

**Ohio Water Resources Center
Annual Technical Report
FY 2017**

Introduction

Pursuant to the Water Resources Research Act of 1964, the Ohio Water Resources Center (WRC) is the federally-authorized and state-designated Water Resources Research Institute for the State of Ohio. The Ohio WRC was originally established at The Ohio State University in 1959, as part of the College of Engineering's Experiment Station. The Ohio WRC continues to be administered through the College of Engineering, in the Department of Civil, Environmental, and Geodetic Engineering.

The Ohio Water Resources Center promotes innovative, water-related research through research grant competitions, coordination of interdisciplinary research proposals, and educational outreach activities. In order to solve current and upcoming water issues, we are focusing on educating new water professionals and directing their efforts to local, state and regional water issues. The Ohio WRC is in ideal position to enable integration of ideas from different stakeholders and facilitate connection among diverse water stakeholders. Additionally, we strive to introduce innovation in water treatment technologies via fundamental research and improve communication of research results to broad audience.

Ohio WRC sponsored researchers enable ecologically and socially sound water management by investigating the sources of nutrients and algal blooms in our environment, developing novel methods and technologies to reduce input of nutrients and other pollutants to water, and characterizing and monitoring the effects of energy development on water resources. By funding researchers early in their careers and developing powerful alliances with partner institutions, Ohio WRC seeds innovative approaches that foster impactful outcomes.

Ohio WRC reaches out to water professionals, educators, and citizens to ensure current and future citizens are water smart. Ohio WRC leaders are active in local and national water research, education and policy organizations such as the Ohio Water Resources Council, Water Management Association of Ohio, National Institutes of Water Resources and University Council on Water Resources.

Research Program Introduction

The Ohio Water Resources Center consistently invests in water related research in the State, growing the number of principal investigators involved in Ohio's water issues, and educating the next generation of water professionals by funding student work on water research projects. Over this past year's reporting period, we sponsored seven new projects and administered five ongoing research projects conducted at four different Ohio universities that totaled \$648,166 in research funding (direct and cost share). The PI's for these projects are five Assistant Professors, three Research Scientists, two Associate Professors and two Full Professors. In total, this research helped support directly and indirectly twenty seven student majoring in environmental engineering, biological sciences, environmental studies, geology, earth science and other water related fields.

The new funded research projects in FY2017 entail studies of important Ohio water resources problems. For example, Dr. Sawyer from the Ohio State University is quantifying the nutrient loads from groundwater discharge to Lake Erie and Dr. Buffam from University of Cincinnati is characterizing the link between algal bloom biomass and methane emissions from drinking water reservoirs in southeastern Ohio. Of the administered research projects, seven projects were finalized during this fiscal year, and six projects will be continued into the next fiscal year 2018. The continuing projects include Dr. Cheng's project on developing nutrient interceptors to treat non-point sources, Dr. Buffam's project on link between algal bloom biomass and methane emissions, Dr. Davies's research of peatlands in Ohio, Dr. Chae's and Dr. Welch's projects on improving technologies for wastewater treatment, and Dr. Bakshi's water-energy nexus project.

In summary, Ohio WRC administered twelve research projects this reporting period, six of which were funded or co-funded by USGS 104(b) base grants. This resulted in the training of twenty seven students, seven published or in preparation manuscripts in peer-review journals and forty two presentations or posters at local, national or international conferences. In this reporting period our PI's have been able to secure an additional \$1,850,000 in research awards using data generated with Ohio WRC funding.

SEPARATION OF PHOSPHORUS- AND NITROGEN-NUTRIENTS FROM AGRICULTURAL DEGRADED WATERS USING PERVIOUS FILTER MATERIAL DEVELOPED FROM INDUSTRIAL BY-PRODUCTS

Basic Information

Title:	SEPARATION OF PHOSPHORUS- AND NITROGEN-NUTRIENTS FROM AGRICULTURAL DEGRADED WATERS USING PERVIOUS FILTER MATERIAL DEVELOPED FROM INDUSTRIAL BY-PRODUCTS
Project Number:	2013OH4360
Start Date:	9/1/2017
End Date:	12/31/2018
Funding Source:	Other
Congressional District:	OH-12
Research Category:	Engineering
Focus Categories:	Treatment, Agriculture, Water Quality
Descriptors:	Industrial by-rproducts, filter material, nutrients
Principal Investigators:	Linda Kay Weavers, ChinMin Cheng

Publications

There are no publications.

SEPARATION OF PHOSPHORUS- AND NITROGEN-NUTRIENTS FROM AGRICULTURALLY DEGRADED
WATERS USING PERVIOUS FILTER MATERIAL DEVELOPED FROM INDUSTRIAL BY-PRODUCTS

Progress Report

Submitted to:

Ohio Water Resources Center

Submitted by:

Principal Investigator:

Linda Weavers, Ph.D., P.E., BCEE.

Professor

Department of Civil, Environmental, and Geodetic Engineering

e-mail: weavers.1@osu.edu; Telephone: 614-292-8263; Fax: 614-292-3780

Co-PI:

Chin-Min Cheng, Ph.D., P.E.

Research Associate II-Engineer

Department of Civil, Environmental, and Geodetic Engineering

ABSTRACT

End-of-tail filtration has been suggested as a more aggressive and effective approach to reduce losses of nutrients from crop lands compared to current best management practices (BMPs) focusing on source reduction and minimizing transportation. A number of industrial by-products, e.g., coal combustion by-products and bauxite leaching residual, have been proven chemically effective in trapping P- and/or N-nutrients, and therefore, are potential low-cost nutrient sorbents for the end-of-tail filtration approach. However, the application of these industrial by-products as the filtration media is limited due to unfavorable hydraulic properties, as well as unknown associated environmental impacts. In this proposed study, pervious filter materials owning both reactivity to nutrients and adequate hydraulic properties are developed using fly ash, stabilized FGD materials, and bauxite leaching residual as the feedstock. By modifying the composition of these industrial by-products, the pervious materials are expected to have selective nutrient-sequestering capabilities, which can be used to separate and recycle phosphorus- and nitrogen-nutrients from agricultural drainage waters (ADWs). This study is carried out in three tasks to (1) investigate the adsorption efficiency and service lifetime of selected pervious materials with synthetic ADW; (2) evaluate the physical and chemical integrity of the pervious materials before and after service; and (3) study the interactions between the prepared filter materials and emerging pollutants commonly found in ADW (e.g., estrone). The goal of this study is to demonstrate the feasibility of applying a low-cost and environmentally-sustainable approach to ADW handling and treatment. This alternative to current BMPs is able to convert agricultural and industrial wastes to value-added products containing concentrated and specific nutrients. Currently, the project is still on going. Results obtained from this study will be used to develop a competitive proposal for external funding.

1. Introduction

Eutrophication of water bodies, a result of release of excessive phosphorous (P) and nitrogen (N) from soil to drainages¹, has been an increasing environmental issue in the US, especially in the Midwest, northeast, and Gulf coast area where the watersheds of major freshwater bodies involve rapid growth and intensification of crop and livestock farming². Not only eutrophication posts unpleasant aesthetic characteristics to water bodies, accumulation of toxic, volatile chemicals produced by algae can cause neurological damage in people and animals being exposed to them. Consequently, eutrophication of water resources results in losses of biodiversity, as well as their amenities and services³. For example, the recent outbreaks of Cyanobacteria, or blue-green algae, in the Grand Lake at St. Mary's area in Ohio has led to state officials to issue water contact and fish consumption advisories.

The major cause of many eutrophication incidents can be directly correlated to fertilizer application⁴. To prevent accumulation of nutrients in surface waters, reduction of nutrients present in the agricultural degraded waters (ADW, i.e., livestock wastewater overflow, subsurface drainages, and surface runoffs from cropland) is perceived as necessary approach⁵. Although many best management practices (BMPs) focusing on source reduction and minimizing transportation have been implemented to reduce losses of nutrients from crop lands, these approaches have shown no control on dissolved phosphorus losses^{6,7}, which is the most readily available form of phosphorus to aquatic organisms⁸. Instead, end-of-tail filtration has been suggested as a more aggressive and effective approach⁶. However, the application is limited. Ideal filter materials, i.e., material with both favorable nutrient-sequestering capability and hydraulic property, have yet been identified⁹.

In this study, low-cost pervious sorption materials prepared from a self-geopolymerization process using agricultural wastes and industrial by-products are tested for their potential as an alternative to current BMPs. The self-geopolymerization process enchains agricultural wastes with chemically-effective, nutrient-sorbing industrial by-products (e.g., coal ash, flue gas desulfurization materials, and bauxite residual) and forms pervious materials. By modifying the composition, the pervious materials are expected to have selective sorption capabilities to nitrogen (N-) and phosphorus (P-) nutrients with adjustable hydraulic properties, which can be used to separate and recycle nutrients from ADWs.

2. Objectives

In this study, a geopolymerization procedure is developed to convert coal combustion by-products (i.e., fly ash and flue gas desulfurization (FGD) material) and alkaline bauxite leaching

residual (bauxite red mud) to pervious filter materials. The materials are tested in a bench-scale setting for their effectiveness and capacity on removing nutrients from simulated agricultural drainage waters. The specific objectives of this proposed project are to:

- (1) Assess the performance of the industrial by-product-derived pervious filter materials with respect to their nutrient removal efficiencies, service lifetime, and hydraulic properties;
- (2) Evaluate the chemical and physical integrity of the materials; and
- (3) Study the interactions between the prepared filter materials and other pollutants contained in ADWs (i.e., estrogens).

3. Materials and Method

The work of this proposed study is divided into three tasks. In summary, the first task focuses on preparing and characterizing the pervious filter materials. At least three sets of P-type (i.e., materials selectively adsorb P-nutrients) and N-type (i.e., materials adsorbed nitrate and/or other N-nutrients) are prepared. In the second task, a series of column experiments are setup to (1) evaluate the adsorption efficiency and capacity of the selected pervious materials with a simulated ADW and (2) study the interactions between estrogens and filtration materials. In addition, the physical and chemical integrities of the pervious filter material during and after service are evaluated. The release of metals and metaloids (e.g., mercury, arsenic, selenium, thallium, and boron), as well as sulfate, from the filter materials during filtration are monitored. In addition, surface characterization techniques, such as X-ray diffraction (XRD) and scanning electron microscopy (SEM), are applied to investigate the transformations of mineral composition and surface morphology before and after the filtration materials are exhausted.

Pervious Filter Material Preparation and Characterization

Coal combustion by-products (i.e., fly ash and stabilized FGD materials) and bauxite leaching residue (i.e., red mud) are used in the preparation of the nutrient-selective pervious filtration materials (Figure 1). Two different types of pervious filtration materials (i.e., P- and N-types) are prepared using a method modified from Cheng et al.¹⁰ and Jin¹¹. Class F fly ash and sulfite-rich stabilized FGD material provided by coal combustion power plants located in eastern Ohio are used to prepare the phosphorous-capture (P-type) filtration materials. Quick lime

(Carmeus USA, Pittsburg, PA), CaO, is added to provide required alkalinity. The nitrogen-capture materials are prepared from red mud, fly ash, and stabilized FGD material. No quick lime is used in the preparation of N-type filter materials. The bauxite red mud provided by a bauxite processing plant located at southeast Texas is oven-dried before use. In one batch, manganese oxide (MnO₂) is also added in the preparation of N-type material. Woodchip is used in the preparation of both N and P-type filter mixtures to modify the hydraulic properties. The prepared mixtures are then cured in a humidity chamber.

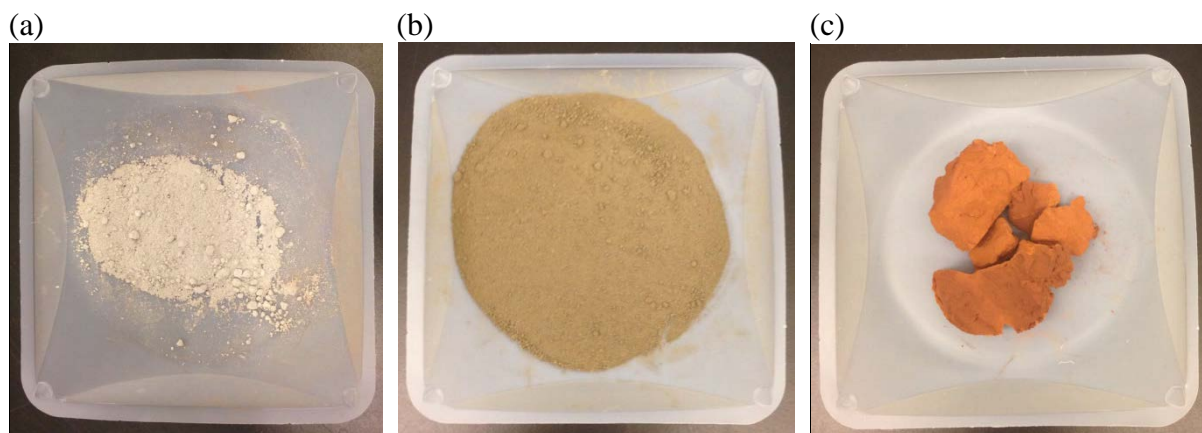


Figure 1. (a) Stabilized FGD material, (b) fly ash, and (c) bauxite red mud used in the preparation of pervious filtration materials.

The cured filter materials are tested for their chemical (i.e., elemental and mineral compositions), physical (density and surface morphology), and engineering (i.e., permeability (k) and/or hydroconductivity (K)) properties as per standard testing protocols. Details on the chemical and physical characterizations of the filter materials are described in the “*Physical and Chemical properties Integrity Evaluation*” section.

Bench-Scale Column Test

A series of column tests are carried out to measure the adsorption capacity and efficiency of prepared pervious materials for P- and N-nutrients with a simulated ADW. In addition to the prepared filter materials, two reference columns, packed separately with granular activated carbon (GAC) and top soil from the OSU’s Waterman Farm Complex, are also included in the column study. A control column, i.e., without packing medium, is included to evaluate the adsorption of nutrients and compounds on the experimental apparatus.

The setup of the column test is illustrated in Figure 2. The ADW used in the column test is synthesized based on formula listed in Table 1. In addition to the constituents listed in the table, one estrogen, e.g., estrone (E1) or 17 α -Estradiol (17 α -E2), commonly found in dairy wastewater¹² is added in selected experimental batches. A peristaltic pump delivers the synthetic ADW to the inlet of a series of two vertically-oriented columns at a constant feed rate (Figure 2). The ADW sequentially passes through the column containing P-type filter material (P-type column) and then the N-Type column. For a given set of filter materials, the column test is carried out under a saturation condition demonstrated in Figure 2.

Table 1. Composition of synthetic dairy wastewater used in this study

Component	Amount (mg/L)
Urea	115.7
NH ₄ Cl	250.0
Na ₂ PO ₄ ·12H ₂ O	385.7
KHCO ₃	257.1
NaHCO ₃	668.6
MgSO ₄ ·7H ₂ O	257.1
FeSO ₄ ·7H ₂ O	10.3
MnSO ₄ ·H ₂ O	10.3
CaCl ₂ ·6H ₂ O	15.4

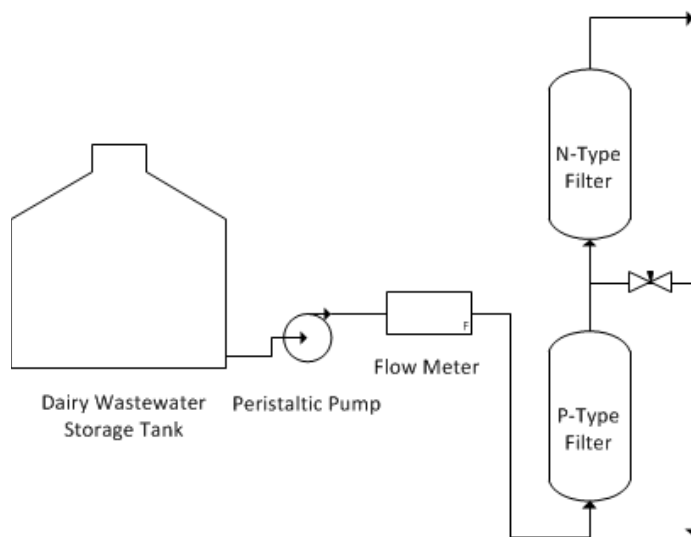


Figure 2. Setup of bench-scale column test

Effluent samples are collected periodically from the outlets of P-type and N-type columns for a list of chemical analyses shown in Table 2. After collection, sample is immediately separated into four sub-samples. The first sub-sample is for pH, conductivity, and redox potential measurements. In the selected batches when estrogen is included in the synthetic ADW, an aliquot of the first subsample is filtered with 1.2µm glass fiber and concentrated by solid-phase extraction for estrogen analysis. Any compounds remained on the sample collection bottle or filter is desorbed by rinsing the bottle and filter with methanol. The concentrated sample is analyzed using a high-performance reverse-phase liquid chromatography tandem electrospray ionization mass spectrometry (HPLC/MS/MS). Deuterated internal standards is added to the samples to correct the interferences caused by the matrix of the sample.

The second sub-sample is filtered and analyzed for alkalinity, total dissolved solids, Cl⁻, SO₄⁻², PO₄⁻³, total Kjeldahl nitrogen, ammonia, and NO₃⁻. The third sub-sample is preserved with 5% HNO₃ and analyzed for “total” elements in the solution. The final sub-sample is filtered through a 0.45-µm syringe filter and preserved with 5% HNO₃ before being analyzed for “dissolved” elements.

Table 2. List of monitoring parameters and respective analytical methods for aqueous samples

Subsample	Parameter	Detection Methods	Instruments	Locations
Subsample I	Conductivity	AWWA Sec. 2510	Thermo Orion 1234	<i>in-situ</i>
	pH		Thermo Orion 1234	<i>in-situ</i>
	Redox Potential		Thermo Orion 1234	<i>in-situ</i>
	Estrogen ^c	HPLC/MS/MS	Micromass Q-TOF II	CCIC ^b
Subsample II	Alkalinity	AWWA Sec. 2310	-	CEGE EER Lab/ OARDC STAR Lab
	Total dissolved solid	AWWA Sec. 2540	-	
	Chloride (Cl)	AWWA Sec. 4110C	Dionex 2100	
	Sulfate (SO ₄ ⁻²)	AWWA Sec. 4110C	Dionex 2100	
	Phosphate(PO ₄ ⁻³)	AWWA Sec. 4110C	Dionex 2100	
	Nitrate (NO ₃ ⁻)	AWWA Sec. 4110C	Dionex 2100	
	Ammonia (NH ₄ ⁺)	AWWA Sec. 4110C	Dionex 2100	
Total Kjeldahl Method	AWWA Sec. 4500 N _{org}	-		
Subsample III/ Subsample IV	Mercury (Hg)	CVAFS	Varian CVAAs,	
	Selected Elements ^a	AWWA Sec. 3120B	Varian VISTA-AX	
	Arsenic (As)/ Thallium(Tl)	AWWA Sec. 3120B	Varian GFAAs, Varian 880Z	
	Selenium (Se)	AWWA Sec. 3120B	Varian GFAAs, Varian 880Z	

^a Aluminum (Al), arsenic (As), barium (Ba), beryllium (Be), boron (B), cadmium (Cd), copper (Cu), chromium (Cr), iron (Fe), lead (Pb), magnesium (Mg), manganese (Mn), nickel (Ni), phosphorous (P), sodium (Na), silver (Ag), zinc (Zn).

^b Campus Chemical Instrument Center at The Ohio State University

^c On selected experimental batches

Chemical and Physical Integrity Evaluations

The exhausted filter materials are preserved using liquid nitrogen and freeze-dried before being analyzed for the mineral and chemical compositions, surface morphology, and forms of adsorbed phosphorus by the methods listed in Table 35. The mineral compositions and morphology of the selected N- and P- type filters materials before and after service are characterized using X-ray diffraction (XRD) and scanning electronic microscopy (SEM), respectively. A Bruker D8 Advance X-ray diffractometer or equivalent is used to identify the mineral composition. The mineral patterns in the diffractograms are matched using the DIFFRACplus EVA software with ICDD Power Diffraction File (PDF2+) database. The complete elemental composition analysis is measured with the assistance of the digestion procedure described in EPA method 3052. A reference coal fly ash, 1633b, provided by the National Institute of Standards and Technology (NIST), is included for analytical quality control. A list of the analyses performed on the materials can be seen in Table 4.

The release potential of trace elements from filter materials before and after service will also be characterized. Standard protocols, i.e., EPA Standard Method 1311, Toxicity Leaching Characteristic Procedure (TCLP), the EPA Standard Method 1312, Synthetic Precipitation Leaching Procedure (SPLP), are used.

Table 3. Physical, mineral, and chemical analyses for selected pervious filter materials

	Method	Instrument	Location
Permeability	ASTM D4525-08		CEGE Soil Lab
Hydraulic Conductivity	ASTM D7100-06		
Morphology	Scanning Electron microscopy	Hitachi S-3000 SEM	OSU Nanotech West Lab
Mineral Composition	X-ray Diffraction	Bruker D8 Advance X-ray diffractometer	SENR Soil Lab ^c
Selected Elements ^a	ASTM D-6357	Milestone Microwave Digestor/ Varian VISTA-AX	CEGE EER Lab ^b
Mercury	ASTM D-6414	Varian CVAAs, Varian 880Z	CEGE EER Lab
Selenium	ASTM D-4606	Varian CVAAs, Varian 880Z	CEGE EER Lab
Arsenic, Thallium	ASTM D-3683	Varian GFAAs, Varian 880Z	CEGE EER Lab

^a aluminum (Al), barium (Ba), beryllium (Be), boron (B), cadmium (Cd), chromium (Cr), lead (Pb), magnesium (Mg), manganese (Mn), nickel (Ni), phosphorous (P), sodium (Na), sulfur (S), and zinc (Zn).

^b Environmental Engineering Research Laboratory at Department of Civil, Environmental, and Geodetic Engineering of The Ohio State University

^c Soil Lab at School of Environment and Natural Resources of The Ohio State University

4. Current Progress and Tasks to be completed

Characterizations of Industrial By-products

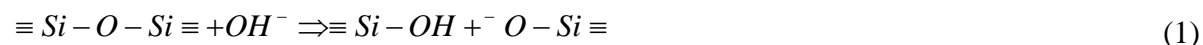
The chemical compositions of fly ash, stabilized FGD material, and bauxite red mud are first characterized and the results are summarized in Table 4. As shown in the table, calcium (Ca) and sulfur (S) are the two most abundant elements in the stabilized FGD material, which is associated with the presence of hannerbachite ($\text{CaSO}_3 \cdot 0.5\text{H}_2\text{O}$), portlandite ($\text{Ca}(\text{OH})_2$), and enttringite ($\text{Ca}_6\text{Al}_2(\text{SO}_4)_3(\text{OH})_{12} \cdot 26\text{H}_2\text{O}$) in the material. The X-ray diffractogram and mineral composition of stabilized FGD material can be seen in Figure 3. Iron (Fe), aluminum (Al), sulfur (S), and silicon (Si) are the major elements in fly ash. Based on XRD analysis, the fly ash used in this study is comprised of amorphous glass, aluminum silicates (e.g., mullite), and iron oxides (hematite, magnetite, and maghemite). Bauxite red mud is consisted of Al, Fe, and Ca. The X-ray diffractograms of fly ash and red mud are not shown.

By properly coalescing fly ash, stabilized FGD material, and red mud under high alkaline environment, fly ash acts as an inorganic polymer binder to enchain active ingredients through a geopolymerization process. After being alkali-activated, the Si-O-Si or Al-O-Si bonds in fly ash and stabilized FGD material are disassociated and subsequently form network-like crystalline and/or amorphous alkaline aluminosilicates with structural framework similar to zeolite¹³. In a previous project, it has been demonstrated that a geotextile material derived from the geopolymerization process with a mixture of fly ash and stabilized FGD material, has effective phosphorus sorption capability by forming Ca- and Fe-precipitates^{10,14,15}. However, the fly ash/stabilized FGD material mixture did not show observable effect on nitrate mitigation¹⁰.

The addition of bauxite red mud is to enhance the nitrogen-nutrients adsorption capability of the fly ash/FGD mixture. Bauxite red mud contains minerals, e.g., iron (III) (hydr)oxides and hydrous aluminum oxides, that have high affinities for nitrate¹⁶. As a result, the material has been shown to be an effective nutrient sorbent¹⁷. Cengeloglu et al¹⁷ used original and acid-treated bauxite red mud to remove nitrate from aqueous solution and reported 70% and over 90% of removal, respectively. They found the alkaline property of bauxite red mud hindered the adsorption performance.

In this study, bauxite red mud is used as the sole alkalinity source in the geopolymerization process, which might promote the nitrate adsorption capacity. During geopolymerization, the OH^- ions from bauxite red mud is consumed (eq. 1) and redistribute the electron density around the silicon atom in fly ash, which weaken the strength of Si-O-Si bond¹⁸

and progress the polymerization process. The reaction neutralizes the negative surface charge of red mud particles, and therefore, might promote the nitrate sorption.



Preparation of P- and N-type pervious filtration

A series of P- and N-type pervious filtration materials have been prepared based on the formulas listed in Tables 5 and 6. Currently, the prepared materials are undergoing a 21-day curing process. The images of two selected prepared materials can be seen in Figure 4. The hydraulic property of the filtration materials are adjusted by the addition of woodchip. Two different sizes of woodchip, i.e., <2.3mm and 2.3-3.6mm, are used. The addition of woodchip creates larger capillary routes for water to pass through. During the geopolymerization process, active ingredients are coated on the surface of woodchip, which allows the nutrients in ADW to react with the active ingredients while passing through the void space.

Table 4. Chemical compositions of fly ash, stabilized FGD material and bauxite red mud used in this study

		Fly Ash	Stabilized FGD material	Red Mud
Phosphorus	P	531	177	1054
Potassium	K	2986	1307	310
Calcium	Ca	9836	172906	33055
Magnesium	Mg	1528	10026	227
sulfur	S	11827	85746	2867
Aluminum	Al	27050	9705	62817
Boron	B	531	313	<3
Copper	Cu	42	<0.4	<0.8
Iron	Fe	59824	18855	240960
Manganese	Mn	85	73	139
Molybdenum	Mo	22	<13	<0.5
Sodium	Na	18851	5296	32412
Zinc	Zn	109	40	22
Arsenic	As	143	36	28
Barium	Ba	177	137	61
Beryllium	Be	<0.18	<0.11	<0.18
Cadmium	Cd	2	6	5
Cobalt	Co	23	4	15
Chromium	Cr	74	25	1397
Lithium	Li	167	106	55
Nickel	Ni	48	7	6
Lead	Pb	28	8	46
Antimony	Sb	<1.5	17	<1.5
Selenium	Se	20	18	1
Silicon	Si	4771	1481	184
Strontium	Sr	229	212	117
Thallium	Tl	129	38	871
Vanadium	V	2	<1.1	<0.6
Mercury	Hg	NA	0.318	NA

NA: Not Available
Unit: mg/kg

Table 5. Formulas of Prepared P-type Filtration Materials

	P-Control	P-type I	P-type II	P-type III
Fly Ash	10.0	10.0	10.0	10.0
Stabilized FGD material	6.0	6.0	6.0	6.0
Quick Lime (CaO)	1.2	1.2	1.2	1.2
Deionized Water	10.5	10.5	10.5	10.5
Wood Chip (<2.3 mm)	0	2.5	5.0	0
Wood Chip (2.3-3.6 mm)	0	0	0	2.5

Unit: g

Table 6. Formulas of Prepared N-type Filtration Materials

	N-Control	N-type I	N-type II	N-type III
Fly Ash	10.0	10.0	10.0	10.0
Stabilized FGD material	6.0	6.0	6.0	6.0
Red Mud (dried weight)	8	8	8	8
Deionized Water	10.5	10.5	10.5	10.5
Wood Chip (<2.3 mm)	0	2.5	5.0	2.5
MnO ₂	0	0	0	2.0

Unit: g

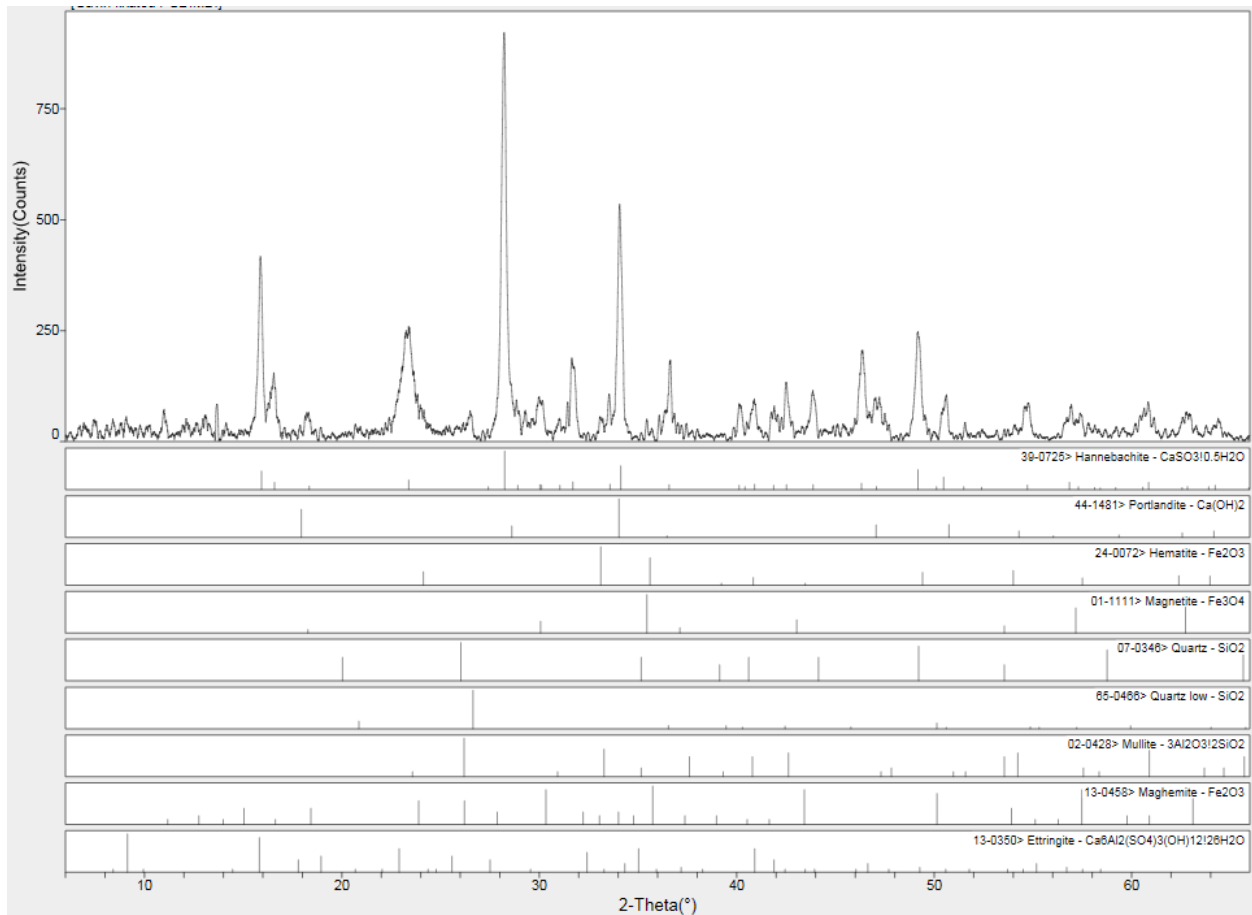


Figure 3. Mineral composition of stabilized FGD material

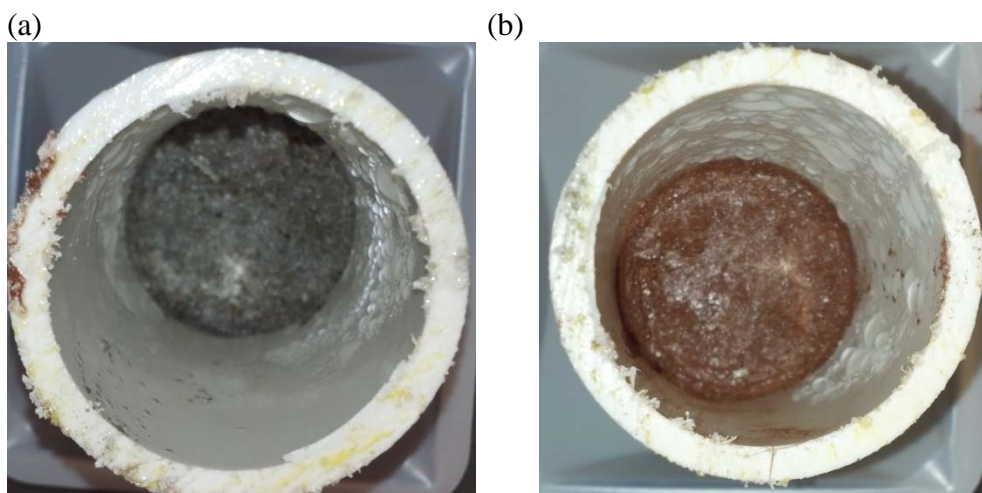


Figure 4. Prepared Pervious filtration materials. (a) P-type and (b) N-type.

These two types (i.e., P- and N-types) of pervious materials are expected to have selective sorption capacity, which can be used to sequentially separate and recover soluble phosphorous and nitrogen in agricultural drainage waters. In practice, two different pervious filter materials can be used in series. The dissolved phosphorous is expected to be selectively retained in the first pervious material (P-type) containing only fly ash and FGD material while allowing nitrate to pass through. Nitrate is captured in the second pervious material (N-Type) containing bauxite red mud, fly ash, and stabilized FGD material.

Adsorption Capacities

The nutrient adsorption capacities of P- and N-type materials were evaluated using the materials prepared from the formulas listed in Tables 5 and 6 for the P-Control and N-Control materials. For either type of the material, the adsorption experiment was carried out by adding six different amounts of the prepared solid, ranging from 0 to 1 gram, into six separate 125-mL HDPE bottles. Each bottle contains 100mL of either 250 mg/L of phosphate or 100 mg/L of nitrate solution. The bottles were then mixing by a tumbler for 24 hours at a rotating speed of 18 rpm. After mixing, the solution collected from each bottle was filtrated with 0.45mm filter and analyzed for NO_3^- or PO_4^{3-} .

The equilibrium concentrations of phosphate and nitrate in the solution after mixing as a function of material dosage are shown in Figure 5. As shown in the figure, over 97% of phosphate was removed by the P-type material with a solid-to liquid (L/S) ratio of 100. With the same L/S ratio, nearly 4% of nitrate was adsorbed by the N-type material.

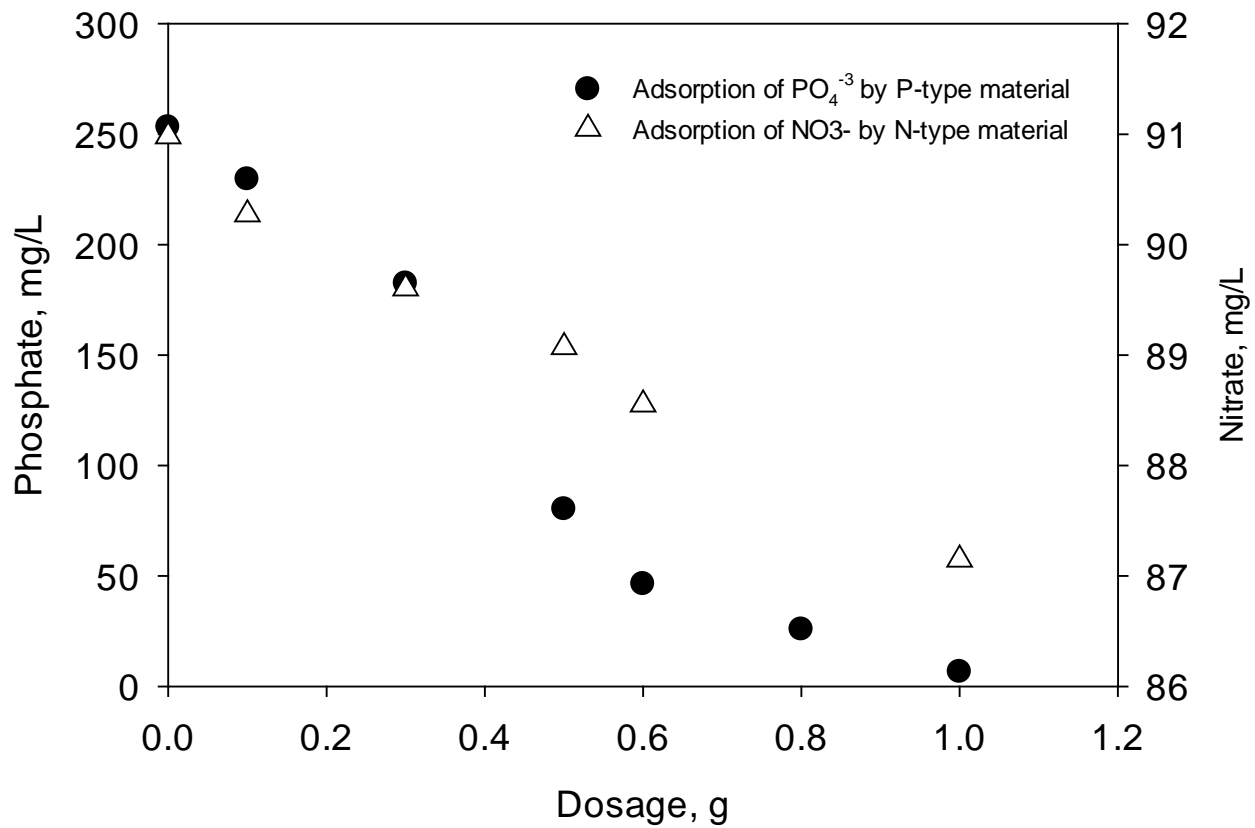


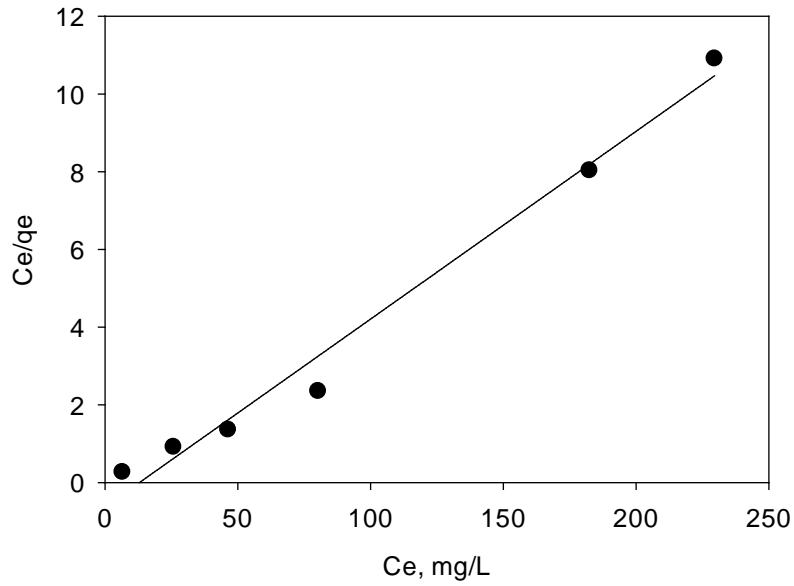
Figure 5. The equilibrium concentrations of phosphate and nitrate in the solution as a function of material dosage

The adsorption isotherms of phosphate on P-type material and nitrate on N-type material are illustrated in Figure 6. As shown in the figure, the adsorption isotherms of phosphate and nitrate can be expressed as Langmuir isotherm. The Langmuir isotherm equation is written as

$$\frac{C_e}{q_e} = \frac{1}{K \cdot Q_a^0} + \frac{C_e}{Q_a^0} \quad \text{Eq. 1}$$

where q_e is mass of material adsorbed (at equilibrium) per mass of adsorbent; Q_a^0 represents the maximum adsorption capacity (monolayer coverage); C_e is the equilibrium concentration in solution when amount adsorbed equals q_e ; K is constant (L/mg).

(a)



(b)

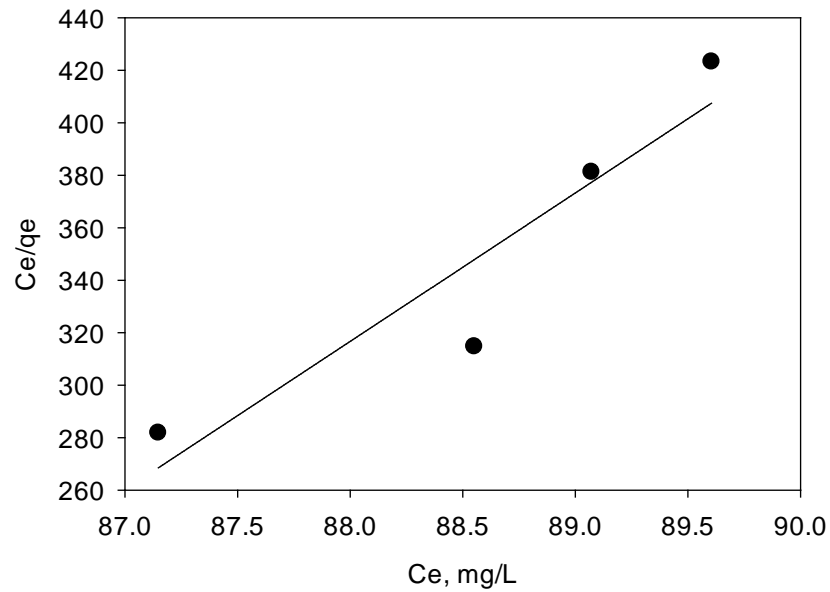


Figure 6. Langmuir isotherms for (a) phosphate and (b) nitrate

It is estimated that the maximum phosphate adsorption capacity of P-type material is 20.7 mg/g. For the N-type material, the adsorption capacity was approximately 0.18 mg/g, which is much less than the expected adsorption capacity.

Column Test

Close-loop Column System

Two series of bench-scale column tests were carried out using P-type and/or N-type columns in a close-loop mode to investigate the removal of nitrate and phosphate with extended contact time. The flow rate was kept at 1.13 ± 0.17 mL/sec for both series. A simplified agriculturally degraded solution prepared with NaH_2PO_4 and NaNO_3 was used. In the first series, the solution was first introduced into P-type column and then N-type column. In the second series, only N-type column was used. A collection schedule was then setup to collect a series of eluent fractions based on pre-scheduled time interval. During each sampling interval, eluents were collected from the inlet and outlet of the first column, as well as the outlet of the second column in the first series, for nitrate and phosphate analyses.

The temporal trends of nitrate and phosphate at the inlet of the first column can be seen in Figure 7, which represent the concentrations in the storage tank. It was found that the concentration of nitrate in the first series decreased over 68.5% (from the original 47.1 mg/L to 14.8 mg/L) after 30 hours of circulation. In the second series, a similar removal efficiency (60.1%) was observed during the first 26 hours when only N-type column was used. However, the concentration of nitrate decreased to a level lower than the detection limit after 146 hours of circulation. In the case of phosphate, over 95% of the phosphate in the solution was removed within 30 hours of circulation in both close-loop series.

Results observed from the two close-loop series of column tests demonstrate that the pervious filter materials prepared in this study can effectively decrease the concentrations of nitrate and phosphate. Although the concentrations of both nitrate and phosphate showed a decreasing trend throughout the testing period in both testing series, for a given sampling interval, no significant changes were observed between the samples collected before and after the columns. It suggests that the time for the solution to travel through the lengths of these columns was not long enough to show any changes.

The decreases of nitration concentration observed in both column tests were unlikely due to adsorption. Results obtained from the adsorption isotherm experiment suggest that the adsorption of nitrate on the N-type material is very limited. Other mechanisms, such as biological reduction, might have involved in nitrate removal. Also, it seems the addition of red mud did not have significant effect on the reduction of nitration concentration.

Flow through Column System

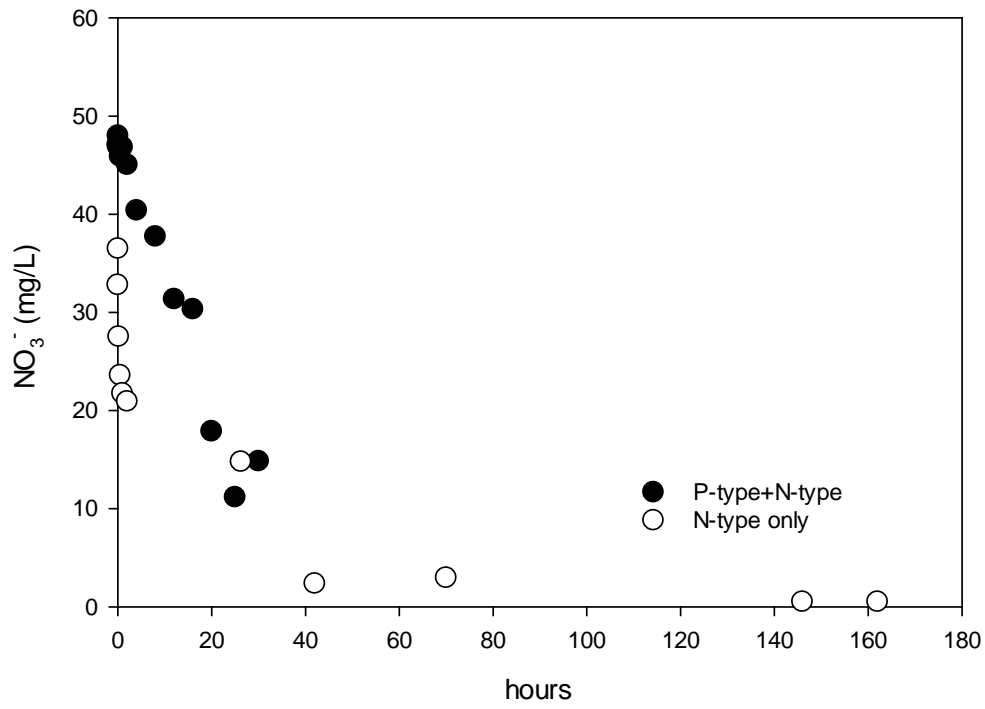
A flow-through column test was setup to further investigate the removal of nitrate and phosphate under the condition that is similar to real application. Only the P-type material was used in the test. The material was packed into a 2.5 ft long acrylic column with a diameter of 6 inches. The flow rate of the simulated agriculturally degraded solution, prepared from the same formula used in the close-loop column test, was controlled at 0.46 mL/min. As a result, the retention time of the solution in the column was maintained at 20 hours.

Results obtained from the test can be seen in Figure 8. As shown in the figure, over 77% of nitrate removal was achieved short after one pore volume passing through the column, which increased to 98% after approximately 168 hours. Compared to the results obtained from the close-loop system, which is also shown in Figure 8, the temporal trends of nitrate removal are very similar between the two systems.

In the case of phosphate, over 99% of removal was achieved after about 560 hours or 28 pore volumes, which increased from the 82.5% observed after about one pore volume. The removal of phosphate kept increasing as more solution passing through the column. It suggests that the adsorption of phosphate was likely controlled by the release of sulfate and the complexation of phosphate on the pore surface of the pervious material. As more solution passing through the column, more sulfate was released from the matrix of the pervious material, which allowed more phosphate to be retained within the pervious material.

Results obtained from the flow through column test confirmed the potential of using the pervious material derived from stabilized FGD material (P-type) to remove both nitrate and phosphate from agriculturally degraded solution.

(a)



(b)

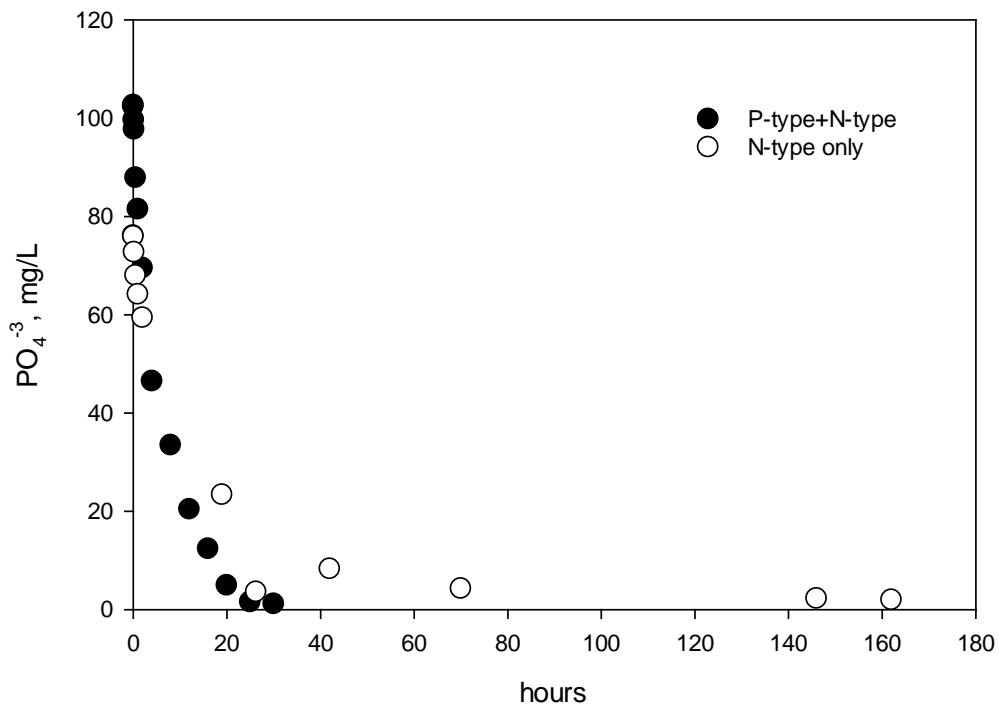
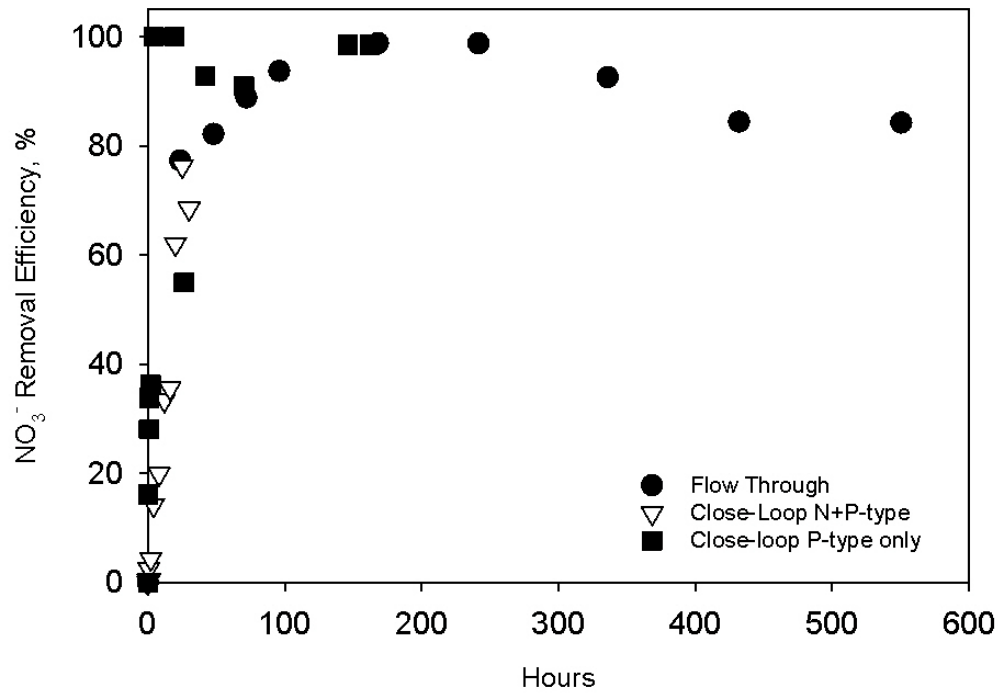


Figure 7. Temporal Trend of nitrate and phosphate in the close-loop column system

(a)



(b)

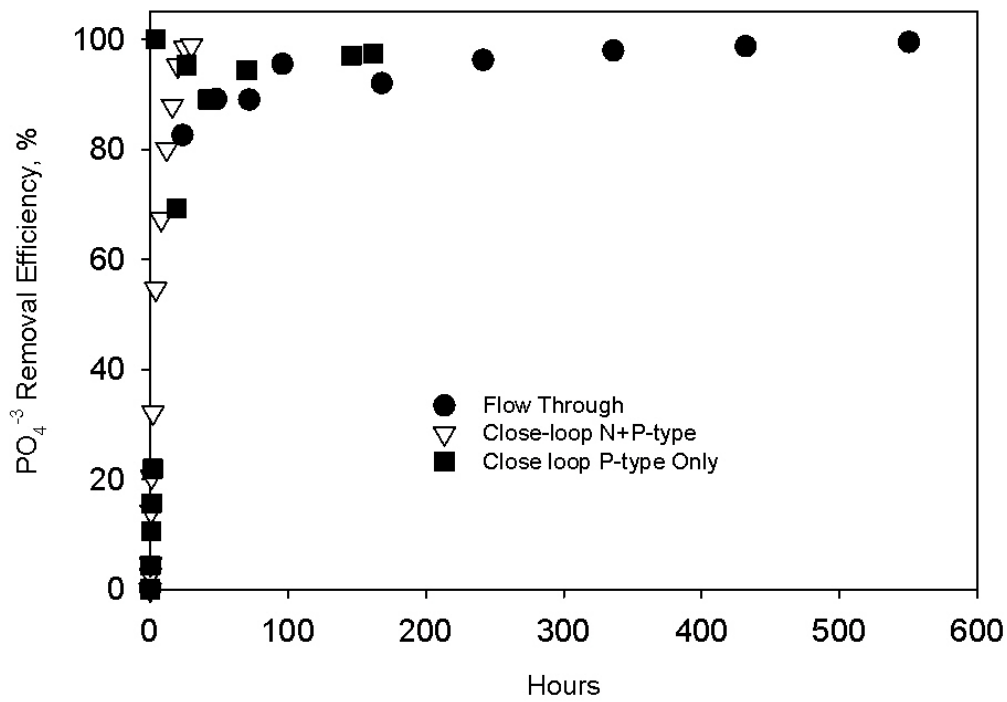


Figure 8. Removal efficiency of (a) nitrate and (b) phosphate using the P-type pervious material with a flow through column

Tasks to be completed

The bench scale column test described in the “*Materials and Methods*” section will be continued. In addition, the mechanisms involved in the removal of N- and P-nutrients will be investigated. The integrities of physical and chemical properties of the pervious materials after adsorption will also be evaluated.

Despite the great potential for the proposed filtration application, the major concern of reutilizing these by-products is the release of trace elements contained in the materials after being contacted with water. Cheng *et al.*²² investigated the water quality impacts associated with using stabilized FGD material as a low permeability liner for a swine manure storage pond. Based on five-year worth of field monitoring data, the concentrations of arsenic (As), boron (B), chromium (Cr), copper (Cu), and zinc (Zn) were consistently found lower in the water passing through the liner than the water collected from the pond. Other trace elements, such as Cd, Se, and Hg were often below the analytical detection limits. Ruyter *et al.*¹⁹ investigated the red mud accident occurred on October 4th 2010 in Ajka, Hungary by testing the plant toxicity and trace element availability with mixtures of red mud and non-contaminated soil. They observed the concentrations of trace elements in the leachate of red mud were either non-detectable or less than 20µg/L. In addition, Peters and Basta¹⁸ added bauxite red mud directly to soil to reduce the bioavailable phosphorus. No excessive soil pH and increases of soil salinity, extractable Al, or heavy metals in soils were found in their study. Based on available field data, the application of coal combustion by-products and bauxite red mud has not been suggested to post adverse impacts on the environments.

However, to comprehend the overall benefits of reusing these by-products, it is vital to understand the leaching properties of the prepared pervious materials under different application scenarios.

Expected Outcomes and Significances

The outcome of this study is expected to provide:

- (1) Initial feasibility evaluation of a potential beneficial utilization for by-products produced from coal combustion and aluminum production processes
- (2) Insights regarding the interaction between nutrients and an agricultural emerging pollutant (i.e., estrogen) of FA zeolite-like material and the properties of biopolymers, and

- (3) Results to be transferred in forms of peer-reviewed publications and conferences, and be based upon in preparing competitive proposal for external funding.

The advantage of using selective sorption materials in the filtration approach is the potential to recycle and reutilize nutrients and industrial by-products, which promotes agricultural production to be in accord with the principles of sustainability. FGD gypsum and stabilized FGD material have shown to improve the yield of crops by providing necessary elements (e.g., calcium), changing soil physical properties, and increasing water infiltration and storage when they are applied as soil amendments^{20,21}. Hylander et al.²², used different filter materials (i.e. limestone, Polonite®, and sand) to capture soluble phosphorus and evaluated the subsequent suitability for plant production. They observed some of recycled phosphorus achieved 76% of the yield increased by commercially available P-fertilizer. As demand for food increases, which results in more land to be used for agricultural purpose and a requirement for increased crop yields, the fertilizer demand have been projected to increase faster than world population²³. With foreseeable increase in demand and depletion in reserve, use of recycled nutrients rather than a raw material is important step toward sustainable agricultural development. Currently, the majority of phosphate rock from mining goes into artificial fertilizer production²⁴. It estimates that sources of high-grade phosphate ore deposits could disappear within the next 100 years at current use rates²⁵.

5. References

- ¹ Alexander, R. B., Smith, R. A., Schwarz, G.E., Boyer, E.W., Nolan, J.V., Brakebill, J.W. (2008) Differences in phosphorous and nitrogen delivery to the Gulf of Mexico from the Mississippi River Basin. *Environ. Sci. Technol.*, 42, 822-830.
- ² Mueller, D.K., Helsel, D.R., Nutrients in the Nation's Waters--Too Much of a Good Thing?. U.S. Geological Survey Circular 1136, <http://pubs.usgs.gov/circ/circ1136/circ1136.html#PUBS>, accessed 2/4/2011.
- ³ Smith, V.H., Tilman, G.D., Nekola, J.C. (1999) Eutrophication: impacts of excess nutrient inouts on freshwater, marine, and terrestrial ecosystems, *Environ. Poll.*, 100, 179-796.
- ⁴ Smil, V. *Enriching the Earth: Fritz Haber, Carl Bosch, and the Transformation of World Food*. The MIT Press, 2001, Cambridge, U.K.
- ⁵ Sharpley A, Foy B, Withers P (2000) Practical and innovative measures for the control of agricultural phosphorus losses to water: An overview. *J. Environ. Qual.*, 29, 1-9.
- ⁶ Kleinman P.J.A., Sharpley, A.N., Buda, A. R., McDowell, R.W., Allen, A.L. (2011) Soil controls of phosphorus in runoff: Management barriers and opportunities. *Can. J. Soil Sci.* 91, 329-338.

- ⁷ Sharpley A., Kleinman, P., and Weld J. (2010) Assessment of best management practices to minimize the runoff of manure-borne phosphorous in the United States, *New Zealand J. Agric. Res.*, 47, 461-477.
- ⁸ Sonzogni, W.C., Chapra, S.G., Armstrong, D.E., Logan, L.T. (1982) Bioavailability of phosphorus inputs to lakes. *J. Environ. Qual.*, 11, 555-563.
- ⁹ King, k.W., McDonald, J., Moore, J.F., Agrawal, S.G., Fischer, E.N., Balogh, J.C. (2010) Nutrient and pesticide removal from laboratory-simulated tile drainage discharge, *Trans. ASABE*, 53, 769-777.
- ¹⁰ Cheng, C.-M., Tu, W., Behrad, Z., Tarunjit B., Wolfe, W., Walker, H. (2007) Beneficial Reuse of FGD Material in the Construction of Low Permeability Liners: Impacts on Inorganic Water Quality Constituents, *J. Environ. Eng.*, 133, 523-531.
- ¹¹ Jin, N. fly ash Applicability in Pervious Concrete, Master Thesis, The Ohio State University, Columbus, OH 2010.
- ¹² Gall, H. E., Sassman S.A., Lee, L.S., and Jafvert, C.T., Hormone discharges from a Midwest tile-drained agroecosystem receiving animal wastes. *Environ. Sci. Tech.*, 2011, 45, 8755-8764.
- ¹³ Buchwald A., Dombrowski, k., and Weil, M. Influence of geopolymer binder composition on conversion reactions at thermal treatment, in *Developments in porous, Biological and Geopolymer Ceramics: A collection of Papers Presented at the 31st international conference on advanced Ceramics and Composites*, eds. Brito, M., Case, E., Kriven, W.M., Ceramic Engineering and Science Proceedings Volume 28. 257-271. Florida 2007,
- ¹⁴ Allred, B. (2010) Laboratory batch test evaluation of five filter materials for removal of nutrients and pesticides from drainage waters. *Transactions of the ASABE*, 53, 39-54.
- ¹⁵ Bryant, R.B., Buda A.R., Kkeinman, P.J.A., Church, C.D., Saporite, L.S., Folmar, G.J., Bose, S., Allen, A. (2012) Using fluegas desulfurization gypsum to remove dissolved phosphorus from agricultural drainage waters. *J. Environ. Qual.* 41, 664-671.
- ¹⁶ Yao, W., Millero, F.J. (1996) Adsorption of phosphate on manganese dioxide in seawater, *Environ. Sci. Technol*, 30, 536-541.
- ¹⁷ Cengeloglu, Y., Tor, A., Ersoz, M., Arslan, G. (2006) Removal of nitrate from aqueous solution by using red mud. *Sep. Purif. Technol*, 51, 374-378.
- ¹⁸ Duxson P, Lukey G.C., Separovic F. van Deventer J.S.J., (2005) Effect of alkali cations on aluminium incorporation in geopolymeric gels, *Ind. Eng. Chem. Res.*, 44, 832-839.
- ¹⁹ Ruters, S., Merten, J., Vassilieva, E., Dehandschutter, B., Poffijn, A., Smolders, E. (2010) The red mud accident in Ajka (Hungary): plant toxicity and trace metal bioavailability in red mud contaminated soil. *Environ. Sci. Technol.*, 45, 1616–1622.
- ²⁰ Chen L., Dick W., Nelson S., (2001) Flue Gas Desulfurization by-product additions to acid soil: Alfalfa productivity and environmental quality, *Environ. Poll.*, 114, 161-168.
- ²¹ Punshon T., Adriano D.C., Weber, J.T. (2001) Effect of flue gas desulfurization residue on plant establishment and soil and leachate quality, *J. Environ. Qual.*, 30, 1071-1080.
- ²² Hylander, L.D., Kietlinska, A., Renman, G., Siman, G. (2006) Phosphorus retention in filter materials for wastewater treatment and its subsequent suitability for plant production. *Biores. Technol.*, 97, 914-921.
- ²³ Haar, A. The Reuse of Phosphorus. Eureau Position Paper EU2-04-SL09, 2005; http://eureau.org/sites/eureau.org/files/documents/2005.02.21_recovery_of_phosphorus_from_sludge.pdf. Accessed 10/6/2012.

- ²⁴ Jasinski S.M., Phosphate rock, 2006 Minerals Yearbook. United States Geological Survey, 2007, http://minerals.usgs.gov/minerals/pubs/commodity/phosphate_rock/myb1-2006-phosp.pdf, accessed 10/2/2012.
- ²⁵ Christen, K. (2007) Closing the phosphorus loop, *Environ. Sci. Technol.*, 41, 2078.

Effectiveness of Data Buoys as Early Warning Systems for cHABs (cyanobacterial Harmful Algal Blooms) in Lake Erie

Basic Information

Title:	Effectiveness of Data Buoys as Early Warning Systems for cHABs (cyanobacterial Harmful Algal Blooms) in Lake Erie
Project Number:	2016OH484B
Start Date:	3/1/2016
End Date:	2/28/2018
Funding Source:	104B
Congressional District:	OH-003 & OH-015
Research Category:	Water Quality
Focus Categories:	Surface Water, Water Quality, Methods
Descriptors:	None
Principal Investigators:	Justin Chaffin, Douglas L Kane

Publications

1. Chaffin, J. "Effectiveness of data buoys for sampling cyanobacterial harmful algal blooms in Lake Erie", Event name: Ohio Academy of Science Annual Meeting, Size of audience: 20, Date: 4/16/2016, Type of presentation: Oral
2. Chaffin, J. "Let's Hear It for the Buoys?- Accuracy of data buoys for monitoring cyanobacterial blooms in Lake Erie" Event name: Great Lakes HABS Collaboratory Webinar, Size of audience: 50, Date: 6/2/2016
3. Chaffin, J. (2016) "Accuracy of Data Buoys for Monitoring Cyanobacterial Blooms in Lake Erie" International Association on Great Lakes Research Conference, Guelph, Canada, Size of audience: 500, Date: 6/6/2016, Oral Presentation
4. Chaffin, J. "Accuracy of data buoys for tracking cyanobacterial blooms in Lake Erie" Lake Erie Millennium Network, Size of audience: 125, Date: 2/21/2017, Type of presentation: Oral
5. Chaffin, J. "The re-eutrophication of Lake Erie: degradation, adaptation, and restoration", oral presentation, São Paulo State University (UNESP)- Botucatu, Brazil, 2/19.2017, audience 20.
6. Chaffin, J. "Yeah buoy: Monitoring cHABS in western Lake Erie using in-situ technology" Event name: International Association on Great Lakes Research Conference, Size of audience: 75, Date: 5/16/2017
7. Chaffin, J. "From Lake to River: Using Plankton to Assess Water Quality in Lake Erie and Its Tributaries." Event Name: University of Toledo- Lake Erie Center Public Lecture Series, Size of audience: 30, Date: 11/16/2017, Oral Presentation
8. Chaffin, J. "Cyanobacterial Harmful Algal Bloom detection in western Lake Erie and the Maumee River using sensor technology" Upper Maumee Watershed Partnership Meeting, Size of audience: 10, Date: 1/10/2018, Type of presentation: Oral
9. Chaffin, J. "Working towards a forecast of Lake Erie cyanobacterial bloom toxicity", Kent State University Biology Department seminar, Size of Audience: 50, 1/19/2018
10. Chaffin, J., "The role of phosphorus, nitrogen, and light on Lake Erie cyanobacterial bloom growth and toxicity", Event name: Midwest Aquatic Plant Management Society, Size of audience: 230, Date: 2/27/2018, Type of presentation: Oral

Effectiveness of Data Buoys as Early Warning Systems for cHABs (cyanobacterial Harmful Algal Blooms) in Lake Erie

11. Chaffin, J. "Development of a Lake Erie HAB toxicity forecast", Event name: Trumbull County Soil & Water Conservation District Lunch and Learn, Size of audience: 20, Date: 3/20/2018
12. Kane, D.D., Chaffin, J.D., Jones, K.W., Johnson, A. Vertical distribution of cyanoHABs and their toxins in a large lake: implications for drinking water treatment. *Water Resources Research*. In preparation.

Ohio WRC Project Final Report

“Effectiveness of Data Buoys as Early Warning Systems for cHABs (cyanobacterial Harmful Algal Blooms) in Lake Erie”

By:

Justin D. Chaffin
Stone Laboratory
Ohio State University and Ohio Sea Grant

And

Douglas D. Kane
Defiance College

Problem and Research Objectives

Harmful cyanobacterial blooms (cHABs) were an annual occurrence in Lake Erie during the mid-1900s due to excessive nutrient loading (Davis 1964). The governments of the United States and Canada agreed to regulate phosphorus (P) loading in the 1970s, which resulted in a lake that was relatively free of cHABs throughout the 1980s and 1990s (DePinto et al. 1986; Makarewicz 1993). However, since the mid-1990s, cHABs have returned, and bloom resurgence has been attributed to increases of dissolved reactive P (Kane et al. 2014; Stumpf et al. 2016), climate change (Michalak et al. 2013). The current cHABs in Lake Erie are dominated by the cyanobacterium *Microcystis* (Chaffin et al. 2011), which is globally-distributed in eutrophic water and can produce high concentrations of the hepatotoxic microcystins (MCYs) (as reviewed by (Harke et al. 2016b)). In August 2014, MCYs were found in the municipal water of Toledo, Ohio, United States, at concentrations that exceeded the World Health Organization’s guideline of 1 µg/L, causing a loss of safe drinking water for nearly 500,000 residents (Qian et al. 2015; Bullerjahn et al. 2016). Additionally, cHABs can disrupt aquatic food web structure (Tillmanns et al. 2008; Davis et al. 2012), have killed pets and livestock (Huisman et al. 2010; Backer et al. 2013), and can adversely impact local economies (Dodds et al. 2009; Bingham et al. 2015).

Ultimately, preventing cHABs from forming in lakes and rivers by decreasing influx of nutrients from the surrounding watershed will aid in the protection of safe drinking water. However, trends in climate and agricultural practices suggest that cHABs will become more common in the future (Paerl and Huisman 2008; Michalak et al. 2013). Thus, the risk of cyanotoxins in water will continue to be present, and societies will need to rely on water treatment plants to provide safe drinking water. Real-time estimates of cHAB biomass at or near the intake pipes of municipal water treatment plants can aid the operators in adjusting treatment accordingly. Moreover, the real-time information on cHAB biomass could be used to notify lake managers, tourists, and the general public of when cHABs cause water quality problems (Read et al. 2010). Early detection of cHABs creates the opportunity to mitigate health risks and adverse economic impacts by warning people before cHABs are a severe problem (Jochens et al. 2010), and allows people know when a cHAB is not causing a problem at a given area of the lake or time.

In response to the Toledo 2014 “do not drink advisory,” several lake-shore communities in northern Ohio, Ohio universities, and the federal government (NOAA) deployed water quality sondes for cyanobacteria on buoys or in water treatment plant intakes to provide real-time cyanobacterial biomass data. Since summer 2015, 9 water quality sondes attached to buoys have been deployed annually, and 11 water quality sondes have been deployed at the intakes of water treatment plants in the western and central basin of Lake Erie (Fig. 1). The data from this network of water quality sondes is freely available online, and serves as an early warning system used by water treatment plant operators who adjust treatment according to cyanobacterial biomass at the intake, beach managers concerned with cHAB-driven beach closures, scientists researching cHABs, and interested members of the general public (Read et al. 2010).

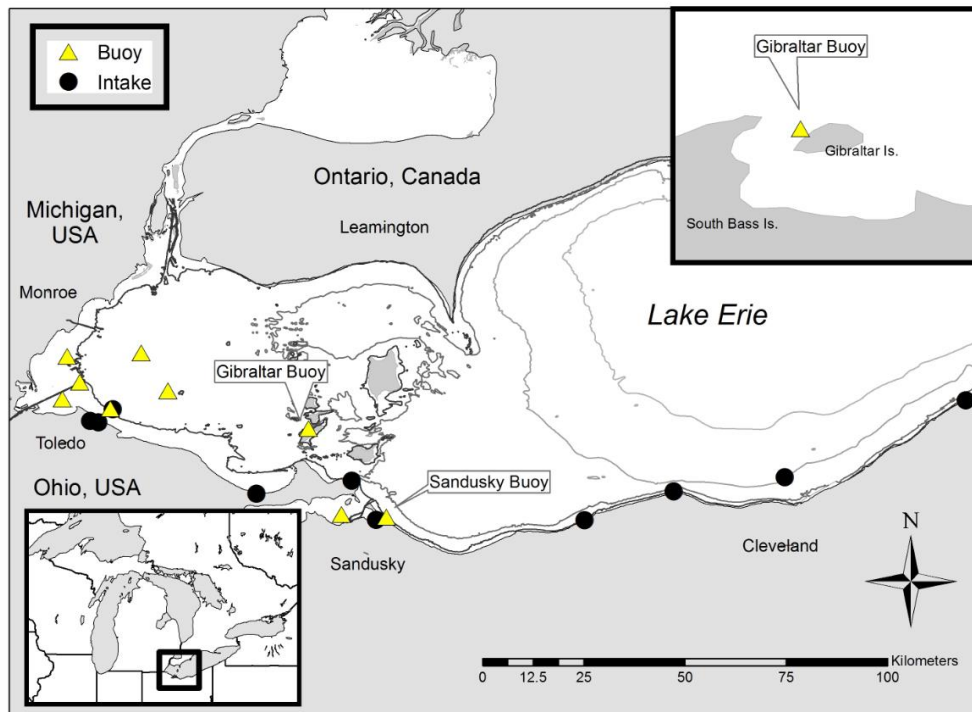


Figure 1. Locations of data buoys (yellow triangles) and water quality sondes mounted to fixed structures (black circles) in Lake Erie used to track cyanobacteria biomass in real time. The location of the two buoys used in this study are highlighted.

Water-quality sondes have sensors that detect and quantify total algae and cyanobacteria with fluorescence from chlorophyll *a* (*chl_a*) and phycocyanin (a pigment specific to cyanobacteria), respectively (Humbert and Törökné 2016). The users of the water quality sondes network interpret higher fluorescence values as increased *chl_a* and phycocyanin concentrations and therefore assume higher biomasses of total algae and cyanobacteria. However, there are several potential issues with long-term deployment of water quality sondes that measure cyanobacteria and total algae biomass by fluorescence. The first problem is the use of fluorescence to measure *chl_a* or phycocyanin concentration. Fluorescence is dependent on the alga’s physiological state because fluorescence per cell can increase under stressful conditions, such as low nutrient concentration and photo-inhibitory high light intensities (Campbell et al. 1998), which could lead to an underestimation or overestimation of cyanobacterial biomass. The second problem arises from the assumption that *chl_a* or phycocyanin concentration is proportional to algal or cyanobacterial biomass. Algae and cyanobacteria can alter their *chl_a* and

phycocyanin content (pigment mass per cell) in response to light conditions (MacIntyre et al. 2002). A long-term Lake Erie plankton study found a weak correlation between *chl a* concentration and phytoplankton biomass (Conroy et al. 2005). Another study discovered that Lake Erie *Microcystis* doubled its *chl a* content, and phycocyanin content increased 6 times, in response to low light conditions in the lake (Chaffin et al. 2012). Hence, data buoys are taking measurements of fluorescence without confirmation the sonde data with biomass data from water samples. A third potential issue is instrument drift. Whether water quality sondes are deployed year-around or seasonally (April-November) they are only calibrated a few times a year (< 5 times) due to the difficulties associated with removing and returning the sondes attached to deployed buoys. It is possible that the water quality sondes lose calibration throughout deployment and give inaccurate data. Finally, biofouling from algae and *Dreissena* mussels (Fig. 2) can reduce water exchange around water quality sondes. The densely packed mussels fouling sondes deployed over long-term intervals can result in inaccurate readings.

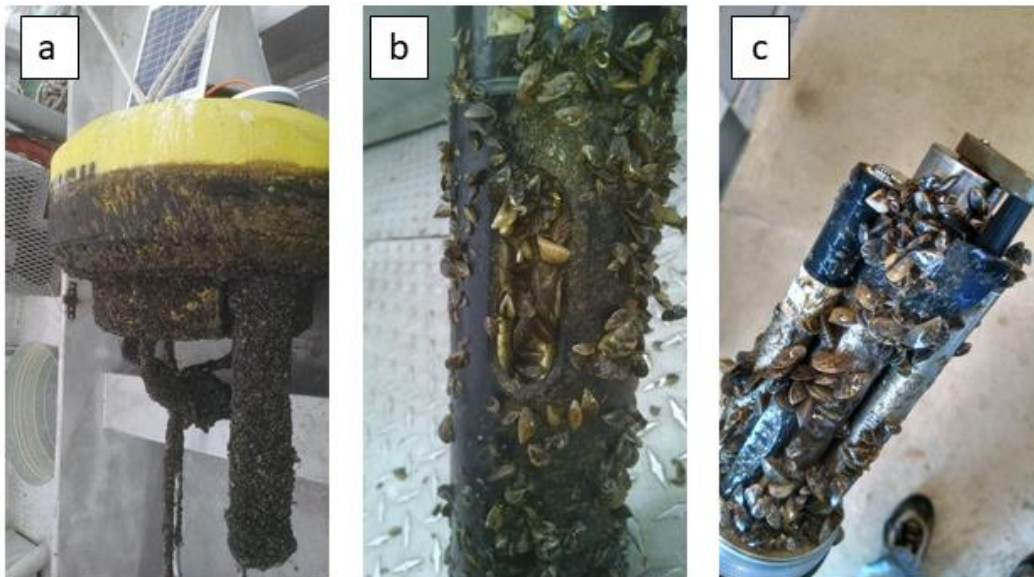


Figure 2. Images of biofouling by filamentous green algae and *Dreissena* mussels on the Sandusky buoy (a), on the YSI sonde (b), and on the YSI sensors (c).

The sensors attached to data buoys are located just below the surface of the water (~0.6 to 1 meter); however, water treatment plant intake pipes are near the bottom of the lake in water that is greater than 6 meters in depth. Thus, there is a potential disconnect between water quality data measured at the surface and water quality being drawn into the plant. Moreover, the different buoyancy regulation strategies of the various cyanobacteria in Lake Erie can further exacerbate that disconnect. For example, *Microcystis* is positively buoyant allowing it to accumulate near the surface in calm waters, whereas, *Planktothrix* is neutrally-to-negatively buoyant and will position itself in the center of the water column or sink to the bottom (Konopka et al., 1987; Reynolds et al., 1987). Thus, a data buoy may overestimate cyanobacteria abundance during a *Microcystis* bloom and underestimate cyanobacteria abundance during a *Planktothrix* bloom. This could result in a plant operator to over-treat (which wastes treatment chemicals and money) or under-treat (which could result in microcystins in tap water) the lake water. *Microcystis* and *Planktothrix* are known microcystins producers and bloom in waters that

serve as source water for several large Ohio shoreline cities such as Toledo and Sandusky, respectively.

Wind speed can also impact how water treatment plant operators interpret buoy data. The lake is calm during low wind weather allowing cyanobacteria to position themselves at desired light levels (i.e., *Microcystis* near the surface and *Planktothrix* lower in the water column). High wind speeds create turbulent mixing of the water column and overpower the buoyancy regulation of cyanobacteria resulting in cyanobacteria to be spread evenly from surface to lake bottom. A potential issue in water treatment can arise when a calm day is followed by a windy day. For example, a buoy measures high cyanobacteria biomass due to *Microcystis* at the surface one day, but then high winds the following day mix the bloom throughout the water column. The buoy data will show fewer cyanobacteria biomass, but the intake is actually drawing in more cyanobacteria biomass because the wind mixed the bloom throughout the water column and down to the intake pipe.

The objective of this study was to determine how well water quality sondes attached to buoys measure total algae and cyanobacterial biomass, and water turbidity. Additionally, because the sonde network in Lake Erie cannot measure MCYs, total MCYs concentrations were measured manually to determine potential correlations with sonde data. While several recent studies have found varying relationships between sonde algae data and biomass estimates (McQuaid et al. 2010; Zamyadi et al. 2012; Loisa et al. 2015; Bowling et al. 2016; Zamyadi et al. 2016; Hodges et al. 2017), none have investigated the utility of water quality sondes for tracking MCYs. Additionally, concentrations of dissolved reactive P, total P, nitrate, ammonium, and total N were measured to aid in interpretation of the relationships between sonde and water sample cyanobacterial biomass and MCY data. The final objective was to determine the vertical position of cyanobacteria throughout the water column in relation to buoy cyanobacteria data and wind speed data.

Methodology

Buoy location and sonde calibration

Two data buoys were used in this study. The Gibraltar buoy was deployed about 200 meters northwest of Gibraltar Island, and the Sandusky buoy was deployed 100 meters off the City of Sandusky lakeside municipal water intake (Fig. 1). The Gibraltar buoy was equipped with a YSI 6600v2 multiprobe sonde during 2015 and a YSI EXO2 sonde during 2016 and 2017. The Sandusky buoy had an EXO2 sonde all three years. The sondes were calibrated together with approximately 20 to 25 other sondes of the Lake Erie sonde network at the University of Toledo's Lake Erie Center to facilitate comparison across sondes. The EXO2 sondes were calibrated together for relative fluorescence units (RFU) for *chl a* and cyanobacteria-PC (surrogates for total algal and cyanobacterial biomass, respectively) with rhodamine dye and for nephelometric turbidity units (NTU) for water clarity (according to YSI instructions) with a YSI NTU standard, and deionized water was used for the 0.0 point. In 2015, the 6600v2 sonde was calibrated to *chl a* $\mu\text{g/L}$ and bluegreen algae cells/mL with rhodamine dye, which also calibrates RFU in the process. The Gibraltar sonde was calibrated and cleaned three times throughout deployment whereas the Sandusky sonde was not cleaned or calibrated until buoy retrieval due to difficulties accessing the sonde from a large vessel while deployed.

Because the Gibraltar buoy had two different sonde models, a laboratory comparison was conducted to determine a PC RFU conversion factor. A rhodamine dye standard was created following the EXOs instruction manual, and RFUs of that standard were recorded using EXO2 and 6600v2 sondes. The standard was diluted by 50% and RFU were recorded for both sondes. This process was repeated 10 times by diluting the standard by 50% each step (0.19% concentration of original standard). This experiment was repeated twice with two different EXO2 and 6600v2 sondes. The 6600v2 RFU values were converted to EXO2 RFU data because all sondes in the Lake Erie sonde network use EXO2 sondes.

Water sample collection

The Gibraltar buoy was visited several times a week by small boats (< 4 meters) to collect samples adjacent to the buoy manually. A total of 56, 81, and 54 samples were collected next to the Gibraltar buoy (May through October) in 2015, 2016, and 2017, respectively. The Sandusky buoy was sampled six and nine times during summers 2015 and 2016, respectively, aboard the RV Erie Monitor; the vessel anchored within 20 meters of the buoy. To determine the relationship between buoy sonde data and water sample data, a 0-2 meter intergraded tube sampler was used to collect surface water. The 0-2 meter sample represents the ‘average’ conditions experienced by the buoys’ sonde as the buoy bobs up and down with waves (the sonde is between 0.7 and 1.0 meters depth). Clean samplers and sample bottles were triple rinsed with surface water before collection. Water from the sampler was dispensed into a clean 5-gallon bucket and then poured into 1) 2-L dark bottle for *chl_a*, PC, total suspended solids (TSS) concentrations, and algal group-specific *chl_a*, 2) 500-mL glass jar and preserved with Lugol’s solution for analysis of phytoplankton identification and quantification, 3) 40-mL amber glass vial for total microcystins concentration, and 4) two separate 250-mL acid washed polycarbonate bottles for analysis of TP and TN. About 50 mL of lake water was filtered upon collection using a 0.45µm polycarbonate membrane syringe filter and stored in a 60-mL bottle for analysis of dissolved reactive P, nitrate, nitrite, and ammonium. An ice chest was used to store samples during transportation back to the laboratory, which was 5 minutes for the Gibraltar buoy and 1.5 hours for the Sandusky buoy. Secchi disk depth was also measured.

On a subset of dates (n = 36), water samples were collected at every meter throughout the water column to determine vertical phytoplankton position. Water was collected with a Van Dorn bottle and poured into 250-mL polycarbonate bottles. Water was analyzed for algal group-specific *chl_a* concentration.

Water sample analysis methods

Total *chl_a* analysis began by filtering 0.25-1.0 L (depending on the density of phytoplankton and suspended solids) onto GF/F filters (47 mm diameter, 0.7 µm pore size), which were then stored on silica gel at -80°C until analysis. Chlorophyll *a* was extracted with dimethyl sulfoxide and quantified with spectrophotometry (Golnick et al. 2016). Algal group-specific *chl_a* was determined within 10 minutes of returning to the laboratory using a FluoroProbe benchtop reader (Chaffin et al. 2013). The FluoroProbe is a fluorometric device that uses *chl_a* and accessory pigment fluorescence to partition total *chl_a* among four functional phytoplankton groups (green algae, cyanobacteria, diatoms, and cryptophytes; (Beutler et al. 2002)). Because the FluoroProbe can underestimate algal biomass (Gregor and Marsálek 2004),

algal group-specific *chl a* concentration was corrected for on each sample date by dividing the algal group-specific *chl a* concentration by the FluoroProbe total *chl a* concentration and then multiplying by the *chl a* concentration determined by DMSO extraction (Bridgeman et al. 2012).

Plankton and solids were filtered (0.25-1.0 L depending on density) onto pre-combusted and weighed GF/F filters (47 mm diameter, 0.7 μm pore size) for analysis of total suspended solids (TSS). Filters with plankton and solids were dried at 103°C overnight and reweighed to determine TSS.

Phytoplankton was quantified with automated imaging flow cytometry (FlowCAM) under 40x, 100x, and 200x magnification on auto-image mode. FlowCAM is a fluid imaging device that was created for the study of phytoplankton that captures images of particles (i.e., plankton) as they flow through the objective lens carried in a medium (i.e., lake water) (Poulton 2016). FlowCAM has been shown to provide results similar to traditional phytoplankton counts (light microscopy with the Utermohl method) (Álvarez et al., 2014). FlowCAM software has a semi-automated image recognition system to aid the user in the sorting of phytoplankton based on 31 recorded parameters for each particle, including length, diameter, and area which were used for calculating biomass (Fluid Imaging Technologies INC. 2011). Sample runs were terminated after 8000 images were captured; the volume analyzed and length of image collection was dependent on the density of particles. Images were first classified using the Auto-Classification function of the Visual Spreadsheet (version 4.0.27) and then manually checked to sort unclassified or incorrectly -classified phytoplankton. Cyanobacteria were identified according to Rosen and St. Amand (2015). Areal measurements were converted to biovolume by assuming a sphere for single cells, a cylinder for filamentous cyanobacteria, and by multiplying by the average cell diameter for colonial cyanobacteria.

Total MCYs were determined after 3 freeze/thaw cycles, filtered with a glass microfiber filter (GMF, 0.45 μm) to remove cellular debris, and quantified using a microcystin/nodularin specific enzyme-linked immunosorbent assay (ELISA) (Abraxis #520011, (Fischer et al. 2001)). When needed, samples were diluted to bring the MCY concentration within the ELISA working range of less than 5 $\mu\text{g/L}$.

Concentrations of nitrate, nitrite, ammonium, and dissolved reactive P were quantified with a SEAL Analytical QuAAatro continuous segmented flow analyzer (SEAL Analytical Inc., Mequon, WI) using standard U.S. EPA methods (EPA 353.1, 354.1, 350.1, and 365.1, respectively). Total P and total Kjeldhal N (TKN) were determined on unfiltered water following digestion and quantified on the SEAL analyzer following standard methods (EPA 365.3, 351.2, respectively). Total N was calculated as the sum of TKN, nitrate, and nitrite, and the TN to TP ratio was calculated by dividing TN by TP.

Buoy data analysis

The buoys recorded data every 15 minutes, which was automatically transmitted to WQDataLive, a website platform (wqdatalive.com). Water sample data were compared to the buoy data on 4 time scales: 1) the single data point closest to the time that the water sample was collected, 2) the average of five buoy data points one hour prior to water sample collection (for example, if water sample was collected at 11:00 the buoy measurements at 10:00, 10:15, 10:30, 10:45, and 11:00 were averaged), 3) averaged for 4 hours prior to water sample, and 4) the daily average (00:00 – 23:45) of the day of sample. Analysis of covariance test (ANCOVA) for homogeneous slopes was conducted to determine if slopes between buoy data (the covariate) and

water sample data (the dependent data) differed among the 3 years (the factors). Then, when ANCOVA indicated non-parallel slopes among years, linear regression was used to determine the relationships between buoy and water sample data separately for each year. IBM SPSS Statistics v23 were used for all data analysis.

Every-meter phytoplankton and wind data analysis

Because the every-meter cyanobacteria biomass data was determined with a FluoroProbe and the data buoy measured cyanobacteria biomass as RFU, buoy RFU data was converted to cyanobacteria-chla with the relationship found below (Table 1). This data analysis was only conducted on data collected next to the Gibraltar buoy because no relationship was found between buoy RFU and cyanobacteria biomass at the Sandusky buoy. Next, the percent relative difference (%RD) between the buoy-converted data and every-meter cyanobacteria biomass data was calculated as:

$$\%RD = (Chla_{@z} - Chla_{buoy}) / Chla_{buoy} \times 100\%$$

Where $Chla_{@z}$ is the cyanobacteria chla concentration measured at depth z (0, 1, 2, 3, 4, or 5 meters) and $Chla_{buoy}$ is the cyanobacteria chla concentration that was converted from the buoy cyanobacteria RFU data. The %RD will always for comparisons between low and high biomass data.

Wind speed data were obtained from NOAA's National Buoy Data Center (http://www.ndbc.noaa.gov/station_page.php?station=sbio1) using South Bass Island site for Gibraltar buoy. We initially proposed to use the buoy's weather station wind data for this project, but we had to find alternate wind data source due to malfunctions to both buoys' weather stations during summer 2016. The average wind speed 1 h, 4 h, 8 h, 12 h, and 24 h before sample collection were calculated. The %RD between buoy and cyanobacteria chla at each depth was plotted against wind speed for each time frame investigated.

Principal Findings and Results

Sonde RFU comparison

In the sonde comparison study, there was a significant linear relationship between PC RFUs values of diluted calibration standards measured by the YSI 6600v2 and EXOv2 sondes ($P < 0.001$, $R^2 = 0.986$); however, the 6600v2 sondes RFU values were 8.3 times greater than that measured by the EXOv2 sondes. There was no difference in slopes for the 2 separate experiment trials with different sondes. Therefore, the conversion factor for converting 6600v2 PC RFU (used in 2015) values to EXOv2 PC RFU (used in 2016 and 2017) values was 0.1204.

Temporal patterns

Cyanobacterial biomass measured by the Gibraltar buoy peaked at 10 cyanobacteria-PC RFUs in late July 2015 and RFUs were between 0.5 and 3.0 during August and September 2015 (Fig. 3a). Cyanobacteria-PC RFUs throughout the entire 2016 season and during May through early September 2017 were between 0.0 to 0.3 RFUs, suggesting lower cyanobacterial biomass

than 2015. Cyanobacteria-PC RFUs increased in September and October 2017 peaking at 1.0 RFUs. Water sample cyanobacteria-*chl**a* followed a similar temporal pattern as buoy cyanobacteria-PC RFU measurements with greatest concentrations in late July 2015 (> 30 µg/L), low concentrations (< 5 µg/L) throughout 2016, and a late summer peak in 2017 (10.5 µg/L). Cyanobacterial biomass measured at the Sandusky buoy was more variable and reached greater PC RFUs than the Gibraltar buoy (Fig. 3b). Cyanobacteria-*chl**a* in the water samples did not follow the temporal pattern of the Sandusky buoy PC RFUs.

Total MCY concentrations followed similar patterns as Gibraltar buoy cyanobacteria-PC RFUs and water sample cyanobacterial biomass (Fig. 3a). Highest MCY concentrations (5.9 µg/L) occurred during the largest peak of cyanobacteria during late-July 2015. Lower total MCY concentrations occurred in 2016 and 2017.

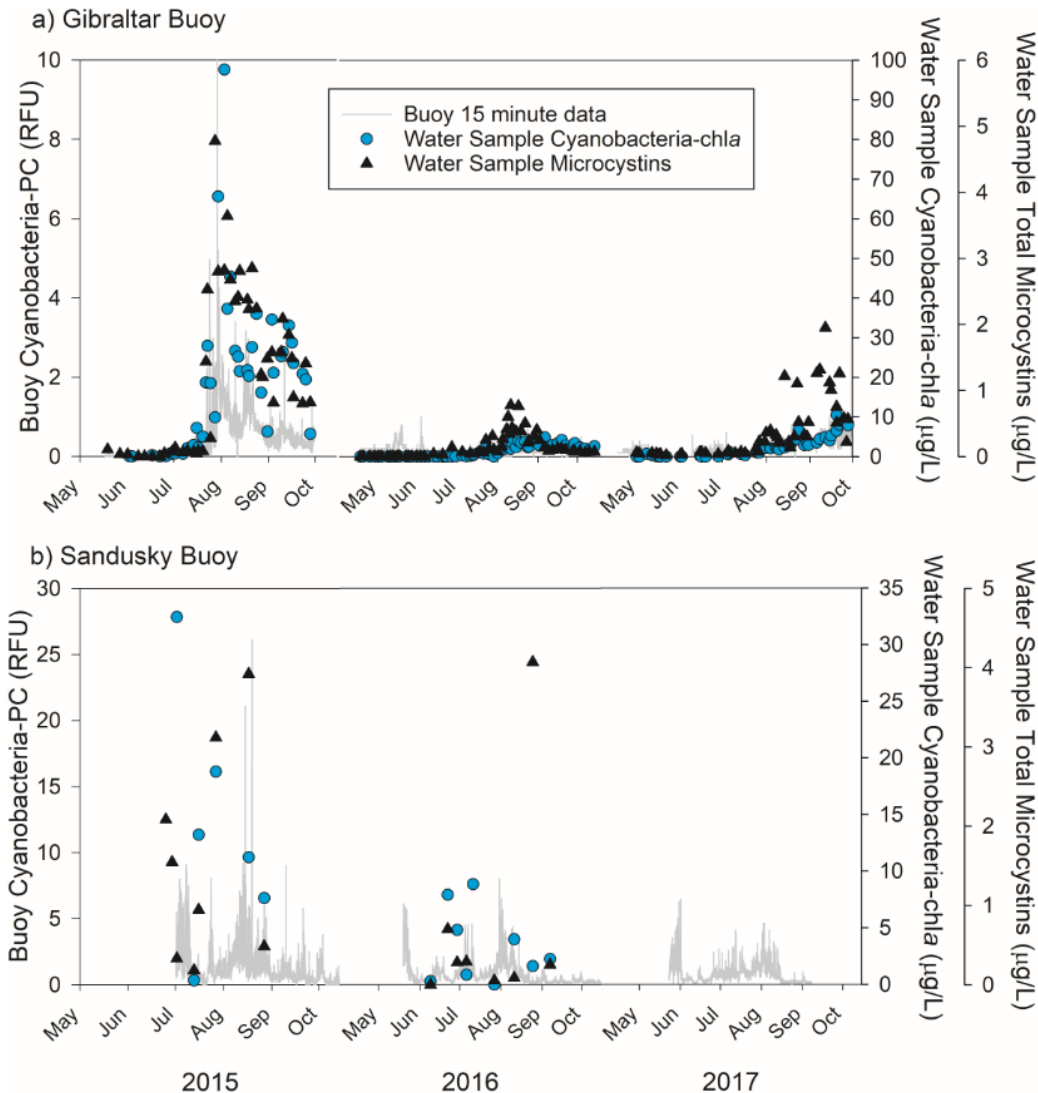


Figure 4. Total phytoplankton abundance at the Gibraltar (A) and Sandusky (B) data buoys during summer 2015, 2016, and 2017 estimated by total chlorophyll *a* sensors (relative fluorescence units; gray lines), and total chlorophyll *a* (green dots) measured in water samples collected next to the data buoys.

In 2015 chlorophyll RFUs followed a similar pattern as cyanobacteria RFUs, except for a minor peak associated with a diatom bloom in late June (Fig. 4a). Chlorophyll RFUs peaked at 9.5 during 2015. Two peaks occurred in each of 2016 and 2017 of similar RFUs values. Diatoms were dominant during the June peaks, whereas cyanobacteria were dominant during the August peaks. Water sample *chl a* concentration followed the pattern of the buoy RFUs measurements with greatest concentrations in late July 2015 ($> 50 \mu\text{g/L}$) and the bimodal peaks in 2016 and 2017 had concentrations around $20 \mu\text{g/L}$. Chlorophyll RFUs measured at the Sandusky buoy was more variable throughout the summers with several peaks per year that reached greater RFUs than the Gibraltar buoy (Fig. 4b). Chlorophyll concentrations in the water samples did not track with buoy RFUs.

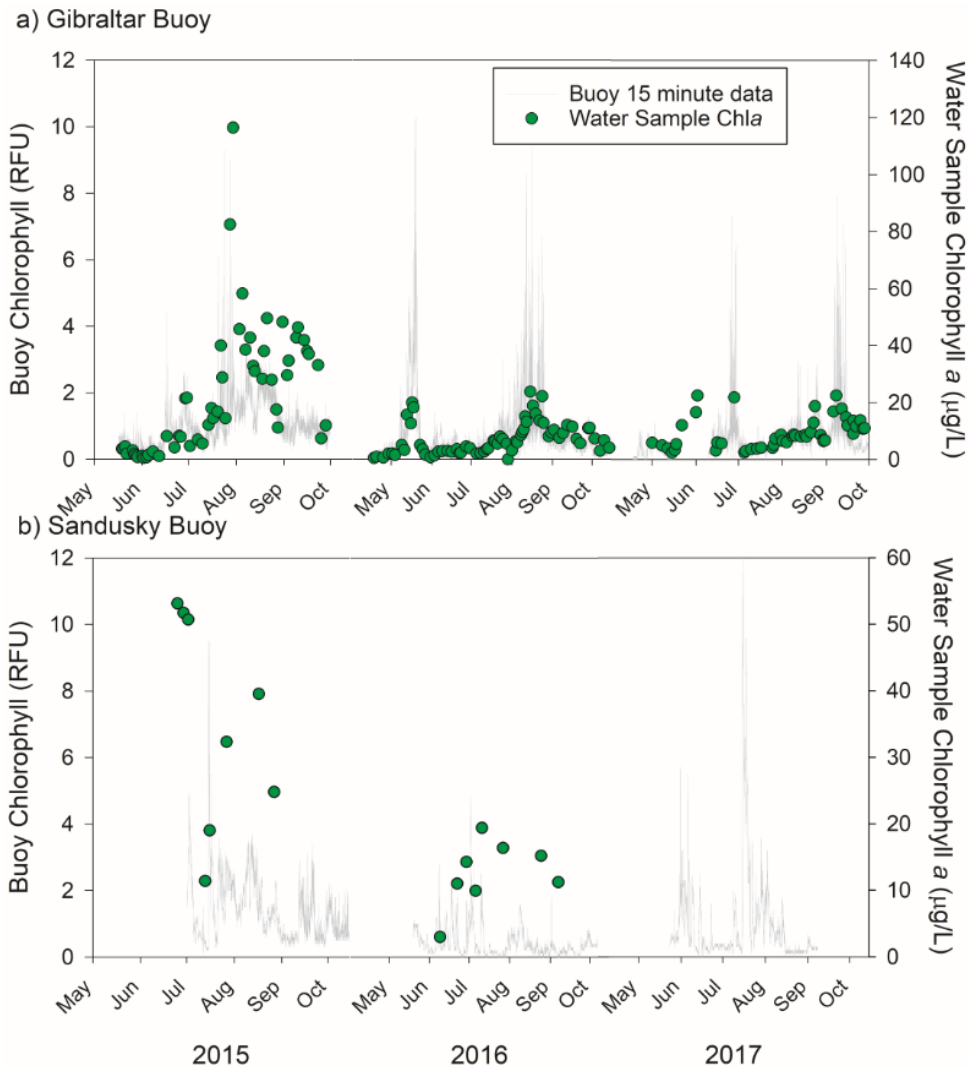


Figure 4. Total phytoplankton abundance at the Gibraltar (A) and Sandusky (B) data buoys during summer 2015, 2016, and 2017 estimated by total chlorophyll *a* sensors (relative fluorescence units; gray lines), and total chlorophyll *a* (green dots) measured in water samples collected next to the data buoys.

Water clarity (NTUs) measured at the Gibraltar buoy during 2015 followed a similar pattern as cyanobacterial biomass peaking 336.8 on July 25, but there were a few minor peaks in May and June (Fig. 5a). NTUs measured in 2016 and 2017 were much lower than 2015, with a

few smaller peaks detected early and late summers. Water sample TSS temporal pattern aligned with buoy NTU each summer. At the Sandusky buoy, extremely high NTUs (>1000 NTUs) were recorded each summer after mid-August (Fig. 5b); however, these high values could be the result of fouling on the water quality sondes (Fig. 2). Before mid-August, higher NTUs were measured during 2015 than 2016 and 2017.

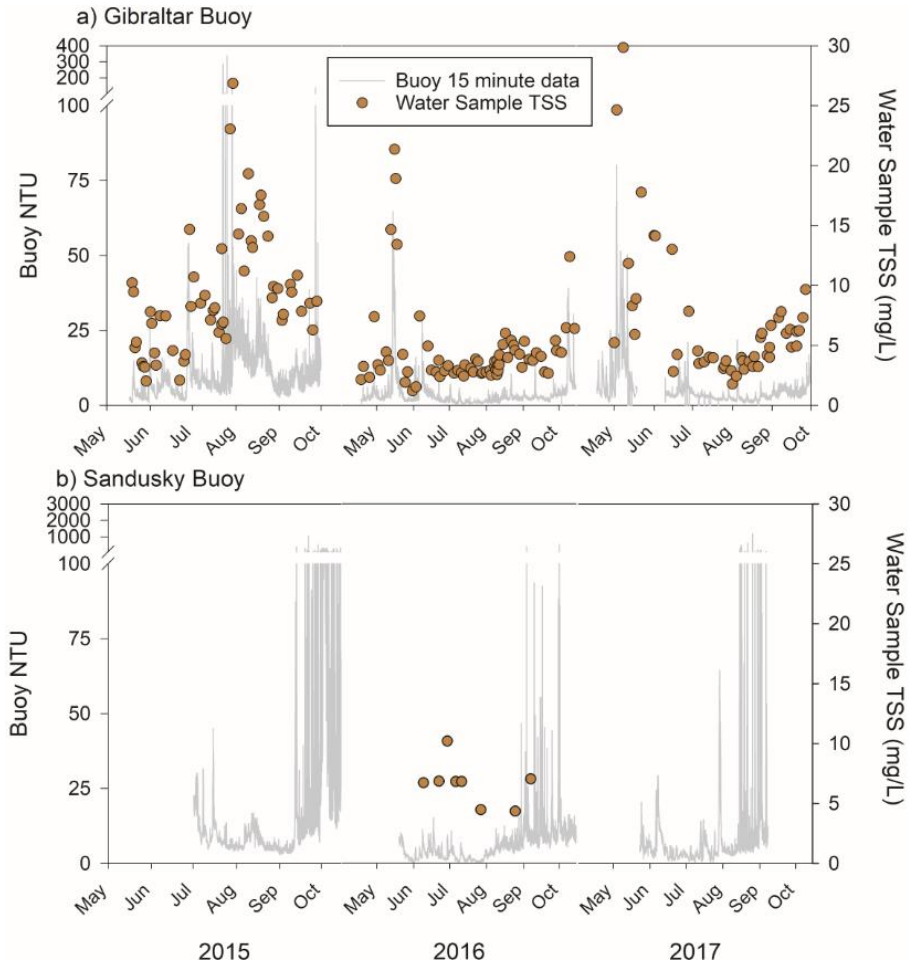


Figure 5. Turbidity (nephelometric turbidity units; gray line) at the Gibraltar (A) and Sandusky (B) data buoys during summer 2015, 2016, and 2017, and total suspended solids (brown dots) measured in water samples collected next to the data buoys.

Correlations between buoy and water samples

For Gibraltar buoy data, an ANCOVA test for homogeneous slopes found significant interactions ($P < 0.05$), among year, buoy data (the covariate) and water sample data (the dependent variable) indicating that regression trends were different each year, and this was true for all 4 time frames investigated and all buoy-water sample data pairs (Table 1). In general, the 1-hour time frame had the most robust relationship (highest R^2 value) for all years and parameters, and Figure 6 displays the relationships between 1-hour averaged buoy data and water sample data.

Table 1. Linear regression statistics between water sample data collected next to the Gibraltar buoy data and the buoy data over 4 time frames. All coefficients were significantly different among years as indicated by failed ANCOVA test for homogeneity each year. Asterisks indicate P values of the regression: * $P < 0.1$; ** $P < 0.01$; *** $P < 0.001$. Bold and italics indicate the best relationship between buoy and water sample data.

Cyanobacteria: Buoy PC RFU vs Water Sample Cyanobacteria-Chl <i>a</i> ($\mu\text{g/L}$)						
	2015 YSI 6600v2		2016 YSI EXO2		2017 YSI EXO2	
Time Frame	Slope	R ²	Slope	R ²	Slope	R ²
Time of Sample	24.549***	0.796	NS	0.000	13.911***	0.729
1 hour prior	27.796***	0.850	NS	0.018	14.142***	0.752
4 hour prior	25.984***	0.828	NS	0.042	15.407***	0.698
Daily Average	28.973***	0.771	NS	0.091	14.912***	0.736
Cyanobacteria: Buoy PC RFU vs Water Sample Cyanobacteria Biovolume ($\mu\text{m}^3/\text{mL}$)						
	2015 YSI 6600v2		2016 YSI EXO2		2017 YSI EXO2	
Time Frame	Slope	R ²	Slope	R ²	Slope	R ²
Time of Sample	3,358,438***	0.843	NS	0.001	2,794,873*	0.440
1 hour prior	3,293,269***	0.850	NS	0.028	2,414,589*	0.377
4 hour prior	2,840,735***	0.816	NS	0.066	NS	0.342
Daily Average	3,657,880***	0.807	NS	0.069	NS	0.318
Total Algae: Buoy Chl RFU vs Water Sample Chl <i>a</i> ($\mu\text{g/L}$)						
	2015 YSI 6600v2		2016 YSI EXO2		2017 YSI EXO2	
Time Frame	Slope	R ²	Slope	R ²	Slope	R ²
Time of Sample	24.072***	0.523	3.999***	0.365	11.640***	0.630
1 hour prior	24.555***	0.516	4.210***	0.396	10.182***	0.674
4 hour prior	27.125***	0.537	3.801***	0.363	11.451***	0.660
Daily Average	27.675***	0.518	5.096***	0.496	10.805***	0.666
Water Clarity: Buoy NTU vs Water Sample TSS (mg/L)						
	2015 YSI 6600v2		2016 YSI EXO2		2017 YSI EXO2	
Time Frame	Slope	R ²	Slope	R ²	Slope	R ²
Time of Sample	0.659***	0.738	1.078***	0.870	0.994***	0.822
1 hour prior	0.703***	0.802	0.938***	0.896	0.949***	0.830
4 hour prior	0.693***	0.788	0.969***	0.829	0.888***	0.845
Daily Average	0.720***	0.752	0.964***	0.799	0.962***	0.792

Significant ($P < 0.001$) and highly correlated ($R^2 > 0.80$) linear relationships occurred between buoy cyanobacteria-PC RFUs and water samples cyanobacterial-chl a (Fig. 6a) and cyanobacterial biovolume (Fig. 6b) for all 4 time frames during 2015 and 2017 as separate datasets (Table 1), but 2016 was not significant (likely due to very little cyanobacteria in 2016). The coefficient for the PC RFU cyanobacteria-chl a relationship in 2015 (27.796 $\mu\text{g chl}a/\text{L}$ per PC RFU) was nearly twice that of 2017 (14.142 $\mu\text{g chl}a/\text{L}$ per PC RFU). Whereas the coefficients for PC RFU-cyanobacterial biovolume were less different among years (2015: 3,293,269 $\mu\text{m}^3/\text{mL}$ per PC RFU; 2017: 2,794,873 $\mu\text{m}^3/\text{mL}$ per PC RFU).

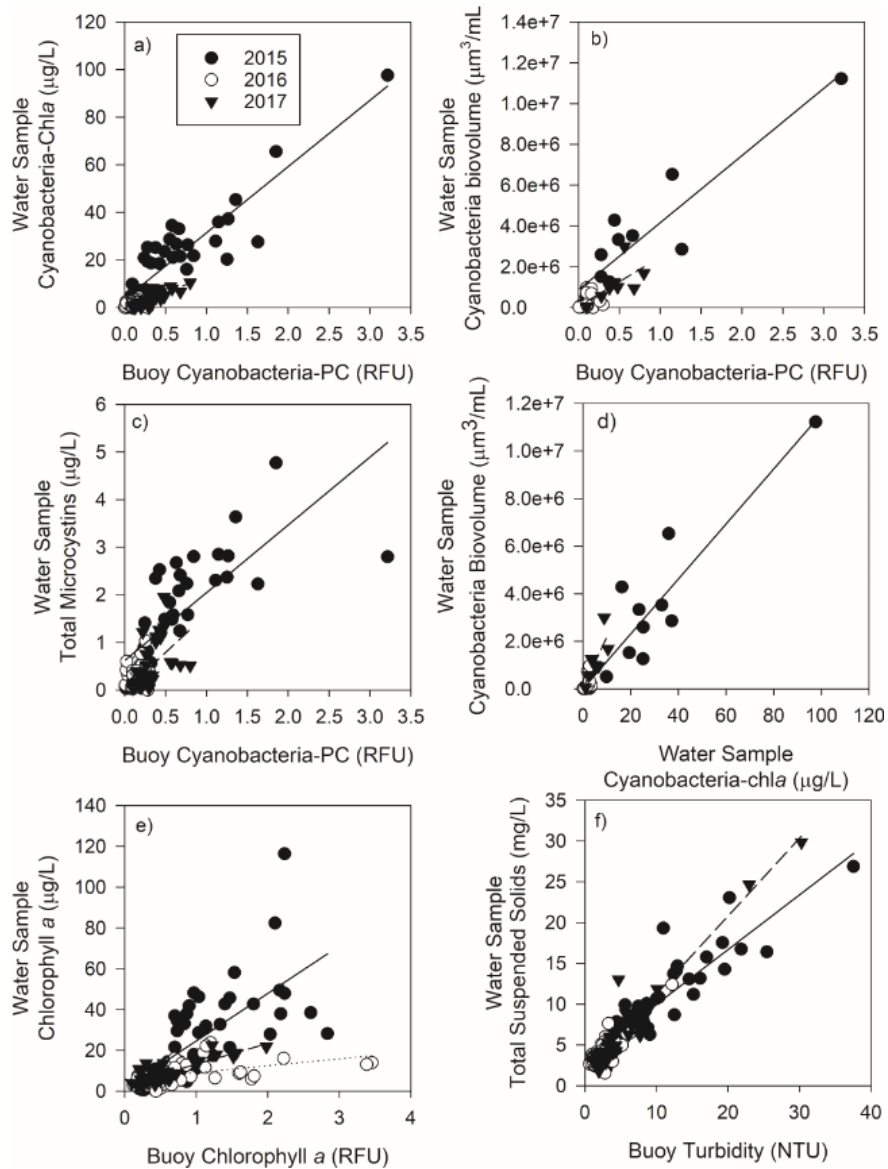


Figure 6. Linear relationships at the Gibraltar buoy between buoy data (averaged 1 hour prior to water sample collection) and water sample data. Linear regression lines: 2015 = solid; 2016 = dotted; 2017 = dashed. The 2016 regression line is often covered by other data points. Linear regression statistics are provided in Tables 1 and 2.

Significant ($P < 0.001$) linear relationships occurred between buoy cyanobacteria-PC RFU and water sample total MCY concentrations during years 2015 and 2017, but not 2016 (Fig. 6c). The relationships between buoy PC RFU and MCY concentration were weaker (2015 $R^2 = 0.593$; 2017 $R^2 = 0.354$) than the buoy PC RFU and cyanobacterial biomass estimate metrics.

Cyanobacterial-chla and biovolume correlated significantly (Table 2; Fig. 6d) and ANCOVA indicated that there was no interaction between data and years. This result suggests that FlouroProbe measured cyanobacterial-chla was an appropriate surrogate for cyanobacterial biovolume.

Table 2. Linear regression statistics between FluoroProbe cyanobacteria-chlorophyll *a* concentration ($\mu\text{g/L}$) and total cyanobacterial biovolume ($\mu\text{m}^3/\text{mL}$). ANCOVA indicated that there was no significant difference among slopes each year.

ANCOVA test for homogeneity of regression slopes		P = 0.579 Slopes homogenous
All years	Slope	112,478.420
	P value; R ²	<0.001; 0.863
2015	Slope	115,666.527
	P value; R ²	<0.001; 0.840
2016	Slope	212,087.958
	P value; R ²	0.024; 0.357
2017	Slope	215,913.477
	P value; R ²	0.020; 0.622

Significant ($P < 0.001$), but less correlated (R^2 between 0.27 and 0.67) relationships occurred between buoy *chl a* RFU and water sample total *chl a* concentration (Table 1; Fig. 6e). However, as indicated by ANCOVA test for homogeneity, the coefficients were highly different among years ranging from 5.096 $\mu\text{g chl a/L}$ per RFU to 27.125 $\mu\text{g chl a/L}$ per RFU. Additionally, the strongest relationship for each year occurred in different time frames.

Significant ($P < 0.001$) and highly correlated ($R^2 > 0.80$) linear relationships occurred between buoy NTUs and water samples TSS for all 4 time frames during all years of study (Table 1; Fig. 6f). The coefficient in 2015 was 0.703 mg TSS/L per NTU and the coefficients for 2016 and 2017 were nearly identical at 0.938 and 0.949 mg TSS/L per NTU, respectively.

For the Sandusky buoy, ANCOVA found no interactions among year, buoy data, and water sample data (Table 3). The cyanobacterial biomass relationships were only significant for the pooled dataset across all years; however, but the highest the R^2 was only 0.36, indicating a weak relationship. The total *chl a* relationship was significant across all years and for 2015 separately (but the all-year relationship was driven by 2015). There was no significant relationship between buoy NTU and water sample TSS at the Sandusky buoy.

Table 3. Linear regression statistics between water sample data collected next to the Sandusky buoy data and the buoy data over 4 time frames. All years included all data pooled together, and ANCOVA indicated there was no significant interaction between year and data suggesting trends were similar each year. Asterisks indicate P values of the regression: * $P < 0.1$; ** $P < 0.01$; *** $P < 0.001$. Bold and italics indicate the best relationship between buoy and water sample data.

Cyanobacteria: Buoy PC RFU vs Water Sample Cyanobacteria-Chl ($\mu\text{g/L}$)						
Time Frame	All years		2015 YSI 6600v2		2016 YSI EXO2	
	Slope	P value; R^2	Slope	P value; R^2	Slope	P value; R^2
Time of Sample	7.358	0.025; 0.331	NS	0.532; 0.104	NS	0.362; 0.119
1 hour prior	7.839	0.032; 0.307	NS	0.445; 0.152	NS	0.677; 0.026
4 hour prior	6.985	0.061; 0.245	NS	0.456; 0.145	NS	0.870; 0.004
Daily Average	9.408	0.021; 0.348	NS	0.158; 0.429	NS	0.883; 0.003
Total Algae: Buoy Chl RFU vs Water Sample Chl <i>a</i> ($\mu\text{g/L}$)						
Time Frame	All years		2015 YSI 6600v2		2016 YSI EXO2	
	Slope	P value; R^2	Slope	P value; R^2	Slope	P value; R^2
Time of Sample	10.316	<0.001; 0.812	10.488	0.012; 0.812	NS	0.894; 0.004
1 hour prior	10.441	<0.001; 0.762	10.638	0.023; 0.765	NS	0.531; 0.083
4 hour prior	9.945	<0.001; 0.674	10.490	0.051; 0.650	NS	0.389; 0.151
Daily Average	8.648	0.002; 0.608	7.386	0.187; 0.388	NS	0.761; 0.020
Water Clarity: Buoy NTU vs Water Sample TSS (mg/L)						
Time Frame	All years		2015 YSI 6600v2		2016 YSI EXO2	
	Slope	P value; R^2	Slope	P value; R^2	Slope	P value; R^2
Time of Sample					NS	0.209; 0.358
1 hour prior	TSS data only in 2016		TSS data only in 2016		NS	0.218; 0.347
4 hour prior					NS	0.237; 0.325
Daily Average					NS	0.702; 0.040

Nitrogen and Microcystins:chl_a ratio

Nitrate concentrations at Gibraltar buoy decreased throughout summer each year (Fig. 7), although the maximum concentration measured in 2015 was approximately 100 $\mu\text{mol/L}$ greater than maximum levels measured in 2016 and 2017. Nitrate concentration declined to levels less than 10 $\mu\text{mol/L}$ by mid-August every year, but in 2017 nitrate concentrations increased to 20 $\mu\text{mol/L}$ by early September and then decreased to low levels throughout September (Fig. 7c).

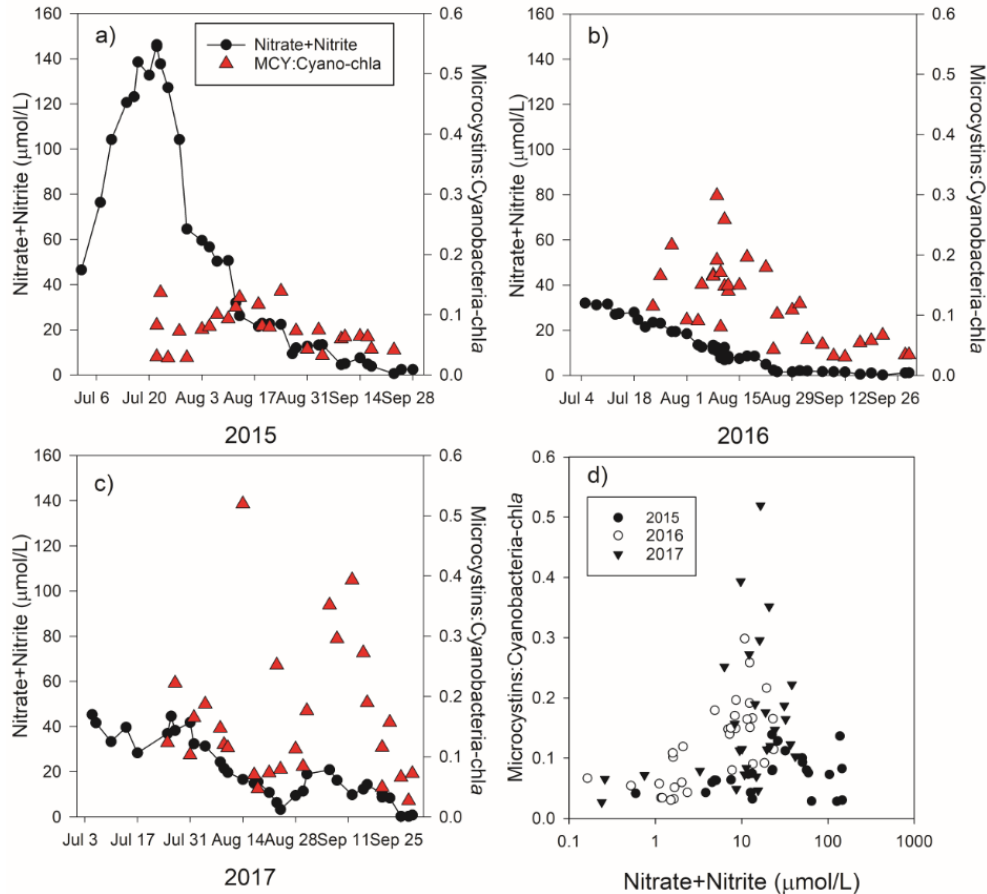


Figure 7. The relationship between nitrate concentration and the ratio of microcystins to cyanobacteria-chla displayed as seasonal patterns for summers 2015 (a), 2016 (b), and 2017 (c), and as a scatter plot (d). Note that highest microcystins to cyanobacteria-chla occurred at intermediate nitrate concentrations and decreased with decreased nitrate concentrations.

The MCY per cyanobacteria-chla ratio (MCY:chla) was calculated to indicate the toxin production per cyanobacteria biomass. During 2015, MCY:chla was less than 0.14 throughout the entire summer and ratio values decreased to less than 0.07 after September 1 (Fig. 7a). During 2016, MCY:chla ranged from 0.08 to 0.30 during July and August, and then decreased to values less than 0.06 in September (Fig. 7b). During July and mid-August of 2017 the MCY:chla was highly variable but, in general, decreased to values less than 0.08 by the end of August (Fig. 7c), and then MCY:chla increased from 0.08 to highest values of 0.39 by mid-September and then again decreased throughout the second half of September. The decreases in MCY:chla were associated with decreases in nitrate concentration in all 3 years, and the lowest MCY:chla values occurred when nitrate concentration was less than 10 $\mu\text{mol/L}$ (Fig. 7d). A similar pattern was observed between MCY:chla and total nitrogen concentration and the ratio of total nitrogen to total phosphorus, but not total phosphorus, dissolved reactive phosphorus, and ammonium-nitrogen concentrations (not shown).

Every-meter phytoplankton data

Buoy measured cyanobacteria RFU and the converted RFU-to-cyanobacteria *chl a* concentrations are displayed in Fig. 8. Highest biomasses of cyanobacteria during late July through September 2015.

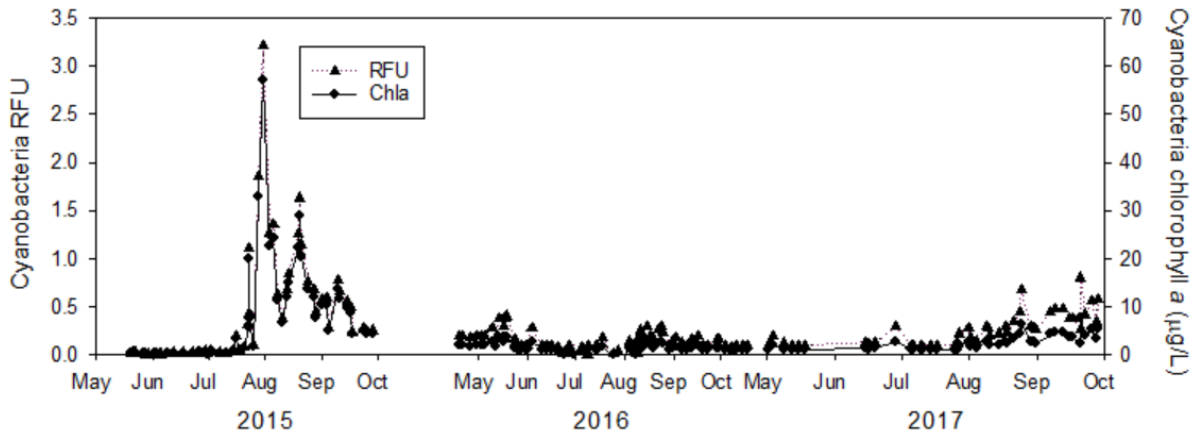


Figure 8. Cyanobacteria abundance at the Gibraltar buoy during summers 2015 as phycocyanin relative fluorescence units (RFU) and RFU converted to cyanobacteria chlorophyll a concentration.

The every meter sampling indicated that cyanobacteria were not evenly distributed throughout the water column on some dates but were evenly distributed on other dates (Fig. 9). For example, on July 28, 2015, cyanobacteria *chl a* concentration peaked at 71.5 µg/L at 0 m and declined throughout the water column to 10.5 µg/L at 5 m. An example of cyanobacteria evenly distributed throughout the water column occurred on August 7, 2015, when *chl a* concentration ranged from 11.2 to 13.8 µg/L. Much lower cyanobacteria *chl a* concentrations were recorded in 2016 and 2017.

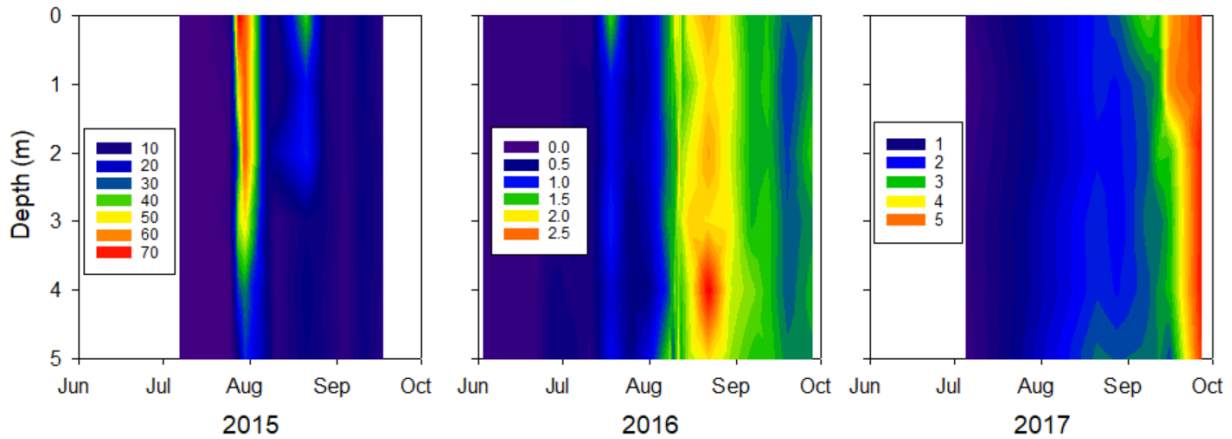


Figure 9. Isopleths of cyanobacteria chlorophyll a concentration measured at every meter from the surface to 5 meters throughout summers 2015, 2016, and 2017. Note the difference in color scale among the three years.

A comparison of buoy RFU converted-cyanobacteria *chl a* to cyanobacteria *chl a* measured throughout the water column showed that there were occurrences when the buoy both under and overestimated the cyanobacteria *chl a* at specific depths (Fig. 10). Data points that lay above the 1 to 1 line (dotted line) indicate the buoy underestimated cyanobacteria *chl a* concentration at the particular depth, whereas those beneath the 1 to 1 line indicate the buoy overestimated

cyanobacteria *chl a* concentration. For example, on July 28, 2015, the buoy estimated the cyanobacteria *chl a* concentration to be 32.9 $\mu\text{g/L}$, but the 0 m and 1 m cyanobacteria *chl a* concentrations exceeded the buoy estimate (71.5 and 51.2 $\mu\text{g/L}$, respectively), whereas the 5 m cyanobacteria *chl a* concentration was much less than the buoy (10.5 $\mu\text{g/L}$). Overall, the buoy tended to underestimate cyanobacteria *chl a* concentrations at 0 m while overestimating the deeper cyanobacteria *chl a* concentrations.

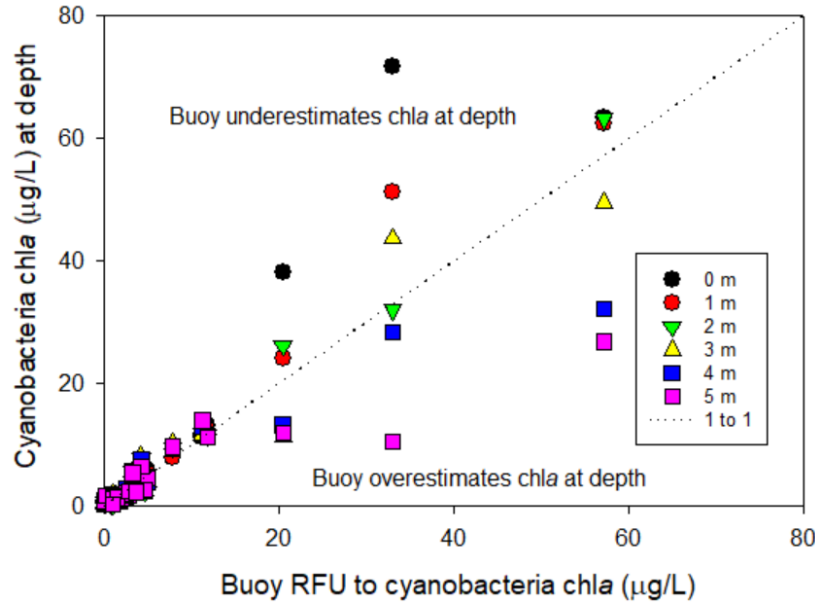


Figure 10. The relationship between buoy measured cyanobacteria chlorophyll a concentration and cyanobacteria chlorophyll a concentration throughout the water column. Data points that lay above the 1 to 1 line (dotted line) indicate the buoy underestimated chl a concentration, whereas those beneath the 1 to 1 line indicate the buoy overestimated chl a concentration.

Wind speed data was used to determine if the differences observed between cyanobacteria *chl a* concentrations measured by the buoy and measured at depth could be explained (Fig. 11). The percent relative difference (%RD) between cyanobacteria *chl a* concentration measured by the data buoy and throughout the water column showed how much cyanobacteria biomass at depth differed from the buoy measurement. The greatest range of wind speed occurred 1 hour before sampling (0.85 to 10.25 m/s) and the wind speed range decreased with longer time frames. There was high %RD across the range of the 1-hour window before sample collection (Fig. 11a), which indicates that cyanobacteria position in the water column was not affected by wind over a short time span. As longer time frames were considered, the %RD decreased with increased wind speed.

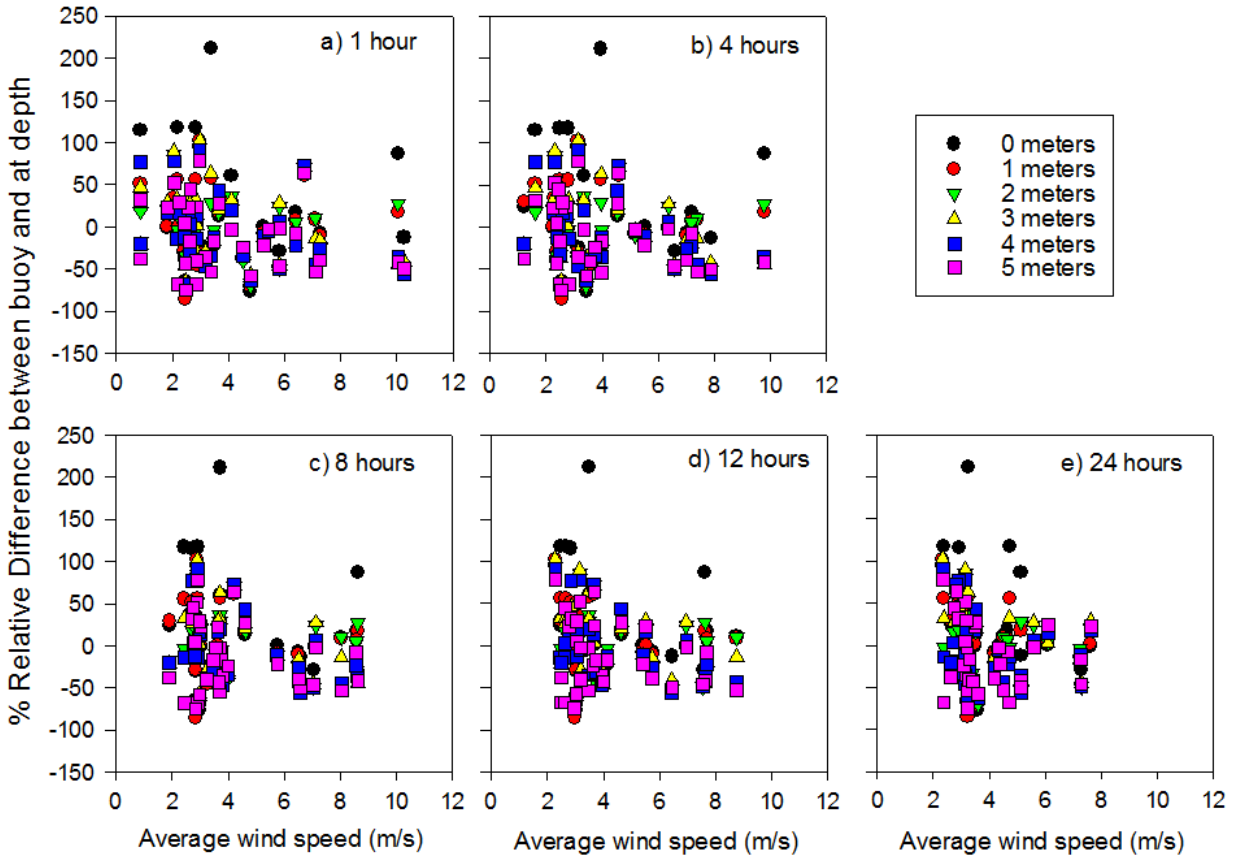


Figure 11. The percent relative difference (%RD) between cyanobacteria *chl a* concentration measured by the data buoy and throughout the water column as a function of wind speed.

Because the %RD decreased with increased wind speed, the average %RD for each depth at wind speeds less than and greater than 4.5 m/s were calculated (Table 4). There was a greater difference in %RD between low and high wind speeds near the surface and less difference in %RD between the wind speeds deeper in the water column. For example, 12 hours before sample, buoy and *chl a* at 0 meter were 52.9% different at low wind speeds and only 18.1% at high wind speeds, whereas, at 5 meters, the differences were 38.9% and 31.2% for low and high winds, respectively. Additionally, surface *chl a* deviated more from the buoy than bottom *chl a* in low vs. high winds, but high winds resulted in the surface *chl a* to be more similar to buoy than bottom *chl a*. The smallest difference (16.8%) between buoy and water sample occurred at the 1 meter depth during high wind speeds when the buoy data 12 hours before sample collection was average.

Table 4. The average of the absolute value of percent relative differences between cyanobacteria chl_a concentration measured by the data buoy and throughout the water column as a function of wind speed less than 4.5 m/s and greater than 4.51 m/s and as time before sample collection.

	1 hour		4 hours		8 hours		12 hours		24 hours	
	<4.5m/s	>4.5m/s	<4.5m/s	>4.5m/s	<4.5m/s	>4.5m/s	<4.5m/s	>4.5m/s	<4.5m/s	>4.5m/s
0 Meter	49.8%	29.4%	52.1%	22.9%	50.7%	20.0%	52.9%	18.1%	47.7%	30.0%
1 Meter	35.6%	27.0%	38.1%	21.3%	37.7%	18.6%	39.3%	16.8%	37.6%	20.7%
2 Meter	29.2%	32.9%	32.1%	27.4%	32.8%	24.5%	33.3%	24.2%	35.1%	20.1%
3 Meter	36.9%	32.2%	38.5%	28.7%	38.4%	26.7%	38.8%	27.0%	38.6%	27.5%
4 Meter	33.9%	35.4%	34.8%	33.7%	35.1%	32.5%	35.9%	31.0%	37.7%	27.0%
5 Meter	37.9%	34.2%	38.6%	32.4%	38.2%	32.2%	38.9%	31.2%	38.0%	33.2%
Overall	37.2%	31.8%	39.0%	27.7%	38.8%	25.8%	39.8%	24.7%	39.1%	26.4%

Microcystins throughout the water column

Total microcystins were measured at every meter on two dates during the 2015 bloom (Fig. 12). On both dates, microcystin concentrations at depth as 0 m, 1 m, and 2 m were 4 to 6 times greater than microcystins at deeper depths. The higher concentrations of microcystins at the surface corresponded to greater biovolumes of cyanobacteria, especially *Microcystis*, near the surface (Fig. 13).

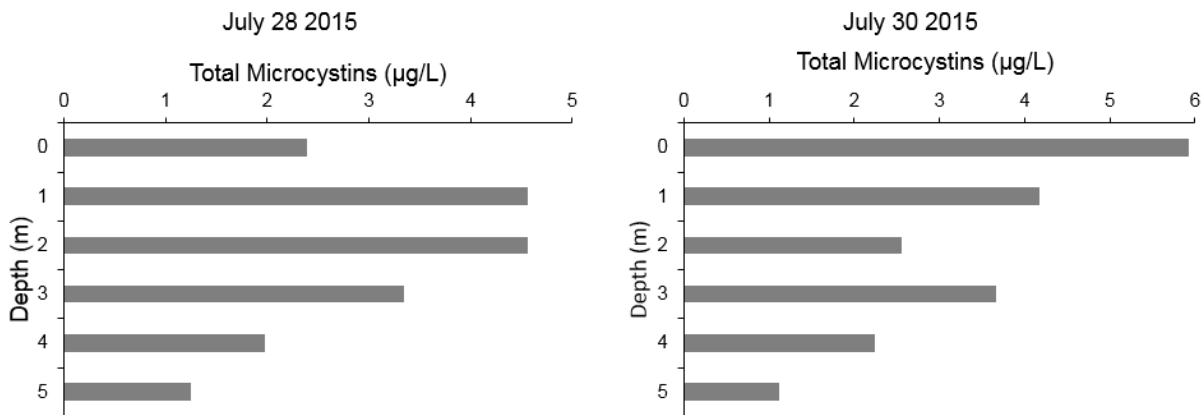


Figure 12. Total microcystin concentrations throughout the water column on two dates in July 2015 at the Gibraltar Island data buoy.

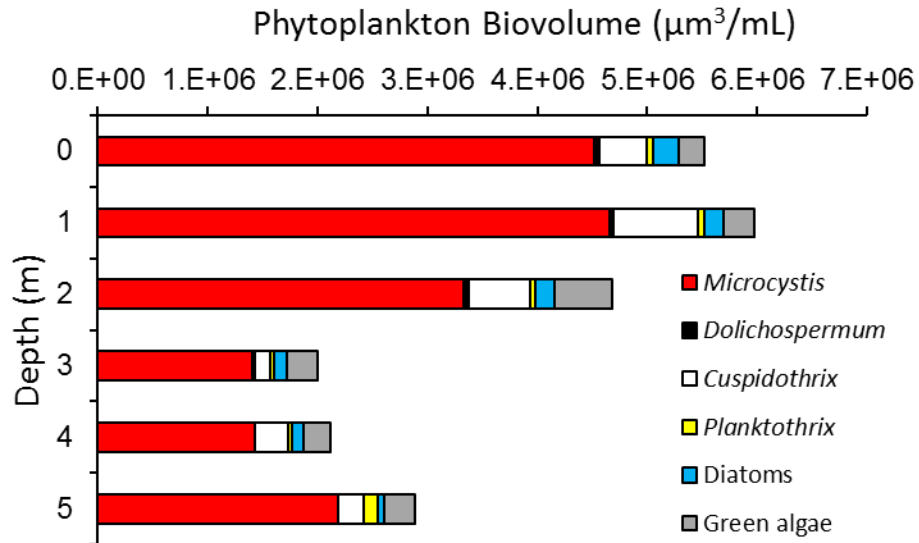


Figure 13. Phytoplankton biovolume measured throughout the water column on July 30, 2015, at the Gibraltar Island data buoy.

Total microcystins were measured weekly from the depth of 5 m throughout summer 2016 (Fig. 14). Microcystins at 5 m followed a similar temporal pattern as surface (0-2 m intergraded sample) microcystin concentration with both depths peaking in mid-August. However, there were 3 occurrences when microcystin concentrations differed between surface and 5 m depth. On August 11, 2016, surface microcystins were $1.03 \mu\text{g/L}$ whereas the 5 m concentration was $0.30 \mu\text{g/L}$. The opposite pattern was observed on August 12 and 15, 2016, as 5 m microcystin concentration exceeded the surface concentrations by nearly a factor of 3.

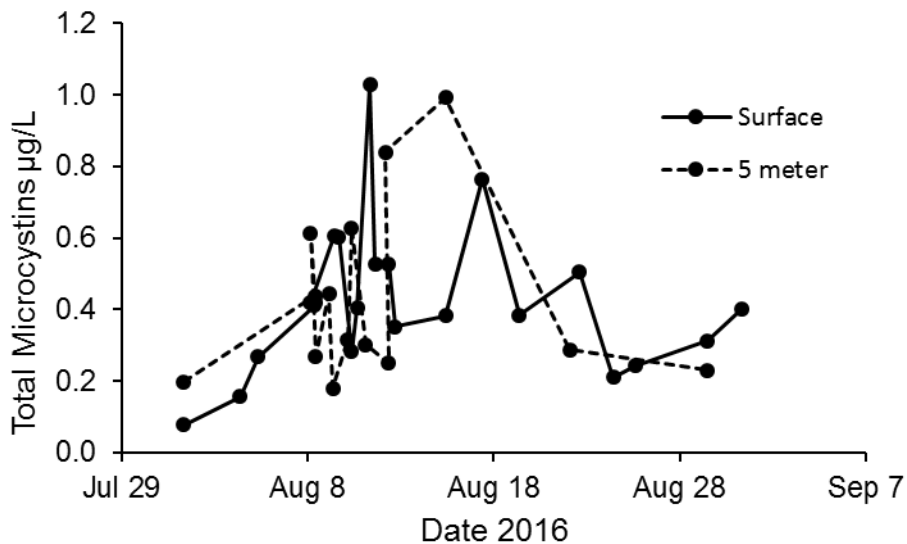


Figure 14. Total microcystin concentrations at the surface (0-2 m intergraded sample) and at 5 meters depth measured throughout summer 2016 at the Gibraltar data buoy.

Finding Significance

Buoys as surrogates for water samples

Since the August 2014 “do not drink” advisory in Toledo, Ohio many data buoys and sondes attached to permanent structures have been deployed in western Lake Erie to serve as an early warning system for potentially toxic cHABs. Cyanobacterial biomass and MCY concentration followed a very similar temporal pattern as buoy cyanobacteria phycocyanin RFUs, suggesting the buoys can serve as an early warning system for cHABs. However, buoy data should only be interpreted as relative biomass data because the trends between buoy and water sample data differed among the 3 years. For example, if a water treatment plant operator noticed increased cyanobacteria RFUs at the intake, it would be safe to assume that more cyanobacteria were entering the water system and treatment should be adjusted to remove higher levels of potentially toxic cyanobacteria. On the other hand, a researcher who wished to use buoy data to calibrate a cHABs-model would first need the exact relationship between buoy data and water sample data. Although, that researcher could compare the temporal trends of model output to *in situ* buoy data.

Buoy *chl a* and cyanobacteria data on the 15-minute time scale was very irregular, which could have led to flawed interpretations. For example, during this study cyanobacteria PC at the Gibraltar buoy ranged from 0.07 to 4.97 RFU and had an average of 1.19 RFU. These large spikes in RFU data were likely due to large *Microcystis* colonies drifting past the sonde as it was recording a measurement (Hodges et al. 2017). Viewing the single most recent value could be misleading, users should consider several data points to get a better interpretation of actual biomass. Indeed, buoy data averaged over a 1-hour before water sample collection had a better correlation with water sample data than the buoy data at the time of sample collection. Furthermore, data over the past 24 hour or several days should be considered to determine trends in potentially toxic cyanobacteria.

This research highlighted two main flaws of *in situ* buoy data. First, data from different buoys may not be directly comparable. There were positive linear relationships found between buoy data and water sample data for the Gibraltar buoy for every parameter tested, but those same correlations did not occur at the Sandusky buoy. This difference could have been due to the lack of service or cleaning of the Sandusky buoy (Fig. 2), which would have minimized water exchange across the water quality sondes and affected results. Alternatively, the difference may have been because of the different cyanobacteria communities at the two buoys (Bowling et al. 2016). *Microcystis* was the only dominant cyanobacteria at the Gibraltar buoy, but a more diverse cyanobacteria community was present at the Sandusky buoy. For example, *Planktothrix*, a filamentous bloom-forming cyanobacterium associated with shallow, light limited waters (Kurmayer et al. 2016), was often found at the Sandusky buoy due to outflow from Sandusky Bay (Conroy et al. 2017). Additionally, in late summer (Aug-Oct) *Microcystis* was found at Sandusky buoy due to the easterly spread of the western basin *Microcystis* bloom (Chaffin et al. 2014b). It is plausible that these two cyanobacteria have different fluorescence properties that result in different RFU readings. The second flaw was year-to-year differences. All three parameters investigated showed significantly different coefficients over the studied years. User error during standard preparation or calibration is a potential source of year-to-year variation that cannot be ruled out, but environmental variables may also be a factor. Cyanobacterial colony morphometry can have significant impacts on the relationship between fluorescence values and

biovolume. Similarly, (Hodges et al. 2017) showed there was a stronger linear relationship between *Microcystis* single cells and fluorescence than colonial *Microcystis* forms. Indeed, single cells of *Microcystis* made up more than 50% of the total cyanobacterial biovolume throughout summer 2015, which had tighter correlations between fluorescence and cyanobacteria biovolume (Table 1). Turbidity was high in 2015, and because algae can alter pigment content per cell with light climate (MacIntyre et al. 2002; Chaffin et al. 2012), cyanobacteria in 2015 could have had more PC and *chl a* per cell than cyanobacteria in 2016 and 2017. Nutrient status of algae can also impact fluorescence (Beardall et al. 2001), and nutrient concentrations during 2015 were much higher than 2016 and 2017. Additionally, variations in the content of PC and *chl a* per cell due to growth phase (Chang et al. 2012) and the presence of extracellular PC (Bastien et al. 2011) can also lead to inaccuracies between sonde data and cyanobacterial biomass estimates (Zamyadi et al. 2016). While calibration of the sondes of the Lake Erie sonde network occurs together (Fig. 1), the data from each sonde may not be directly comparable across time and space.

Turbidity is a commonly measured parameter as an indicator of water quality. Turbidity is primarily associated with phytoplankton biomass and suspended solids (sediments from tributary loading or resuspension from the lake bottom), but high concentrations of colored dissolved organic matter can also impact turbidity (Wetzel 2001). Buoy measured turbidity, and water sample TSS were highly correlated, and the trends were similar but significantly different, among years (Table 1).

Microcystins correlations

Cyanobacterial blooms are troublesome due to their potential to produce high concentrations of the toxin MCYs. Many lake managers and water treatment facilities have opted to use real-time water quality sondes that estimate cyanobacterial biomass; however, the water quality sondes cannot directly measure MCYs. Therefore, users interpreting sonde data are left to assume that MCYs and cyanobacterial abundance are proportional; conversely, cyanobacterial biomass and MCYs concentrations often do not correlate in the environment (Dyble et al. 2008; Millie et al. 2009; Wang et al. 2009; Rinta-Kanto et al. 2009). Additionally, the MCY to cyanobacteria-*chl a* ratio decreased throughout summer and differed year-to-year (2015 had lower MCY:cyanobacteria-*chl a* than 2016 and 2017; Fig. 7), which indicates that amount of MCY produced per unit cyanobacterial biomass was not constant. Nonetheless, within each bloom season, peaks in buoy cyanobacteria-PC RFU were often associated with an increase MCY concentrations, but the magnitude of the MCY peak was not scalable with the RFU peak.

Microcystin production by cyanobacteria has been linked to N availability by numerous studies (Orr and Jones 1998; Long et al. 2001; Horst et al. 2014; Gobler et al. 2016). Nitrate concentrations at the Gibraltar buoy decreased to low levels throughout each year of the study (Fig. 7), which is a temporal pattern that has been documented in other years in the western basin of Lake Erie (Chaffin et al. 2013; Gobler et al. 2016). The MCY to cyanobacteria-*chl a* ratio pattern followed nitrate concentrations and only low MCY:cyanobacteria-*chl a* ratios occurred at low nitrate concentrations (Fig. 7d). Additionally, during late August 2017 nitrate concentrations increased by 20 $\mu\text{mol/L}$ and there was a corresponding increase in the MCY:cyanobacteria-*chl a* ratio (Fig. 7c). Furthermore, nitrate enrichments to late summer bloom water under experimental conditions resulted in increased toxin production (Chaffin et al. in review; Harke and Gobler

2015; Harke et al. 2016a). Taken together, previous studies and the results presented agree that low N availability constrains cyanobacterial bloom toxicity.

Water quality sonde networks have been deployed in Lake Erie and elsewhere to track potentially toxic cyanobacterial blooms, with the goal of protecting the public from cyanobacterial toxins (Jochens et al. 2010). As discussed above, several factors interfere with relationships between PC RFU data and cyanobacterial abundance, and there is no sound correlation between cyanobacteria biomass and toxin concentration. Therefore, due to the multiple layers of uncertainty, sonde PC RFU data should not be used as a direct estimate of MCY concentration. Although, nitrate concentration data or a general understanding of the temporal patterns of nitrate concentrations at a given site can improve the decision-making process. For example, it is known that the highest nitrate concentrations occur in Lake Erie during early summer and decrease to low levels by the end of August (Chaffin et al. 2013), and therefore, spikes of PC RFU during early summer should be considered to be highly toxic whereas peaks of PC RFU later in the season could be assumed to be less toxic. Following that logic, a water treatment plant operator should use higher treatment doses (such as more activated carbon) per PC RFU during early summer blooms to potentially remove more cyanobacterial toxins per PC RFU than late summer blooms. Nevertheless, these guidelines should be used only as a tool, and not a replacement for sample testing where decisions with enormous ramifications (such as drinking water safety) are concerned and need to be confirmed by sample testing.

Water column cyanobacteria and relation to buoy data

Cyanobacteria can migrate throughout the water column and often concentration near the surface of the water (Reynolds et al. 1987; Ganf et al. 1989; Brookes et al. 2003). The vertical migration of cyanobacteria can be problematic for data buoys with water quality sondes fixed at one depth. Indeed, the *chl_a* concentration measured at a depth of 1 meter by the data buoy often did not match the *chl_a* concentration measured at the surface (above the sonde) or below the sonde at deeper depths (Fig. 10). Therefore, interpretation of a data buoy's *chl_a* data that is recorded from a fixed depth cannot be assumed to be equal to the concentration above or below the sonde.

Wind speed can affect phytoplankton position in the water column. In light winds and calm water, buoyant cyanobacteria will concentrate near the surface (Hutchinson and Webster 1994; Soranno 1997), whereas, negatively buoyant phytoplankton, such as diatoms, will sink towards the lake bottom (Webster and Hutchinson 1994; Huisman et al. 2002). In high winds and rough waters, the buoyancy of cyanobacteria and the sinking rate of diatoms is over-powered by the water turbulence, and the phytoplankton will be evenly distributed throughout the water column (Huisman et al. 2002; Brookes et al. 2003). There were more considerable differences between cyanobacteria *chl_a* measured by the buoy at depth during low wind speeds and the relative difference decreased as wind speed before sampling increased (Fig. 11, Table 4). This indicates that the cyanobacteria became more-mixed throughout the water column and that the buoy estimates of cyanobacteria biomass were more extractable to other depths.

The period over which wind speed was averaged affected how to interpret the relationship between buoy and at-depth measurements of cyanobacteria *chl_a*. In the 1-hour before sampling period, large relative differences between the buoy and at depth occurred at high wind speeds (Fig. 11a), which likely indicates high winds started just recently before sampling and there was not enough time to mix the water column. The decreases in relative difference

between buoy and *chl a* at depth became apparent when 12 and 24 hours of wind speed data were averaged (Fig. 11d and e), and indicates that cyanobacteria vertical position was more affected by long-term (12+ hours) than short-term (< 1 hour) wind speeds.

The relationship between buoy and surface (0 m) cyanobacteria *chl a* was different from the relationship between the buoy and deep *chl a* (5 m). Under calm winds, surface and buoy *chl a* differed by 52.9%, which indicated that buoyant cyanobacteria migrated above the buoy's water quality sonde (0.6-1.0 m in depth). Buoy data would have misled data users by the presence of noticeable scum at the surface. Contrary to low winds, the smallest difference between the buoy data and *chl a* at the surface and 1 m (18.1% and 16.8%, respectively) was recorded under high winds. This indicated that surface buoy measurements are most accurate at high wind speeds because water turbulence inhibited surface scum formation. However, the difference between the buoy data and *chl a* at the 5 m was not affected by wind speed (31.2% at low wind speeds and 38.9% at high wind speeds). Therefore, there is going to be an error associated with interpretation surface buoy data and cyanobacteria biomass at deeper depths. For example, a water treatment plant operator cannot assume surface buoy biomass data is proportional to biomass being drawn into the plant from deeper depths, and the difference cannot be corrected for by wind speed.

Conclusions

Significant correlations occurred between buoy data and water sample data for cyanobacterial biomass, total algae, and turbidity; however, the trends differed between buoys and among years. Further, relative trends in the data over time and space can be gleaned, but these methodologies do not replace laboratory methods for estimation of actual phytoplankton biomass. In spite of that, cyanobacterial biomass and MCY concentration data from water samples collected next to the Gibraltar buoy followed a similar temporal pattern as the buoy cyanobacteria-PC RFU data, which indicates their usefulness as a guidance tool for sectors like water treatment and beach management. Additionally, the inclusion of nitrate concentration data can lead to more robust predictions on the relative toxicity of blooms. Low wind speeds over the previous 12 hours (< 4.5 m/s) led to an underestimation of cyanobacteria biomass at the surface, whereas high wind speeds (> 4.5 m/s) resulted in more accurate measurements. However, cyanobacteria biomass estimates 5 meters below the surface were between 31% to 39% different from the buoy estimate and were not improved when wind speed was considered. Overall, deployed buoys and water quality sondes that are routinely cleaned and calibrated can efficiently track relative cyanobacteria abundance and can be used as an early warning system for potentially toxic blooms.

A flow chart was created to help interpretation of data buoys better cyanobacteria biomass and extrapolate the buoy data to other water depths. Additionally, the relative risk of microcystins was also included. The flow chart is specific to systems dominated by *Microcystis*. The first division was based on nitrate concentration because highest ratios of microcystin concentration to cyanobacteria-*chl a* corresponded to nitrate concentrations greater than 7 $\mu\text{mol/L}$ (0.1 mg $\text{NO}_3\text{-N/L}$, Fig. 7), and phytoplankton growth is considered N-limited at nitrate concentrations less than 7 $\mu\text{mol/L}$ (Chaffin et al. 2014a). Nitrate concentrations higher than 7 $\mu\text{mol/L}$ are to be associated with a higher risk of microcystins, but additional factors could limit microcystin concentration, such as low light levels (Chaffin et al. 2018). Summer 2015 had high nitrate concentrations (Fig. 7) but low water clarity and low microcystin concentrations relative

to the high *Microcystis* biomass. The second division on the flow chart is wind speed and the division is 4.5 m/s (10 miles per hour) averaged over the previous 12 hours. The final division is depth of concern (surface or at depth). At calm wind speeds, *Microcystis* will float above the buoy sensors resulting in an underestimation at the surface, but high wind speeds will mix the water column and result in biomass estimates that are within 20% of the actual surface measurements. Wind speeds did not impact the relationship between buoy and cyanobacteria *chl a* data at depth, and therefore, the users must be aware that there will be an error of 30% to 40% when relying on surface buoy as an estimate of cyanobacteria biomass near the lake bottom, for example, a water intake.

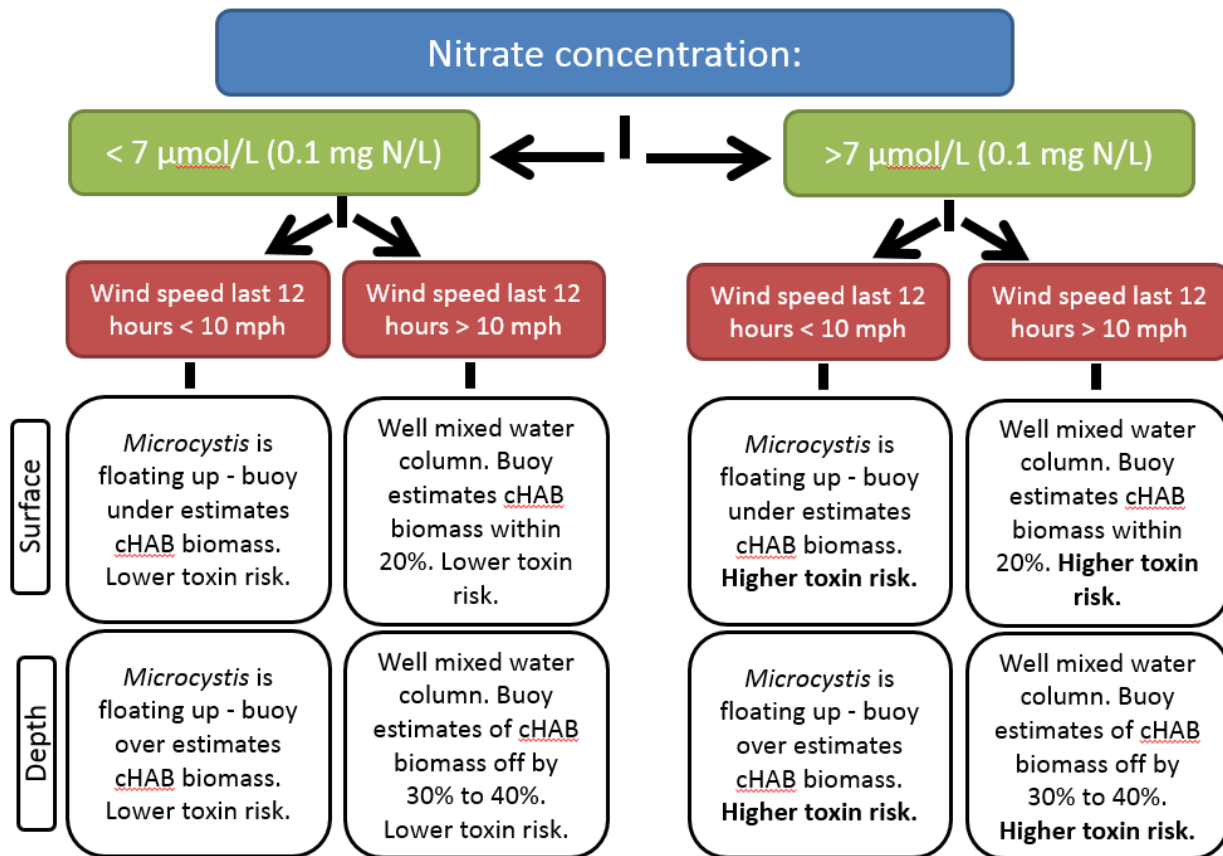


Figure 15. A flow chart for better interpretation of cyanobacteria biomass data measured by surface buoys in a *Microcystis*-dominated system based on nitrate concentration and wind speed.

References

- Backer LC, Landsberg JH, Miller M, et al (2013) Canine cyanotoxin poisonings in the United States (1920s-2012): Review of Suspected and Confirmed Cases from Three Data Sources. *Toxins* 5:1597–1628. doi: 10.3390/toxins5091597
- Bastien C, Cardin R, Veilleux É, et al (2011) Performance evaluation of phycocyanin probes for the monitoring of cyanobacteria. *J Environ Monit* 13:110–118. doi: 10.1039/C0EM00366B
- Beardall J, Young E, Roberts S (2001) Approaches for determining phytoplankton nutrient limitation. *Aquat Sci* 63:44–69

- Beutler M, Wiltshire KH, Meyer B, et al (2002) A fluorometric method for the differentiation of algal populations in vivo and in situ. *Photosynth Res* 72:39–53
- Bingham M, Sinha S, Lupi F (2015) Economic Benefits of Reducing Harmful Algal Blooms in Lake Erie. Environmental Consulting & Technology, Inc., Environmental Consulting & Technology, Inc.
- Bowling LC, Zamyadi A, Henderson RK (2016) Assessment of in situ fluorometry to measure cyanobacterial presence in water bodies with diverse cyanobacterial populations. *Water Res* 105:22–33. doi: 10.1016/j.watres.2016.08.051
- Bridgeman TB, Chaffin JD, Kane DD, et al (2012) From River to Lake: Phosphorus partitioning and algal community compositional changes in western Lake Erie. *J Gt Lakes Res* 38:90–97
- Brookes JD, Regel RH, Ganf GG (2003) Changes in the photo-chemistry of *Microcystis aeruginosa* in response to light and mixing. *New Phytol* 158:151–164
- Bullerjahn GS, McKay RM, Davis TW, et al (2016) Global solutions to regional problems: collecting global expertise to address the problem of harmful cyanobacterial blooms. A Lake Erie case study. *Harmful Algae* 54:223–238. doi: 10.1016/j.hal.2016.01.003
- Campbell D, Hurry V, Clarke AK, et al (1998) Chlorophyll fluorescence analysis of cyanobacterial photosynthesis and acclimation. *Microbiol Mol Biol Rev* 62:667–683
- Chaffin JD, Bridgeman TB, Bade DL (2013) Nitrogen Constrains the Growth of Late Summer Cyanobacterial Blooms in Lake Erie. *Adv Microbiol* 03:16–26. doi: 10.4236/aim.2013.36A003
- Chaffin JD, Bridgeman TB, Bade DL, Mobilian CN (2014a) Summer phytoplankton nutrient limitation in Maumee Bay of Lake Erie during high-flow and low-flow years. *J Gt Lakes Res* 40:524–531
- Chaffin JD, Bridgeman TB, Heckathorn SA, et al (2012) Role of suspended sediments and mixing in reducing photoinhibition in the bloom-forming cyanobacterium *Microcystis*. *J Water Resour Prot* 4:1029
- Chaffin JD, Bridgeman TB, Heckathorn SA, Mishra S (2011) Assessment of *Microcystis* growth rate potential and nutrient status across a trophic gradient in western Lake Erie. *J Gt Lakes Res* 37:92–100. doi: 10.1016/j.jglr.2010.11.016
- Chaffin JD, Davis TW, Smith DJ, et al (2018) Interactions between nitrogen form, loading rate, and light intensity on *Microcystis* and *Planktothrix* growth and microcystin production. *Harmful Algae* 73:84–97. doi: 10.1016/j.hal.2018.02.001
- Chaffin JD, Sigler V, Bridgeman TB (2014b) Connecting the blooms: tracking and establishing the origin of the record-breaking Lake Erie *Microcystis* bloom of 2011 using DGGE. *Aquat Microbiol Ecol* 73:29–39
- Chang D-W, Hobson P, Burch M, Lin T-F (2012) Measurement of cyanobacteria using in-vivo fluoroscopy – Effect of cyanobacterial species, pigments, and colonies. *Water Res* 46:5037–5048. doi: 10.1016/j.watres.2012.06.050
- Conroy JD, Kane DD, Dolan DM, et al (2005) Temporal trends in Lake Erie plankton biomass: roles of external phosphorus loading and dreissenid mussels. *J Gt Lakes Res* 31, Supplement 2:89–110. doi: 10.1016/S0380-1330(05)70307-5
- Conroy JD, Kane DD, Quinlan EL, et al (2017) Abiotic and biotic controls of phytoplankton biomass dynamics in a freshwater tributary, estuary, and large lake ecosystem: Sandusky Bay (Lake Erie) chemostat. *Inland Waters* 7:473–492. doi: 10.1080/20442041.2017.1395142

- Davis CC (1964) Evidence for the eutrophication of Lake Erie from phytoplankton records. *Limnol Oceanogr* 9:275–283
- Davis TW, Koch F, Marcoval MA, et al (2012) Mesozooplankton and microzooplankton grazing during cyanobacterial blooms in the western basin of Lake Erie. *Harmful Algae* 15:26–35. doi: 10.1016/j.hal.2011.11.002
- DePinto JV, Young TC, McIlroy LM (1986) Great Lakes water quality improvement. *Environ Sci Technol* 20:752–759
- Dodds WK, Bouska WW, Eitzmann JL, et al (2009) Eutrophication of U.S. Freshwaters: analysis of potential economic damages. *Environ Sci Technol* 43:12–19. doi: 10.1021/es801217q
- Dyble J, Fahnenstiel GL, Litaker RW, et al (2008) Microcystin concentrations and genetic diversity of *Microcystis* in the lower Great Lakes. *Environ Toxicol* 23:507–516
- Fischer WJ, Garthwaite I, Miles CO, et al (2001) Congener-Independent Immunoassay for Microcystins and Nodularins. *Environ Sci Technol* 35:4849–4856. doi: 10.1021/es011182f
- Ganf GG, Oliver RL, Walsby AE (1989) Optical properties of gas-vacuolate cells and colonies of *Microcystis* in relation to light attenuation in a turbid, stratified reservoir (Mount Bold Reservoir, South Australia). *Aust J Mar Freshw Res* 40:595–611
- Gobler CJ, Burkholder JM, Davis TW, et al (2016) The dual role of nitrogen supply in controlling the growth and toxicity of cyanobacterial blooms. *Harmful Algae* 54:87–97. doi: 10.1016/j.hal.2016.01.010
- Golnick PC, Chaffin JD, Bridgeman TB, et al (2016) A comparison of water sampling and analytical methods in western Lake Erie. *J Gt Lakes Res* 42:965–971. doi: 10.1016/j.jglr.2016.07.031
- Gregor J, Marsálek B (2004) Freshwater phytoplankton quantification by chlorophyll a: a comparative study of in vitro, in vivo and in situ methods. *Water Res* 38:517–522. doi: 10.1016/j.watres.2003.10.033
- Harke MJ, Davis TW, Watson SB, Gobler CJ (2016a) Nutrient-Controlled Niche Differentiation of Western Lake Erie Cyanobacterial Populations Revealed via Metatranscriptomic Surveys. *Env Sci Technol* 50:604–615. doi: 10.1021/acs.est.5b03931
- Harke MJ, Gobler CJ (2015) Daily transcriptome changes reveal the role of nitrogen in controlling microcystin synthesis and nutrient transport in the toxic cyanobacterium, *Microcystis aeruginosa*. *BMC Genomics* 16:1068
- Harke MJ, Steffen MM, Gobler CJ, et al (2016b) A review of the global ecology, genomics, and biogeography of the toxic cyanobacterium, *Microcystis* spp. *Harmful Algae* 54:4–20. doi: 10.1016/j.hal.2015.12.007
- Hodges CM, Wood SA, Puddick J, et al (2017) Sensor manufacturer, temperature, and cyanobacteria morphology affect phycocyanin fluorescence measurements. *Environ Sci Pollut Res* 1–10. doi: 10.1007/s11356-017-0473-5
- Horst GP, Sarnelle O, White JD, et al (2014) Nitrogen availability increases the toxin quota of a harmful cyanobacterium, *Microcystis aeruginosa*. *Water Res* 54:188–198
- Huisman J, Arrayás M, Ebert U, Sommeijer B (2002) How do sinking phytoplankton species manage to persist? *Am Nat* 159:245–254
- Huisman J, Matthijs HCP, Visser PM (eds) (2010) *Harmful Cyanobacteria*, Softcover reprint of hardcover 1st ed. 2005 edition. Springer, Place of publication not identified

- Humbert J-F, Törökné A (2016) New Tools for the Monitoring of Cyanobacteria in Freshwater Ecosystems. In: Meriluoto J, Spoof L, Codd GA (eds) Handbook of Cyanobacterial Monitoring and Cyanotoxin Analysis. John Wiley & Sons, Ltd, pp 84–88
- Hutchinson PA, Webster IT (1994) On the distribution of blue-green algae in lakes: Wind-tunnel tank experiments. *Limnol Oceanogr* 39:374–382
- Jochens AE, Malone TC, Stumpf RP, et al (2010) Integrated Ocean Observing System in Support of Forecasting Harmful Algal Blooms. *Mar Technol Soc J* 44:99–121. doi: 10.4031/MTSJ.44.6.16
- Kane DD, Conroy JD, Richards RP, et al (2014) Re-eutrophication of Lake Erie: Correlations between tributary nutrient loads and phytoplankton biomass. *J Gt Lakes Res* 40:496–501
- Kurmayer R, Deng L, Entfellner E (2016) Role of toxic and bioactive secondary metabolites in colonization and bloom formation by filamentous cyanobacteria *Planktothrix*. *Harmful Algae* 54:69–86. doi: 10.1016/j.hal.2016.01.004
- Loisa O, Kääriä J, Laaksonlaita J, et al (2015) From phycocyanin fluorescence to absolute cyanobacteria biomass: An application using in-situ fluorometer probes in the monitoring of potentially harmful cyanobacteria blooms. *Water Pract Technol* 10:695–698. doi: 10.2166/wpt.2015.083
- Long BM, Jones GJ, Orr PT (2001) Cellular microcystin content in N-limited *Microcystis aeruginosa* can be predicted from growth rate. *Appl Environ Microbiol* 67:278–283. doi: 10.1128/AEM.67.1.278-283.2001
- MacIntyre HL, Kana TM, Anning T, Geider RJ (2002) Photoacclimation of photosynthesis irradiance response curves and photosynthetic pigments in microalgae and cyanobacteria. *J Phycol* 38:17–38
- Makarewicz JC (1993) Phytoplankton biomass and species composition in Lake Erie, 1970 to 1987. *J Gt Lakes Res* 19:258–274
- McQuaid N, Zamyadi A, Prévost M, et al (2010) Use of in vivo phycocyanin fluorescence to monitor potential microcystin-producing cyanobacterial biovolume in a drinking water source. *J Env Monit* 13:455–463
- Michalak AM, Anderson EJ, Beletsky D, et al (2013) Record-setting algal bloom in Lake Erie caused by agricultural and meteorological trends consistent with expected future conditions. *Proc Natl Acad Sci* 110:6448–6452. doi: 10.1073/pnas.1216006110
- Millie DF, Fahnenstiel GL, Dyle Bressie J, et al (2009) Late-summer phytoplankton in western Lake Erie (Laurentian Great Lakes): bloom distributions, toxicity, and environmental influences. *Aquat Ecol* 43:915–934
- Orr PT, Jones GJ (1998) Relationship between microcystin production and cell division rates in nitrogen-limited *Microcystis aeruginosa* cultures. *Limnol Oceanogr* 43:1604–1614. doi: 10.4319/lo.1998.43.7.1604
- Paerl HW, Huisman J (2008) Blooms like it hot. *Science* 320:57–58. doi: 10.1126/science.1155398
- Poulton NJ (2016) FlowCam: Quantification and Classification of Phytoplankton by Imaging Flow Cytometry. In: *Imaging Flow Cytometry*. Humana Press, New York, NY, pp 237–247
- Qian SS, Chaffin JD, DuFour MR, et al (2015) Quantifying and reducing uncertainty in estimated microcystin concentrations from the ELISA method. *Environ Sci Technol* 49:14221–14229. doi: 10.1021/acs.est.5b03029

- Read J, Klump V, Johengen T, et al (2010) Working in Freshwater: The Great Lakes Observing System Contributions to Regional and National Observations, Data Infrastructure, and Decision Support. *Mar Technol Soc J* 44:84–98. doi: 10.4031/MTSJ.44.6.12
- Reynolds CS, Oliver RL, Walsby AE (1987) Cyanobacterial dominance: The role of buoyancy regulation in dynamic lake environments. *N Z J Mar Freshw Res* 21:379–390
- Rinta-Kanto JM, Konopko EA, DeBruyn JM, et al (2009) Lake Erie *Microcystis*: Relationship between microcystin production, dynamics of genotypes and environmental parameters in a large lake. *Harmful Algae* 8:665–673. doi: 10.1016/j.hal.2008.12.004
- Rosen BH, St. Amand A (2015) Field and laboratory guide to freshwater cyanobacteria harmful algal blooms for Native American and Alaska Native communities. U.S. Geological Survey, Reston, VA
- Soranno PA (1997) Factors affecting the timing of surface scum and epilimnetic blooms of blue-green algae in a eutrophic lake. *Can J Fish Aquat Sci* 54:1965–1975
- Stumpf RP, Johnson LT, Wynne TT, Baker DB (2016) Forecasting annual cyanobacterial bloom biomass to inform management decisions in Lake Erie. *J Gt Lakes Res* 42:1174–1183. doi: 10.1016/j.jglr.2016.08.006
- Tillmanns AR, Wilson AE, Pick FR, Sarnelle O (2008) Meta-analysis of cyanobacterial effects on zooplankton population growth rate: species-specific responses. *Fundam Appl Limnol Arch Für Hydrobiol* 171:285–295. doi: 10.1127/1863-9135/2008/0171-0285
- Wang H, Gruden CL, Bridgeman TB, Chaffin JD (2009) Detection and quantification of *Microcystis* spp. and microcystin-LR in Western Lake Erie during the summer of 2007. *Water Sci Technol* 60:
- Webster IT, Hutchinson PA (1994) Effect of wind on the distribution of phytoplankton cells in lakes revisited. *Limnol Oceanogr* 39:365–373
- Wetzel RG (2001) *Limnology : lake and river ecosystems*. Academic Press, San Diego
- Zamyadi A, Choo F, Newcombe G, et al (2016) A review of monitoring technologies for real-time management of cyanobacteria: Recent advances and future direction. *TrAC Trends Anal Chem* 85:83–96. doi: 10.1016/j.trac.2016.06.023
- Zamyadi A, Mcquaid N, Dorner S, et al (2012) Cyanobacterial detection using in vivo fluorescence-probes: Managing interferences for improved decision-making. *J - Am Water Works Assoc* 104:E466–E479. doi: 10.5942/jawwa.2012.104.0114

Determining components for a phosphorus interceptor to reduce harmful algal blooms in the western Lake Erie basin

Basic Information

Title:	Determining components for a phosphorus interceptor to reduce harmful algal blooms in the western Lake Erie basin
Project Number:	2016OH5000
Start Date:	3/1/2016
End Date:	2/28/2018
Funding Source:	Other
Congressional District:	OH-009
Research Category:	Water Quality
Focus Categories:	Nutrients, Non Point Pollution, Agriculture
Descriptors:	None
Principal Investigators:	Daryl F Dwyer

Publication

1. Bartos, A., D. F. Dwyer, R. W. Jackwood. September 2016. Effectiveness of Natural and Industrial Byproducts to Adsorb Dissolved Phosphorus as a Water Quality Management Technique in the Maumee River Watershed". Presented as a poster at the University of Toledo Undergraduate Research Symposium, Toledo, OH.

Final Report – Determining Components for a Phosphorus Interceptor to Reduce Harmful Algal Blooms in the Western Lake Erie Basin. PI – Daryl F. Dwyer, Ph.D., Department of Environmental Sciences, The University of Toledo, Toledo, OH.

1.a. Problem and Research Objectives - Harmful algal blooms (HABs) have been observed annually in the western Lake Erie basin since the mid-1990s; some of the most extensive blooms were observed in recent years (Bridgeman et al., 2012; Michalak et al., 2013). HABs are due to complex interactions among multiple factors that may include nutrient input from agricultural fields, climate change-induced increases in temperature and in the frequency and severity of storms, and the unique geomorphology of Lake Erie, which is shallow and warm (Michalak et al., 2013; Smith et al., 2015). HABs in Lake Erie appear closely linked to agricultural nutrients, specifically nitrogen (N) and soluble phosphorus (SP) (Chaffin et al., 2011; Bridgeman et al., 2012). An estimated 50% of the total phosphorus (TP) loading to Lake Erie is derived from the Maumee River (Dolan and McGunagle, 2005) with 49% from agricultural sources (Robertson and Saad, 2011). Studies indicate (Smith et al., 2015) that approximately 50% of phosphorous emissions may be derived from subsurface tiles, which suggests that tile drainage is equally as important as surface runoff. Unfortunately, tile drainage has been overlooked by the traditional best management practices (BMPs) implemented by agricultural conservation programs that focus on management and reduction of nutrient transport as surface runoff (Sharpley et al., 2006). Therefore, we proposed to develop a “nutrient interceptor” to harvest phosphorus from agricultural-derived water emitted via drainage tiles.

The proposed nutrient interceptor is a simple, easy to install device that can be implemented throughout the Maumee River watershed and is basically a surface container filled with mesh bags of replaceable filter media with the appropriate properties to adsorb SP. We previously evaluated several types of filter media including commercial sorbents, biochar, and mussel shells, which proved to be the best sorbent with an average 13% reduction in SP. We proposed to evaluate additional types of natural filter media, including locally-derived limestone, for comparison with the initial results. The sorbent with the highest SP removal was to be field tested in nutrient interceptors stationed at farm fields within the Wolf Creek watershed to test the efficiency of SP-removal. Thus, for this project, three specific objectives were created: (1) determine the most appropriate filter media and hydraulic retention time for P nutrient interceptors, (2) investigate rain event-based P loadings from agricultural fields, and (3) quantify the reduction in P using the nutrient interceptors.

Unfortunately, the field work portion of the project was not successful due to two factors: (1) the drain tile mains were below the water level in the ditches into which they emptied during rain storms that occurred after fertilization of the farms fields. Thus, we were unable to place the interceptors into position. (2) When the water levels were low enough to access the drain tile mains, fertilizer had not been applied to the fields. To substitute for the field work, we brought the drainage water to the laboratory, added phosphorous to attain concentrations relevant to those observed in the field, and set up the nutrient interceptors in the laboratory for testing their effect on this amended water.

1.b. Methodology

PSM characterization. The selection of a phosphorous-sorbing material (PSM) was prefaced on availability, cost, and performance. Three materials that were both readily available and inexpensive were chosen for comparison with respect to performance – each of the test materials (water treatment plant residuals, quarry-derived limestone, and crushed zebra mussel shells) was calcium-based; sand was used as a control. Water treatment plant residuals were acquired from the Toledo Water Treatment Plant, ground and passed through a sieve to obtain sizes less than 850 μm . Limestone gravel was obtained from a local quarry. Zebra mussel shells were obtained from the shoreline of Lake Erie, passed through a series of three sieves to obtain fractions of the following sizes: < 850 μm ; 850 μm to 2 mm; 2mm and 4mm. Each material (including all three size fractions of zebra mussel shells) was characterized (Lyngsie et. al, 2015) in triplicate as follows: (i) Bulk Density. PSM (100 cm^3) was weighed and the density calculated. (ii) Porosity. PSM (40 cm^3) was saturated with DI water within a graduated cylinder and the volume divided by the measured quantity of water. (iii) pH Bench Test. PSM (15 g) was added to DI water (150 mL) and to Maumee River water (150 mL) in 250 mL Erlenmeyer flasks; pH was measured using a Toledo Mettler Seven Go Pro.

Rates of phosphorus adsorption. PSM (2 g) was placed into solutions (30 mL) containing known concentrations of SP (0.5, 1.0, 5.0, 10 and 25 mg P/L). The stock solution of SP was made by dissolving 0.2129 g of KH_2PO_4 into 1 L of 18-ohm reverse osmosis filtered water, resulting in a solution of 50 mg P/L. In the initial experiments, to maintain a controlled experimental setting, the 30 ml of solution was modified Hoagland's solution containing per liter, 0.0379 g of K_2SO_4 , 0.0254 g of NaCl, 0.0568 g of MgSO_4 , and 0.448 g of CuSO_4 . This solution approximated the nutrient composition of the Maumee River. Each setup was done in triplicate and placed on a bench shaker; water samples (1 mL) were taken at 1, 10, 30, 60 min, 5 and 24 hours after shaking (120 rpm) commenced, centrifuged to remove solids, and tested (EPA method 365.2, Rice et al., 2012) for PO_4^{3-} and reported as mg P/L adsorbed to each PSM.

Phosphorous sorption capacity. Water treatment plant residuals were selected for further experimentation based on the initial analysis. Samples (5 g) were mixed evenly with laboratory grade sand (95 g) and placed into six PVC columns (3.8 cm diameter by 20 cm height) in triplicate (Figure 1). A 45- μm filter was added to the bottom of each column to prevent PSM from passing into collection flasks. Phosphorus solution (1 mg P/L) was added to each column with constant head pressure, allowed to percolate through the PSM mixture and effluent samples collected every 30 min for 5 hr. Samples were then analyzed for SP.



Figure 1. Experimental setup to determine the phosphorous sorption capacity of water treatment plant residuals.

Efficacy of the nutrient interceptor. The nutrient interceptor (Figure 2) was constructed using two 19 L open top buckets, two 1.27 cm diameter bulkhead fittings, and a 5-micron industrial filter. Tile drainage water from a farm field (located in Oregon, OH) was amended with the stock P-solution to attain a concentration of 2.5 mg P per liter. The water was first tested to ascertain that the field water did not alter the sorption efficiency or capacity of the nutrient interceptor. The interceptor contained water treatment plant residual (18% by weight) mixed with sand to a final mass of 3 kg. Water (40 L) was gravity fed through the interceptor using a 2 meter head at a rate of 3 liters per minute. Water samples (10 mL) from the inflow and outflow of the interceptor were taken over time until the water was depleted.

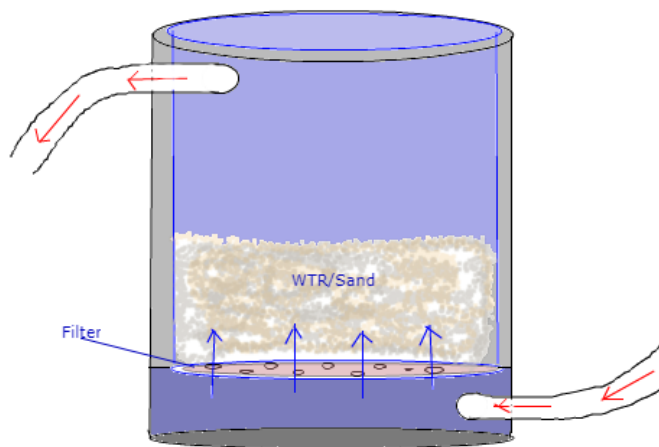
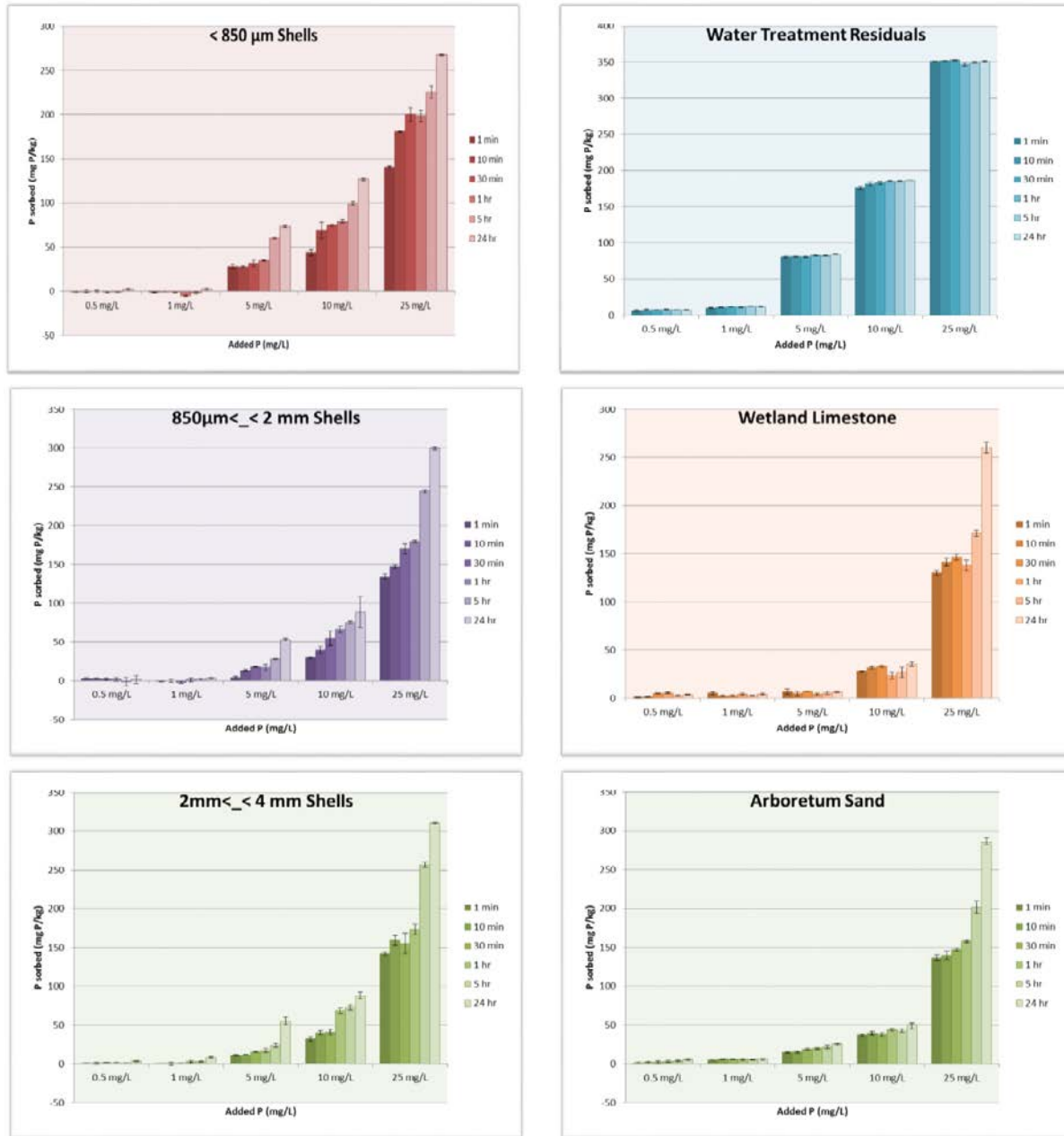


Figure 2. Diagram of the nutrient interceptor designed to test the phosphorous-removal efficacy of the water treatment plant residuals. A photograph of the system in the laboratory is provided with this report.

1.c. Principal Findings and Results

Rates of phosphorous adsorption. Over a period of 24 hours, the amount of phosphorous adsorbed to each PSM increased (Figure 3). The water treatment plant residuals demonstrated the relatively quickest sorption for each tested concentration – sorption was complete within 1 minute when compared to the slower rates for the remaining PSMs. For this reason, water treatment plant residuals were selected for further testing.

Figure 3. The quantity of phosphorus adsorbed by each PSM over a 24-hour period. The most rapid adsorption rate occurred with the water treatment plant residuals.



Phosphorous sorption capacity. Data for each experimental trial – using sand as a control and the water treatment plant residuals - is provided in Figure 4. The amount of phosphorous adsorbed by sand decreased over time, which is an anomaly that may be explained only if the sand had attached phosphorous that was released. More noteworthy are the results using water treatment plant residuals to which P adsorbed over the 300-minute trial. Note that compared to the batch systems, in which adsorption occurred almost instantaneously, the flow through systems used in these experiments allowed for continuous removal of phosphorous over time, but did attain what appears to be saturation of the PSM.

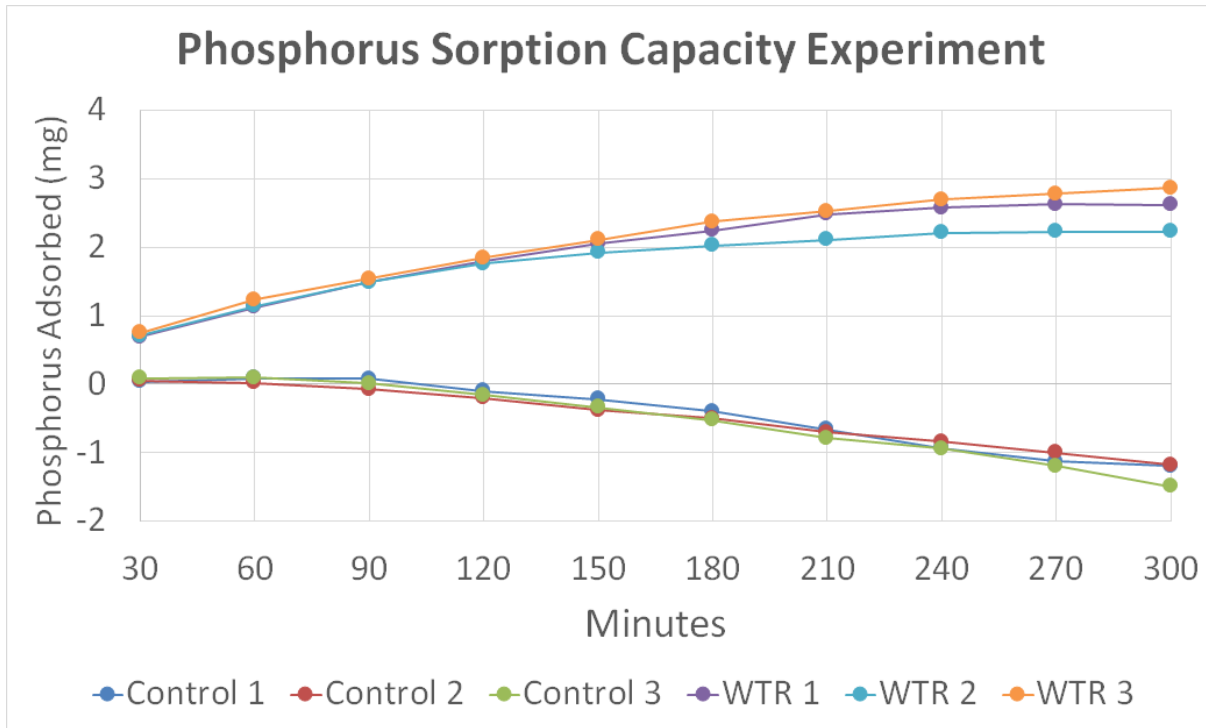
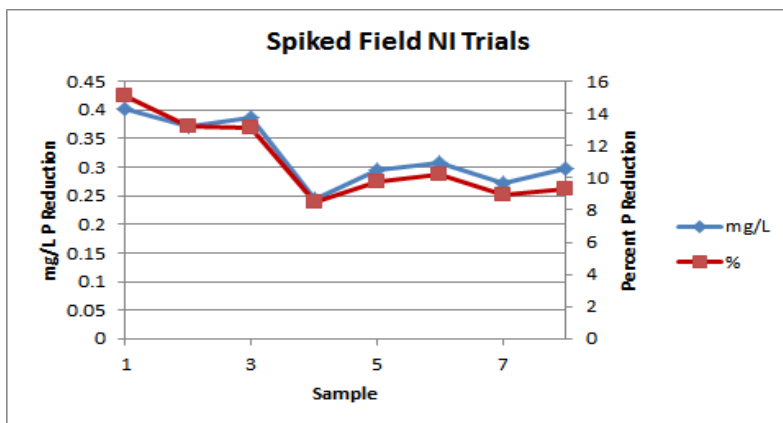


Figure 4. The sorption of phosphorous in flow-through systems occurred continuously over time and leveled-off near the end of the 5-hour experiment, presumably due to saturation of the PSM.

Efficacy of the nutrient interceptor. The nutrient interceptor (Figure 5) had farm field water to which phosphorous had been amended passed through and samples of water analyzed to determine the amount of adsorbed phosphorous with the data presented as both the reduction in concentration of P and percentage of P. Initially, reductions of 15% occurred, but this percentage decreased to 10% as the PSM, presumably, became saturated.

Figure 5. Average reduction of phosphorus (mg/L; red line) and average percent reduction of phosphorus (%; blue line) of spiked tile drainage water (2.5 mg P/L) calculated for each effluent sample for the nutrient interceptor (NI) trials. Discrete phosphorus reduction decreases indicating the gradual tendency to saturation of the WTR.



1.d. Finding Significance. The water treatment plant residuals worked relatively well within the scope of this project, especially when compared to other potential PSM material. We are currently continuing with this project to formulate the residuals into a material that can be used in large scale nutrient interceptors. Interest in media that can be used to remove nutrients from agricultural field water is not new. However, the results here demonstrate that a waste product from water treatment plants can function as a PSM. It is worth noting that the City of Toledo currently spends millions of dollars each year to dispose of the residuals. Conversion to a PSM instead of disposal would potentially save municipalities money and create a product that can be used to improve water quality.

1.e. Literature Cited

Bridgeman, T.B., Chaffin, J.D., Kane, D.D., Conroy, J.D., Panek, S.E., Armenio, P.M. 2012. From River to Lake: Phosphorus partitioning and algal community compositional changes in Western Lake Erie. *J. Great Lakes Res.* 38: 90-97.

Chaffin, J.D., Bridgeman, T.B., Heckathorn, S.A., Mishra, S. 2011. Assessment of *Microcystis* growth rate potential and nutrient status across. *J. Great Lakes Res.* 37(1): 92-100.

City of Toledo. 2014. Microcystin event preliminary summary. Monday, August 4, 2014, Department of Public Utilities.

Dolan, D.M., McGunagle, K.P. 2005. Lake Erie total phosphorus loading analysis and update: 1996–2002. *J. Great Lakes Res.* 31(Suppl. 2):11–22.

Lyngsie, Gry, Chad J. Penn, Henrik L. Pederson, Ole K. Borggaard, and Hans C.B. Hansen. "Modelling of Phosphate Retention by Ca- and Fe-rich Filter Materials under Flow-through Conditions." *Ecological Engineering* 75 (2015): 93-102. Web. <Ecological Engineering>

Michalak, A.M., Anderson, E.J., Beletsky, D., Boland, S., Bosch, N.S., Bridgeman, T.B., et al., 2013. Record-setting algal bloom in Lake Erie caused by agricultural and meteorological trends consistent with expected future conditions. *Proc. Natl. Acad. Sci.* 110 (16): 6448–6452.

Sharpley, A.N., Daniel, T., Gibson, G., Bundy, L., Cabrera, M., Sims, T., Stevens, R., Lemunyon, J., Kleinman, P., Parry, R. 2006. Best management practices to minimize agricultural phosphorus impacts on water quality. U.S. Department of Agriculture, Agricultural Research Service ARS-163, 50 pp.

Smith, D.R., King, K.W., Williams, M.R., 2015. What is causing the harmful algal blooms in Lake Erie? *J. Soil Water Conserv.* 70 (2): 27A-29A.

Improved Estimates of Peak Water Demand in Buildings: Implications for Water-Energy Savings

Basic Information

Title:	Improved Estimates of Peak Water Demand in Buildings: Implications for Water-Energy Savings
Project Number:	2016OH506O
Start Date:	3/1/2016
End Date:	12/31/2017
Funding Source:	Other
Congressional District:	1
Research Category:	Engineering
Focus Categories:	Models, Water Supply, Conservation
Descriptors:	None
Principal Investigators:	Steve Buchberger

Publications

1. Omaghom, T. and Buchberger, S. G. (February, 2017) Residential Water Demand Calculator Poster presentation in 2017 Graduate Student Expo & Poster Forum, Cincinnati, OH
2. Omaghom, T. and Buchberger, S. G. (2017) Residential Water Demand Calculator Poster presentation in the 13th Annual OVALS Conference: Water Technology: The Wave of the Future, Cincinnati, OH
3. Omaghom, T and Buchberger, S. (2018), “A Model of In-Home Hot Water Distribution Systems Energy Losses Using EPANET, Public Domain Software for Pipe Networks”, Invited Presentation at ACEEE Hot Water Forum, Portland, Oregon
4. Omaghom, T and Buchberger, S. (2018) “Residential Water and Energy Savings in Right-Sized Premise Plumbing” in Proceedings, WDSA / CCWI 2018 Joint Conference, Kingston, Canada

Improved Estimates of Peak Water Demand in Buildings: Implications for Water-Energy Savings

Prepared by

Toritseju Omaghomi and Steven Buchberger, PhD
College of Engineering and Applied Science



Final Report for
Project 2016OH506B

May 2018

ACKNOWLEDGMENTS

The authors appreciate helpful discussions with James D. Lutz of the Lawrence Berkeley National Laboratory and with Daniel Cole of the International Association of Plumbing and Mechanical Officials.

TABLE OF CONTENTS

ACKNOWLEDGMENTS	ii
LIST OF FIGURES	iv
LIST OF TABLES	v
LIST OF NOTATION.....	vi
ABSTRACT	1
INTRODUCTION	2
METHODOLOGY.....	3
Part 1 – Parameters for estimating peak water demand	4
Part 2 – Estimating peak water demand	5
Part 3 – Sizing premise plumbing in single-family home.....	6
Part 4 – Simulating hot water demand pulses and estimating energy consumed.....	8
Background	8
Simulating PRP Demand Pulses.....	9
EPANET Setup	14
Energy Calculations.....	16
RESULTS AND DISCUSSION	18
Inefficient and Efficient Fixtures.....	18
Premise Plumbing Configuration.....	19
Pipe Sizing Method	21
Building Size.....	21
CONCLUSION	23
REFERENCES.....	24

LIST OF FIGURES

Figure 1: Binomial Distribution and Zero Truncated Binomial Distribution (ZTBD) of busy fixtures in a group of (a) $n = 5$ (b) $n = 20$ fixtures each with a probability $p = 0.20$ of being in use.	6
Figure 2: Hot water distribution in single-family home for a) trunk-and-branch layout and b) manifold layout	7
Figure 3: Flowchart to generate PRP pulses necessary and perform hydraulic simulations in EPANET	10
Figure 4: Fixture demand multipliers for weekday and weekend water use	13
Figure 5: Illustration of adjusted pulse duration with preserved mass	14
Figure 6: Energy balance in a building's pipe network.....	16
Figure 7: 24-hour timeline of hot water demand pulses and temperature decay resulting from use of two fixtures in a 2-bath unit in Figure 2a.....	18
Figure 8: Annual hot water volume, energy consumed and energy cost in a 2-bath home with inefficient and efficient water fixtures.....	19

LIST OF TABLES

Table 1: Peak hour p -values and q -values for six fixture groups in a single-family home (Buchberger et al. 2017).....	4
Table 2: Estimated water demand and corresponding pipe sizes (Copper L) for current practice and the proposed improved method (WDC) for trunk and branch layout shown in Figure 2	8
Table 3: Criteria for fixture efficiency	11
Table 4: 24-hour base demand for individual fixtures in six fixture groups in single-family home ..	11
Table 5: PRP fixture parameters - Pulse characteristics.....	12
Table 6: Expected and simulated pulse characteristics for hot water fixtures.....	13
Table 7: Heat decay coefficient for different sizes of uninsulated Copper L pipes from equation [5]	15
Table 8: Typical hot water temperatures at fixtures and implied hot/cold water mix	15
Table 9: Cincinnati mean monthly temperatures (U. S. Climate Data 2017).....	16
Table 10: Annual hot water/energy consumed in a 2-bath residence with trunk-and-branched network sized by Hunters curve and new WDC.....	20
Table 11: Annual hot water/energy consumed in a 2-bath residence with trunk-and-branch and manifold pipe network sized with a new WDC method	20
Table 12: Annual hot water/energy per unit consumed in a building with 2-bath units sized with the new WDC method	20
Table 13: Pipe sizes for water demand in large buildings.....	22

LIST OF NOTATION

- α_k : Fixture mean intensity, (*gpm*)
 $\lambda_{j,k}$: Fixture average hourly pulse arrival rate (*hour*⁻¹)
 $\pi_{j,k}$: Fixture hourly multiplier
 τ_k : Fixture mean duration, (*minutes*)
 ϵ : Surface emittance

 A : Pipe surface area, (*ft*²)
 C_p : Specific heat of water, ($\frac{Btu}{lb \cdot ^\circ F}$)
 D_i : Inside pipe diameter, (*ft*)
 D_o : Outside pipe diameter, (*ft*)
 h_{air} : Overall film heat transfer coefficient, ($\frac{Btu}{hr \cdot ft^2 \cdot ^\circ F}$)
 h_{cov} : Convection surface coefficient, ($\frac{Btu}{hr \cdot ft^2 \cdot ^\circ F}$)
 h_{rad} : Radiation surface coefficient, ($\frac{Btu}{hr \cdot ft^2 \cdot ^\circ F}$)
 h_w : Convective film heat transfer coefficient, ($\frac{Btu}{hr \cdot ft^2 \cdot ^\circ F}$)
 k : Thermal conductivity of copper, ($\frac{Btu}{hr \cdot ft \cdot ^\circ F}$)
 k_d : Heat decay coefficient of copper L pipes, (*day*⁻¹)
 L : Pipe length, (*ft*)
 \dot{m} : Mass flowrate of water, ($\frac{lb_m}{hr}$)
 m_l : Mass of water per length of pipe, ($\frac{lb}{ft}$)
 p_k : Fixture probability of use
 q_k : Fixture flow rate, (*gpm*)
 Q_k : Fixture 24-hour base demand flow, (*gpm*)
 R : Time between consecutive pulses, (*seconds*)
 T_a : Air temperature surrounding pipe, (*°F*)
 T_s : Pipe surface temperature, (*°F*)
 ΔT : Change in temperature, (*°F*)
 U_o : Overall heat transfer coefficient, ($\frac{Btu}{h \cdot ft^2 \cdot ^\circ F}$)
 $V_{j,k}$: Hourly volume of water used at fixture, (*gallon*)
 V_k^* : Average daily volume of water used at fixture, (*gallon*)

ABSTRACT

Current methods for estimating peak hot and cold water demands in buildings were developed 80 years ago in the seminal work of Dr. Roy Hunter at the US National Bureau of Standards. Hunter's design curve has been incorporated into the Uniform Plumbing Code (UPC) and adopted by water agencies around the world. Over the years, the performance of water fixtures and demands of water consumers have changed. Consequently, it is now widely recognized that Hunter's iconic design curve significantly over-estimates peak demand for indoor hot and cold water use. Inflated peak flow values have led to over-sized premise plumbing and improperly sized water meters, heaters, and softeners.

The hot water component of premise plumbing exemplifies the water-energy nexus on a local scale. When a building's water supply system is over-sized, it triggers a cascade of potential water-energy related problems, including:

- Inflated construction cost,
- Over-sized water meters and heaters,
- Lost revenue from inaccurate water metering,
- Wasted energy from inefficient water heating and delivery,
- Potential health issues from opportunistic bacteria (e.g., *Legionella*)

This research computes the water and energy consumption resulting from hot water use in residential plumbing systems serving households with efficient and inefficient fixtures. A novel Water Demand Calculator (WDC) is developed to estimate peak water demand expected in residential settings ranging from single-family homes to a large apartment complex. Not surprisingly, plumbing systems that serve efficient water fixtures can be smaller in scale (i.e., reduced pipe diameters, meters, heater) than the plumbing system serving standard (inefficient) water fixtures. Simulation of instantaneous water and energy consumption in a typical 2-bath residential unit shows that annual savings for both water and energy can approach 30 percent each when rightly-sized plumbing is coupled with highly efficient fixtures.

INTRODUCTION

An estimate of peak water demand is the most important factor for sizing a building's water supply system. Water demand in buildings is a random process dependent on other variables such as building size, fixture type, time of the day, occupancy rate and so on. In 1940, Dr. Roy Hunter, using the binomial distribution, developed a theoretically rigorous method to estimate the 99th percentile for peak water demand in buildings subject to congested use patterns. Hunter's design curve has been incorporated into the various plumbing codes and adopted by water agencies at home and abroad. However, with changes in fixture performance and consumer water use habits over the years, Hunter's curve significantly over-estimates peak demand for indoor hot and cold water use in contemporary applications (AWWA 2004; NIBS 2012).

Although theoretically sound, the overprediction of peak water demand by Hunter's method reflects its inability to incorporate recent water saving measures or accommodate the complexity of fixtures and other characteristics of modern plumbing (NIBS 2012). A study of residential water use trends by Coomes *et al.* (2010) suggests that low flow fixtures and appliances account for a 16 percent decline in the average daily water use over the last 20 years, thus effectively reducing water demand in buildings (Price *et al.* 2014). Consequently, following the current design practice, premise plumbing in new buildings is often designed to supply more water than necessary. To compensate for design discrepancies, ASHRAE (1987) and other professional organizations introduced modifications to Hunter's curve. Unfortunately, this makeshift approach is inconsistent and subjective. Furthermore, it does not provide a precise foundation for the design of smart high efficiency (water/energy) buildings for the future generations.

Inaccurate design guidance for water supply (i.e., premise plumbing) has profound consequences for today's new generation of water and energy conserving buildings. Obsolete water supply design guidelines produce over-sized plumbing systems and improperly sized water meters. This leads to a myriad of water – energy problems including: [i] inflated construction costs, [ii] inaccurate water monitoring and billing, [iii] wasted energy and water through inefficient water heating, and [iv] increased potential health hazards from the risk of microbial contamination (*Legionella*) (ANSI/ASHRAE Standard -188 2015). These issues can adversely impact owners, residents, and users of facilities throughout the public and private sectors.

According to the US Energy Information Administration (2015), energy consumption in the residential sector accounted for 22 percent of the total energy consumed in the US in 2014. In this vein, water heating is the second highest sole source of energy consumption in residential buildings next to space heating. On the average, heating water accounts for about 18 percent of total residential energy consumption in the US (US EIA 2013). Heating water is also the most energy-intensive part of the urban water-use cycle compared to the collection, treatment, and distribution of water (Vieira *et al.* 2014; Siddiqi and Fletcher 2015). There has been scant attention on the water energy-nexus at the design phase in the residential water sector.

The relationship between building water and building energy use is complex and depends on the building type, user behavior and fixture characteristics (Agudelo-Vera *et al.* 2014). Recent research on hot water distribution systems has found that many factors influence hot water energy consumption: fixture flow rates, pipe size, pipe material (Klein 2013), pipe layout (Hiller 2012; Klein 2013) and hot water waste at different fixtures (Lutz 2005; Lutz *et al.* 2014). These studies focus on one or two factors at a time. The unknown effect of combined factors on hot water energy consumption reinforces the importance of understanding the relationship between designing for hot water distribution and hot water energy consumption.

This research aims to investigate and quantify potential water and energy savings in residential buildings in which supply pipes serving efficient water fixtures are sized by an improved method. To achieve this aim, the performance of a hot water distribution system and the corresponding energy consumed a 2-bath residential building will be evaluated using combinations of the following conditions:

- **Fixture efficiency:** inefficient fixtures or efficient fixtures,
- **Pipe layout:** trunk-and-branched layout or manifold layout, and
- **Pipes sizing method:** current practice (Hunter's curve) or improved method (WDC).

METHODOLOGY

This work extends research on defining water use parameters and developing methods for estimating peak water demand necessary to right size indoor premise plumbing in buildings. The method is presented in four parts:

- **Part one** involves the estimation of fixture water use parameters from high-resolution water demand measurements at single-family homes.
- **Part two** applies the estimated fixture water use parameters to develop new methods for estimating peak water demand.
- **Part three** compares a building’s premise plumbing sized by current conventional design to a similar building sized using improved estimates of peak water demand.
- **Part four** examines the impacts of the hot water pipe diameter on a building’s energy consumption.

Part 1 – Parameters for estimating peak water demand

The key parameters needed to estimate peak water demand in a building are n - the number of fixtures, p - the probability that a fixture is busy, and q - the fixture flowrate. These three parameters (n, p, q) apply to both Hunter’s (1940) binomial approach and Wistort’s (1994) normal approximation of the binomial distribution to estimate the expected peak water demand.

In a review of the methods to estimate peak water demand, Omaghomi and Buchberger (2014) suggested that both Hunter and Wistort’s method can be improved by using a data-centered approach to estimate parameters reflecting today’s water use habits. The parameter n is a physical feature that can easily be measured, while the parameter q can be obtained from the fixture manufacturer or easily measured on site. However, the probability that a fixture is busy, p can only be estimated from an extensive water use survey. The peak hour probability that a fixture is busy (i.e., fixture p -value) was calculated from a residential water use survey (IAPMO data set) with over 1000 single-family homes each having six unique fixture types. Table 1 shows the representative peak hour p -values and q -values for fixtures in a single-family residential home.

Table 1: Peak hour p -values and q -values for six fixture groups in a single-family home (Buchberger et al. 2017)

Fixture Group	Bathtub	Clothes washer	Dishwasher	Faucet (Lavatory)	Faucet (K. Sink)	Shower	Water closet
Probability of use	0.010	0.055	0.005	0.020	0.020	0.045	0.010
Flow rate (gpm)	5.5	3.5	1.3	1.5	2.2	2.0	3.0

Part 2 – Estimating peak water demand

In developing his curve for peak water demand, Hunter focused on large buildings with a bank of fixtures experiencing congested use (i.e., a queue of people has formed to use a fixture). Under these conditions, it was virtually certain that at least one fixture in the building would be using water at any instant during the peak period. Congested use effectively pulls the probability distribution of busy water fixtures away from the lower boundary of zero. The assumption of congested use works well with large public buildings, but complications arise in single-family homes and other small-scale dwellings with few people and few fixtures.

In smaller buildings like single-family homes, idle fixtures are the norm even during the period of peak use. The high probability of idle fixtures in the single-family home implies zero flow (stagnation) which, in turn, exerts a strong “downward pull” on the predicted peak flow. Wistort’s method, a simplified version of Hunter’s method is a normal approximation of the binomial distribution. Similar to Hunter’s method, Wistort’s method has limitations in its application to small buildings due to their high probability of idle fixtures.

A zero-truncated binomial distribution (ZTBD) was introduced to address the “downward pull” on predicted peak flow due to a high probability of idle fixtures in single-family residential homes. The ZTBD is the conditional distribution of busy fixtures in a building given that at least one fixture is busy. The ZTBD arises from the parent binomial distribution. By truncating the mass probability of zero demand and rescaling the remaining probability mass to ensure the conditional ZTBD sums to one, the predicted flows will represent the demand from at least one busy fixture.

Figure 1 illustrates two cases of binomial distribution and their corresponding ZTBD. As the number of fixture increases and the probability of zero flow approaches zero ($P_0 \rightarrow 0$), there is a smooth transition from the ZTBD to the binomial distribution. Hence, the ZTBD provides the missing link needed to extend the binomial design framework across the full spectrum from large public buildings to small private dwellings.

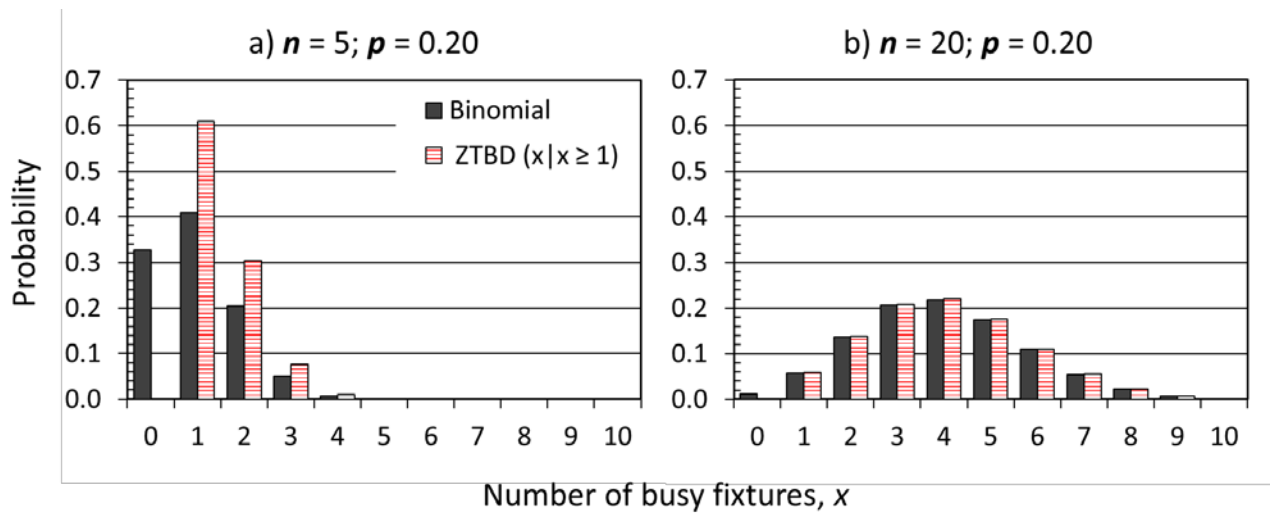


Figure 1: Binomial Distribution and Zero Truncated Binomial Distribution (ZTBD) of busy fixtures in a group of (a) $n = 5$ (b) $n = 20$ fixtures each with a probability $p = 0.20$ of being in use.

Findings by Buchberger *et al.* (2017) indicate that no single method is suitable to estimate peak water demand for all sizes of building. As a building size and its number of fixtures increases, the building's water demand transitions from discrete to continuous random pulses. A water demand calculator (WDC) was created in Microsoft Excel to select an appropriate method for estimating peak water demand depending on the combination of parameters n, p, q . The WDC selects from methods such as the exhaustive enumeration of the binomial method, a modified Wistort's method using the ZTBD and Wistort's method. Results from the WDC represent the improved estimates of peak demand used in this report. Further details on the WDC can be found in Buchberger *et al.* (2017).

Part 3 – Sizing premise plumbing in a single-family home.

The hot water premise plumbing layout for a typical 2-bath home is shown in Figure 2. Results of pipe sizing for hot water use at this home are summarized in Table 2 for two instances: (1) Estimated peak demand and size pipe using Hunter's Curve (current practice) and (2) Estimated peak demand and size pipe using WDC (improved method).

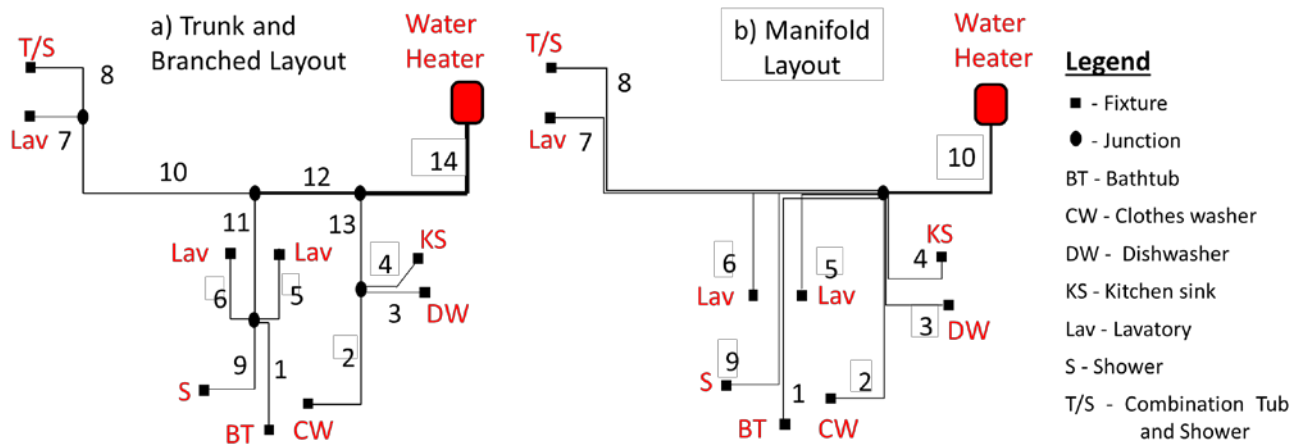


Figure 2: Hot water distribution in a single-family home for a) trunk-and-branch layout and b) manifold layout

Comparing estimates from current practices to the improved WDC method in Table 2 reveals that the design demand for single fixtures using the current method differs from the actual fixture flow rate. For instance, pipes sized by the current practices gives a 3.3 gpm for a bathtub, while the improved method gives a 5.5 gpm. This is due to the fact that Hunter’s method is not suitable for premise plumbing design with single fixtures. To arrive at design demand values for single fixtures using the current method, Hunter’s curve had to be extrapolated from 5 Fixture Units (FU) and 4 gpm to 1 FU and 1 gpm. Furthermore, to reconcile the inconsistency in design demand and demand flows, the UPC set a minimum allowable pipe size of 1/2 inch. This minimum allowable pipe size over compensates for dishwashers and lavatory faucets, but ironically under compensates for bathtubs and combination tub showers.

Table 2: Estimated water demand and corresponding pipe sizes (Copper L) for current practice and the proposed improved method (WDC) for trunk and branch layout shown in Figure 2

Link	Single fixtures and links with more than one fixture serviced by pipe	Current Practice			Improved Method (WDC)		Pipe length (feet)
		UPC Fixture Units (FU)	Peak Demand (gpm)	Pipe Size (in)	Peak Demand (gpm)	Pipe Size (in)	
1	BT	4	3.3	1/2	5.5	3/4	5.3
2	CW	4	3.3	1/2	3.5	1/2	10.1
3	DW	1.5	1.4	1/2	1.3	3/8	12.8
4	KS	1.5	1.4	1/2	2.2	1/2	9.7
5	Lav	1	1.0	1/2	1.5	3/8	8.4
6	Lav	1	1.0	1/2	1.5	3/8	9.5
7	Lav	1	1.0	1/2	1.5	3/8	2.1
8	T/S	4	3.3	1/2	5.5	3/4	7.2
9	S	2	1.8	1/2	2.0	3/8	5.8
10	Links 7, 8	5	4.0	1/2	5.5	3/4	13.0
11	Links 1, 5, 6, 9	8	6.5	3/4	7.0	3/4	10.5
12	Links 10, 11	13	10.0	1	7.5	3/4	11.8
13	Links 2, 3, 4	7	6.3	3/4	4.8	3/4	8.6
14	All fixtures	20	14.0	1-1/4	9	1	27.4

- Grey cells indicate links where the pipe diameters for current practice differ from diameters for the improved method.
- Bold red font indicates the case with the larger pipe diameter.
- Pipe sizes are for hot water pipes, based on peak demand and maximum water velocity of 5 ft/sec

Part 4 – Simulating hot water demand pulses and estimating energy consumed.

Background

The daily energy needed to heat the hot water tank depends on the total daily volume of water used rather than the peak water demand. Because the WDC tool (mentioned in Part 2) gives peak flow rates but not daily water volumes, a different approach was needed to simulate the volume of hot water drawn during household fixture use. The Poisson Rectangular Pulse (PRP) concept developed by Buchberger and Wu (1995) was used to generate indoor residential hot water pulses on a 1-second time scale. The generated demands were input to the public domain computer code EPANET to simulate instantaneous hot water use at fixtures inside a typical household for a period of one year. Figure 3 shows the flowchart linking PRP water demands with EPANET.

Simulating PRP Demand Pulses

With the PRP approach, residential users are assumed to arrive during hour j at household fixture group k according to a Poisson process with a constant rate $\lambda_{j,k}$ given by,

$$\lambda_{j,k} = \pi_{j,k} \left(\frac{Q_k}{\alpha_k \tau_k} \right) \quad [1]$$

In this expression, $\pi_{j,k}$ is the dimensionless hourly multiplier reflecting the diurnal demand pattern of indoor water use at fixture group k (see Figure 4). Q_k is the average continuous 24-hr base demand for a *single* fixture in group k (see Table 4). The denominator in Equation [1] is the product of the mean intensity α_k and mean duration τ_k of the water pulse for fixture group k (see Table 5). The four terms on the right-hand-side of Equation [1] were estimated from residential water use information in the IAPMO database.

The 24-hr base demand for a *single* fixture in fixture group k having n_k identical fixtures is given by,

$$Q_k = \frac{V_k^* / n_k}{1440 \text{ minutes/day}} \quad [2]$$

Where V_k^* is the average volume of water used per day at a fixture group of n_k identical fixtures. If V_k^* is expressed as gallons per day, then the resulting value for Q_k given in Equation [2] is gpm per fixture.

The dimensionless multiplier during hour j for fixture group k is the ratio of the hourly consumption at the fixture group $V_{j,k}$ to the average volume of water used per hour at the fixture group and is given by.

$$\pi_{j,k} = \frac{V_{j,k}}{V_k^* / 24} \quad [3]$$

At each fixture group k , the daily average of the hourly multipliers is unity, $\frac{1}{24} \sum_{j=1}^{24} \pi_{j,k} = 1.0$

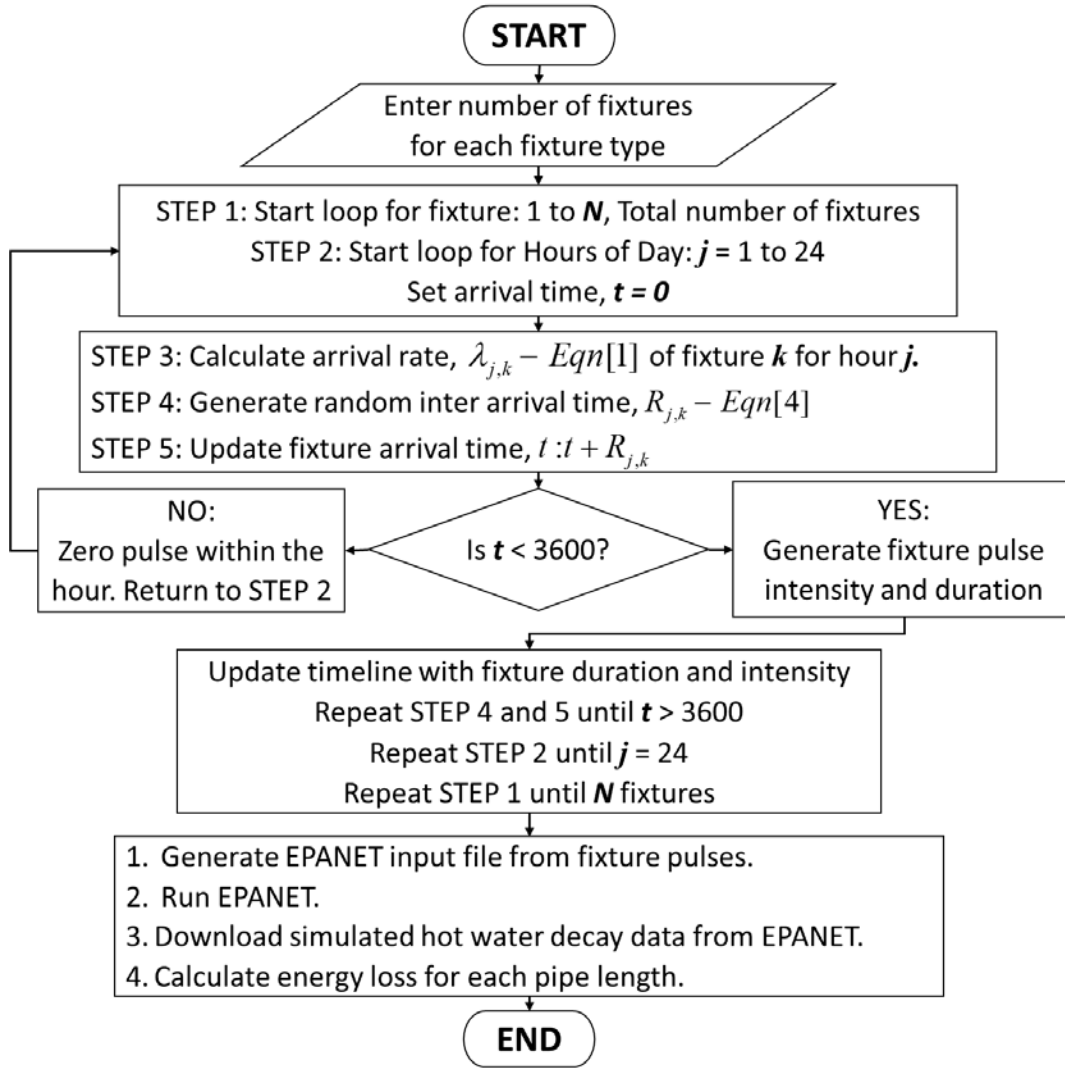


Figure 3: Flowchart to generate PRP pulses necessary and perform hydraulic simulations in EPANET. Since the arrival rate at a fixture follows the Poisson process, the time between water pulses is exponentially distributed. The time $R_{j,k}$ between consecutive pulses during hour j at fixture group k is

$$R_{j,k} = -\frac{\text{Ln}(U)}{\lambda_{j,k}} \quad [4]$$

where U is a uniform random variable between $[0, 1]$. For generated pulse arrivals, random pulse intensities and duration are simulated with a log-normal distribution. The necessary parameters to simulate fixture pulse characteristics using the PRP method were derived from the IAPMO data set for six unique fixtures groups identified in the IAPMO database. Each fixture was categorized as

either efficient or inefficient based on the water consumption per use. Table 3 shows the fixture classification criteria. Note that Bathtubs and Faucets (Kitchen sink and Lavatory) were not categorized by efficiency.

Table 3: Criteria for fixture efficiency

Fixture	Efficiency Criteria	Efficient Fixtures	Inefficient Fixtures
Clothes water	Gallon per load	≤ 30	> 30
Dishwasher	Gallon per use	≤ 3	> 3
Shower	Gallon per minute	≤ 2.5	> 2.5

The fixture PRP parameters namely daily base flow, mean and standard deviation of pulse intensity and duration are in Tables 4 and 5, respectively. Results from the water use survey showed a slight difference in weekend water use consumption and patterns when compared to weekday water use. Hence, the simulations of demand pulses included the weekday-weekend effect using the fixture base flows in Table 4 and multipliers shown in Figure 4 to generate the arrival rate at a fixture. There was no difference in the pattern of water use between efficient and inefficient fixtures.

Table 4: 24-hour base demand for individual fixtures in six fixture groups in single-family home

Fixture	Inefficient Fixtures (gpm)		Efficient Fixtures (gpm)	
	Weekday Base Flow	Weekend Base Flow	Weekday Base Flow	Weekend Base Flow
Bathtub	0.0035	0.0040	0.0035	0.0040
Clothes washer	0.0243	0.0364	0.0130	0.0198
Dishwasher	0.0018	0.0020	0.0017	0.0020
Faucet*	0.0055	0.0060	0.0055	0.0060
Shower	0.0149	0.0162	0.0120	0.0131
Water Closet	0.0158	0.0172	0.0080	0.0092

* Faucet represents both kitchen sink and lavatory

Table 5: PRP fixture parameters - Pulse characteristics

Fixture	Pulse characteristics	Inefficient Fixtures		Efficient Fixtures	
		α , Intensity (gpm)	τ , Duration (minutes)	α , Intensity (gpm)	τ , Duration (minutes)
Bathtub	<i>Average</i>	4.47	4.99	4.47	4.99
	<i>Standard dev.</i>	1.22	2.73	1.22	2.73
Clothes washer	<i>Average</i>	3.79	12.96	2.36	10.54
	<i>Standard dev.</i>	0.95	2.98	0.90	2.33
Dishwasher	<i>Average</i>	1.16	4.06	1.02	2.05
	<i>Standard dev.</i>	0.27	2.22	0.26	0.59
Faucet*	<i>Average</i>	0.97	0.61	0.97	0.61
	<i>Standard dev.</i>	0.23	0.22	0.23	0.22
Shower	<i>Average</i>	3.14	7.26	1.87	8.55
	<i>Standard dev.</i>	0.56	2.64	0.33	2.85
Water Closet	<i>Average</i>	2.78	1.29	2.14	0.91
	<i>Standard dev.</i>	0.75	0.54	0.57	0.34

* Faucet represents both kitchen sink and lavatory

Note that different methods were employed to arrive at the parameters for the WDC and the PRP method. The fixture peak hour p -values shown in Table 1 were estimated from fixture duration of use, while the fixture base flow (see Table 4) and hourly multipliers (see Figure 4) were estimated from the volume of water use at the fixture.

Since the IAPMO database did not distinguish between water use at the lavatory and kitchen sink, the PRP parameters for faucet were applied to generate arrival times for both the lavatory and the kitchen sink. About 20 percent of the measured faucet flow rates in the database was greater than 2 gpm. Therefore, the arrivals at faucet were split 80-20 for pulses at a lavatory and kitchen sink respectively. For example, only 80 percent of the arrivals at a lavatory was actual water use pulses at the lavatory. Similarly, only 20 percent of arrivals at a kitchen sink were actual pulses at the kitchen sink. The kitchen sink pulse characteristics were 1.52 (\pm 0.50) gpm and 1.01 (\pm 0.52) minute for the intensity and duration of flow respectively.

The simulated frequency and volume of hot water demand pulses at fixtures were remarkably similar to the expected values based on the input parameters supplied in Tables 4, 5 and Figure 4. Table 6 shows good agreement between the expected and simulated daily fixture frequency of use

and volume. The difference between the expected and simulated daily number of events and volume was less than ± 2 percent. Also, the small standard error indicates the accuracy of the mean simulated pulse arrivals and pulse characteristics.

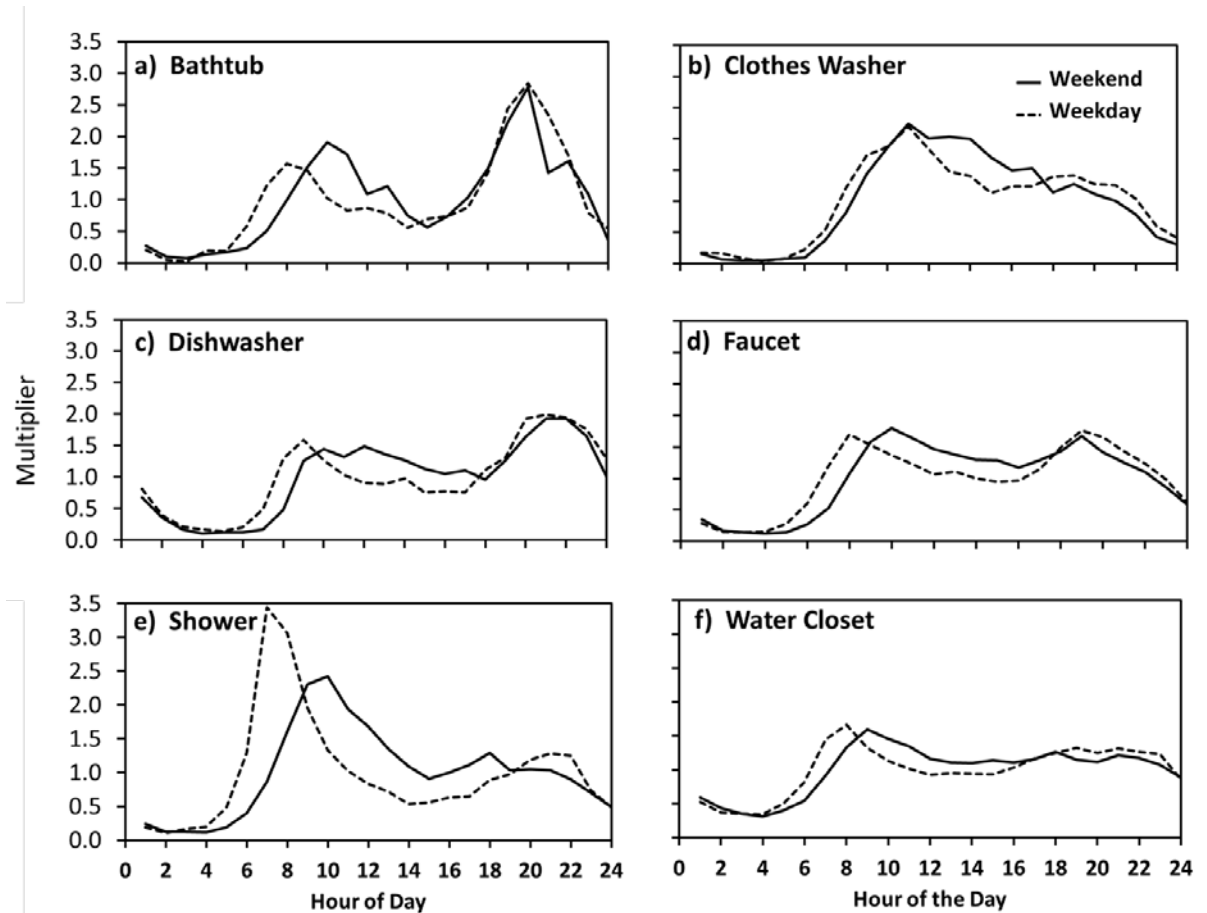


Figure 4: Fixture demand multipliers for weekday and weekend water use

Table 6: Expected and simulated pulse characteristics for hot water fixtures

Fixtures	[A] Expected		[B] Simulated		Percentage difference between [A] and [B]		Standard error in simulation	
	Events /Day	Hot Water Volume/Day (gallons)	Events /Day	Hot Water Volume/Day (gallons)	Events /Day	Volume /Day	Events /Day	Volume /Day (gallons)
Bathtub	0.23	4.52	0.23	4.61	-1.3	1.9	0.02	0.47
Clothes washer	0.95	16.14	0.94	15.82	-1.1	-2.0	0.05	1.04
Dishwasher	1.26	2.64	1.27	2.65	0.7	0.5	0.06	0.13
Kitchen Sink	2.75	3.30	2.77	3.36	0.9	1.9	0.09	0.13
Lavatory	10.98	5.13	10.94	5.12	-0.4	-0.3	0.17	0.09
Shower	1.11	15.43	1.11	15.38	0.1	-0.3	0.06	0.83

EPANET Setup

EPANET has a minimum 1-minute timescale for its hydraulic simulations. Therefore, the fixture pulses generated on a 1-second scale were consolidated into a 1-minute time scale before performing hydraulic simulations in EPANET. The duration of the pulse flow was rounded to the nearest minute (i.e., 85 seconds is rounded down to 1 minute, while 95 seconds rounded up to 2 minutes). To preserve the simulated pulse volume, the pulse intensity was adjusted to fit the new pulse duration (See Figure 5).

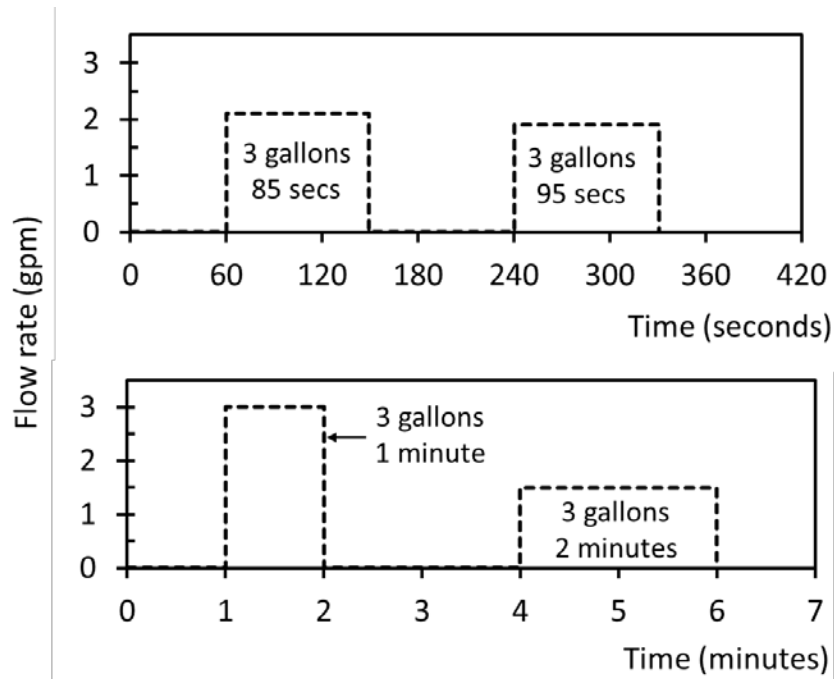


Figure 5: Illustration of adjusted pulse duration with preserved mass

The EPANET first-order decay function for chlorine concentration was applied to simulate hot water cooling in pipes. Depending on the pipe size and material, the rate at which heat dissipates through the pipe wall differs. The decay coefficient, k_d of heat through copper L pipes as shown in Table 7, was calculated using Equation [5] for the different pipe sizes. Note that Equation 5 is a derived expression from combining the heat capacity formula $Q = mc\Delta T$ and heat transfer formula $Q = \frac{kA\Delta T}{d}$. A step by step procedure can be found in Omaghomi (2018) - in review. These derived decay coefficients for copper L pipes are the bulk coefficient for each link in the EPANET network setup.

$$k_d = \frac{AU_o}{m_l C_p} \quad [5]$$

Where $U_o = 1 / \left(\frac{D_o}{D_i h_w} + \frac{D_o \ln(D_o/D_i)}{2k} + \frac{1}{h_{air}} \right)$

$$h_{air} = h_{cov} + h_{rad}$$

$$h_{cov} = 0.27 \left[\frac{|T_s - T_a|}{D_o} \right]^{0.25}$$

$$h_{rad} = \frac{\epsilon \times 0.1714 \times 10^{-8} [(T_a + 459.6)^4 - (T_s + 459.6)^4]}{(T_a - T_s)}$$

Dull $\epsilon = 0.44$, Bright $\epsilon = 0.08$

Stefan-Boltzman Constant = $0.1714 \times 10^{-8} \left(\frac{Btu}{hr-ft^2-R^4} \right)$

Table 7: Heat decay coefficient for different sizes of uninsulated Copper L pipes from equation [5]

Nominal pipe size (inches)	1/4	3/8	1/2	3/4	1	1-1/4	1-1/2	2
k_d, Heat decay coefficient, (day⁻¹)	129	87.5	65.5	41.7	30.1	23.4	19.0	13.7

Other assumptions considered for running EPANET are the desired temperature depending on the type of fixture and the ambient water temperatures as detailed in Tables 8 and 9.

Table 8: Typical hot water temperatures at fixtures and implied hot/cold water mix

Fixture	Usage Temperature (°F)	% Hot	% Cold
Bath Filling	95	63	37
Clothes washer (hot)	118	100	0
Clothes washer (warm)	87	51	49
Dishwasher	118	100	0
Faucet	105	79	21
Shower and Tubs	110	87	13

NOTE:

Hot Water Temperature (°F) 118

Cold Water Temperature (°F) 55

- Fixture usage temperatures are based on recommendations from ASHRAE Applications Handbook.
- Cold water temperature represents an annual average temperature for Cincinnati Ohio adopted from US Climate Data.
- Cold water temperature was used ONLY to estimate the mixing ratio of hot to cold water for a usage temperature.
- Clothes washer warm wash temperature is assumed to be a simple average of cold and hot water temperatures.
- Water heater set temperature is assumed to be 120 (°F).
- Clothes washer (hot) and dishwasher are set at maximum temperature.

Table 9: Cincinnati mean monthly temperatures (U. S. Climate Data 2017)

Month	Temperature (°F)	Month	Temperature (°F)
January	30.5	July	76.5
February	35.5	August	74.5
March	44.5	September	68.0
April	54.0	October	55.5
May	64.0	November	45.5
June	72.5	December	35.4

Energy Calculations

For this research, the energy calculations on heated water are focused on hot water distribution system (HWDS) excluding the water heater. Figure 6 shows two different outcomes of energy in hot water after it has left the heater: it is dissipated (between uses) along the pipe, or it is delivered (during use) to the end use fixture. The water heater is assumed to be 100 percent efficient, always delivering hot water at a set temperature of 120 °F. The pipes in HWDS are a control volume in which previously heated water cools to room temperature. It is assumed that there is no water loss from leaking pipes and no extra energy is required to move the water through the HWDS. Other assumptions relevant to the calculations are, water temperature is constant across the pipe length, the effect of longitudinal mass dispersion (or energy) is ignored as EPANET assumes plug flow, and finally, the pipes are not insulated. The ambient temperatures were also assumed to be constant throughout the month. The water temperature at the fixture during use represents actual usage temperature, needed to calculate the energy delivered. The water temperature in the pipes was used to calculate the energy dissipated between uses.

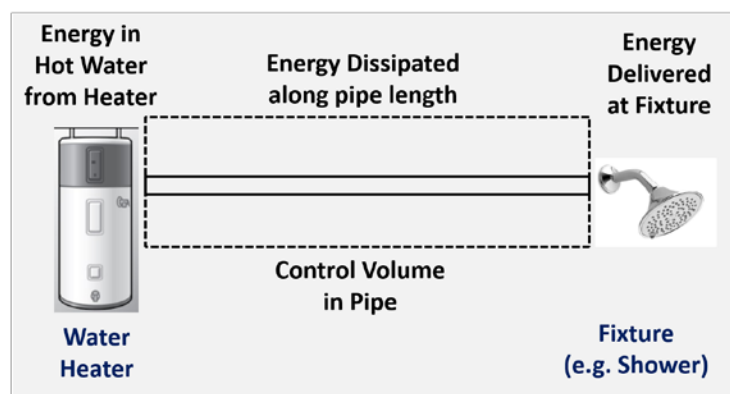


Figure 6: Energy balance in a building's pipe network

The energy consumed related to hot water demand was analyzed for the HWDS in a 2-bath residential building for the following four scenarios:

- (i) inefficient fixtures versus efficient fixtures,
- (ii) trunk-and-branch versus manifold layout with efficient fixtures,
- (iii) pipe sizes determined by the current practices (Hunter’s curve) versus improved estimates (WDC) and,
- (iv) hot water use per unit in a multi-unit building versus single unit building.

Since energy is conserved, the energy required to raise the temperature of one gallon of water through 1 °F is the energy dissipated when the temperature of one gallon of water cools by 1 °F. Therefore, the total energy delivered and dissipated from a hot water draw is calculated using Equation [6].

$$E_{Total} = \int_t c_p \dot{m} \Delta T_i dt + \int_t A U_o \Delta T_i dt \quad [6]$$

$E_1 \qquad E_2$

Note that the calculation differentiates between flowing and zero-flow states. In a zero-flowing state, $\dot{m} = 0$ so the flow-dependent term (first part of Equation [6]) disappears. The second part of Equation 6 (E_2) is the heat loss through the pipes in the flowing and zero-flow states. E_2 is calculated by integrating the heat transfer rate through the pipe over time, t .

In a trunk-and-branch network, there are situations where the cooling of hot water in a pipe with multiple fixtures downstream is interrupted by another hot water pulse from a different fixture. The energy loss in the shared pipe is assigned to the fixture with the most recent pulse until another fixture becomes active. For instance, Link 10 in Table 2 is shared by the lavatory and tub/shower-nodes 7 and 8 respectively. Figure 7 shows overlap in heat loss from the 2nd and 6th pulse. The energy dissipated after the 2nd and 6th pulses will be attributed to node 7 even if the heat from the 1st and 5th pulse at node 8 primed the system.

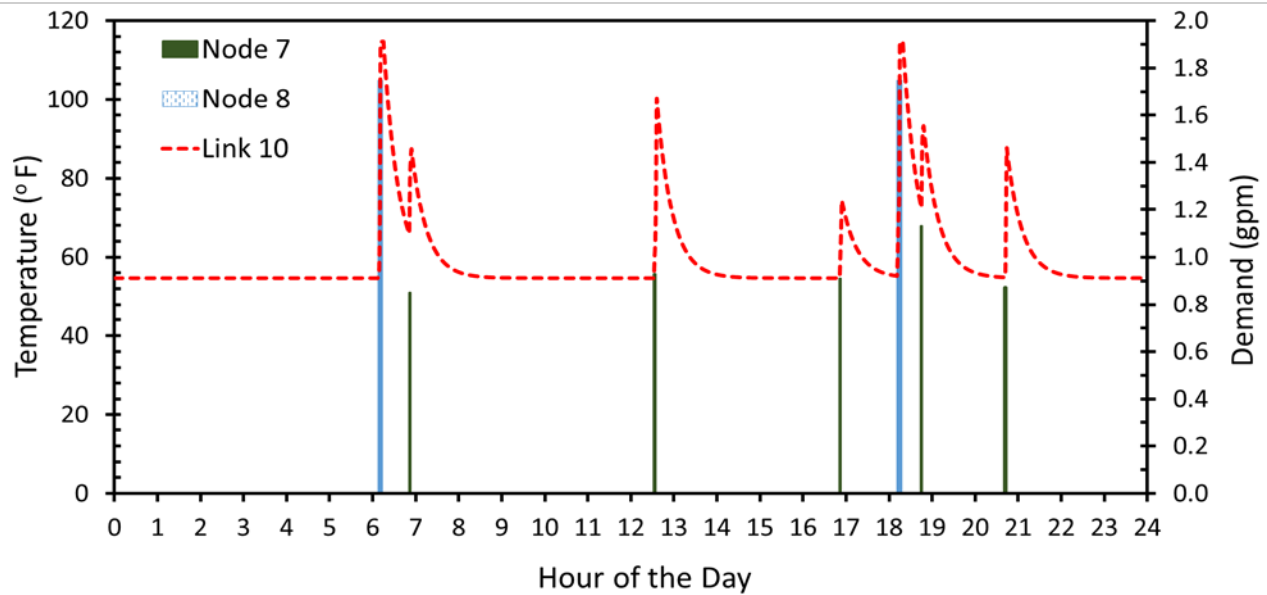


Figure 7: 24-hour timeline of hot water demand pulses and temperature decay resulting from the use of two fixtures in a 2-bath unit in Figure 2a

RESULTS AND DISCUSSION

EPANET was used to simulate the flow and change in temperature of hot water through a typical 2-bath premise plumbing system. The water use demands at individual fixtures were generated using the PRP process. Temperature readings were taken at the fixtures and their connecting pipes. Results for simulated hot water demand pulse and the energy consumed are summarized in Tables 10, 11 and 12 for various scenarios concerning fixture efficiency, network configuration and network sized by current practice and improved estimates. The total energy entering the pipes as hot water was categorized into two parts: Energy utilized at the fixtures due to hot water delivered (E_1), and energy dissipated due to heat loss through the pipe walls (E_2).

Inefficient and Efficient Fixtures

Due to only fixture efficiency, Figure 8 and Table 10 shows a 30.6 percent reduction in the volume of hot water consumed and a corresponding 30.6 percent reduction in total energy consumed. The amount of annual savings in energy is directly related to the reduction of hot water delivered.

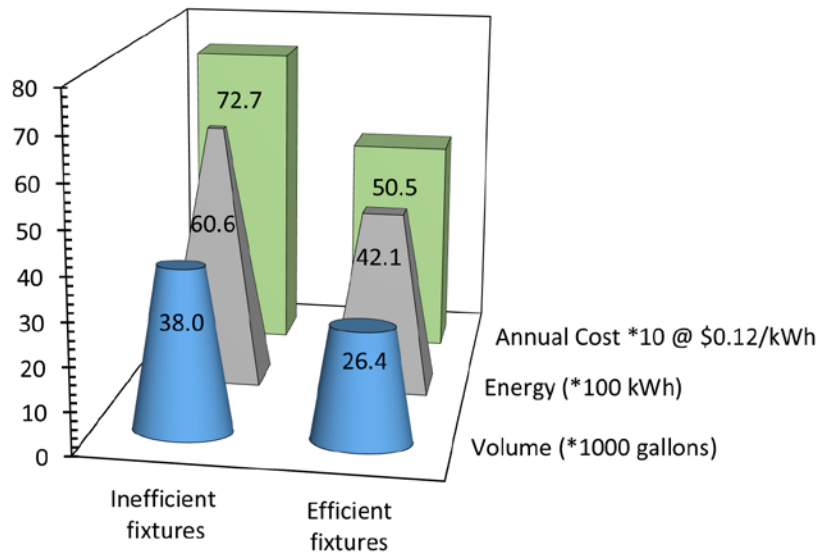


Figure 8: Annual hot water volume, energy consumed and energy cost in a 2-bath home with inefficient and efficient water fixtures

Premise Plumbing Configuration

The effect of pipe size is important when comparing the annual energy consumed in a 2-bath building with a trunk-and-branch network to a similar building with a manifold network with efficient fixtures. In the manifold network, each fixture had a dedicated pipe that runs the full length as the corresponding fixture in the trunk-and-branch layout (see Figures 2a and 2b).

The total length of pipes in the manifold layout was 263.2 feet holding 4.1 gallons of water, while the trunk-and-branch layout was 142.5 feet with 3.1 gallons of water. However, for the hot water line to any given fixture, the volume of the manifold layout never exceeded the volume of water in the trunk-and-branch layout. This means that, during a hot water use event, less water required flushing, thus hot water was delivered at higher temperatures to the fixtures in the manifold system. Furthermore, owing to its smaller pipe volume, the heat lost during waiting periods between hot water demand was less for the manifold system than the trunk and branch system. Table 11 shows the average annual energy delivered (E_1) in the manifold network was 11.3 percent greater than the trunk-and-branch layout, meanwhile the average annual energy loss in the pipe (E_2) reduced by 5.9 percent.

Table 10: Annual hot water/energy consumed in a 2-bath residence with trunk-and-branch network sized by Hunter's curve and new WDC

Scenario	Statistics	Volume (gallons)	E ₁ (kWh)	E ₂ (kWh)	Total Energy Consumed (kWh)	Percentage Difference in Average Volume	Percentage Difference in Average Total Energy Consumed
Hunters Curve and Inefficient Fixture	Average	38050	4260	1380	6060	Reference Case	
	Standard dev.	849	112	7	132		
Hunters Curve and Efficient Fixture	Average	26400	2640	1360	4210	- 30.6	- 30.6
	Standard dev.	483	66	8	75		
New WDC and Efficient Fixture	Average	26400	2670	1230	4210	- 30.6	- 30.6
	Standard dev.	483	65	7	75		

Table 11: Annual hot water/energy consumed in a 2-bath residence with trunk-and-branch and manifold pipe network sized with a new WDC method

Scenario	Statistics	Volume (gallons)	E ₁ (kWh)	E ₂ (kWh)	Total Energy Consumed (kWh)	Percentage Difference in Energy Delivered	Percentage Difference in Energy Dissipated
New WDC and Efficient Fixture	Average	26400	2670	1230	4210	Reference Case	
	Standard dev.	483	65	7	75		
Trunk-and-Branch Layout	Average	26400	2670	1230	4210		
	Standard dev.	483	65	7	75		
Manifold Layout	Average	26400	2970	1160	4210	11.3	- 5.9
	Standard dev.	483	70	7	75		

Table 12: Annual hot water/energy per unit consumed in a building with 2-bath units sized with the new WDC method

Scenario	Statistics	Volume (gallons)	E ₁ (kWh)	E ₂ (kWh)	Total Energy Consumed (kWh)	Percentage Difference in Average Volume	Percentage Difference in Average Total Energy Consumed
1 Unit/ Building	Average	26400	2670	1230	4210	Reference Case	
	Standard dev.	483	65	7	75		
2 Units/ Building	Average	26450	2740	1320	4220	0.18	0.23
	Standard dev.	370	52	8	59		
4 Units/ Building	Average	26480	2710	1360	4220	0.28	0.33
	Standard dev.	299	41	5	48		

NOTE: The terms E₁ and E₂ are as described in Equation 6

Pipe Sizing Method

Updating the peak demand estimates and right-sizing the premise plumbing accordingly (improved method) for a 2-bath home resulted in an 18 percent decrease in the total volume of hot water within the distribution network. There was a mix of increase and decrease in single fixture pipe size. For the 2-bath home example, the decrease in volume is largely from pipes serving two or more fixtures downstream. Reduced pipe sizes result in a corresponding decrease in the waiting time or hot water at a fixture, given the same flow rate.

As shown in Table 7, the heat decay coefficient of a small pipe is greater than those of larger pipe (e.g., 65.5 per day for 1/2" pipe and 41.7 per day for a 3/4" pipe). Given the same demand pulse characteristics and pipe length between the heater and a fixture, the temperature at a fixture will differ solely due to the pipe size difference. The temperature of hot water delivered at a fixture with a smaller pipe will be slightly lower than that of a similar fixture at the end of a larger pipe. The higher heat decay coefficient in smaller pipes are responsible for the higher rate of heat loss from the pipes.

Due to the difference in pipe sizes from the pipe sizing methods, about 1 percent increase in the annual energy delivered and 9.7 percent decrease in the annual energy dissipated can be calculated from the values in Table 10. Depending on the fixture efficiency, pipe sizing method and pipe layout, the average annual energy consumed related to pipe characteristics (E_2) accounted for about 23 percent to 32 percent of the total annual energy consumed. Correspondingly, the bulk of the annual energy consumed related to water heating, i.e. energy delivered (E_1), accounted for about 62 percent to 70 percent of the total annual energy consumed.

Building Size

The energy simulations were extended to buildings with multiple of 2-bath units to investigate hot water and energy consumption in larger buildings. The national average annual energy consumed due to water heating was 4,471 kWh and 5,403 kWh per single-family household attached and detached respectively (US EIA 2013). In the same report, the average annual energy consumed by water heating decreased per household for multi-apartment buildings. The results

in Table 12 show no notable change in the average annual energy consumed per unit in buildings with 2 or 4-units. This is because the demand pulses for the multi-unit building were simply multiple simulations of hot water use in a single unit.

Although this research did not report any effect of reduced pipe size on energy consumption in multi-apartment buildings, Table 13 shows there will be significant reductions in the expected demand and the corresponding pipe size for pipe mains supplying water to multiple units. There is greater than 47 percent reduction in estimated demand leading to a drop in two or more pipe sizes in larger buildings with multiple units.

Table 13: Pipe sizes for water demand in large buildings

Building Size: Number of Units	Number of Fixtures	Hunters Curve		New WDC		Percentage Decrease in Expected Flow	Number of Pipe Size Drop
		Demand (gpm)	Pipe Size (inches)	Demand (gpm)	Pipe Size (inches)		
1	11	17	1-1/4	9	1	-47.1	1
2	22	29	2	11	1	-62.1	3
4	44	44	2	15	1-1/4	-65.9	2
10	110	75	3	22	1-1/2	-70.7	3
20	220	125	3-1/2	35	2	-72.0	3
50	550	240	5	71	2-1/2	-70.4	4
100	1100	375	6	125	3-1/2	-66.7	3

These results are subject to the following limitations:

- Fixture parameters extracted from the IAPMO database were calculated per unit fixture. No adjustments were made based on the number of residents in the surveyed households. Therefore, the simulated demand pulses are representative of an average of 2.72 residents per household.
- A Lutz (2005) discussed, 20 percent of hot water wasted. The IAPMO water use database had results for all water use events (cold and hot). Therefore, the fixture pulse parameters from the IAPMO database already incorporates the peculiar human behavior of waiting for hot water. The energy delivered (E_1) in this report accounts for both wasted and useful hot water.

CONCLUSION

Hot water distribution is a key component of premise plumbing. It is therefore important to understand how changes in fixture efficiency and pipe sizing affect hot water and energy consumption in residential buildings. In this study, the generation of realistic hot water pulses at individual fixtures using MATLAB and simulation of temperature changes within pipes using EPANET provided clear insights on the water/energy implications of right-sized premise plumbing systems.

Sizing pipes with the new WDC method reduce the amount of water between the heater and a fixture, thus minimizing structural waste by reducing the waiting time for hot water at a fixture. Similarly, the use of efficient fixtures in rightly-sized premise plumbing systems reduces water and energy consumption associated with hot water use in the building. The 2-bath example in this report shows a 30 percent reduction in annual energy consumed resulting in about \$222 of annual cost saving for a single-family residence at a Cincinnati rate of \$0.12/kWh.

Review of simulated short duration, low flow pulses especially at the lavatory and kitchen sink reveals that only about half of the hot water drawn from the heater is delivered to the fixture. This result is consistent with field observation of Lutz *et al.* (2014).

If the time between consecutive hot water use exceeds two hours, the hot water line will cool to room temperature. In this case, energy added by the water heater does not reach the end use, but instead dissipates along the supply line. Insulating pipes will reduce the rate of heat loss in the pipe. Investigating the effect of insulated pipes on the total energy consumed is suggested to quantify the cost-effectiveness of hot water pipe insulation. EPANET does not simulate longitudinal mass or heat dispersion in pipes. Future work should consider comparing measured hot water pulses to EPANET simulated water demands to assess the importance of including dispersion when simulating the temperature of the water reaching a fixture.

REFERENCES

- Agudelo-Vera, C., Pieterse-Quirijns, I., Scheffer, W., and Blokker, M. (2014). "Water and Energy Nexus at the Building Level." *REHVA Journal*, 12-15.
- ANSI/ASHRAE Standard -188. (2015). "Legionellosis: Risk Management for Building Water Systems." *ASHRAE*: <https://www.Ashrae.Org/>.
- ASHRAE. (1987). *American Society of Heating, Refrigerating and Air-Conditioning Engineers Handbook*. American Society of Heating, Refrigerating, and Air-Conditioning Engineers, Inc., Atlanta, GA.
- AWWA. (2004). *Sizing Water Service Lines and Meters: Manual of Water Supply Practices (M22)*. American Water Works Association, Denver, CO.
- Buchberger, S., and Wu, L. (1995). "Model for Instantaneous Residential Water Demands." *J.Hydraul.Eng.*, 121(3), 232-246.
- Buchberger, S., Omaghomi, T., Wolfe, T., Hewitt, J., and Cole, D. (2017). "Peak Water Demand Study: Probability Estimates for Efficient Fixtures in Single and Multi-family Residential Buildings " *Rep. No. Executive Summary*, IAPMO, Online.
- Coomes, P., Rockaway, T., Rivard, J., and Kornstein, B. (2010). "North America Residential Water Usage Trends Since 1992 ." Water Research Foundation, Denver, CO; 148 p; accessed May 30 2015 at <http://www.waterrf.org/PublicReportLibrary/4031.pdf>.
- Hiller, C. C. (2012). "Comparison of Heat Loss and Water Waste Characteristics of Bundled vs. Single Pipe Hot Water Distribution Systems." *ASHRAE Trans*, 118(1), 901-907.
- Hunter, R. B. (1940). "Methods of Estimating Loads on Plumbing Systems." *Rep. No. BMS65*, US National Bureau of Standards, Washington DC.
- Klein, G. (2013). "Efficient hot-water piping: smarter layouts and right-sized pipes save time, water, and energy." *The Journal of Light Construction*, 31(6), 73.
- Lutz, J. (2005). "Estimating Energy and Water Losses in Residential Hot Water Distribution Systems." *Rep. No. Paper LBNL-57199*, Lawrence Berkeley National Laboratory, University of California, Berkeley, CA.
- Lutz, J., Lanzisera, S., Liao, A., Fitting, C., Stiles, C., and Kloss, M. (2014). "Reducing Waste in Residential Hot Water Distribution Systems." *Rep. No. CEC- 500-2015-004.*, California Energy Commission, Lawrence Berkeley National Laboratory, CA.

NIBS. (2012). "Moving Forward: In-Depth Findings and Recommendations from the Consultative Council." National Institute of Building Science, 2012 Consultative Council Report.

Omaghomi, T., and Buchberger, S. (2014). "Estimating Water Demands in Buildings." *Procedia Engineering*, 89(0), 1013-1022.

Omaghomi, T. (2018). "Estimating Peak Water Demand in Buildings with Efficient Fixtures: Methods, Merits, and Implications". University of Cincinnati, Cincinnati, Ohio.

Price, J. I., Chermak, J. M., and Felardo, J. (2014). "Low-flow appliances and household water demand: An evaluation of demand-side management policy in Albuquerque, New Mexico." *J. Environ. Manage.*, 133(0), 37-44.

Siddiqi, A., and Fletcher, S. (2015). "Energy Intensity of Water End-Uses." *Curr Sustainable Renewable Energy Rep*, 2(1), 25-31.

U. S. Climate Data. (2017). "Climate Cincinnati - Ohio." <https://www.usclimatedata.com/climate/cincinnati/ohio/united-states/usoh0188> (August 28, 2017).

U.S. Energy Information Administration. (2015). "Monthly Energy Review - June 2015." *Rep. No. DOE/EIA -0035(2015/06)*, U.S. Energy Information Administration, 214 p, accessed: June 30, 2015 at <http://www.eia.gov/totalenergy/data/monthly/>.

US EIA. (2013). "Residential Energy Consumption Survey (RECS) 2009 Survey Data." U S Energy Information Administration, accessed August 20, 2017 at <https://www.eia.gov/consumption/residential/data/2009/index.php?view=consumption#end-use>.

Vieira, A. S., Beal, C. D., and Stewart, R. A. (2014). "Residential water heaters in Brisbane, Australia: Thinking beyond technology selection to enhance energy efficiency and level of service." *Energy Build.*, 82(0), 222-236.

Wistort, R. A. (1994). "A new look at determining water demands in building: ASPE direct analytic method." *American Society of Plumbing Engineers Convention*, Kansas City, MO, 17-34.

Baseline measurements of methane emissions from Piedmont Lake - current and future fracking area

Basic Information

Title:	Baseline measurements of methane emissions from Piedmont Lake - current and future fracking area
Project Number:	2016OH507B
Start Date:	3/1/2016
End Date:	2/28/2018
Funding Source:	104B
Congressional District:	3
Research Category:	Climate and Hydrologic Processes
Focus Categories:	Climatological Processes, Non Point Pollution, Wetlands
Descriptors:	None
Principal Investigators:	Gil Bohrer

Publication

1. Vines C, Rey Sánchez AC, Bohrer G. Using footprint analysis to determine flux measurements source over a heterogeneous surface. Poster, 10/2017. Fifth Annual Water and Land Symposium at Kent State University, Kent, OH.

Final Report 2016-2018

Contract Information

Title	Baseline measurements of methane emissions from Piedmond Lake - current and future fracking area
Project Number	G16AP00076
Start Date	3/1/2016
End Date	2/28/2018 (including a 12 Month no-cost extension)
Lead Institute	The Ohio State University
Principal Investigators	Gil Bohrer

Abstract

Methane is the second most important green-house gas (GHG). Methane is emitted from natural wetlands ad lakes, and also from natural gas extraction and production operations. The large uncertainty surrounds both the quantity and mechanisms producing natural methane emissions from lakes and wetlands, and fugitive methane emissions during hydrofracking, compound in areas where fracking is conducted near and/or under lakes and wetlands. In such cases, there is a strong need for baseline observations of the natural emissions which will be used to distinguish those from additional emissions, if present, related to fracking.

The direct result of this project will be the development of a dataset of observations of baseline emissions from Piedmont Lake, OH, and an empirical model for the emission rates from the lake. Though the modelling approach is general and could be applied anywhere, we will use the depth of data at our field site in the 4H camp at the shore of Piedmont Lake, near future potential fracking sites. Some of the area around the lake was cleared for fracking activity, and production may start in the next few years.

Methodology

- 1) The establishment of an OSU fracking research site in Piedmont Lake by the USEEL center has failed and an OSU site will not exist. Our project was leveraging on that site, and therefore, we were forced to locate a flux tower with measurements of methane emissions.
- 2) A site to locate methane measurements was set up in partnership with Derrek Johnson in West Virginia University. A 20 m tall flux tower was located downwind a planned well pad locations near Morgantown West Virginia. The tower is relatively tall to allow a wide footprint area (Figure 1).
- 3) Ongoing measurements of meteorological conditions (air temperature, pressure and humidity, wind, precipitation and incoming radiation) and methane and CO₂ fluxes using eddy-flux are conducted continuously at the West Virginia site since 7/2017 and will continue until 12/2018. The tower includes an LI7700 open path methane analyzer, and a closed path isotopic methane analyzer. This tower was funded by NSF.
- 4) A campaign for chamber measurements of the fluxes from the river near the tower and fracking site will start in May 2017 and be repeated monthly June-September 2018.
- 5) We used the EC measurements with a neural network modeling approach to model the baseline fluxes before the start of fracking activity. We will identify fracking related peaks as

peaks above the baseline after the start of fracking. Fracking-related peaks will also have an isotopic signature indicative of fossil methane source.

- 6) We will use a large eddy simulation model (PALM) to combine chamber and EC flux measurements to determine the potential source locations of emission peaks.

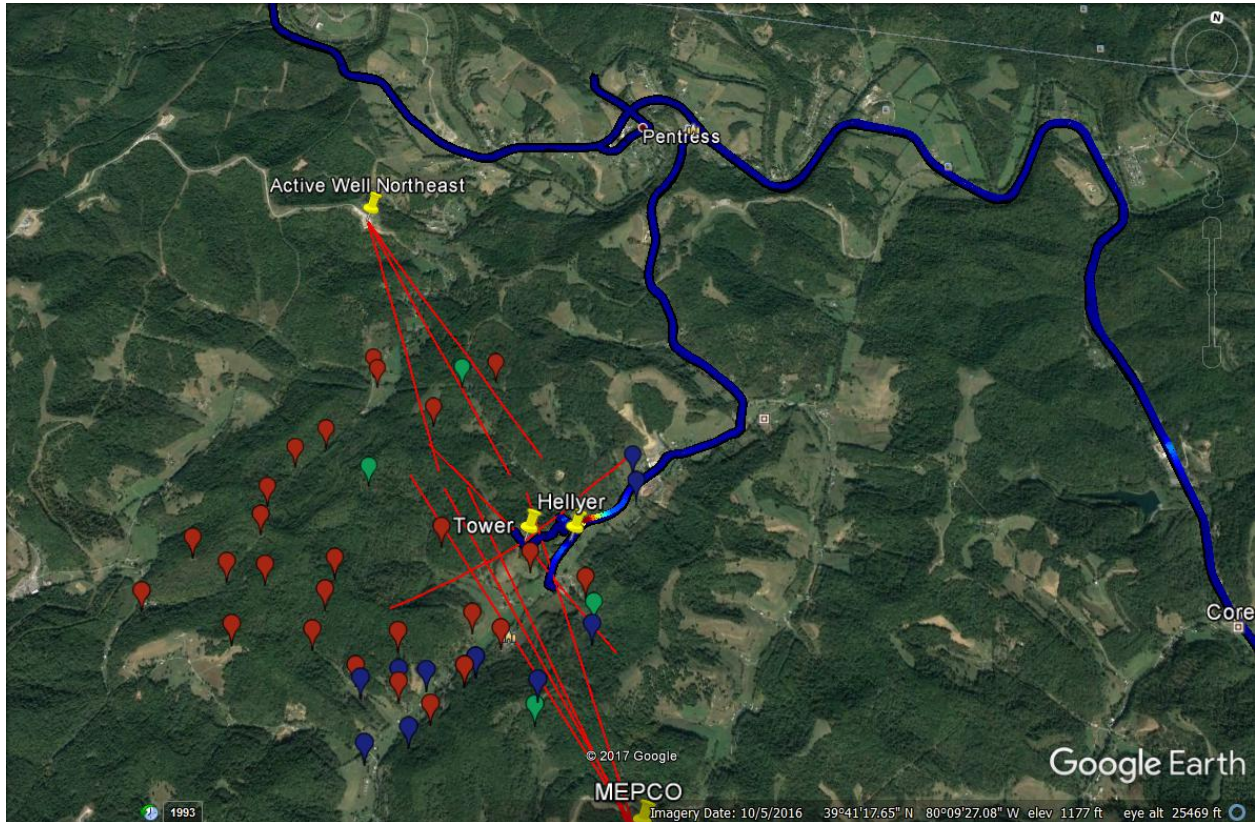


Figure 1. A site for the flux tower was established in Pentress WV. A 20 m tall flux tower was constructed and instrumented (yellow tack "Tower"). The closest active and planned fracking pads (yellow tack marks), planned horizontal fracking well paths (red lines), abandoned wells (blue markers), plugged wells (red markers), and active wells (green markers) are illustrated. A campaign for measurement of methane concentrations in the air using the West Virginia Mobile air quality lab was conducted in 5/2017. The mobile lab drove from WVU campus in Morgantown to our tower site, and around the county roads near or tower site. Methane concentrations are illustrated in color (blue - ambient, near 0 to red - high concentrations) along a thick line overlaying the mobile lab sampling path. We found clean (low methane concentrations) throughout the region, except when in proximity to some active wells.

Major Activity

Unfortunately, the NETL project has failed to secure a study site and activities in the USEEL Will not be possible. Therefore, it was impossible for us to start our fieldwork at the planned project period. A 1-year no-cost extension for the project was requested and approved. We have secured an alternative field site in collaboration with Prof. Derek Johnson in West Virginia University. The site is near Morgantown WV, on private land, near a fracking pad (Fig 1). Fracking activity has started in December 2017, a few months after we started measuring the baseline emissions. This project provide an additional components of chamber measurements in

a larger NSF-funded project that will fund the construction of a flux tower and the flux analysis activity. A subcontract from the NSF funding was signed with WVU and field work at the new site started in May 2017. The tower construction was completed and the site is fully operational and reporting data since July 2017. We have been coordinating the tower construction planning through teleconference with Derek Johnson in WVU. We have secured an agreement with the Olentangy River Wetland Research Center for access to the GCMS for analyzing the chamber observations and in the process of preparing the needed supplies for the chamber measurement campaign (sterilizing and evacuating vials).

Findings

A chamber measurement campaign took place in May 2017. We measured baseline methane fluxes from the field surrounding the tower, and from the near-by river. At each patch type (field, river) duplicate chamber measurements were taken at 3 locations. The grass field produces no methane, and some very low rate of methane oxidation occur in the soil. This is important for the interpretation of the measurements from the flux tower, as it indicates that observations will represent remote sources of methane and are not influenced by baseline emissions at the local field around the tower. As expected, some methane emission occurred from the river. Any wet ecosystem typically produces some methane. Nonetheless, the emissions from the river were very low. For example, they are about 2 orders of magnitude lower than emissions we typically observe in natural wetlands. The resulting fluxes we observed are illustrated in figure 2.

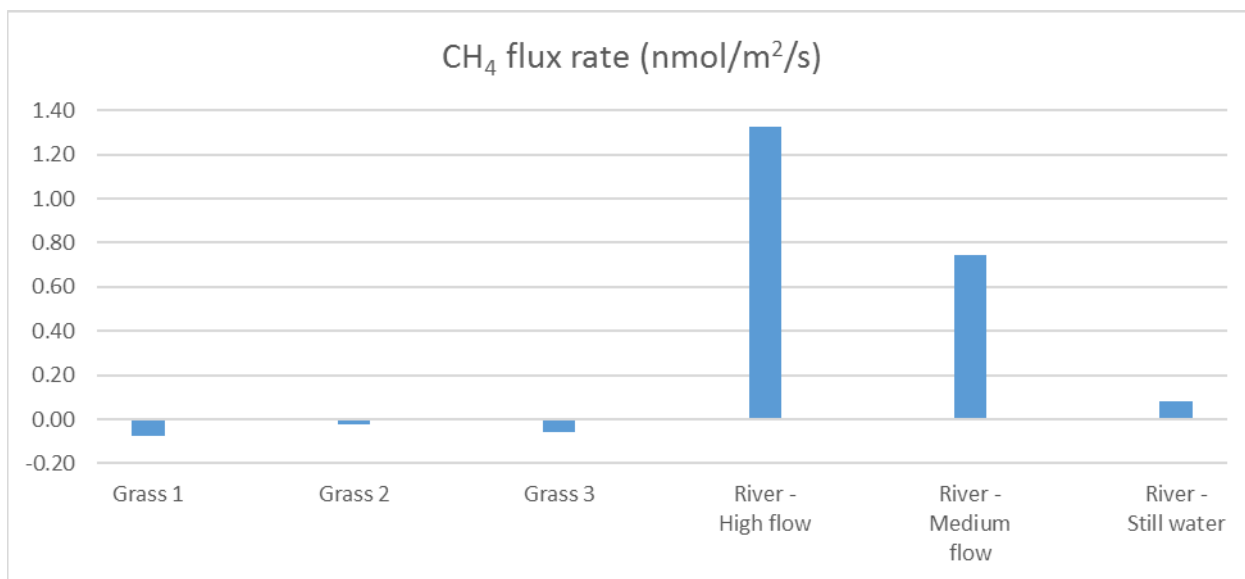


Figure 2. Methane fluxes from grass field and river near flux tower location and fracking site

An automated neural network (ANN) model of the methane concentration at the

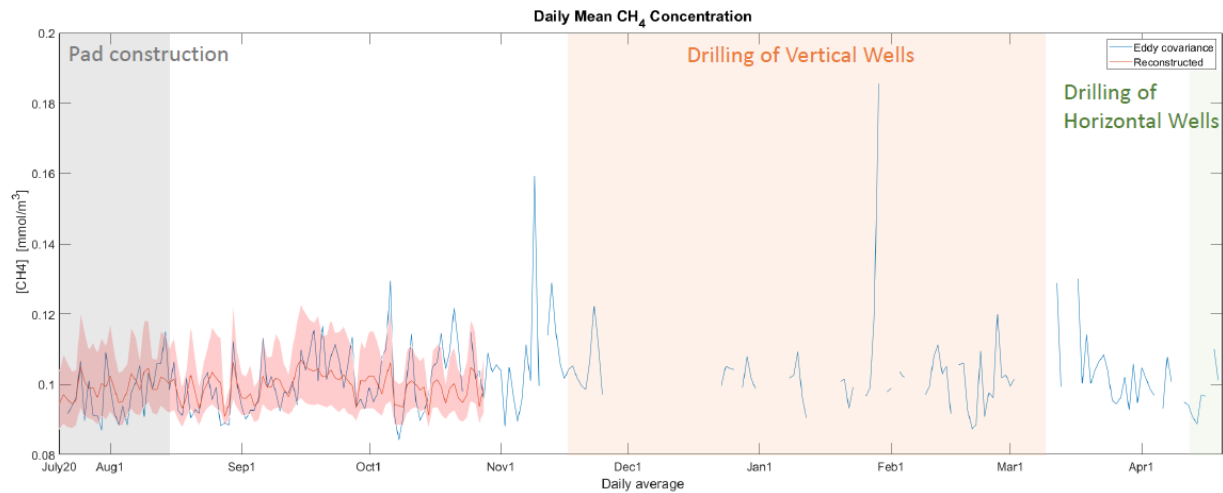


Figure 3. CH_4 concentration from WV site. Neural network model is used to estimate CH_4 concentration during baseline period (July 20- Oct 1, red line). Horizontal drilling is currently ongoing. 5% to 95% uncertainty levels of the ANN model are calculated and shown in red shading. Projecting the model forward to the drilling period will allow identifying above-baseline peaks.

Significance

The project will provide baseline measurements of methane emissions from natural and agricultural aquatic ecosystems around the proposed locations of a hydrofracking site. These observations will allow developing an empirical model for the natural methane emissions from the water system at the site and will allow determining whether these emissions increase due to diffused methane release into the ground water after the drilling operations started.







Bog HELPR: Bog History, Ecosystem status and Land-use for Peatland Restoration in Ohio

Basic Information

Title:	Bog HELPR: Bog History, Ecosystem status and Land-use for Peatland Restoration in Ohio
Project Number:	2017OH532B
Start Date:	3/1/2017
End Date:	2/28/2019
Funding Source:	104B
Congressional District:	
Research Category:	Biological Sciences
Focus Categories:	Wetlands, Ecology, Management and Planning
Descriptors:	None
Principal Investigators:	Gwilym Matthew Davies, Gil Bohrer

Publications

1. Rey-Sanchez AC, Slater J, Hao Y, Grau-Andres R, Davies M, Bohrer G. (2017). Measuring Methane Emissions in a Peat Bog in Ohio with Fluctuating Water Level: Comparison of Disturbed vs. Undisturbed Areas. 46th Annual Water Management Association of Ohio Conference. 11/01/2017. Worthington, Ohio
2. Rey-Sanchez AC, Morin TH, Bohrer G. (2017). Techniques for monitoring and modelling carbon dioxide and methane fluxes in wetlands. University La Sallista. 02/10/2017. Antioquia, Colombia
3. Slater JM, Davies GM, Rich VI, Bohrer G, Hao Y & Ray Sanchez AC (2017). A comparison of plant communities in intact and damaged Ohio peat bogs. Society for Ecological Restoration Mid-West Great Lakes Chapter Annual Meeting. Grand Valley State University, Grand Rapids, Michigan, 24th – 26th March 2017.
4. Slater JM, Davies GM, Rich VI, Bohrer G. (2017). Plant community composition across environmental and disturbance gradients in Ohio's peat bogs [poster]. Ohio Academy of Science Annual Meeting. University of Cincinnati, Cincinnati, Ohio, 8th April 2017.

Bog HELPR: Bog History, Ecosystem status and Land-use for Peatland Restoration in Ohio

PIs: G. Matt Davies^{1*} & Gil Bohrer^{2*}

Contributing authors: Julie Slater¹, Yushan Hao^{1,3}, Roger Grau Andres¹, Yueh-Fen Li³, Virginia Rich³, Camilo Rey Sanchez²

¹School of Environment and Natural Resources, The Ohio State University, Kottman Hall, 2021 Coffey Road, Columbus, OH 43210.

²Department of Civil and Environmental Engineering, The Ohio State University, Hitchcock Hall, 2070 Neil Ave, Columbus, OH 43210.

³Department of Microbiology, 105 Biological Sciences Building, 484 W. 12th Ave, Columbus OH, 43210

*Corresponding authors: G. Matt Davies - Tel: 614 292 3567, Email: davies.411@osu.edu; Gil Bohrer - Tel: 614 292 4178, Email bohrer.17@osu.edu

Contents

PART 1 – RESEARCH REPORT	2
1. Problem and Research Objectives	2
2. Methodology.....	3
2.1 Mapping and classifying Ohio’s peat bogs.....	3
2.2 Peat bog hydrochemistry.....	4
2.3 Vegetation community composition	5
2.4 Soil microbial community composition	5
3. Principal Findings and Results.....	6
3.1 Mapping and classifying Ohio’s peat bogs.....	6
3.2 Peat bog hydrochemistry.....	6
3.3 Vegetation community composition	9
3.4 Soil microbial community composition	9
4. Finding Significance.....	11
4. References	12
PART II. PUBLICATION CITATIONS.....	12
PART III. STUDENTS SUPPORTED	13
PART IV. PROFESSIONAL PLACEMENT OF GRADUATES	13
PART V. AWARDS OR ACHIEVEMENTS	13

PART 1 – RESEARCH REPORT

1. Problem and Research Objectives

In Ohio historically-abundant wetland ecosystems have suffered declines of up to 85% since the 18th century (Dahl 1990). Wetlands provide a wide range of ecosystem services such as regulating hydrological processes, water quality improvement, sequestering atmospheric carbon via peat formation, supporting biodiversity including wildfowl and rare plants and providing opportunities for recreation and education (Zedler & Kercher 2005). The degradation of wetland ecosystems, such as peatlands, has large financial costs associated with the. For example, Zedler & Kircher (2005) estimated costs of up to \$7,600 ha⁻¹ yr⁻¹ from lost water supply, between \$3,677 and \$21,100 ha⁻¹ yr⁻¹ from alterations to nutrient cycling and between \$2 and \$3,008 ha⁻¹ yr⁻¹ from lost recreational opportunities.

Ohio once contained a diverse and abundant array of wetland ecosystems including marshes, swamps, fens, and bogs. Peatland ecosystems in Ohio are of significant conservation concern as, in addition to being degraded or destroyed during land-use conversion, remaining systems are at the limits of their climatic range (Halsey et al. 2000), and have been impacted by drainage, disturbance and nutrient inputs from surrounding human land-use. Ohio's bogs therefore are a "canary in the coalmine" for interactions between climate change and human disturbance. However, we currently have little quantitative evidence on their current status, history or condition. That is important as the restoration of remnant peatland areas could provide a significant opportunity to improve the ecological, hydrological and chemical characteristics of many catchments. Human impacts on peatland ecosystems in Ohio (and elsewhere) have left them in a parlous state. By the late 1980's only 2% of Ohio's peat bogs were thought to remain (Andreas & Knoop 1992) but there has been no intensive survey of their status since that time.

Developing a peatland restoration agenda will require better knowledge of Ohio's existing peatland resource and the links between historical disturbance, land-use and the ecological structure of these sites. Our project's draws on three important historical studies that collectively document the extent and location of Ohio's peatlands between the early- and mid-20th century (Dachnowski 1912, Herrick 1974, Andreas & Knoop 1992). These studies vary in coverage and completeness but include sufficient information to allow historical, degraded and intact sites to be relocated. They also provide some qualitative assessment of historical site vegetation. They do not provide information on how sites have changed over the last ca. 40 years or quantitative data on their ecological status, functioning, or restoration potential.

Our specific objectives were to:

- Use historic maps, reports and aerial imagery to identify and map the locations of existing and historic peat bogs in Ohio.
- Combine historic maps, aerial images and ground survey to quantify changes in peat bog extent during two key periods – the 1860s-1950s and 1950s-2010s.
- Map and quantify variation in broad vegetation composition and structure within and between bogs representing a range of historic disturbance/management histories.
- Relate variation in community composition to land-use and environmental gradients in soil, weather, and hydro-chemical conditions within and between bogs.

2. Methodology

2.1 Mapping and classifying Ohio's peat bogs

Peatland classification is complicated by the often interchangeable use of terms such as bog, fen, swamp, bog forest, marsh, wet prairie, and many others. In recent decades, the usage of these terms has been debated and standardized (Bridgham et al. 1996), but their definition in older texts can vary even within those by the same author (Wheeler and Proctor 2000). Our project was focused on Ohio's bog ecosystems, defined as acidic, low alkalinity peatlands dominated by *Sphagnum* mosses, conifers, and ericaceous shrubs without any assumptions about hydrological process, as suggested by Bridgham et al. (1996). We began by attempting to relocate all sites defined by Andreas (1985) as bogs, and when not included in her study, sites with the word bog in the name, or described as bogs in historical or current site descriptions.

Andreas and Knoop (1992) qualitatively documented changes in peatland extent in Ohio up to the 1980's. As the article does not include specific site locations, we relocated sites using the authors' primary sources: a turn-of-the-century survey of peat deposits in Ohio (Dachnowski 1912) and other historical peatland studies. Andreas and Knoop also referred to herbarium records for their study, but these have not been included in our study at this time. Historical studies included any of the following relevant information: township and section, location relative to natural and manmade landmarks, landowner names (which were searched in county deed records), and rarely, site coordinates. Protected bog sites with unchanged names were easy to locate by internet search.

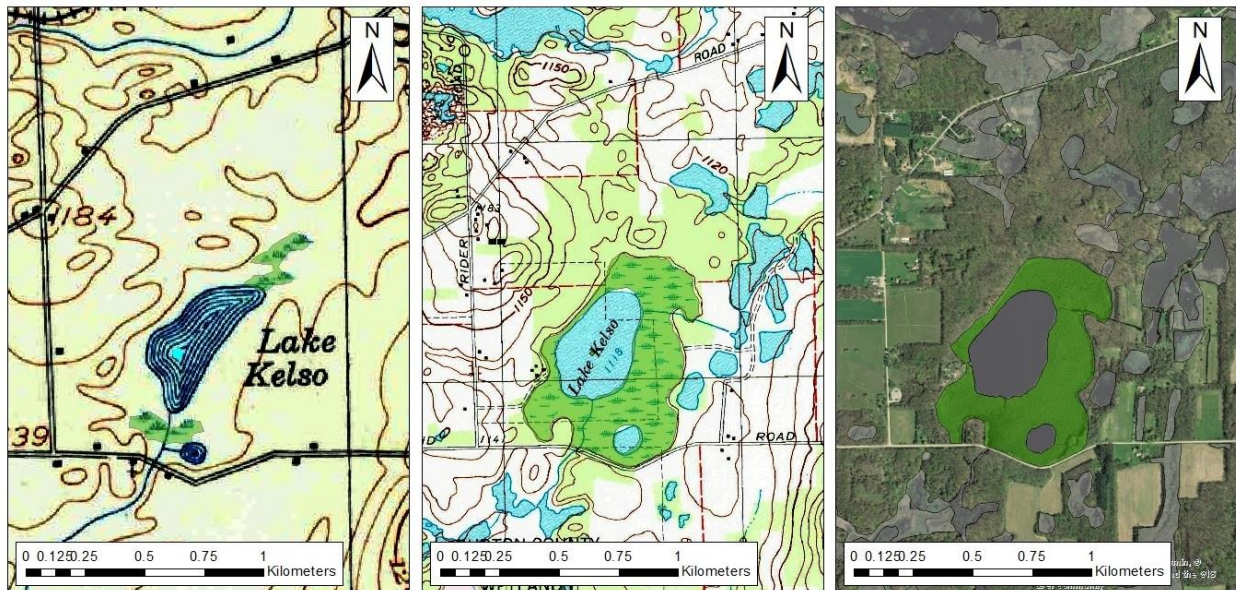


Figure 1: Examples of digitized maps used to evaluate the efficacy of utilizing historical sources to locate peat bog sites across Ohio and document changes in their extent. From left to right the pictures show a 1900's era USGS Topo Map, a 1994 USGS Topo Map and an aerial image from 2007. Areas mapped as peat bog are shown in green.

As a first step in evaluating the efficacy of historical maps for calculating historical bog extent we assessed 15 bog sites that could be clearly delineated from aerial photographs. This criteria favored kettle hole bogs and excluded large peatland complexes with wide variation in hydrology and plant communities. Topographic maps from three different time periods were evaluated for their efficacy in estimating historical bog extent. United States Geological Survey (USGS) maps from 1900-1920 were chosen to correspond with Dachnowski's 1910-1911 peat survey, USGS maps from 1960-1994

corresponded with Andreas and Knoop's 1976-1991 field inventories, and current National Wetland Inventory (NWI) maps based on data collected in 2007 were used to represent present-day extent (Figure 1).

When multiple options were available, the map created closest to 1911 and 1991, respectively, was selected. Georeferenced historical USGS maps were accessed using topoView, the USGS's historical map download portal. The NWI provides wetland extent for current USGS topographic maps. Shapefiles were created by digitizing wetland extent or selecting polygons that corresponded to descriptions in historical studies. Wetland area was calculated from these shapefiles in ArcGIS. We continue to add to this dataset by systematically searching for representations of peat bogs on older 19th Century county and township maps, to date relatively few of these have been found to reliably show areas of wetland.

Andreas (1985) uses the presence of indicator species to systematically classify Ohio's peatlands into bogs and fens, with the occurrence of a single indicator species enough to classify an entire site. However, few true bog indicator species exist; rather, bog vegetation is distinguished by a lack of calcareous fen indicator species (Wheeler and Proctor 2000). Tamarack, for example, is used by Andreas (1985) as a bog indicator, although it can be found outside that habitat. As a result, some fens appear to be misidentified as bogs. Frame Bog is thus defined by Andreas as a bog, but has now been protected under the name Herrick Fen, and in Andreas's own site description was said to have calcareous indicators. With this in mind, historical site descriptions were revisited, and plant community descriptions used to divide these "bogs" into high, medium, or low confidence in their classification as bogs. High confidence was assigned to bogs whose status was confirmed by historical site descriptions, medium confidence was assigned to bogs whose identity could be neither confirmed or denied due to lack of data (herbarium records were not referenced in the current project), and low confidence was assigned to sites whose descriptions included dominant characteristic fen vegetation.

2.2 Peat bog hydrochemistry

We selected nine sites for extensive monitoring of hydrochemistry. These sites selected to represent largely-intact peat bogs with differing land-use histories and surrounding land-use pressures. At each site we established multiple transects across the bogs to capture the ecological gradient from lag/moat conditions at the peatland margin to the core of the bog (Figure 2). Sites varied in their structure. While many had an open-water zone at their core others consisted of a floating peat dome. The depth and width of the lag or moat varied noticeably between sites and appeared to be a function of the physiography of the basin in which the peatland formed. Along each transect we placed multiple dipwells to monitor groundwater chemistry and measure water table depth. Dipwells were placed to capture representative locations within each broad vegetation zone crossed by the transect. We also installed one or more potentiometers to assess variation in water table position at fine temporal scales and collected monthly samples for detailed nutrient analyses. pH and electric conductivity (EC) of peat pore water was measured with a portable meter (YSI Pro1030). We completed five measurements per well approximately monthly from 20-Jun-2017 to 28-Nov-2017. Differences in environmental variables between broad vegetation type zones were investigated using linear mixed effects models with "site" as a random factor (R packages "nlme" Pinheiro et al., 2017 and "multcomp" Hothorn et al., 2008)

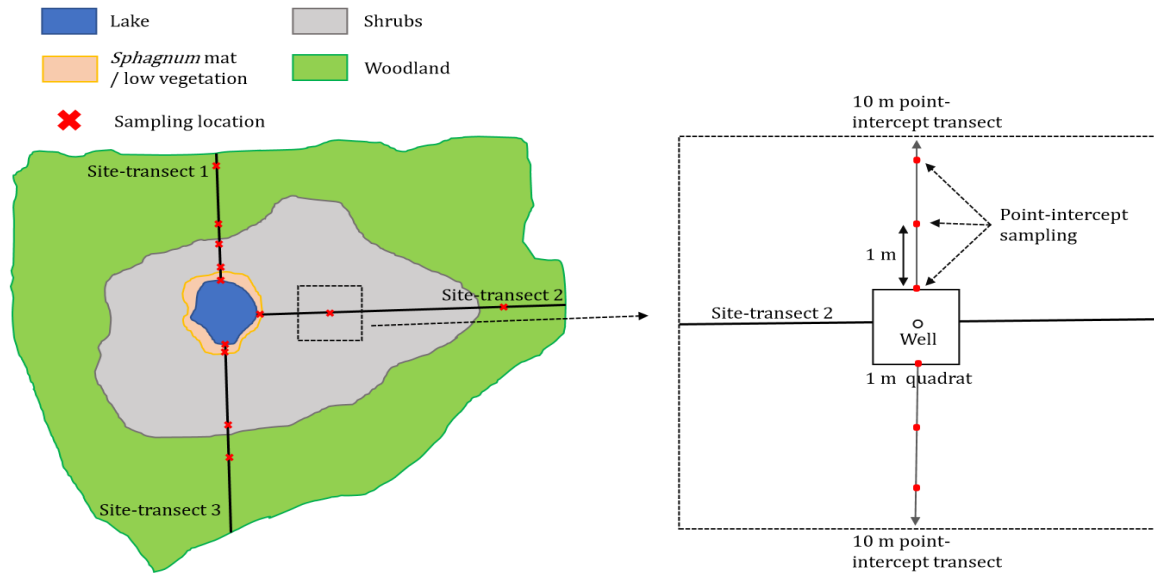


Figure 2: Example of sampling design for one site, showing (left) sampling locations within site-level transects, and (right) a quadrat and point-intercept transects for a single sampling location. Quadrats were centred at the well, and point-intercept transects were divided into two 10 m parts, starting at each side of the quadrat and perpendicular to the core to edge site-transect.

2.3 Vegetation community composition

We surveyed vegetation community composition at the nine extensively monitored peatlands used for the hydrochemical monitoring. Within each transect we selected one to seven sampling locations to adequately represent the variety of broad vegetation zones (Figure 2). This resulted in 81 sampling locations across all sites (six to twelve per site, mean = 9). Initial surveying and data analysis has focused on assessing variation in bryophyte composition as we wished to test the extent to which this could act as an indicator of variation in abiotic and biotic conditions within and between peat bogs. Bryophyte abundance was surveyed once between 12-Jul-2017 and 15-Sep-2017 using quadrat and transect methods (Figure 2). We also recorded total cover of vascular plants by adding cover of individual species (well quadrats) and presence counts (point-intercept). Non-metric multidimensional scaling (NMDS) was used to visualise variation in bryophyte community composition (function “metaMDS” in package “vegan”; Oksanen et al., 2017). We fitted environmental variables onto ordination using the “envfit” function in “vegan”, restricting permutations to within-site groups.

2.4 Soil microbial community composition

Samples for microbial community characterization were collected from Browns Lake Bog (n=99) and Flatiron Bog (n=374), from several habitats at each site: Sphagnum mat zones at both sites, blueberry shrubland zones at both sites, and tamarack-dominated, historically disturbed, and runoff-impacted zones at Flatiron. Soil samples were kept at -20C until DNA extraction. DNA was extracted from 0.25g of soil sample using DNeasy PowerSoil Kit (Qiagen, Germantown, MD) following manufacturer’s procedures. Extracts were shipped to Argonne National Lab for amplification and sequencing; 16S rRNA gene amplicons were generated using the Earth Microbiome Protocol pre-2015 primers 515F/806R, and were sequenced on the Illumina MiSeq with the 2x150bp protocol. Amplicon data were processed with the bioinformatics software QIIME 1.9.1 (Caporaso et al., 2010) using the 16S-RDS pipeline (Nelson et al, 2014), and removing lineages assigned to the family mitochondria and the class chloroplast. Sequences

in each sample were rarefied to 3000 for beta diversity analysis, and the results were visualized with principal coordinates analysis.

3. Principal Findings and Results

3.1 Mapping and classifying Ohio's peat bogs

A total of 70 potential bog sites were evaluated in our study (Appendix A), adding 10 sites to Andreas and Knoop's list of bogs (1992). Of these, 55 were relocated with a high degree of confidence (Figure 3). We were highly confident in the bog status of 40% of the sites. Bog classification confidence was moderate for 31.4%, of cases and low for 28.6%. Most large bogs, which in reality are likely to have consisted of wetland complexes including areas of fen, bog and swamp forest, have been lost or heavily mined. The majority of sites we identified were located in NE Ohio, though important clusters were found in NW Ohio, in the area formerly dominated by the Great Black Swamp, and in central Ohio.

In order to evaluate the efficacy of historical maps for calculating historical bog extent, 15 bog sites with clearly delineated margins were selected (Figure 4). Eight of fifteen (53%) sites are not indicated as wetlands on early 1900s historical maps. Bogs have not been created between then and the 1980s, so the discrepancy between maps of different time periods can be attributed to differences in scale or wetland mapping criteria. Early 1900s maps are at 1:62,500 scale, while more recent USGS topographic maps have a scale of 1:24,000. The criteria for wetlands to be marked on USGS maps in the early 1900s are unclear, but they appear to be less accurate and consistent when depicting wetland shape and area.

In three cases, bogs appear only on the most recent NWI maps. It is possible that smaller bogs were passed over in older maps, or that bogs with open water were less likely to be marked as wetlands due to already being displayed on the map as ponds. However, Young's Bog is a counterexample to both of these ideas, having no open water and being relatively large at 48 ha.

Two of the analyzed bogs show a decrease in area since the early 1900s. Cranberry Bog is a floating bog island in the Buckeye Lake reservoir, where wave action from boating activity has been decreasing the size of the island. The area of Camden Lake Bog in the early 1900s map included surrounding wetlands as well as the bog proper, resulting in an inflated estimate.

Seven sites display a noticeable trend of a slight decrease in wetland extent in the NWI compared to the 1980s-1990s USGS map. Areas extracted from these two more recent maps were visualized alongside areas listed by Andreas and Knoop (1992) in order to compare evaluate the accuracy of the three data sources (Figure 5). The NWI was more likely to feature peatlands listed by Andreas as historical (destroyed), as in the case of Camden Lake Bog and Fox Lake Bog, and less likely to not recognize an extant peatland, as in the case of Bonnett Pond Bog, and Young's Bog. However, the classification system used in NWI does not reflect the unique ecological and hydrological conditions of peat bog systems.

3.2 Peat bog hydrochemistry

Across the nine sites we sampled, average water table depth (WTD) was 0.6 cm, i.e. just below the ground but varied greatly between plots as indicated by its high standard deviation (21.2 cm) (Table 1). Water table was significantly higher (26.9 cm above the ground vegetation on average) in the central Sphagnum mat zone than in zones closer the margin of the bog. No significant differences in WTD fluctuation (8.9 ± 7.7 cm), pH (4.8 ± 0.6) and EC ($0.097 \pm 0.079 \mu\text{S cm}^{-1}$) were observed between vegetation zones. As of May 2018 the potentiometers remain in position and lab analysis of hydrochemistry is on-going.

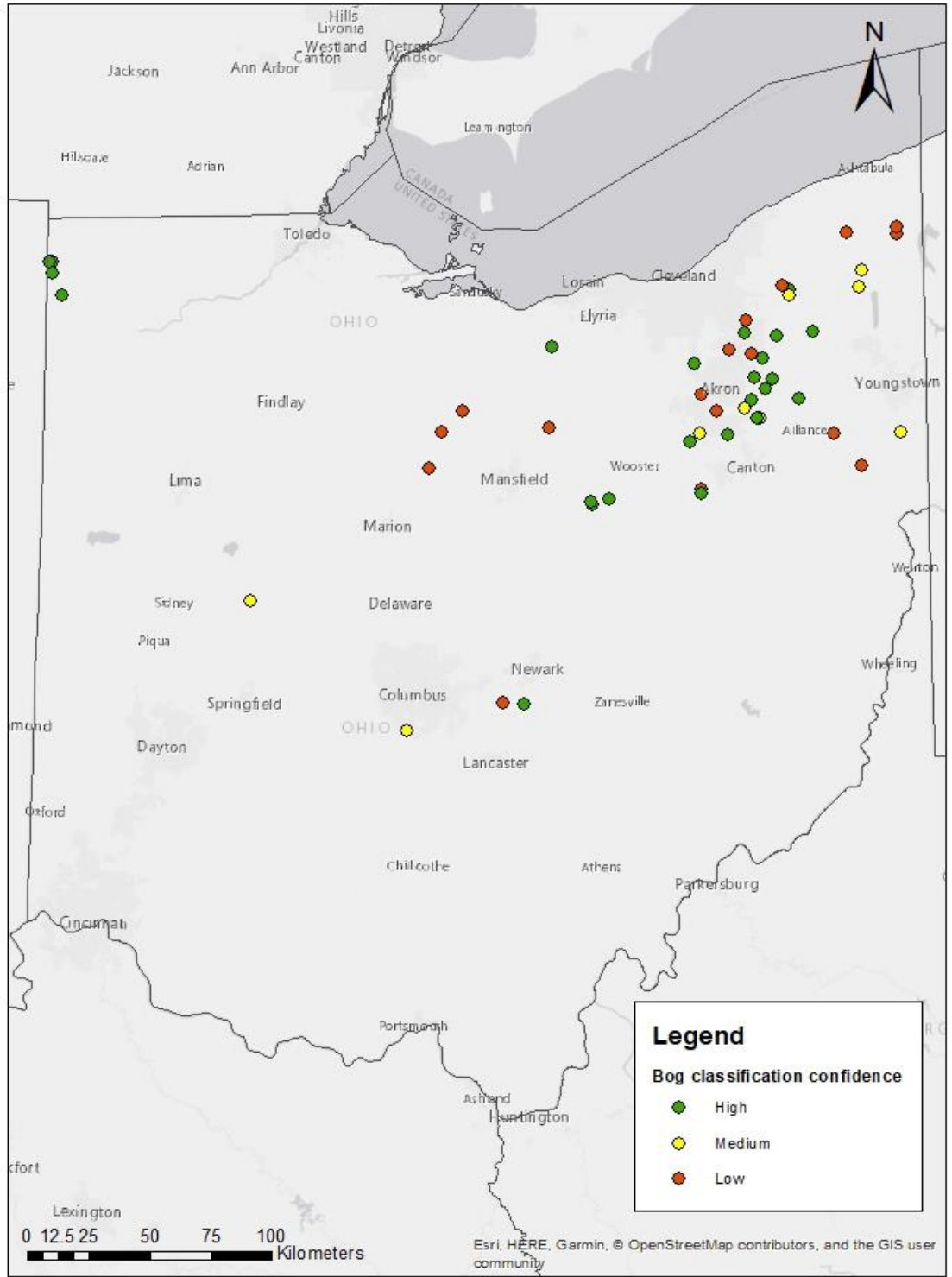


Figure 3: Distribution of relocated peatland sites, colored according to confidence in their bog classification.

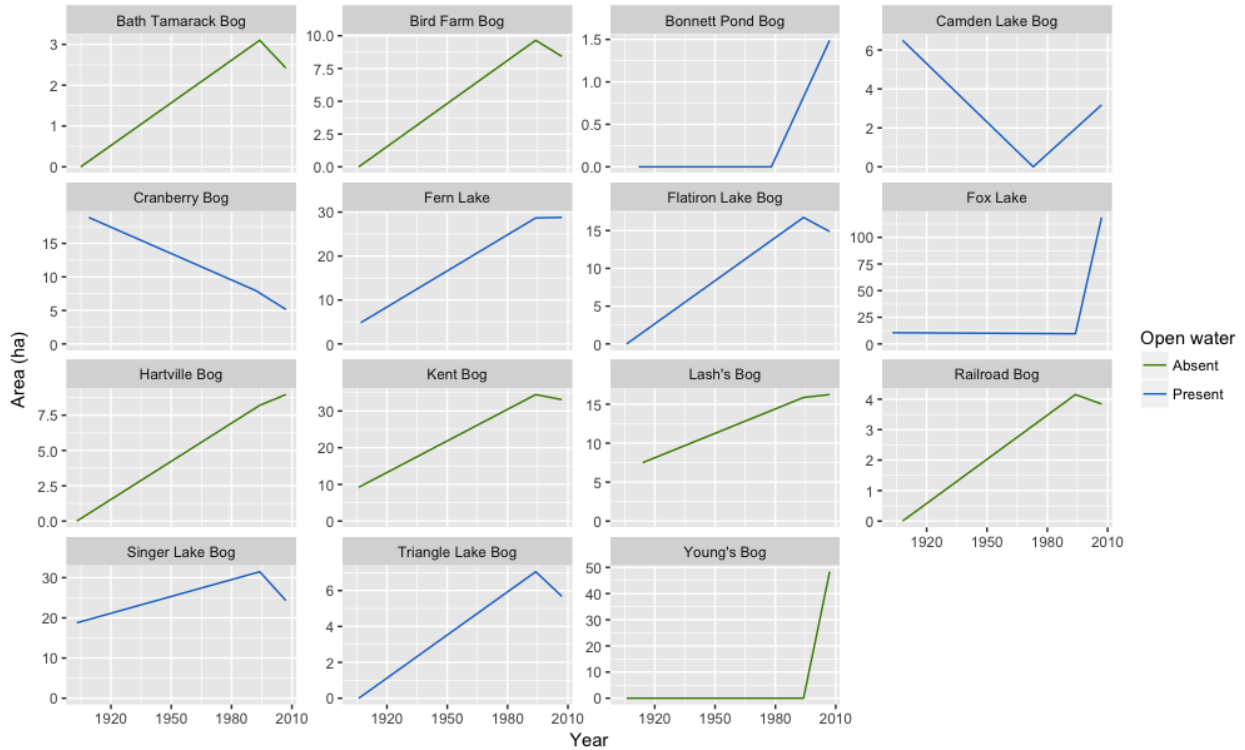


Figure 4: Change in extent of select Ohio bog sites as described by three historical USGS maps. Note that the y-axis varies, and graphs indicate patterns in relative (rather than absolute) area. Color indicates the presence or absence of open water at each site.

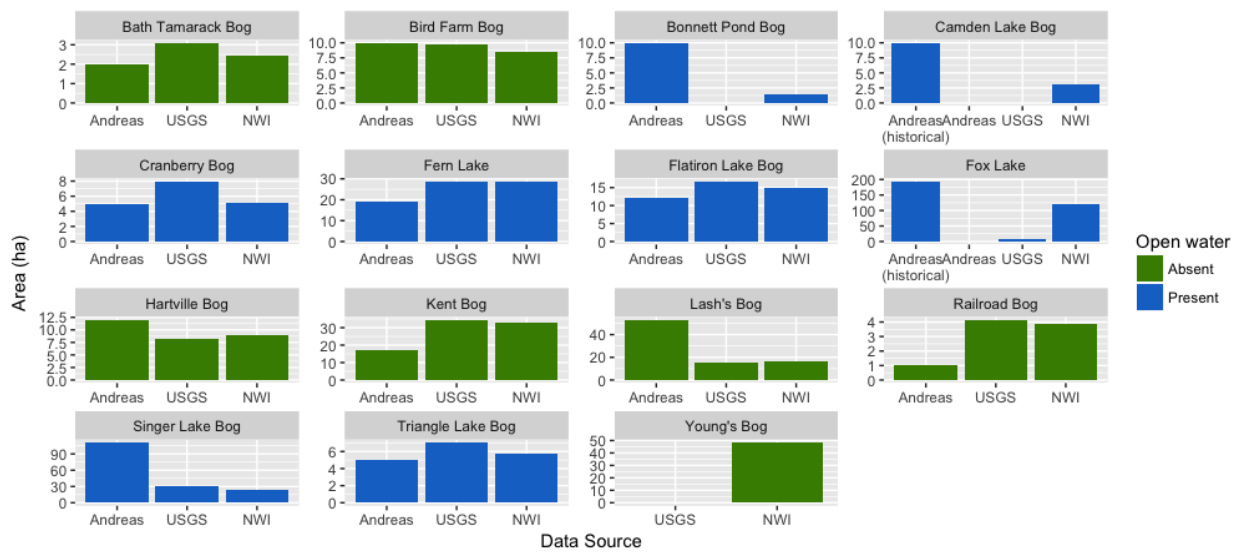


Figure 5: Comparison of bog extent listed by Andreas and Knoop (1992) to that displayed in USGS maps from the 1980s-1990s and NWI maps from 2007, including estimates of historic bog extent of destroyed bogs.

Table 1: Average values (standard deviation in parenthesis) of the environmental variables per broad vegetation zone. Same letters within the same row indicate differences were not statistically significant ($\alpha = 0.05$).

	Floating mat	Low shrubs	Tall shrubs	Woodland
Water table depth (cm)	-26.9 (15.6) a	9.9 (11.5) b	-5.3 (24) c	8.9 (16.6) bc
WTD fluctuation (cm)	9.6 (4.3) a	6.1 (5.4) a	10.6 (8.6) a	10.4 (9.5) a
Microtopography heterogeneity (cm)	17.6 (8.2) a	8.4 (4.2) b	9.4 (4.6) b	7.4 (5.4) b
pH	5.3 (0.7) a	4.7 (0.5) a	4.8 (0.6) a	4.7 (0.7) a
Electric conductivity ($\mu\text{S cm}^{-1}$)	0.14 (0.1) a	0.07 (0.05) b	0.11 (0.1) a	0.08 (0.02) ab
Cover (%)	95 (44) a	101 (43) a	122 (44) a	175 (60) b

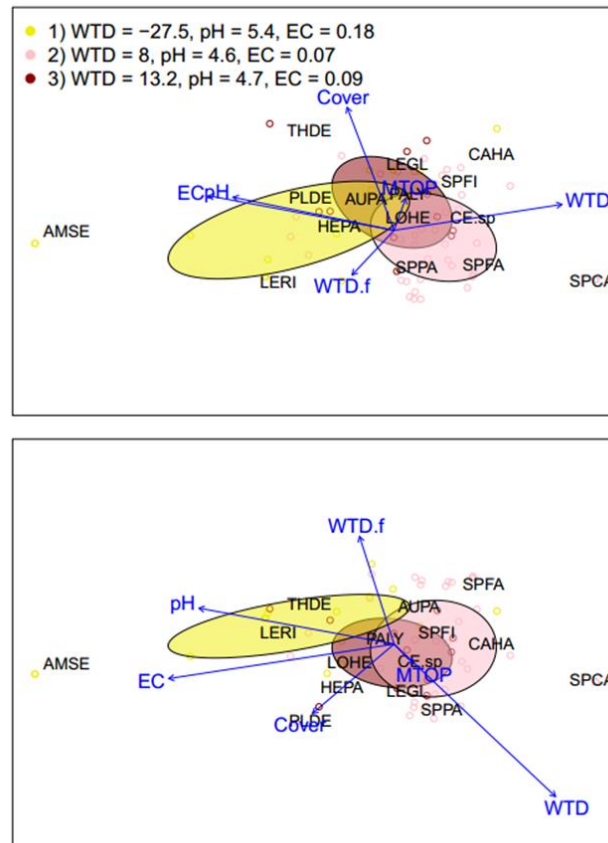


Figure 6: NMDS ordination of bryophyte cover in quadrats – top = axes 1 v 2, bottom = axes 1 v 3. Ellipses show standard deviations for clusters of plots with similar abiotic characteristics. Arrows are fitted covariates (length is proportional to the correlation with ordination): water table depth “WTD”, its fluctuation “WTD.f”, heterogeneity in microtopography “MTOP”, pH, electric conductivity “EC” and cover of vascular plants “Cover”.

3.3 Vegetation community composition

At our nine surveyed sites, we identified 39 different bryophyte taxa in 74 plots from the quadrat survey (7 plots were excluded due to lack of bryophytes). The point-intercept transect survey yielded 34 taxa

from 69 plots. The ordination of bryophyte species composition varied along a first NMDS axis associated with WTD, EC and pH, and a second axis associated with vascular plant cover (Figure 6). These environmental vectors had a significant effect on community composition when fitted onto the ordination, and were used to classify sampling locations, resulting in three groups of distinct hydrology and hydrochemistry.

3.4 Soil microbial community composition

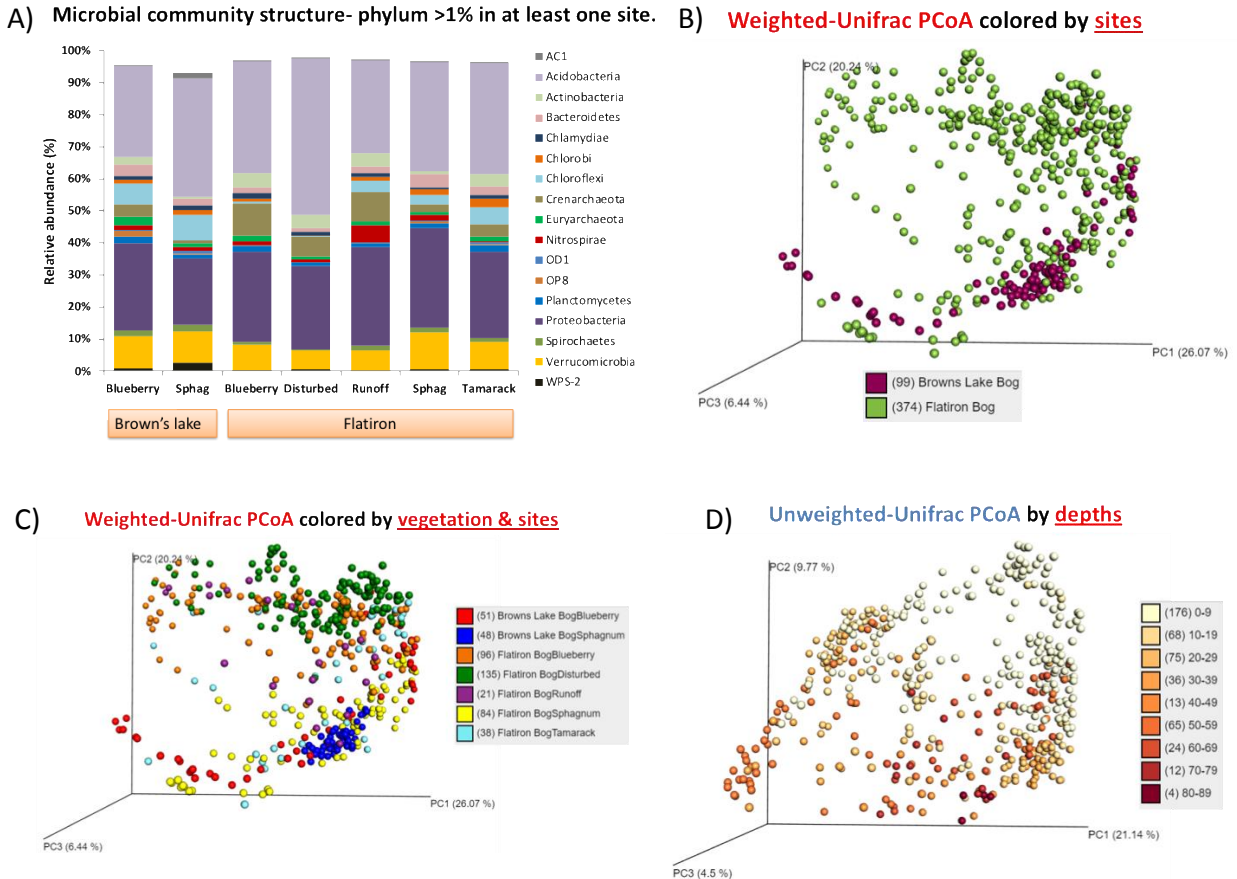


Figure 7: Microbiota differ by site, habitat, and depth. (A) Communities across all sites were consistently dominated by Acidobacteria and Proteobacteria, and showed similar overall phylum-level relative compositions among sites. (B) Principal coordinates analysis, accounting for genetic relatedness of communities (via Unifrac distances) and weighted by the relative abundances of members, indicated that Flatiron Bog was home to a larger diversity of microbial communities than Browns Lake Bog, and the latter was a discrete subset of the former. (C) Overlaying habitat type information on the same analysis suggested some habitat cohesion across sites. (D) Communities also diverged gradually by depth; this was clearest when plotting communities by genetic relatedness but not weighting by relative abundances, indicating that the presence/absence of rarer or more genetically divergent, low-abundance members may drive the depth patterning.

After processing, 8.15M reads remained for the 473 samples, with an average of 17,085 (SD 6,081) reads per sample. Acidobacteria (28-49%), proteobacteria (21-31%), and Verrucomicrobia (6-12%) were the three most relatively abundant phyla across the sites irrespective of site or habitat (Figure 7A), with differences in known nitrogen- and methane-cycling organisms we are currently investigating. For example, markedly higher Nitrospirae, and high Crenarchaeota (which include the archaeal ammonia oxidizers), were present in the runoff-impacted site. PCoA analysis showed sample separation by site (flatiron vs brown lake), habitat, and sample depths (0-90cm) (Figure 7B-D). Notably, Sphagnum

dominance caused similar overall community compositions between the two sites (Figure 7C), while the dominance of blueberry did not. *Sphagnum* spp., high in secondary compounds and generally lowering site pH as is well described in the literature, acted as a control on belowground community structure and processes. We continue to explore the specific lineages, and geochemical and vegetation correlations, in the microbiota at these two sites.

4. Finding Significance

Mapping historic peatlands: Shape files of our identified and classified bogs are available from the authors and will be publicly archived once the classification is complete and results published. The maps we've developed will provide an important resource for researchers wanting to understand Ohio's peatland ecology and managers seeking information relating to targets and contexts for wetland restoration. We conclude that attempts to estimate changes in historic bog extent based on early USGS maps are confounded by too many factors to be accurate. Differences in scale, wetland mapping criteria, and difficulty in identifying the borders of certain sites make accurate estimates of area problematic. However, historical maps still contain valuable information on the locations of former peatlands and can provide insights into land use changes and site history. Our mapping will provide an invaluable resource that catalogues areas where peatland cover has been lost and that should be a priority for ground survey to assess restoration potential. The NWI can be used in conjunction with site descriptions from the literature to define current bog extent. On-going research is focused on quantifying uncertainty in changes in peatland extent and developing a conservative estimate of peatland loss. We also aimed to develop a more detailed classification of the sites' current and past land-use and land-cover to assess surrounding land-cover, this work is on-going. Our map of current bog extent can be used to examine current land use pressures on extant sites. Andreas and Knoop's (1992) study listed the cause of destruction of historic peatland sites, but the pressures facing Ohio's remaining bogs have not been quantified. Using the National Land Cover Database and aerial imagery, we can gain an understanding of the threats to Ohio's bogs at a landscape scale.

It appears that, being more difficult to drain, kettle hole peatlands such as those evaluated above are likely to diverge in land use history from much larger peatland complexes. While the latter pose unique challenges for delineation, historical maps could be an important source of information on the history of such sites.

Fifteen sites listed by Andreas and Knoop (1992) could not be located due to a lack of data. Records from throughout Ohio's herbaria, including Andreas's own collections, can be accessed online through the Consortium of Midwest Herbaria. These fifteen sites and more may be located relatively easily by searching for herbarium specimens used by Andreas and Knoop (1992).

Peatland hydrochemistry: We have established a detailed initial baseline to understand variation in hydrochemistry within and between remaining peat bogs. This information can be used as a basis against which to assess hydrochemistry in sites undergoing restoration. Our sites had a pH at the higher end of the range typical for bogs. This could indicate some influence from surrounding land use and/or a non-negligible influence of surface run-off and groundwater. The latter finding would suggest that, hydrologically, Ohio's peat bogs are more likely poor fen systems. This is supported by the high EC with a wide range (33–597 $\mu\text{S cm}^{-1}$; median = 70 $\mu\text{S cm}^{-1}$) compared to 35–78 $\mu\text{S cm}^{-1}$ reported by Andreas and Bryan (1990). Our results have demonstrated significant hydrochemical gradients within Ohio's peat bogs that serve to differentiate important differences in above- and below-ground community structure.

Community composition: Our research has revealed the utility of using bryophytes as indicators of peatland hydrochemical status. This will facilitate monitoring where resources for detailed assessments

of varying water table and water quality conditions is not possible. Our microbial data will help us understand the above- below-ground linkages that determine the carbon balance and ecosystem function of remaining peatland sites.

5. References

- Andreas B.K. 1985. The relationship between Ohio peatland distribution and buried river valleys. *Ohio Journal of Science* 85:116–125.
- Andreas B.K. & Knoop J.D. 1992. 100 years of changes in Ohio peatlands. *Ohio Journal of Science* 92:130–138.
- Bridgham S.D., Pastor J., Janssens J.A., Chapin C. & Malterer T.J. 1996. Multiple limiting gradients in peatlands: A call for a new paradigm. *Wetlands* 16:45–65.
- Caporaso J.G., Kuczynski J., Stombaugh J., Bittinger K., Bushman F.D., Costello E.K., Fierer N., Peña A.G., Goodrich J.K., Gordon J.I., Huttley G.A., Kelley S.T., Knights D., Koenig J.E., Ley R.E., Lozupone C.A., McDonald D., Muegge B.D., Pirrung M., Reeder J., Sevinsky J.R., Turnbaugh P.J., Walters W.A., Widmann J., Yatsunencko T., Zaneveld J., Knight R. 2010. QIIME allows analysis of high-throughput community sequencing data. *Nature Methods* 7:335-336.
- Dahl T.E. 1990. *Wetlands – Losses in the United States, 1780’s to 1980’s*. US Fish and Wildlife Service, Washington DC.
- Dachnowski A. 1912. *Peat Deposits of Ohio: Their Origin, Formation, and Uses*. Geological Survey of Ohio, Columbus, Ohio, USA.
- Halsey L.A., Vitt D.H. & Gignac L.D. 2000. *Sphagnum*-dominated peatlands in North America since the last Glacial Maximum: their occurrence and extent. *The Bryologist* 103: 334-352.
- Herrick J.A. 1974. *The Natural Areas Project: a summary of data to date*. Ohio Biological Survey Informative Circular 1. The Ohio State University, Columbus, Ohio.
- Hothorn T., Bretz F. & Westfall P. 2008. Simultaneous inference in general parametric models. *Biometrical Journal* 50:346-363.
- Nelson M.C., Morrison H.G., Benjamino J., Grim S.L. & Graf J. 2014. Analysis, optimization and verification of Illumina-generated 16S rRNA gene amplicon surveys. *PLoS One* 10:e94249.
- Oksanen J., Blanchet F.G., Friendly M., Kindt R., Legendre P., McGlenn D., Minchin P.R., O’Hara R.B., Simpson G.L., Solymos P., Stevens M.H.H. Szoecs, E. & Wagner H. 2017. *vegan: Community Ecology Package*. URL: <https://CRAN.R-project.org/package=vegan>. r package version 2.4-5.
- Pinheiro J., Bates D., DebRoy S., Sarkar D. & R Core Team. 2017. *nlme: Linear and Nonlinear Mixed Effects Models*. URL: [https://CRAN.R-project.org/ package=nlme](https://CRAN.R-project.org/package=nlme). r package version 3.1-131.
- Wheeler B.D. & Proctor M.C.F. 2000. Ecological gradients, subdivisions and terminology of north-west European mires. *Journal of Ecology* 88:187-203.
- Zedler J.B. & Kercher S. 2005. Wetland resources: status, trends, ecosystem services, and restorability. *Annual Review of Environment and Resources* 30:39-74.

APPENDIX A – LIST AND CLASSIFICATION OF CURRENT AND HISTORIC PEAT BOGS IN OHIO

Table A.1: Peat bogs identified based on analysis of records reported in Dachnowski (1912), Andreas (1985) and Andreas & Knoop (1992). Where not Latitude and Longitude are given it was not possible to identify even an approximate location beyond the county and township. Confidence reflects our reanalysis of the ecological status of the sites and our confidence the vegetation community was reflective of an acidophilous vegetation type. It is not a reliable indicator of the sites' current or historic hydrological regime. Status reports our assessment of whether the site is extant (E), degraded (D) or historic/destroyed (H).

Site Name	Alternate names	Latitude	Longitude	County	Township	Section	Andreas 1985 Classification	Confidence	Status
Atwater Center		41.0451	-81.1377	Portage	Atwater		Bog	H	D
Barnacle Bog				Portage	Ravenna		Bog	M	
Bath Tamarack Bog		41.1773	-81.6437	Summit	Bath			H	E
Baughman Bog		40.7194	-81.6151	Stark	Sugar Creek			L	E
Bird Farm Bog	Bird Bog	41.0841	-81.2955	Portage	Rootstown		Bog	H	E
Bloody Run Swamp		39.9375	-82.5706	Licking	Harrison		Bog	L	H
Bloomfield Bog		41.4515	-80.8336	Trumbull	Bloomfield		Bog	M	H
Bonnett Pond Bog	Bonnet Lake, Long Lake, Cranberry Marsh	40.6631	-82.1388	Holmes	Washington		Fen	H	E
Brown's Lake Bog		40.6821	-82.0627	Wayne	Clinton		Bog	H	E
Bucyrus Bog		40.7972	-82.9333	Crawford	Bucyrus			L	H
Burned Bog				Portage	Hiram		Bog	M	H
Camden Lake Bog	Cambden Lake Bog	41.2428	-82.3351	Lorain	Camden		Bog	H	D
Caston Pond Bog	Caston Road Bog	40.9576	-81.5287	Summit	Green		Bog	M	E
Congress Lake		40.9776	-81.3263	Stark	Lake		Bog	M	H
Cranberry Bog	Cranberry Island, Buckeye Lake	39.9314	-82.4687	Licking	Licking			H	D
Eagle Creek Bog		41.2919	-81.0619	Portage	Nelson			H	E
Eckert Bog		41.1959	-81.3093	Portage	Ravenna		Bog	H	H
Fern Lake	Lake Kelso, Bradley Pond, Kellmore Lake	41.4444	-81.1750	Geauga	Burton		Bog	H	E
Flatiron Lake Bog		41.0448	-81.3665	Portage	Suffield		Bog	H	E
Florence Bog		41.5331	-84.7786	Williams	Florence			H	H
Forquier Bog				Richland	Cass		Bog	M	
Fox Lake Bog		40.8913	-81.6661	Wayne	Baughman	1 & 12	Bog	H	D

Frame Bog	Herrick Fen, Frame Lake Fen	41.2112	-81.3666	Portage	Streetsboro		Bog	L	E
Garfield Bog		40.9173	-80.9659	Mahoning	Goshen	30 & 31	Bog	L	D
Grand River Terraces				Ashtabula	Morgan		Bog	M	E
Guilford Bog		40.7942	-80.8396	Columbiana	Center	7 & 8	Bog	L	D
Hartville Bog		40.9752	-81.3422	Stark	Lake		Bog	H	E
Infirmiry Road Bog	Tummonds Nature Preserve	41.2784	-81.2407	Portage	Mantua		Bog	H	D
Karlo Bog	Karlo Fen			Summit	Coventry		Bog	M	
Kent Bog	Brimfield Bog? Check	41.1256	-81.3542	Portage	Brimfield		Bog	H	E
Kline Farm Bog		41.5352	-84.7972	Williams	Florence			H	H
Lake Township Bog				Stark	Lake		Bog	M	
Lash's Bog	Brewster Bog	40.7011	-81.6143	Stark	Sugar Creek	16		H	E
Lehman Bog	Big Lake, Leman's Lake, Lehman Lake	41.4121	-84.7270	Defiance	Milford	2 & 11	Bog	H	D
Leon Bog		41.6468	-80.6456	Ashtabula	Morgan		Bog	L	D
Similar to Leon Bog		41.6700	-80.6414	Ashtabula	Dorset			L	D
Long Lake Bog		41.0024	-81.5371	Summit	Coventry			L	E
Luna Lake Bog		40.9216	-81.6211	Summit	Clinton		Bog	M	D
Lyman Bog				Stark	Sugar Creek		Bog	H	
McCracken Bog		40.3048	-83.7858	Logan	Liberty			L	E
Morgan Swamp		41.6516	-80.8937	Ashtabula	Morgan		Bog	L	E
Mud Lake Bog		41.2302	-81.4719	Summit	Hudson		Bog	L	D
New Haven Bog	New Haven Marsh, Huron Bog	41.0088	-82.7691	Crawford/ Huron	Auburn/ New Haven		Bog	L	D
New Washington Bog	Crawford Bog, Cranberry Marsh	40.9297	-82.8698	Crawford	Cranberry	24,25,26		L	H
Norton Bog	Part of Copley Swamp, Copley Bog			Summit	Norton		Bog	H	
Orrville Bog	Orville Bog			Wayne	Orrville	29	Bog	L	H
Orwell Tamarack Bog	Orwell Swamp, Orwell Bog	41.5157	-80.8216	Ashtabula	Orwell		Bog	M	D
Panzer wetland	Part of Copley Swamp, Copley Bog	41.0662	-81.6098	Summit	Copley			L	D
Pettibone Swamp				Cuyahoga	Solon		Bog	M	
Punderson Lake		41.4624	-81.2102	Geauga	Newberry		Bog	L	E

Railroad Bog	Railroad Cranberry Bog	41.2917	-81.3973	Summit	Twinsburg		Bog	H	E
Rider Road Bog				Geauga	Burton			L	
Rockwell Bog				Portage	Franklin		Bog	M	
Round Lake	Mud Lake	40.6722	-82.1448	Ashland	Lake		Bog	H	H
Savannah Lakes		40.9456	-82.3518	Ashland	Clear Creek			L	D
Seville Bog				Lorain	Camden		Bog	M	
Singer Lake Bog		40.9167	-81.4862	Summit	Green	33	Bog	H	E
Snow Lake	South Pond	41.4259	-81.1755	Geauga	Troy		Bog	M	E
Snyder Bog		40.9167	-80.6415	Mahoning	Beaver		Bog	M	H
Solon Bog	Geauga Lake/Pond, Aurora Lake/Pond	41.3377	-81.3859	Cuyahoga	Solon		Bog	L	H
St Joseph Bog		41.4959	-84.7763	Williams	St Joseph	8	Bog	H	H
Steinert's Bog				Summit	Bath		Bog	M	
Stratton Pond				Portage	Franklin		Bog	M	
Torrens Bog				Licking	Burlington		Bog	H	
Triangle Lake Bog		41.1181	-81.2617	Portage	Rootstown		Bog	H	E
Turkeyfoot Lake Bog				Summit	New Franklin		Bog	H	
Utica Bog	Cranberry Prairie			Licking	Washington		Bog	M	
Utzinger Bog		39.8333	-83.0289	Franklin	Jackson			M	H
West Swamp				Trumbull	Braceville		Bog	M	
Youngs Bog		41.0149	-81.4038	Summit	Springfield			M	E

Characterizing the Link Between Algal Bloom Biomass and Methane Production in Ohio Reservoirs

Basic Information

Title:	Characterizing the Link Between Algal Bloom Biomass and Methane Production in Ohio Reservoirs
Project Number:	2017OH533B
Start Date:	3/1/2017
End Date:	2/28/2019
Funding Source:	104B
Congressional District:	1
Research Category:	Biological Sciences
Focus Categories:	Nutrients, Ecology, Water Quality
Descriptors:	None
Principal Investigators:	Ishi Buffam, Trinity L Hamilton

Publications

1. Berberich, M.E. 2017. Spatial variability of methane production and methanogen communities in a reservoir: importance of organic matter source and quantity. MS Thesis, Department of Biological Sciences, University of Cincinnati.
2. *Berberich, M., I. Buffam, J. Beaulieu, T. Hamilton, S. Waldo, and X. Li. December 2016. Sediment characteristics and microbial communities associated with methane production in a eutrophic reservoir. American Geophysical Union Fall 2016 Conference, San Francisco, CA, USA (poster).

Annual Progress Report 2017-18

Characterizing the Link Between Algal Bloom Biomass and Methane Production in Ohio Reservoirs

*Grant# OSURF 60059469 - Sub G16AP00076 USGS: 3/1/2017 – 2/28/2018
This progress report includes results from the first year of the project, which is under a no-cost extension through Feb. 2019.*

Ishi Buffam and Trinity Hamilton
University of Cincinnati

Table of Contents

1. SUMMARY	2
2. PROBLEM AND RESEARCH OBJECTIVES	2
3. SPECIFIC AIM #1: WITHIN-RESERVOIR SPATIAL VARIABILITY IN METHANE PRODUCTION	4
3.1 METHODOLOGY	4
3.2 PRINCIPAL FINDINGS.....	7
4. SPECIFIC AIM #2: COMPARISON OF METHANE PRODUCTION RATES AMONG OHIO RESERVOIRS	11
4.1 METHODOLOGY.....	11
4.2 PRINCIPAL FINDINGS.....	12
5. SIGNIFICANCE	12
6. PUBLICATION CITATIONS	13
7. STUDENTS SUPPORTED BY THE PROJECT.....	13
8. PROFESSIONAL PLACEMENT OF STUDENTS	14
9. NOTABLE AWARDS AND ACHIEVEMENTS.....	14
10. REFERENCES	15

1. Summary

In this study, we examined the link between eutrophication and methane production in Ohio Reservoirs, with a focus on sediment microbial processes. Algal blooms and the associated negative environmental impacts caused by nutrient enrichment have been identified as a leading cause of impairment of surface waters in Ohio. One of the understudied negative consequences of eutrophication is the increased potential for in-lake production and emissions of methane (CH_4), a potent greenhouse gas with a global warming potential 21 times that of CO_2 . Lab-scale studies have indicated the potential for increased methane production in lake/reservoir sediments with labile algal organic matter added, but it is not known whether this relationship translates to the field scale. This is an important question for Ohio water resource management, as Ohio has a large number of reservoirs, many of which suffer from eutrophication due to high nutrient inputs, mainly from agricultural landscapes. The *overall objective* of this project was to determine the relationship between the occurrence of algal blooms and sediment CH_4 production rates in Ohio reservoirs, as mediated by sediment organic matter quantity and quality and the sediment microbial community. We examined these relationships at two spatial scales, highlighting both within-reservoir and among reservoir variation.

To date we have carried out the analysis for the within-reservoir variability in Harsha Lake, and those results are presented here; in the coming year we will continue to compile results from the among-reservoir Ohio-wide sampling as well as finishing off lab analyses. For Harsha Lake, areal CH_4 production rates were highest in the riverine portion of the reservoir below the main inlet where sediment organic matter (OM) quantity was greatest, presumably due to high OM sedimentation rates. The pattern of high CH_4 production rates in the riverine portion of the reservoir persisted even when rates were normalized to OM quantity, suggesting that not only was OM more abundant in the riverine zone, it was more readily utilized by methanogens. Sediment stable isotopes and elemental ratios indicated a greater proportion of allochthonous (terrestrial) OM in the riverine zone than other areas of the reservoir, suggesting that watershed derived OM is an important driver of CH_4 production in the system. Methanogens were abundant at all sampling sites but the functional diversity of methanogens was highest in the riverine zone, likely reflecting differences in decomposition processes or OM quality across the reservoir. Notably, in contrast to our expectation that water column algal productivity would be a key predictor of CH_4 emission rates, we found that the highest production rates occurred at sites with a strong contribution of terrestrial OM – indicating that both algal OM and terrestrial OM may be important substrates for CH_4 production in this eutrophic reservoir.

2. Problem and Research Objectives

Increased nutrient loading to lakes and reservoirs can cause eutrophication and an associated suite of environmental impacts including toxic algal blooms, water column anoxia, fish kills, and taste and odor problems. As such, nutrient enrichment has been identified as a leading cause of impairment of surface water ecosystems in Ohio (Ohio EPA, 2014). Eutrophication also has other less well-known negative consequences, notably the potential for in-lake production and emissions of methane (CH_4), a potent greenhouse gas (GHG) with a global warming potential 21 times that of CO_2 . Research in southwest Ohio has shown that GHG emissions from reservoirs draining agricultural watersheds can be exceptionally high (Beaulieu et al. 2014) and a recent review study indicates that reservoir productivity is the best predictor of CH_4 emissions (Deemer et al. 2016). Methanogenesis (microbial methane production) in aquatic ecosystems is an important source of methane to the atmosphere, and there is compelling evidence that CH_4

emissions from reservoirs is underestimated and thus not adequately quantified in the global GHG budget (Bastviken 2011, Deemer et al. 2016). Meanwhile, lab studies have demonstrated that the addition of fresh algal material to lake/reservoir sediments can stimulate CH₄ production under anoxic conditions by providing a labile carbon source (West et al. 2012, Schwarz et al. 2008). These data suggest that increased algal blooms resulting from nutrient loading may stimulate *in situ* methanogenesis, leading to increased CH₄ emissions from eutrophic reservoirs. This would be a significant environmental disservice, but there is a critical knowledge gap regarding the relationship between algal bloom occurrence and CH₄ production at the scale of whole ecosystems. A better understanding of this process is required to evaluate the extent of negative impacts caused by nutrient loading, and to properly place value on nutrient loading reductions resulting from regulatory or water quality trading approaches (US EPA, 2003).

The **objective** of this project was to quantify the relationship between algal bloom formation, sediment organic matter quality, and sediment microbial CH₄ production in Ohio reservoirs. We highlight reservoirs rather than natural lakes, because (1) reservoirs are understudied relative to natural lakes, yet cover more area than natural lakes (aside from Erie) within Ohio and many regions, and are growing in prevalence globally (Downing et al., 2006); (2) reservoirs typically have a high watershed area:lake area ratio, thus tend to receive high sediment and nutrient loads and are prone to eutrophication (Jones et al. 2004, Dodds and Whiles 2010); (3) recent measurements in a SW Ohio reservoir have revealed CH₄ emissions among the highest ever reported for freshwaters (Beaulieu et al., 2014, Beaulieu et al., 2016).

Our *central hypothesis* was that sediment CH₄-production rates would be higher and methanogens more abundant in reservoirs (and at locations within a given reservoir) where sediment characteristics reflect large contributions of algal-derived organic matter, that in turn reflect spatial variation in algal blooms. We approached our overall objective by testing the central hypothesis at two different spatial scales, with the following specific aims:

Specific Aim #1: Determine the relationship between algal-derived organic matter, CH₄ production and microbial community structure in sediments from Harsha Lake, over a within-reservoir spatial gradient in nutrient and algal organic matter loading. Our working hypothesis is that sediment CH₄ production rates and the abundance of methanogens will co-vary with sediment organic matter quantity and quality, which will in turn co-vary with algal productivity and deposition rates, and will thus be highest near the sediment delta formed downstream of the inlet of this well-studied reservoir in SW Ohio.

Specific Aim #2: Determine the relationship between algal-derived organic matter, CH₄ production and microbial community structure in sediments from 18 Ohio (and nearby) reservoirs, varying across a gradient of watershed land-use/land-cover and predicted trophic status. Our working hypothesis is that sediment CH₄ production rates and the abundance of methanogens will co-vary with sediment organic matter quantity and quality, which will in turn vary among reservoirs as a function of watershed agricultural cover.

We addressed these aims by determining sediment CH₄ production rates, methanogen abundance and microbial community structure, and labile organic matter content along a transect of 15 sites in Harsha Lake, and for two sediment locations (one deep, one near the main river inlet) in each of 18 Ohio reservoirs varying across a gradient of land-use.

3. Specific Aim #1: Within-Reservoir Spatial Variability in Methane Production

3.1 Methodology

Site description. William H. Harsha Lake (Figure 1) is a reservoir in southwest Ohio that was built on the East Fork of the Little Miami River in 1978. The primary functions of this reservoir include flood control, drinking water supply, recreation, and wildlife habitat. It has a surface area of 7.9 km², is seasonally stratified, and reaches 32.8 m at its maximum depth. Harsha Lake's watershed is 882 km², with agriculture (including corn, soybean and pasture) as the dominant land-use (Beaulieu et al. 2016).

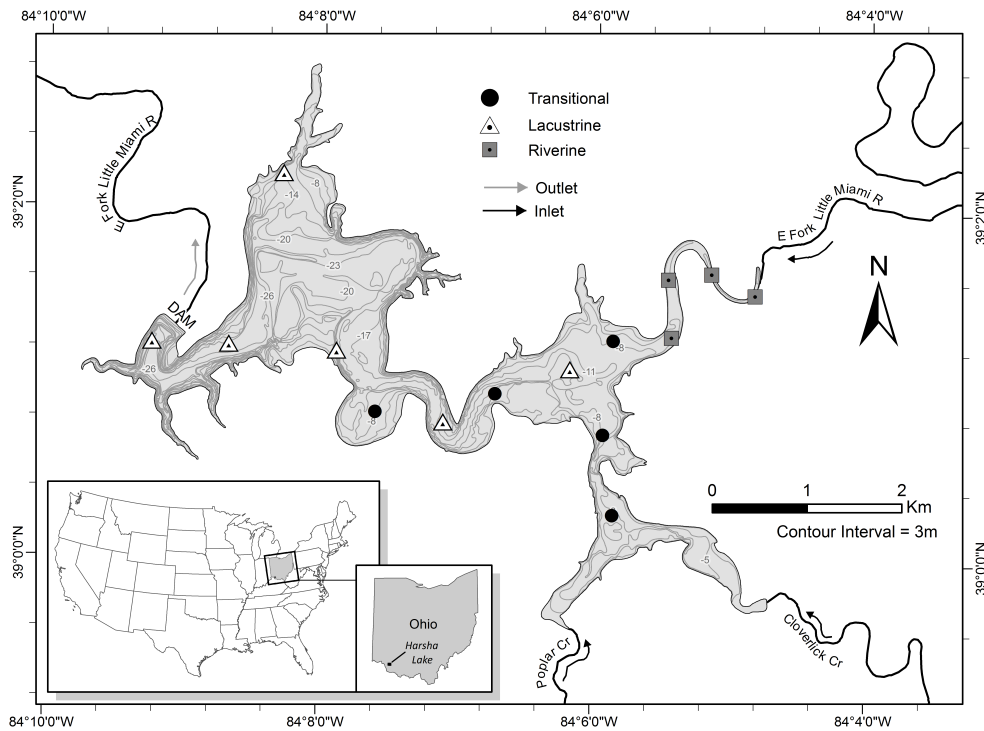


Figure 1. Harsha Lake sampling sites and site categories. The legend indicates which sites were assigned to the riverine, transitional, and lacustrine zones.

Sample collection. Triplicate sediment cores, water samples, and water column measurements were collected from 15 sites across the reservoir (Figure 1) within a 7-day window in late May. Sites were selected to span the length of the reservoir and encompass a range of water depths, temperature, oxygen, productivity, and inputs to the sediment. Sites were categorized into reservoir zones (riverine, transitional or lacustrine) based on thermal stratification from temperature-depth profiles measured at each site in July, when stratification was expected to be strongest. On each date, three sediment cores (Figure 2) were collected from each of five sites distributed across the three reservoir zones using a K-B Corer. Epilimnion (0.1 m) and hypolimnion (0.5-2 m above sediment) water samples were collected at each site using a Niskin bottle. Depth profiles of water temperature, pH, dissolved oxygen, specific conductivity were measured using a YSI ProDSS multiparameter sonde, and depth profiles of chromophoric dissolved organic matter (CDOM), in vivo chlorophyll a, and turbidity were measured using a Turner C3 Submersible Fluorometer at each site. Secchi depth and depth profiles of photosynthetically active radiation (PAR) were also measured.

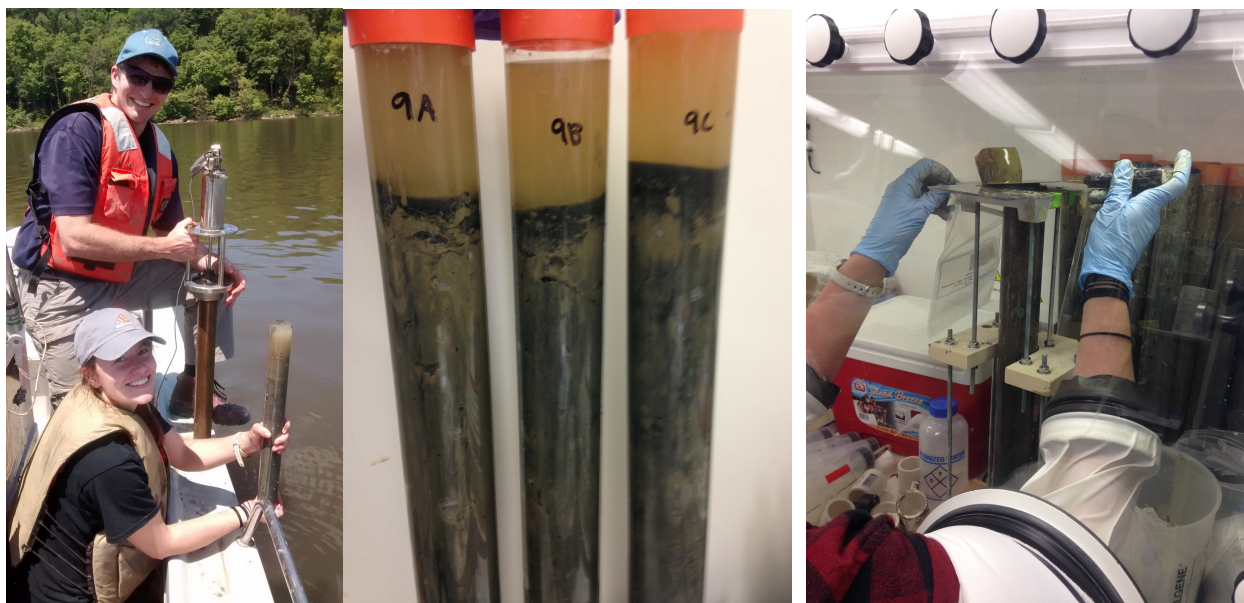


Figure 2. Left: Dr. Jake Beaulieu and Megan Berberich collecting sediment cores with K-B corer. Middle: Triplicate cores from a single site in Harsha Lake. Right: Core extrusion under N₂ atmosphere in glove box to retain anaerobic conditions while subsampling.

Water sample processing. Water samples collected from each site were stored on ice or refrigerated until they were processed (within 24 hours). Water samples were analyzed for chlorophyll *a*, dissolved nutrients, and total suspended solids (TSS). The spectrophotometric method was used to measure chlorophyll *a* following acetone extraction (APHA 2012).

Sediment processing. Sediment cores were sectioned and processed within 24 hours of collection. The top 5 cm of each core was extruded, homogenized, and subsampled in a glove box under N₂ atmosphere (Figure 2). Subsamples of sediment were used for CH₄ potential production rate assays, sediment characterization, porewater collection and nucleic acid extraction. Sediment slurries were prepared in the glove box by adding 15 mL of sediment and 15 mL of lake water to a 120 mL serum bottle using syringes. Slurries were capped with a rubber stopper, crimp sealed, and wrapped in aluminum foil.

Sediment slurries – potential CH₄ production rates. All slurries were stored in the dark at room temperature (~23 °C) during the 9-day incubation. 11 mL gas samples were taken on days 1, 2, 3, 5, 7 and 9. After taking the gas sample, 11 mL of N₂ gas was returned to the serum bottle to maintain the same pressure. Gas samples were analyzed on a gas chromatograph (Bruker 450, Massachusetts, U.S.A.) equipped with a flame ionization detector (FID). Methane production rates for the slurries were calculated by accounting for dilution during sampling, then determining the change of moles of methane over time. Methane production rates were expressed either normalized to sediment volume, sediment dry mass, or mass of sediment organic matter.

Sediment characterization. Sediment was dried at 60 °C for 3 days or until constant weight, and then ground to a fine powder before further analysis. Elemental analysis and stable isotope analysis (¹³C and ¹⁵N) were conducted using an elemental analyzer connected to an isotope ratio mass spectrometer (EA-IRMS). Sediment was fumigated with hydrochloric acid prior to C and ¹³C analysis to removed carbonates (Harris et al. 2001). Density was calculated from the weight

of a known volume of sediment. Organic matter content was calculated by determining weight loss after ignition (550°C, 4 hours). Elemental and isotopic composition of sediment was used to determine the proportion of autochthonous and allochthonous organic matter (see *Mixing model*).

Porewater analyses. Porewater was extracted from a subsample of sediment for determination of volatile fatty acids (VFA), dissolved organic carbon (DOC), and for excitation emission matrix (EEMs) fluorescence. We extracted porewater by centrifuging sediment in 50 mL tubes at 7800 rpm. The porewater was filtered at 0.45 µm prior to measurement of optical absorbance and fluorescence using a scanning spectrofluorometer. The optical data were used to calculate the fluorescence index (FI), biological index (BIX), relative fluorescence efficiency (RFE), and the specific ultraviolet absorbance at 254 nm (SUVA₂₅₄), which provide information about the composition and source of dissolved organic matter. A summary of these and other optical properties is described by Hansen et al (2016).

Sediment traps. Sediment traps (Figure 3) were deployed at 3 of the 15 sampling sites (one per reservoir zone) to determine sedimentation rates and composition of the water column particulate matter. Sediment traps were deployed for seven weeks during summer, with the initial deployment in early June. Traps were constructed using 2" PVC pipe and caps for a final height to diameter ratio of 5:1 (Bloesch & Burns 1980), and were deployed 2 m from the sediment surface for the transitional and lacustrine sites, and 1.5 m above the sediment for the riverine site due to the shallow water depth at this location. Traps were sampled weekly to minimize OM decomposition. Sedimentation rates were determined by calculating the total solids (TS) per sediment trap area, and dividing by the number of days the trap was deployed. Organic matter, chlorophyll *a*, elemental composition (C, N) and stable isotope composition (¹³C and ¹⁵N) for a subset of the samples were measured to evaluate the composition of the sediment trap material using the methods described above.



Figure 3. Sediment trap deployment in Harsha Lake.

DNA extraction and analysis. DNA was extracted from ~500 mg (wet weight) of sediment from each core using a MoBio PowerSoil® DNA Isolation Kit following the manufacturer's protocol. DNA concentration was determined using a Qubit dsDNA HS Assay kit and a Qubit 3.0 Fluorometer. DNA was used in *Microbial community analysis* and *qPCR*. **Microbial community analysis.** The V4 region of the 16S rRNA gene was amplified and sequenced using the paired-end Illumina MiSeq sequencing platform with the primers 515f and 806rB (Caporaso et al. 2012; Apprill et al. 2015). All sequencing was performed at the Center for Bioinformatics & Functional Genomics at Miami University (Oxford, OH, USA). **qPCR.** Quantitative polymerase chain reactions (qPCR) were performed to determine the abundance of *mcrA* (a biomarker for methanogens), and archaeal 16S rRNA genes on a StepOne Plus™ Real-Time PCR System. *mcrA* encodes a protein necessary for methanogenesis and has been widely used as a marker for methanogens (Luton et al. 2002). Further details of the *Microbial community analysis* and *qPCR* methods, including quality control approach, can be found in Berberich 2017.

Mixing model for determining contribution of autochthonous OM to sediment. A mixing model was generated to estimate the proportion of autochthonous (aquatic) vs. allochthonous

(terrestrial) organic matter found in each sediment sample, using the MixSIAR package version 3.1.7 (Stock & Semmens 2013) in R. The model used as input the C/N ratios and $\delta^{15}\text{N}$ isotopic signature of terrestrial and aquatic end-members (sources) of OM. Terrestrial samples were taken from the surrounding watershed and included stream-bank soil, leaf litter, corn field soil, and corn stalk litter from tributary streams and a field along the perimeter of the reservoir. Aquatic end members came from epilimnion water samples from each of the 15 sites in late May.

Statistical methods and data analysis. All statistical analyses were performed using R version 3.4.0 (R Core Team 2017). One-way nested ANOVAs were used to evaluate differences in sediment characteristics, methane production, and microbial community characteristics among reservoir zones. Partial least square (PLS) regression analysis with the R package ‘plsdepot’ was used to investigate which measured parameters best explained variation in methane production rates (Gaston Sanchez 2012). One response variable, methane production rates ($\mu\text{mol CH}_4 \text{ cm}^{-3} \text{ day}^{-1}$), was used. Explanatory variables included water column variables (water chemistry, temperature, dissolved oxygen, chlorophyll, etc.), sediment variables (density, organic matter content, organic matter source, etc.) and biological variables (percent of different methanogen genera).

3.2 Principal Findings

In summary, we found distinct differences among reservoir zones in Harsha Lake sediments for physicochemical parameters including organic matter (OM) quantity and source, and for the methane production rates. Methanogens were abundant at all sampling sites but the functional diversity of methanogens was highest in the riverine zone. Variation in functional diversity of methanogens likely reflects differences in decomposition processes or OM quality across the reservoir. Methane production rate was highest in the shallow riverine zone near the inlet, as hypothesized as this was also the area of highest surficial methane emissions and an area of extensive algal blooms. Methane production was also correlated with both sediment organic matter quantity and source. As hypothesized, higher overall OM content gave rise to higher CH_4 production rates. However, the relationship with OM source was not a simple positive correlation with sediment algal OM in the way that we had initially hypothesized. In fact, the zone with the highest methane production rates, the shallow riverine zone, also had the highest proportion of terrestrial (as opposed to algal-derived) organic matter in the sediment. Thus, overall sediment methane production rates were negatively correlated with algal-derived OM proportion in the solid sediment, at the same time positively correlated with algal-derived OM proportion in the dissolved phase (porewaters) of the sediment.

We have several working hypotheses for why this may be the case, and continue to explore this as we develop this project. One possibility is that it is the dissolved fraction of OM that is primarily driving methane production, therefore the relationship that is seen between methane production rates and the solid fraction of OM is of less consequence. More likely, both terrestrial and algal-derived OM may be important for CH_4 production, and the algal sources are rapidly degraded but the terrestrial OM is degraded over both short and longer time scales (see Guillemette et al. 2017; Grasset et al. 2018). Overall, the riverine zone has more OM, and definitely more terrestrial OM than the other zones. Thus, the terrestrial OM source in this zone may be degraded at a more consistent rate over time and contribute to CH_4 production along with the algal OM, leading to an overall higher CH_4 production rate.

Key results from each component of the Harsha Lake study are detailed below.

Site characteristics. The depth of the water column averaged 3.6 m in the riverine zone, 9.6 m in the transitional zone, and 20.3 m in the lacustrine zone. All sites were nutrient rich, with epilimnion total nitrogen (TN) concentrations ranging from 1210 – 2040 $\mu\text{g/L}$ and total phosphorus (TP) concentrations ranging from 166 – 232 $\mu\text{g/L}$. The riverine zone had the highest average TN and TP concentrations (1745 and 210 $\mu\text{g/L}$, respectively), and the lacustrine zone had the lowest average concentrations (1380 and 180 $\mu\text{g/L}$, respectively). Similarly, chlorophyll *a* was highest in the riverine zone (47.6 $\mu\text{g/L}$). Secchi depth increased from the riverine zone (average 0.33 m) to the lacustrine zone (average 0.78 m).

Methane production among reservoir zones. Potential CH_4 production rates normalized by slurry volume and by grams of organic matter were greater in riverine zone compared to the transitional or lacustrine zones (Figure 4), which is consistent with previous reports of higher CH_4 emission rates in the riverine zone compared to other areas of this reservoir (Beaulieu et al. 2014, 2016). Published areal surface CH_4 emission rates from the Harsha Lake riverine zone (Beaulieu et al. 2016) and the average of our measured riverine zone sediment CH_4 production rates from this study were in remarkable agreement (33.0 $\text{mg CH}_4 \text{ m}^{-2} \text{ h}^{-1}$ and 30.8 $\text{mg CH}_4 \text{ m}^{-2} \text{ h}^{-1}$, respectively). However, CH_4 surface emission rates in the riverine zone in Harsha can be six-fold (Beaulieu et al. 2016) to 1-2 orders of magnitude (Beaulieu et al. 2014) higher than other areas of the reservoir, while sediment CH_4 production rates were only two-fold higher in the riverine zone compared to other zones. This contrast is likely due to methane oxidation in lacustrine and transitional zones where the water column is deeper and more strongly stratified.

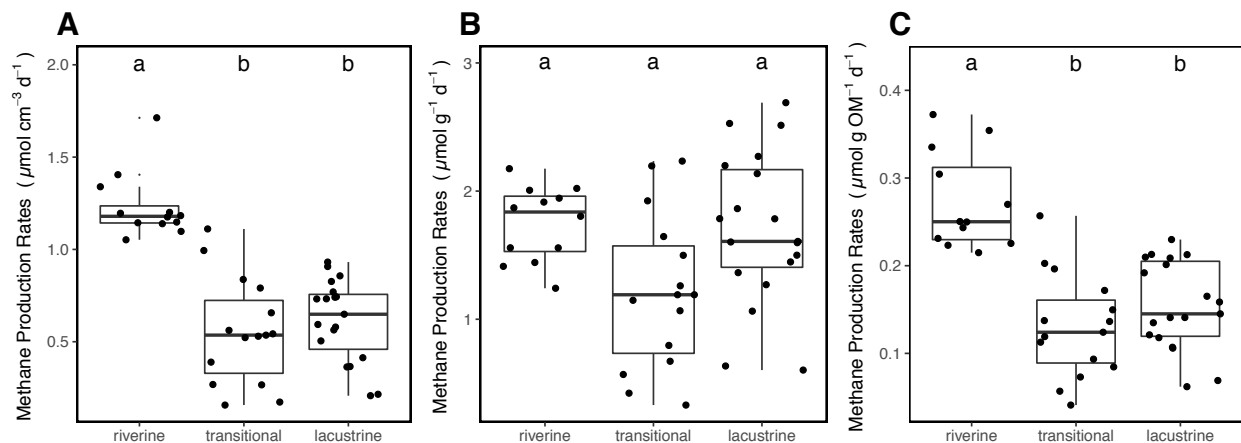


Figure 4. Potential methane production rates from sediment slurries in each of the reservoir zones, normalized to sediment volume (A), sediment mass (B), and sediment organic matter (C). Dots represent the potential methane production rate calculated from each sediment core by a sediment slurry assay. Different lowercase letters indicate significant differences between reservoir zones.

Sediment characteristics among reservoir zones. Sediment was the densest in the riverine zone, intermediate in the transitional zone, and the least dense in the lacustrine zone. The quantity of organic matter was greatest in the riverine zone for both the solid fraction of OM (g OM cm^{-3}) and the dissolved fraction of OM from the sediment porewater (DOC, g mL^{-1}) (Figure 5), but the differences among zones for the solid fraction of OM were not significant. The dissolved fraction of OM was greater in the riverine zone than either the transitional or lacustrine zones. Stable isotope and elemental composition data indicated that the source of OM varied significantly among reservoir zones in the solid fraction (Figure 6). The proportion of autochthonous solid-

fraction OM (calculated from the mixing model) was lowest in the riverine zone, intermediate in the transitional zone, and highest in the lacustrine zone (Figure 6). Optical properties of the dissolved OM showed some evidence of differences in DOM source across reservoir zones. FI values of DOM were significantly higher in the riverine zone than the lacustrine or transitional zones, indicating a higher proportion of DOM derived from microbial sources (e.g. bacteria and algae) relative to terrestrial OM (McKnight et al. 2001; Cory et al. 2010).

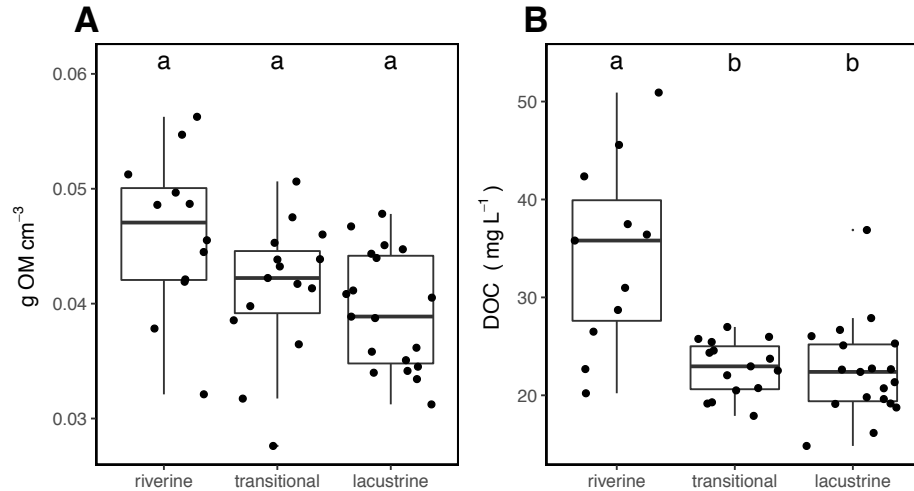


Figure 5. Comparison of the quantity of OM among reservoir zones. Panel A represents the amount of OM found in the bulk sediment, normalized to sediment volume. Panel B represents the concentration of the dissolved fraction of OM found in the sediment porewater, measured as DOC. One riverine value with an exceptionally high DOC concentration was excluded from the plot for readability. Different lowercase letters indicate significant differences between reservoir zones.

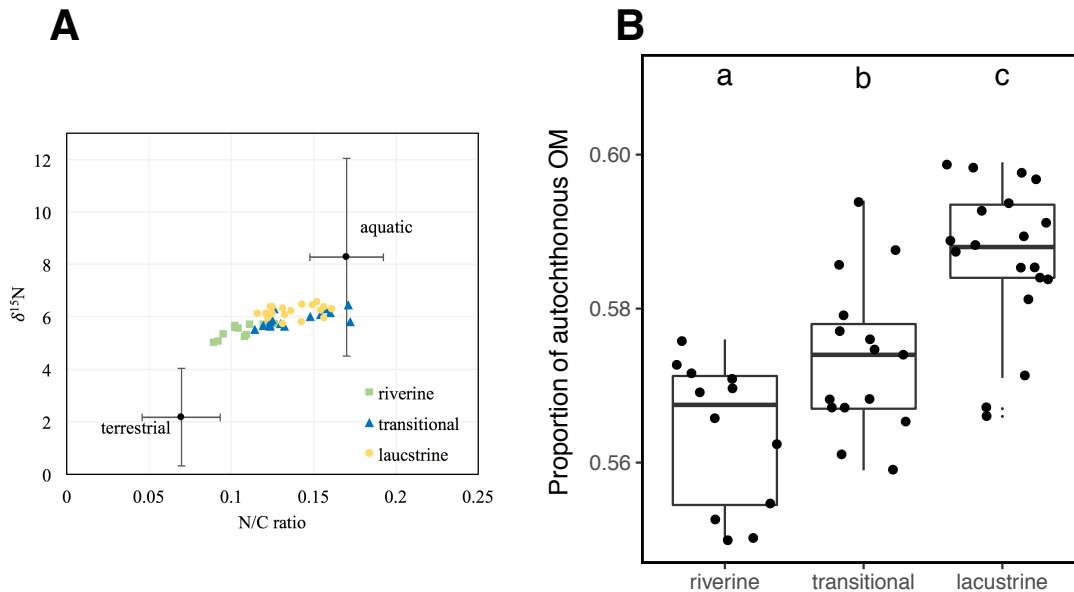


Figure 6. Plot of $\delta^{15}\text{N}$ vs. N/C elemental ratios of terrestrial and aquatic OM sources, and the sediment mixtures for each core across the three reservoir zones (A). The center dots for the two sources represent the mean values ($n = 13$ for terrestrial sources, $n = 16$ for aquatic sources), and error bars represent the standard deviation. Panel B depicts the proportion of autochthonous (aquatic) OM found in each core grouped by reservoir zones calculated from the stable isotope mixing model. Different lowercase letters indicate significant differences among reservoir zones.

Methanogen communities among reservoir zones. There were no differences in copy number for either the *mcrA* gene (an indicator of methanogen community abundance in the sediments) or the archaeal 16S rRNA gene (an indicator of total archaeal abundance in the sediments) among reservoir zones. On average, methanogens represented 34% of total archaea. Representative operational taxonomic units (OTUs) from the order Methanomicrobiales accounted for 53%, 77% and 76% of total methanogen sequences from the riverine, transitional, and lacustrine zones, respectively. The order Methanosarcinales comprised 34%, 16% and 17% of riverine, transitional and lacustrine methanogens. The most notable difference in methanogen communities among reservoir zones was the abundance of *Methanosarcina*, a genus of the Methanosarcinales order, which composed 15% of methanogens at the riverine sites, but < 1% of transitional and lacustrine methanogens.

Similar to results of other studies in freshwater systems, we found no correlation between methanogen abundance and CH₄ production rates, likely because methanogen activity, rather than abundance, determines rates of methanogenesis (West et al. 2012; Chaudhary & Blaser 2017). We observed higher methanogen functional diversity in the zone with the highest methane production rates and high OM diversity—the riverine zone where the water does not stratify. The elevated rates of CH₄ production in the riverine zone could be due to higher processing of OM in the presence of oxygen before it reaches the anoxic sediment layers, resulting in high substrate availability for methanogenesis.

Sediment deposition rates and deposited sediment composition. Over the 6-week sediment trap deployment period, average sediment deposition rates were highest in the riverine sediment trap site, and lowest in the lacustrine sediment trap site (Table 1). Similar to the benthic sediment, the proportion of organic matter of the deposited sediment was lowest in the riverine site and highest in the lacustrine site. Despite this, the rate of chlorophyll deposition in the lacustrine sediment trap over the 6-week period averaged less than that of the riverine and transitional sites. In short, the quantity and source of OM observed in the sediment traps, matched well with the patterns observed in the bottom sediments for the respective reservoir zones.

Table 1. Average sedimentation rates, and %OM for the three sites that were sampled regularly.

Site (Zone)	Sedimentation rates (mg/cm ² /day)	OM percent	Sedimentation rates (mg OM/cm ² /day)
EFL (Lacustrine)	1.53	22.57	0.33
ENN (Transition)	4.66	18.91	0.82
EUS (Riverine)	53.07	19.37	6.52

Predicting CH_4 production rates from all measured variables. PLS analysis confirmed that the three reservoir zones have distinct sediment, water column, and microbial community characteristics, and that the triplicate cores show tight grouping within zones, with a few exceptions (Figure 7). The first and second components from PLS regression explained 70.0% and 15.8% of the variance among cores, respectively. Axis 1 depicts the main gradient in the data, which shows the transition from lacustrine to terrestrial (riverine) sites across many co-varying variables, and is reflected in methane production rates which increase across the gradient from lacustrine to terrestrial/riverine.

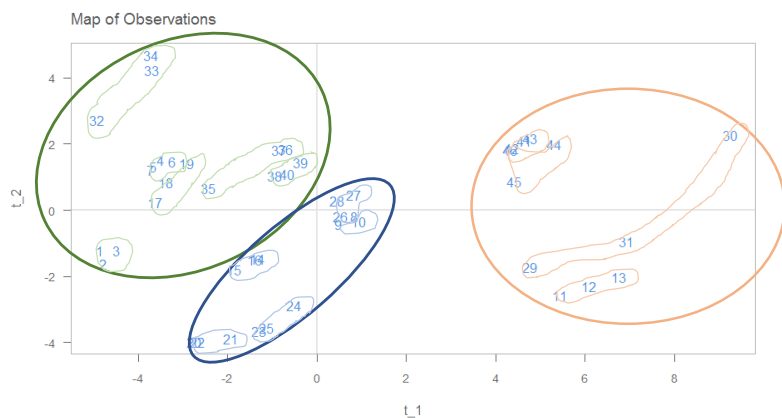


Figure 7. Results of Partial Least Squares Regression (PLS) multivariate analysis relating sediment methane production rates to characteristics of the sediments, water column, and microbial community at each core site in Harsha Lake. Each number represents a single core. The x-axis is the first PLS component, and the y-axis the second PLS component. The orange oval includes all cores from riverine sites, the blue oval includes all cores from the transitional sites, and the green oval includes all cores from the lacustrine sites. Smaller shapes are drawn around each set of three replicate cores from a given location.

The riverine zone is characterized by denser sediments with lower % OM, but a greater overall amount of OM per unit area due to the higher density. The riverine zone is also characterized by a higher proportion of terrestrially-derived OM, a higher apparent functional diversity of archaeal methanogen communities, and a higher CH_4 production rates. In short, the riverine zone is an area of active organic matter production, deposition, and decomposition, and consequently, CH_4 production. Our results show evidence for high sedimentation rates of OM of both algal and terrestrial origin, and both likely contribute to the high sediment CH_4 production rates. Because of the shallow nature of this zone, the CH_4 produced here is also likely able to quickly evade to the atmosphere, with little removal by CH_4 oxidation in the water column. Further work is needed to more fully partition the algal vs. terrestrial source of the carbon used to produce the CH_4 , and to determine whether similar patterns are seen in riverine vs. lacustrine zones of other reservoirs.

4. Specific Aim #2: Comparison of Methane production rates among Ohio reservoirs

4.1 Methodology

In conjunction with a regional assessment of reservoir CH_4 emissions undertaken by the US EPA, our collaborator Dr. Jake Beaulieu provided our group with sediment samples from 18 reservoirs in the states Ohio, Kentucky, and Indiana (United States) collected during the summer of 2016 (Figure 8). The reservoirs were selected to span gradients of agriculture/forest land-use

(7 – 83% forested) and water depth (max depth: 3- 35 m). Ebullitive CH₄ emissions were measured using 15 – 24 hour inverted funnel deployments, and diffusive emissions via 5 minute floating chamber deployments. Emissions were dominated by ebullition in most systems and were positively correlated with agricultural land use (Waldo and Beaulieu, unpublished data), in keeping with our overarching hypothesis.

Regional Reservoirs Sediment Sampling. Sediment was collected from the 18 regional reservoirs

using a ponar grab sampler. Upon retrieval, sediment was collected and stored in 500 mL amber Nalgene bottles without headspace on ice (~4°C) until processed.

Sediment Analysis. Sediment samples were processed and analyzed for methane production rates, sediment characteristics including organic matter source and quantity. A subset of samples were also analyzed for microbial community with a focus on methanogens. All analyses are carried out as described in the Methodology for Specific Aim #1 above. Analysis is currently underway for this part of the project, and will continue during the coming year.

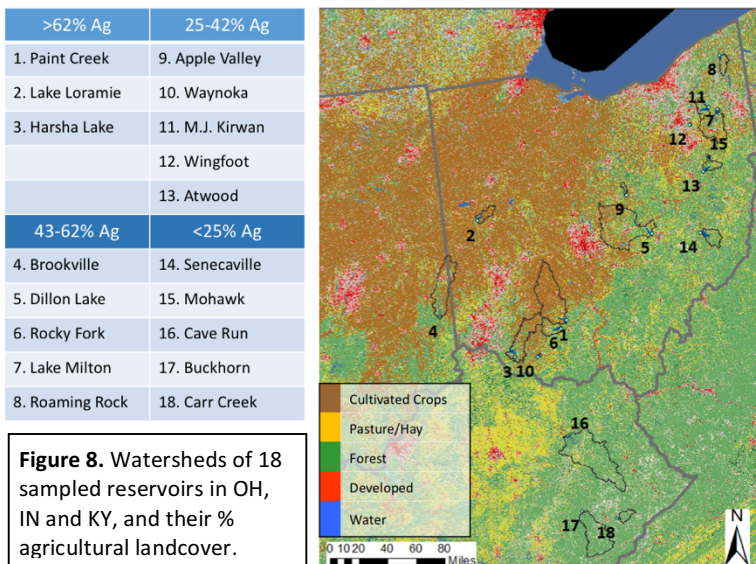
4.2 Principal Findings

At this point all samples have been collected and many of the laboratory analyses have been carried out for this second Specific Aim, but we have not yet undertaken overall synthesis and analysis of the data from the multi-reservoir survey. During the coming year we will complete lab analyses, analyze and synthesize the data.

5. Significance

We found that within the eutrophic Harsha Lake reservoir, the riverine zone was an area of particularly active organic matter production, deposition, and decomposition, and consequently, CH₄ production. Our results show evidence for high sedimentation rates of OM of both algal and terrestrial origin in this zone, and both likely contribute to the high sediment CH₄ production rates. Because of the shallow nature of this riverine zone, the CH₄ produced here is also likely able to quickly evade to the atmosphere, with little removal by CH₄ oxidation in the water column. Based on the high degree of spatial variation in CH₄ production rates, studies of reservoirs as well as natural lakes with substantial riverine inputs, would do well to take a spatially-aware sampling approach to determine CH₄ production and emissions, rather than sampling only at a single deep location. We recommend placing special attention on the riverine zone, as this zone is important in carbon biogeochemistry of reservoirs.

Another finding of significance was that source and quantity of organic matter are both important for methane production rates in reservoir sediments. This has important implications for global carbon cycling, as the amount of sediment OM transported to reservoirs is expected to increase as a function of land use change and with the number of reservoirs globally increasing.



Terrestrial OM may play an important role in fueling methane production in the zone with the highest potential rates. However, to verify this, this needs to be tested more directly. Future work should focus on specifically evaluating the role of terrestrial OM in methane production, particularly in depositional/riverine zones. A follow-up study would be useful to more fully partition the algal vs. terrestrial source of the carbon used to produce the CH₄, and our work in the coming year to complete the project will help to determine whether similar patterns are seen in riverine vs. lacustrine zones of other reservoirs in Ohio.

10. References

- Apprill, A., McNally S., Parsons R. & Weber L. (2015) Minor revision to V4 region SSU rRNA 806R gene primer greatly increases detection of SAR11 bacterioplankton. *Aquat. Microb. Ecol.* 75: 129–137. doi:10.3354/ame01753.
- Bastviken D., Tranvik L.J., Downing J.A., Crill P.M. & Enrich-Prast A. (2011) Freshwater Methane Emissions Offset the Continental Carbon Sink. *Science* 331: 50.
- Beaulieu J.J., McManus M.G., Nietch C.T. (2016) Estimates of reservoir methane emissions based on a spatially balanced probabilistic-survey. *Limnol. Oceanogr.* 61: S27-S40.
- Beaulieu J.J., Smolenski R.L., Nietch C.T., Townsend-Small A. & Elovitz M.S. (2014) High Methane Emissions from a Midlatitude Reservoir Draining an Agricultural Watershed. *Environ. Sci. Technol.* 48: 11100-11108.
- Berberich, M.E. 2017. Spatial variability of methane production and methanogen communities in a reservoir: importance of organic matter source and quantity. *MS Thesis*, Department of Biological Sciences, University of Cincinnati.
- Bloesch J. & Burns N.M. (1980) A critical review of sedimentation trap techniques. *Schweizerische Zeitschrift fur Hydrologie*, **42(1)**, 15-55.
- Caporaso J.G., Lauber C.L., Walters W.A., Berg-Lyons D., Huntley J., Fierer N., Owens S.M., Betley J., Fraser L., Bauer M., Gormely M., Gilbert J.A., Smith J., Knight R. (2012) Ultra-high-throughput microbial community analysis on the Illumina HiSeq and MiSeq platforms. *The ISME Journal* 6: 1621–1624.
- Chaudhary P.P., Rulík M., Blaser M. (2017) Is the methanogenic community reflecting the methane emissions of river sediments?-comparison of two study sites. *Microbiology Open* 7:947–9.
- Cory R. M., McNeill K., Cotner J.P., Amado A., Purcell J.M., and Marshall A.G. (2010) Singlet oxygen in the coupled photochemical and biochemical oxidation of dissolved organic matter. *Environ. Sci. Technol.* 44: 3683–3689.
- Deemer B.R., Harrison J.A., Li S., Beaulieu J.J., DelSontro T., Barros N., Bezerra-Neto J.F., Powers S.M., dos Santos M.A., Vonk J.A. (2016) Greenhouse gas emissions from reservoir water surfaces: A new global synthesis. *BioScience* 66: 949-964.
- Diggle P.J., Heagerty P., Liang K.Y., Zeger S.L. (2002) *The Analysis of Longitudinal Data*. Second Edition. Oxford University Press, Oxford, England.
- Dodds W. & Whiles M. (2010) *Freshwater Ecology: Concepts and Applications of Limnology*, 2nd edition. Elsevier, Amsterdam, 811 pp.
- Downing, J.A., Prairie, Y.T., Cole, J.J., Duarte, C.M., Tranvik, L.J., Striegl, R.G. *et al.* (2006). The global abundance and size distribution of lakes, ponds, and impoundments. *Limnol. Oceanogr.* 51: 2388-2397.

- Grasset, C., R. Mendonça, G. Villamor Saucedo, D. Bastviken, F. Roland, and S. Sobek. 2018. Large but variable methane production in anoxic freshwater sediment upon addition of allochthonous and autochthonous organic matter. *Limnol. Oceanogr.* **91**: 1225–14. doi:10.1002/lno.10786
- Guillemette F., Bianchi T.S., Spencer R.G.M. (2017) Old before your time: Ancient carbon incorporation in contemporary aquatic foodwebs. *Limnol Oceanogr* 33:2–19.
- Hansen A.M., Kraus TEC, Pellerin BA, Fleck JA, Downing BD, Bergamaschi BA. (2016) Optical properties of dissolved organic matter (DOM): Effects of biological and photolytic degradation. *Limnol. Oceanogr.* 61:1015–1032.
- Harris D., Horwath W.R., & van Kessel C. (2001) Acid fumigation of soils to remove carbonates prior to total organic carbon or carbon-13 isotopic analysis. *Soil Sci. Soc. Am. J.* 65: 1853-1856.
- Jones J.R., Knowlton M.F., Obrecht D.V., Cook E.A. (2004) Importance of landscape variables and morphology on nutrients in Missouri reservoirs. *Can J Fish Aquat Sci*, **61**, 1503–12.
- Luton P.E., Wayne J.M., Sharp R.J., Riley P.W. (2002) The mcrA gene as an alternative to 16S rRNA in the phylogenetic analysis of methanogen populations in landfill. *Microbiology* 148: 3521–3530.
- McKnight D.M., Boyer E.W., Westerhoff P.K., Doran P.T., Kulbe T., Andersen D.T. (2001) Spectrofluorometric characterization of dissolved organic matter for indication of precursor organic material and aromaticity. *Limnology and Oceanography* 46: doi: 10.4319/lno.2001.46.1.0038.
- Ohio EPA (2014). Nonpoint Source Program: Nonpoint Source Management Plan Update. 1-78. http://www.epa.ohio.gov/Portals/35/nps/NPS_Mgmt_Plan.pdf.
- R Core Team (2017). R: A language and environment for statistical computing. R Foundation for Statistical Computing, Vienna, Austria. <https://www.R-project.org/>.
- Schwarz J.I.K., Eckert W. & Conrad R. (2008) Response of methanogenic microbial community of a profundal lake sediment (Lake Kinneret, Israel) to algal deposition. *Limnol. Oceanogr.* 53: 113-121.
- Stock B.C. & Semmens B.X. (2013) MixSIAR GUI User Manual. Version 3.1. <https://github.com/brianstock/MixSIAR>.
- US EPA (U.S. Environmental Protection Agency), 2003. US Water Quality Trading Policy. Office of Water, Washington, D.C. <http://water.epa.gov/type/watersheds/trading/finalpolicy2003.cfm>.
- West W.E., Coloso J.J. & Jones S.E. (2012) Effects of algal and terrestrial carbon on methane production rates and methanogen community structure in a temperate lake sediment. *Freshwater Biol.* 57: 949-955.

Quantifying direct groundwater discharge to Lake Erie and vulnerability to hidden nutrient loads

Basic Information

Title:	Quantifying direct groundwater discharge to Lake Erie and vulnerability to hidden nutrient loads
Project Number:	2017OH534B
Start Date:	3/1/2017
End Date:	2/28/2019
Funding Source:	104B
Congressional District:	3rd
Research Category:	Ground-water Flow and Transport
Focus Categories:	Groundwater, Nutrients, Surface Water
Descriptors:	None
Principal Investigators:	Audrey Hucks Sawyer

Publications

1. Knights, Deon, Kevin C. Parks, Audrey H. Sawyer, Cédric H. David, Trevor N. Browning, Kelsey M. Danner, and Corey D. Wallace, (2017), Direct groundwater discharge and vulnerability to hidden nutrient loads along the Great Lakes coast of the United States, *Journal of Hydrology*, 554, 331-341, doi: 10.1016/j.jhydrol.2017.09.001
2. Knights, Deon, Parks, Kevin C, Sawyer, Audrey H, David, Cedric H, Browning, Trevor T, Danner, Kelsey M, & Wallace, Corey D. (2017). Output files corresponding to "Direct groundwater discharge and vulnerability to hidden nutrient loads along the Great Lakes coast of the United States" [Data set]. Zenodo. <http://doi.org/10.5281/zenodo.1011074>.
3. Sawyer, A.H. (2017) "Hidden chemical exchange due to lake-groundwater interactions." Presented at Water Management Association of Ohio luncheon series, April 19.
4. Knights, D., K.C. Parks, and A.H. Sawyer (2017). "Estimation of Groundwater Discharge and Nutrient Inputs to a Lake Erie Shoreline." Presented at Northwestern's Black Graduate Student Association Graduate Research Conference, Chicago, April 15.
5. Knights, Deon, Sawyer, Audrey H and Parks, Kevin (2016). "Estimation of direct groundwater discharge and nutrient inputs to a Lake Erie Shoreline." Presented at the Geological Society of America Annual Meeting in Denver, Colorado, September 25-29.

Final Report for Ohio Water Resources Center

Title: Quantifying direct groundwater discharge to Lake Erie and vulnerability to hidden nutrient loads

PI: Audrey Sawyer

1. Main Text

Problem and Research Objectives

Elevated nutrient inputs to the Great Lakes contribute to eutrophication and harmful algal blooms [Michalak *et al.*, 2013; National Wildlife Federation, 2011]. Harmful algal blooms are a major concern for federal and state governments and local communities because of negative impacts to aquatic ecosystems, fishery and tourism revenues, and essential drinking water resources. For example, a prolonged harmful algal bloom near Toledo, Ohio triggered a ban on tap water for 500,000 people in August of 2014. Lake Erie's shallow depth and short residence times render it particularly susceptible to nutrient contamination and harmful algal blooms [Richards *et al.*, 2010].

Nutrients can enter large lakes through river and groundwater inputs. Nutrient inputs from groundwater to the Great Lakes are poorly constrained, mainly because they are highly heterogeneous and broadly distributed along the coast [Kornelsen and Coulibaly, 2014; Robinson, 2015]. Groundwater fluxes to lakes can range by over five orders of magnitude [Rosenberry *et al.*, 2015]. Chemical fluxes are also obscured by variations in nutrient concentrations along discharging flow paths [Frape and Patterson, 1981; Kroeger and Charette, 2008; LaBaugh *et al.*, 1997; Sawyer, 2015]. For example, mineralization of organic matter may increase dissolved phosphorus concentrations, while sorption to sediment grains may reduce it [Lewandowski *et al.*, 2015]. Nitrate can be removed via denitrification in anoxic zones with a sufficient supply of organic carbon. Despite the potential for removal, nitrate concentrations in groundwater can exceed nitrate concentrations in rivers by an order of magnitude [Valiela *et al.*, 1990].

If nutrient concentrations in discharging groundwater are high, the groundwater-borne nutrient load can be high even if the rate of groundwater discharge is low [Valiela *et al.*, 1990]. In a review of lake studies, Lewandoski *et al.* [2015] found that typically groundwater-borne P loads across the sediment-water interface vary widely from 0.74 to 2900 mg PO₄-P m⁻² yr⁻¹, while N loads vary widely from 0.001 to 640 g m⁻² yr⁻¹. Groundwater inputs of phosphorus have been implicated as a possible contributor to algal fouling along the Lake Huron coast, although loads were not quantified [Barton *et al.*, 2013].

Deteriorating water quality in the Great Lakes and large uncertainties in nutrient sources motivate new studies on groundwater. A 2015 report for the Great Lakes Executive Committee identified several priority science needs for understanding groundwater effects on lake chemical, physical and biological integrity [Grannemann and Van Stempvoort, 2015]. The first two priority science needs are: 1) tools to characterize heterogeneity in groundwater/surface water exchanges, and 2) accurate quantification of groundwater discharge to surface water. Our study addresses both needs. ***Our first objective was to use a water budget approach to quantify direct groundwater discharge to Lake Erie and other parts of the Great Lakes coast. Our second objective was to use this information to assess areas that are vulnerable to high groundwater-borne nutrient loads and relate these vulnerability estimates to field***

measurements of groundwater-borne nutrient loads.

Methodology

Geospatial analysis. We estimated direct groundwater discharge rates to the Lake Erie coast using the water budget method of *Sawyer et al.* [2016]. In short, recharge zones for direct groundwater discharge were defined with NHDPlus [*McKay et al.*, 2012], a high-resolution hydrographic data available for the United States portion of the coast (43% of the entire Great Lakes coastline). We assumed that recharge zones are the wedge-shaped land areas outside stream catchments where water flows directly to the coast (Figure 1). We then assumed that recharge across these coastal catchments is the component of precipitation that infiltrates and would become base flow to a stream, if a stream were present, but instead flows to the coast.

Two types of data products from NHDPlus were used in this study: 1) the networks of rivers, streams and coastlines (a polyline product), and 2) their associated contributing catchments (a polygon product). These data products were obtained for the Great Lakes Region (Figure 1). A two-step process was used to estimate the geometry and size of recharge areas. First, coastlines were extracted from the polyline product using the feature type attribute. Second, the contributing catchments corresponding to each of the coastlines were extracted using the common NHDPlus integer identifier

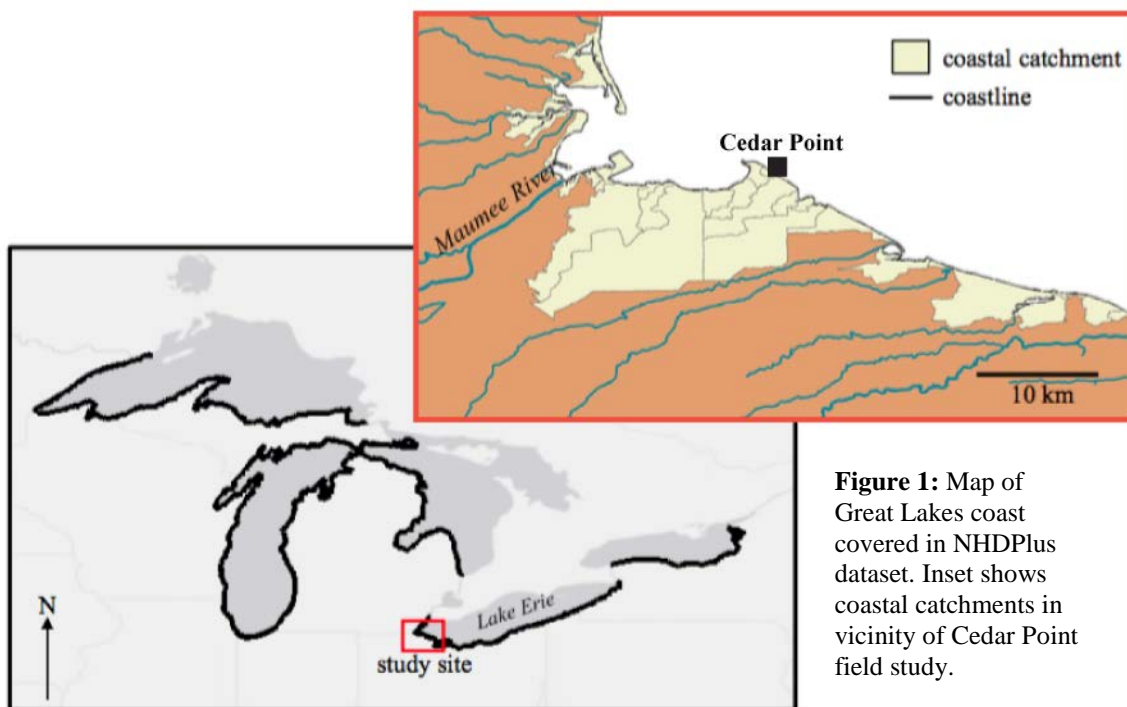


Figure 1: Map of Great Lakes coast covered in NHDPlus dataset. Inset shows coastal catchments in vicinity of Cedar Point field study.

relating polylines and polygons. Coastal catchments were then grouped by reach code. By construction, none of the coastal catchments contained streams, and instead the catchments were wedged between known intersections of streams and coast. The infiltrating precipitation within coastal catchments is assumed to flow to the coast and become direct groundwater discharge.

Infiltrating runoff was acquired from the second phase of NASA's North American Land Data Assimilation System, NLDAS2 [*Xia et al.*, 2012]. NLDAS2

provides a 30-year average monthly (1980-2009) dataset of terrestrial hydrologic quantities on a 1/8th degree (approximately 12.5 km) latitude-longitude grid over North America. We computed the recharge rate at each grid cell as the average of monthly infiltrating runoff from the NLDAS2 output based on the Variable Infiltration Capacity land surface model (VIC) [Liang *et al.*, 1994]. We excluded non-infiltrating runoff (another NLDAS2 product) because it presumably discharges to the coast as overland flow. We calculated annual recharge volume (m³/y) across each coastal catchment by multiplying the catchment area by the annual recharge rate nearest to the catchment centroid. This calculation assigns the recharge rate at the NLDAS2 grid cell that is closest to the catchment centroid to the entire catchment, which is a valid assumption because the contributing catchments are much smaller than the size of the NLDAS2 grid cell. Finally, we divided the annual recharge volume by the corresponding coastline length to produce a flux (m²/y). Uncertainty in the direct groundwater discharge rate was estimated using a multi-model ensemble produced with NLDAS2 output from the models VIC [Liang *et al.*, 1994], Mosaic [Koster and Suarez, 1994], and Noah [Chen *et al.*, 1997].

Next, we combined our estimates of direct groundwater discharge rates along the United States Great Lakes coast with land use data to map vulnerability to groundwater-borne nutrient loading. Where the direct groundwater discharge rate was above average and the fraction of total developed and agricultural land area was above average, we assumed that potential nutrient fluxes could be above average and designated these coastlines vulnerable to nutrient inputs from direct groundwater discharge. We determined the fraction of developed and agricultural land in each coastal catchment using the 2011 National Land Cover Database (<http://www.mrlc.gov/nlcd2011.php>). Specifically, we converted the raster dataset to a polygon shape file and summed the areas of developed, crop, and pasture land in each coastal recharge zone.

Field observations. Because vulnerability maps only indicate coastal regions with a greater likelihood of high nutrient inputs from groundwater, we conducted a detailed field study of a vulnerable coastal site to quantify groundwater-borne nutrient loads. The study site was located at Cedar Point Wildlife Refuge in the Western Lake Erie Basin (41°41'57.62"N, 83°19'32.95"W, Figure 1). Cedar Point is underlain by silty glacial till with a thin (1-2 m) veneer of highly permeable sand. The site is bordered by coastal wetlands, but the predominant land use within the entire coastal catchment is agricultural.

At the site, we measured direct groundwater seepage rates with Lee-type seepage meters (Figure 2). Specifically, twenty-four Lee-type seepage meters were deployed in three shore-perpendicular transects on the lake bed. Seepage meters were constructed from the ends of steel drums (internal diameter of 57 cm) modified from the design of Lee [1977] (Figure 2). Meters were spaced evenly in 5 or 10 meter intervals within each transect. The use of multiple transects allowed us to explore long-shore variation in seepage rates. We recorded the positions of the meters with a handheld GPS.

After installation of the meters, groundwater flow was allowed to equilibrate for one day prior to measurements. We measured seepage rates at a time with relatively calm nearshore conditions [Shinn *et al.*, 2002]. Measurements were conducted in two rounds and averaged to improve accuracy. Measurements were performed by connecting plastic autoclave bags to the meters via a quick connect valve (Figure 2). Bags were prefilled with 1.89 liters of lake water to allow measurement of recharge in addition to discharge. The prefilled bags were first weighed with a digital scale (± 0.05 kg precision). The

collection bags were then attached to the seepage meters for 3 hours. After collection, the bags were again weighed, and the volumetric seepage rate was calculated from the difference between the initial and final water mass in the bag and the density of water. The linear seepage rate was then calculated from the known cross-sectional area of the meter.

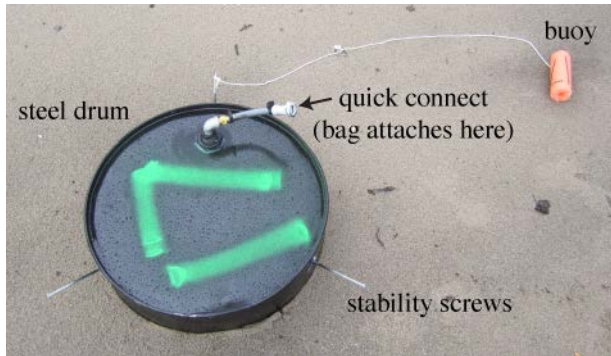


Figure 2: Photograph of a Lee-type seepage meter used by PI Sawyer's laboratory.

To understand fluxes of nutrients across the sediment-water interface, pore water samples were collected near each seepage meter (~1 m away) at 25 cm below the sediment-water interface. The samples were collected next to the meters instead of from the autoclave bags because the large steel meters restrict the supply of oxygen and can influence redox chemistry in the underlying groundwater. The sampling depth of 25 cm is somewhat arbitrary but was chosen to be deep enough to avoid drawing down lake water into the sampler but sufficiently close to the sediment-water interface to reflect the final chemistry of discharging groundwater as it flows through legacy lakebed sediments [Lewandowski *et al.*, 2015]. Pore water was collected by inserting a perforated steel tube with a 0.5-cm inner diameter and 0.6-cm outer diameter into the lakebed. The tube was purged by hand using a syringe, and the contents were discarded. The syringe was then used to collect 12 mL of pore water, which was filtered to 0.45 μm and placed immediately in a cooler on ice. Samples were transferred from the cooler to a freezer within 12 hours of collection. Additional samples were collected for end-member waters that mix in shallow lakebed sediments (lake water and onshore groundwater). Onshore groundwater samples were collected from piezometers screened near the water table on the adjacent beach.

Samples were analyzed in the Geochemistry Lab at The Ohio State University for basic anions, including dissolved reactive phosphate (PO_4^{3-}), using Ion Chromatograph (IC). Samples were analyzed for ammonium (NH_4^+), and nitrate plus nitrite ($\text{NO}_2^- + \text{NO}_3^-$) using a Skalar flow-injection nutrient analyzer.

We calculated the mass flux of nitrate plus nitrite, ammonium, and dissolved phosphorus per unit length of coast by assuming fluxes are purely advective. This calculation neglects dispersive fluxes and may be an underestimate.

Principal Findings and Results

Estimated rates of direct groundwater discharge along the Great Lakes coast are highly variable, but generally are greatest for Lake Erie and Lake Michigan [Knights *et al.*, 2017] (Figure 3). The average direct groundwater discharge rate for Lake Erie is 477 $\text{m}^3 \text{y}^{-1} \text{m}^{-1}$. At our Cedar Creek field site, measured discharge rates were significantly

lower than water budget-based estimates ($354 \pm 25 \text{ m}^3 \text{ y}^{-1} \text{ m}^{-1}$ compared to $588 \pm 181 \text{ m}^3 \text{ y}^{-1} \text{ m}^{-1}$). This comparison underscores the uncertainties in attempting to estimate direct groundwater discharge rates, which can vary by orders of magnitude across different lithologies or sediment types.

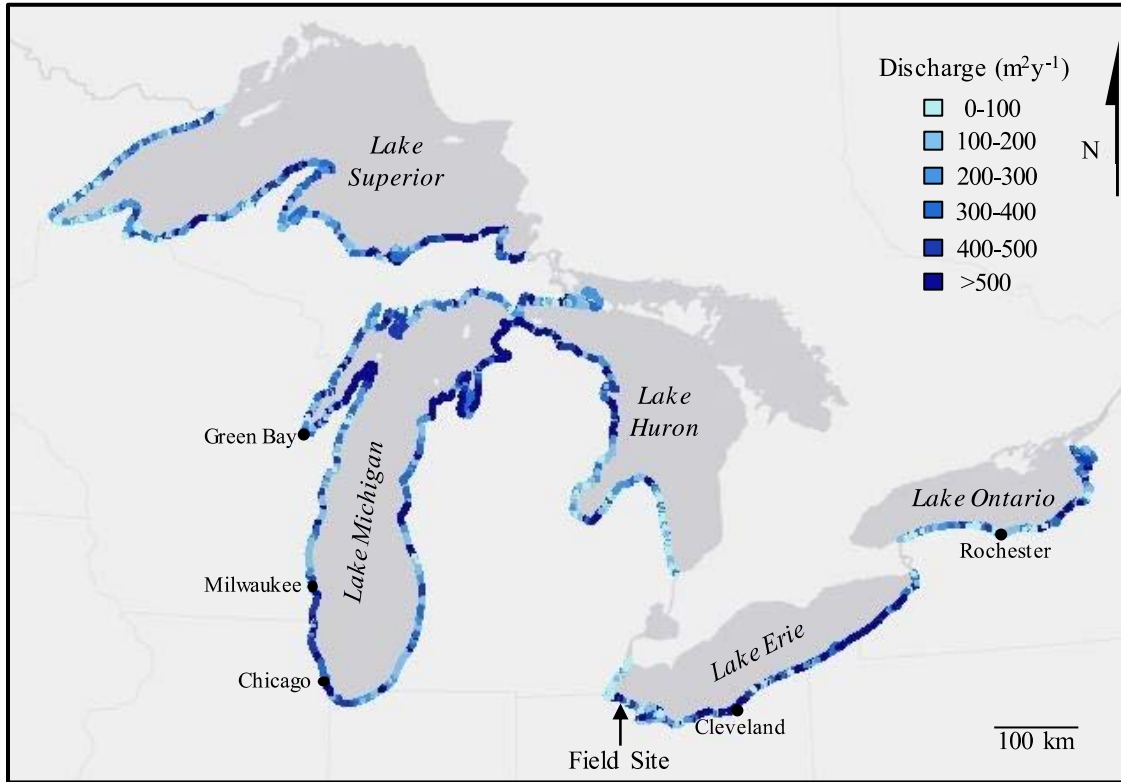


Figure 3: Direct ground water discharge to the Great Lakes. Discharge rates are high along the eastern and central sections of Lake Erie.

Approximately 15% of the analyzed Great Lakes coast is vulnerable to nutrient inputs from groundwater, and Lake Erie shoulders the highest vulnerability [*Knights et al.*, 2017]. Almost one-third of Lake Erie's United States coastline is vulnerable (Figure 4).

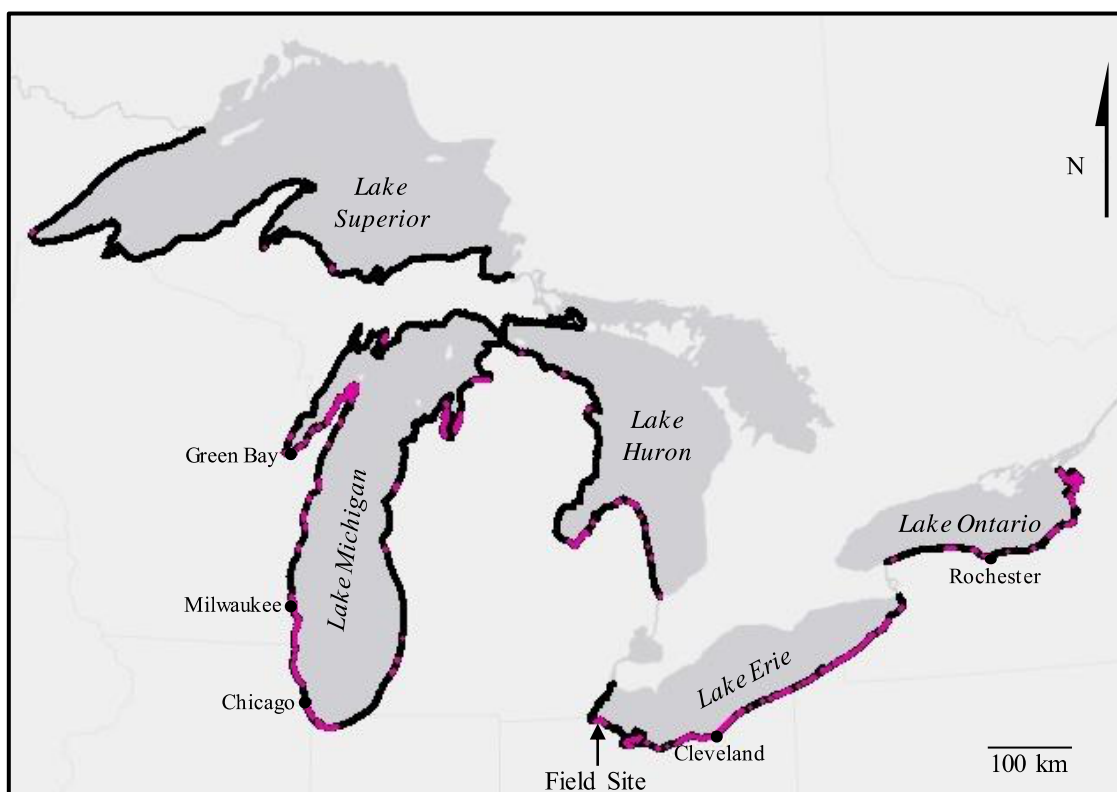


Figure 4: Vulnerability of Great Lakes to contaminant inputs from groundwater. Bright color represents vulnerable areas.

At our vulnerable field site, the mass flux of DP per unit length of shoreline was $86 \pm 6.1 \text{ mg m}^{-1} \text{ d}^{-1}$. Dissolved phosphorous concentrations in lakebed pore waters were elevated (average of 0.12 mg L^{-1}) compared to lake water and onshore groundwater (both below detection). Some of the measured phosphorus may be locally sourced from desorption of legacy P or mineralization of organic matter in the lakebed, which our vulnerability framework does not include.

The mass flux of DIN per unit length of shoreline was $2022 \pm 141.3 \text{ mg m}^{-1} \text{ d}^{-1}$. The average DIN concentration in lakebed pore water was 2.57 mg L^{-1} , which was greater than lake water but less than onshore groundwater. Much of the land-derived nitrogen may be removed by uptake or denitrification along groundwater flow paths prior to discharge.

An important question is whether groundwater is a significant source of nutrients to Lake Erie. We lack distributed chemical data from around Lake Erie to estimate the total flux of groundwater-borne nutrients. However, if we assume nutrient concentrations in groundwater discharge zones around Lake Erie are similar to those at the field site (average DP and DIN concentrations of 0.12 and 2.57 mg L^{-1} , respectively) and use an average direct groundwater discharge rate of $477 \text{ m}^2 \text{ y}^{-1}$ over a coastline length of 1400 km , the total DP and DIN fluxes to Lake Erie are 2.5 and 54.3 g s^{-1} , respectively [Knights *et al.*, 2017]. For comparison, these fluxes represent 13% of the DP load and 4% of the DIN load to Lake Erie by the Maumee River [Baker *et al.*, 2014; Stow *et al.*, 2015]. In summary, groundwater is potentially a small but non-negligible source of nutrients to

Lake Erie. Unlike discharge from a river, direct groundwater discharge is diffuse and exhibits high spatial heterogeneity. The complexity in quantifying direct groundwater discharge as a nonpoint source of contamination makes management difficult compared to point source loading.

Discharging groundwater tends to be nitrogen-rich and can therefore influence primary production [Lapointe, 1997; Weiskel and Howes, 1992]. Groundwater at our field site delivers a DIN:DP ratio of 147:1, far exceeding the Redfield ratio [Knights *et al.*, 2017]. In comparison, a N:P ratio of 21:1 was reported in lake water within the western basin of Lake Erie near Maumee Bay during the 2008 algal bloom [Chaffin *et al.*, 2011]. Assuming field measurements are representative of average P and N concentrations, discharging groundwater has the potential to exacerbate P limitation.

Finding Significance

We have produced a new understanding of the “hidden” water and nutrient inputs from coastal aquifers to the Great Lakes, which can guide our understanding of coastal water quality and ecosystem health. Our findings are highly pertinent to government officials at federal and state levels, as well as city planners. In a 2015 report, *Granneman and Van Stempvoort* stated: “No conceptual frameworks are available that can be applied as screening tools to evaluate the potential for direct groundwater discharge along a shoreline, and moreover to evaluate if groundwater may be an important pathway in delivering nutrients to nearshore waters” [Grannemann and Van Stempvoort, 2015]. This study has provided the highly sought framework. We produced maps of direct groundwater discharge rates and identified coastal areas that are vulnerable to groundwater-borne nutrient loads.

Our map products, which are freely available on Zenodo, can be used by scientists, practitioners, and stakeholders in a number of ways:

- 1) The groundwater discharge rates can be integrated in improved water budgets for Lake Erie and other Great Lakes. With additional groundwater chemistry information, nutrient fluxes can be estimated and used in nutrient budgets for whole lakes or localized nearshore areas.
- 2) Maps can be used to target areas for groundwater and lake water quality monitoring.
- 3) Vulnerability estimates can be improved with local information and used to guide coastal development strategies or best management practices. For example, maps of groundwater discharge rates can be combined with site-specific data on agricultural practices or septic tank distributions to further understand potential nutrient inputs. These areas can then be targeted for improved sewer infrastructure, wetland reconstruction, precision fertilizer application, or a number of other projects designed to improve groundwater quality.

Many factors control nutrient fluxes to the coast (including rates of key reactions such as denitrification, residence times, and the history of land use change or fertilizer applications). Therefore, our vulnerability designation is only a qualitative assessment of areas that may have high groundwater-borne nutrient loads. We recommend more field measurements of groundwater-borne nitrogen and phosphorus loads to provide additional context for our vulnerability maps and determine when and where the vulnerability designation is most reliable (for which nutrients and hydrogeologic conditions).

Highlights:

- 43% of the U.S. Great Lakes' coast is vulnerable to groundwater-borne nutrients.
- Lake Erie has the greatest fraction of vulnerable shoreline.
- Lakebed sediments are a source of dissolved phosphorous at discharge zones.
- Some nitrate removal occurs along groundwater flow paths prior to discharge.

References

- Baker, D. B., R. Confesor, D. E. Ewing, L. T. Johnson, J. W. Kramer, and B. J. Merryfield (2014), Phosphorus loading to Lake Erie from the Maumee, Sandusky and Cuyahoga rivers: The importance of bioavailability, *Journal of Great Lakes Research*, 40(3), 502-517, doi: <https://doi.org/10.1016/j.jglr.2014.05.001>.
- Barton, D. R., E. T. Howell, and C. L. Fietsch (2013), Ecosystem changes and nuisance benthic algae on the southeast shores of Lake Huron, *Journal of Great Lakes Research*, 39(4), 602-611, doi: 10.1016/j.jglr.2013.09.010.
- Chaffin, J. D., T. B. Bridgeman, S. A. Heckathorn, and S. Mishra (2011), Assessment of *Microcystis* growth rate potential and nutrient status across a trophic gradient in western Lake Erie, *Journal of Great Lakes Research*, 37(1), 92-100, doi: <https://doi.org/10.1016/j.jglr.2010.11.016>.
- Chen, F., Z. Janjic, and K. Mitchell (1997), Impact of atmospheric surface-layer parameterizations in the new land-surface scheme of the NCEP mesoscale Eta model, *Boundary-Layer Meteorology*, 85(3), 391-421, doi: 10.1023/a:1000531001463.
- Frape, S. K., and R. J. Patterson (1981), Chemistry of interstitial water and bottom sediments as indicators of seepage patterns in Perch Lake, Chalk-River, Ontario, *Limnol. Oceanogr.*, 26(3), 500-517.
- Grannemann, N. G., and D. Van Stempvoort (2015), Groundwater science relevant to the Great Lakes Water Quality Agreement: A status report, Lansing, MI.
- Knights, D., K. C. Parks, A. H. Sawyer, C. H. David, T. N. Browning, K. M. Danner, and C. D. Wallace (2017), Direct groundwater discharge and vulnerability to hidden nutrient loads along the Great Lakes coast of the United States, *Journal of Hydrology*, 554, 331-341, doi: <https://doi.org/10.1016/j.jhydrol.2017.09.001>.
- Kornelsen, K. C., and P. Coulibaly (2014), Synthesis review on groundwater discharge to surface water in the Great Lakes Basin, *Journal of Great Lakes Research*, 40(2), 247-256, doi: 10.1016/j.jglr.2014.03.006.
- Koster, R. D., and M. J. Suarez (1994), The components of a SVAT scheme and their effects on a GCMs hydrological cycle, *Adv. Water Resour.*, 17(1-2), 61-78, doi: 10.1016/0309-1708(94)90024-8.
- Kroeger, K. D., and M. A. Charette (2008), Nitrogen biogeochemistry of submarine groundwater discharge, *Limnol. Oceanogr.*, 53(3), 1025-1039, doi: 10.4319/lo.2008.53.3.1025.
- LaBaugh, J. W., T. C. Winter, D. O. Rosenberry, P. F. Schuster, M. M. Reddy, and G. R. Aiken (1997), Hydrological and chemical estimates of the water balance of a closed-basin lake in north central Minnesota, *Water Resources Research*, 33(12), 2799-2812, doi: 10.1029/97wr02427.

- Lapointe, B. E. (1997), Nutrient thresholds for bottom - up control of macroalgal blooms on coral reefs in Jamaica and southeast Florida, *Limnol. Oceanogr.*, 42(5part2), 1119-1131, doi: doi:10.4319/lo.1997.42.5_part_2.1119.
- Lee, D. R. (1977), A device for measuring seepage flux in lakes and estuaries, *Limnol. Oceanogr.*, 22, 140-147.
- Lewandowski, J., K. Meinikmann, G. Nutzmann, and D. O. Rosenberry (2015), Groundwater - the disregarded component in lake water and nutrient budgets. Part 2: effects of groundwater on nutrients, *Hydrol. Process.*, 29(13), 2922-2955, doi: 10.1002/hyp.10384.
- Liang, X., D. P. Lettenmaier, E. F. Wood, and S. J. Burges (1994), A Simple Hydrologically Based Model of Land-Surface Water and Energy Fluxes for General-Circulation Models, *J. Geophys. Res.-Atmos.*, 99, 14415-14428.
- McKay, L. D., T. R. Bondelid, T. G. Dewald, C. M. Johnston, R. B. Moore, and A. Rea (2012), NHDPlus Version 2: User Guide (Data Model Version 2.1), 181 pp, available online at ftp://ftp.horizon-systems.com/nhdplus/nhdplusv21/documentation/nhdplusv2_user_guide.pdf.
- Michalak, A. M., E. J. Anderson, D. Beletsky, S. Boland, N. S. Bosch, T. B. Bridgeman, J. D. Chaffin, K. Cho, R. Confesor, I. Daloglu, J. V. DePinto, M. A. Evans, G. L. Fahnenstiel, L. He, J. C. Ho, L. Jenkins, T. H. Johengen, K. C. Kuo, E. LaPorte, X. Liu, M. R. McWilliams, M. R. Moore, D. J. Posselt, R. P. Richards, D. Scavia, A. L. Steiner, E. Verhamme, D. M. Wright, and M. A. Zagorski (2013), Record-setting algal bloom in Lake Erie caused by agricultural and meteorological trends consistent with expected future conditions, *Proc. Natl. Acad. Sci. U. S. A.*, 110(16), 6448-6452, doi: 10.1073/pnas.1216006110.
- National Wildlife Federation (2011), Feast and famine in the Great Lakes: How nutrients and invasive species interact to overwhelm the coasts and starved offshore waters, Ann Arbor, Michigan.
- Richards, R. P., D. B. Baker, J. P. Crumrine, and A. M. Stearns (2010), Unusually large loads in 2007 from the Maumee and Sandusky Rivers, tributaries to Lake Erie, *Journal of Soil and Water Conservation*, 65(6), 450-462, doi: 10.2489/jswc.65.6.450.
- Robinson, C. (2015), Review on groundwater as a source of nutrients to the Great Lakes and their tributaries, *Journal of Great Lakes Research*, 41(4), 941-950, doi: 10.1016/j.jglr.2015.08.001.
- Rosenberry, D. O., J. Lewandowski, K. Meinikmann, and G. Nutzmann (2015), Groundwater - the disregarded component in lake water and nutrient budgets. Part 1: effects of groundwater on hydrology, *Hydrol. Process.*, 29(13), 2895-2921, doi: 10.1002/hyp.10403.
- Sawyer, A. H. (2015), Enhanced removal of groundwater-borne nitrate in heterogeneous aquatic sediments, *Geophys. Res. Lett.*, 42(2), 403-410, doi: 10.1002/2014gl062234.
- Sawyer, A. H., C. H. David, and J. S. Famiglietti (2016), Continental patterns of submarine groundwater discharge reveal coastal vulnerabilities, *Science*, doi: 10.1126/science.aag1058.
- Shinn, E. A., C. D. Reich, and T. D. Hickey (2002), Seepage meters and Bernoulli's revenge, *Estuaries*, 25(1), 126-132, doi: 10.1007/bf02696056.

- Stow, C. A., Y. Cha, L. T. Johnson, R. Confesor, and R. P. Richards (2015), Long-Term and Seasonal Trend Decomposition of Maumee River Nutrient Inputs to Western Lake Erie, *Environmental Science & Technology*, 49(6), 3392-3400, doi: 10.1021/es5062648.
- Valiela, I., J. Costa, K. Foreman, J. M. Teal, B. Howes, and D. Aubrey (1990), Transport of groundwater-borne nutrients from watersheds and their effects on coastal waters, *Biogeochemistry*, 10(3), 177-197.
- Weiskel, P. K., and B. L. Howes (1992), Differential transport of sewage-derived nitrogen and phosphorus through a coastal watershed, *Environmental Science & Technology*, 26(2), 352-360, doi: 10.1021/es00026a017.
- Xia, Y., K. Mitchell, M. Ek, J. Sheffield, B. Cosgrove, E. Wood, L. Luo, C. Alonge, H. Wei, J. Meng, B. Livneh, D. Lettenmaier, V. Koren, Q. Duan, K. Mo, Y. Fan, and D. Mocko (2012), Continental-scale water and energy flux analysis and validation for the North American Land Data Assimilation System project phase 2 (NLDAS-2): 1. Intercomparison and application of model products, *J. Geophys. Res.*, 117, D03109.

Addressing the Water-Energy Nexus of Fossil Power Generation by Considering Technological, Agro-Ecological, and Economic Options in the Muskingum Watershed

Basic Information

Title:	Addressing the Water-Energy Nexus of Fossil Power Generation by Considering Technological, Agro-Ecological, and Economic Options in the Muskingum Watershed
Project Number:	2017OH540B
Start Date:	3/1/2017
End Date:	2/28/2019
Funding Source:	104B
Congressional District:	OH-3
Research Category:	Not Applicable
Focus Categories:	Management and Planning, Surface Water, Economics
Descriptors:	None
Principal Investigators:	Bhavik R Bakshi, Brent Sohngen, Sami Khanal

Publication

1. Lee, K., Khanal, S., and Bakshi, B.R. The Energy-Water Nexus of Thermoelectric Power Generation and Its Impacts in the Muskingum River Watershed in Ohio. 2018 AIChE Annual Meeting. Pittsburgh, PA.

Final Report: Addressing the Water-Energy Nexus of Fossil Power Generation by Considering Technological, Agro-Ecological, and Economic Options in the Muskingum Watershed

1 Problem and Research Objectives

Thermoelectric power plants generate electricity and flue gas scrubbers mitigate emissions from the plants. However, at the same time the power plants withdraw large quantities of water from the watershed, which corresponds to 45% of the total 2010 US water use [1], and emissions from the scrubbers cause deposition of nutrients in the watershed. Therefore, increasing electricity generation could increase water stress and deteriorate water quality. Also, in the watershed where power plants are located, other activities, such as farming, interact with the power plants since these activities also require water as well as energy from the power plants and release nutrients to the watershed. To prevent shifting of environmental impacts across multiple flows [2], the Energy-Water nexus between different activities in the watershed needs to be understood in assessing the impacts of power plants.

Fossil fuel power plants not only require a huge amount of water, but also emit 28% of the 2016 US greenhouse gas emissions [3], 67% of the 2014 US SO₂ emissions, and 12% of the 2014 US NO_x emissions [4]. Therefore, ecosystem services, such as water quality regulation, air quality regulation, and climate change regulation, play an important role in mitigating those pollutants and emissions. To account for the role of ecosystems, Techno-Ecological Synergy (TES) framework is applied in analyzing the impacts of activities in the watershed [5,6]. In such an analysis, the trade-offs between water quality, water quantity, net electricity generation, climate change, air quality, and monetary objective are identified. Various scenarios need to be investigated to suggest better solutions that are ‘win-win’ in terms of multiple objectives.

Muskingum River Watershed (MRW) in Ohio ranks fourth as the most polluted watershed in the US [7], and two coal-fired power plants and three natural gas-fired power plants are located in the MRW. In this work, a holistic analysis approach is employed to evaluate the water-energy nexus in the MRW. Various technological alternatives in terms of fossil power generation are considered. The alternatives include fuel mining options, power generation technology options, and cooling technology options. Scenarios for each alternative are analyzed to understand trade-offs between multiple flows and address the nexus.

2 Methodology

To address the water-energy nexus in the watershed, a holistic analysis approach needs to be employed since most activities in the watershed require water and energy, and cause air and water emissions. Also, many activities in the watershed interact with each other. Figure 1 shows the analysis scope of this work to address the water-energy nexus in the watershed.

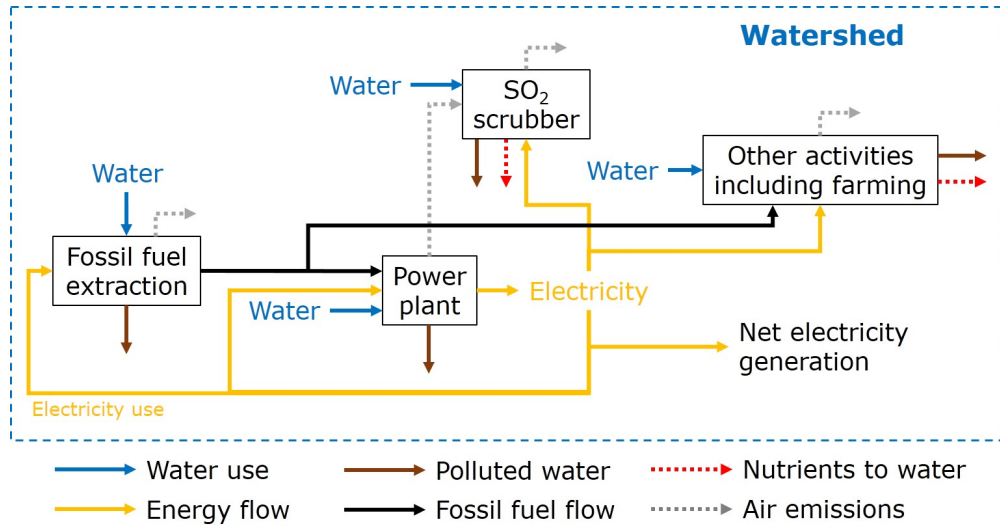


Figure 1: Analysis scope of the water-energy nexus in the Muskingum River Watershed.

2.1 Fossil Power Generation

In the Muskingum River Watershed (MRW), there are two coal-fired steam turbine power plants and three natural gas-fired combined cycle (NGCC) power plants, as shown in Fig. 2. One of the coal-fired plants, which is the Muskingum River Power Plant, has been retired in 2015 due to environmental regulations [8]. Since some databases do not have data for the years after 2015, we assume the Muskingum River Power Plant is still operating to keep the consistency of data.

Coal and natural gas account for 55% and 44% of energy sources that are used to generate electricity from fossil fuels in the US, respectively [9]. Depending on which fossil resources are exploited, total environmental interventions from the fossil power generation are varied. This is mainly attributed to the fact that each fossil resource contains different chemical compositions. Furthermore, in the case of natural gas extraction, the hydraulic fracturing of shale gas requires a lot of water compared to the conventional natural gas extraction. In terms of the power generation technology of power plants, coal-fired power plants usually employ steam turbine boilers (99% of total US coal-fired plants), while NG-fired power plants employ combined cycle boilers (84% of total US NG-fired plants) [10].

Fossil power generation is responsible for almost 40% of freshwater withdrawals in the US. Most of the water withdrawn is used for the cooling of boilers. Depending on which cooling methods are employed in the plant, water and energy requirements are varied. Once-through cooling technology, also known as the open-loop system, withdraws massive amounts of water, but return most of it at high temperature. On the other hand, recirculating cooling technology, also known as the closed-loop system and cooling tower, withdraws only a fraction of the water that systems require, but consume most of it. On the contrary to those wet cooling methods, the dry cooling technology uses no water, but requires high cost and results in low efficiency. Among the five power plants in the MRW, only one coal-fired plant, the Muskingum River Power Plant, employs once-through cooling technology and other four plants employ recirculating cooling technology.

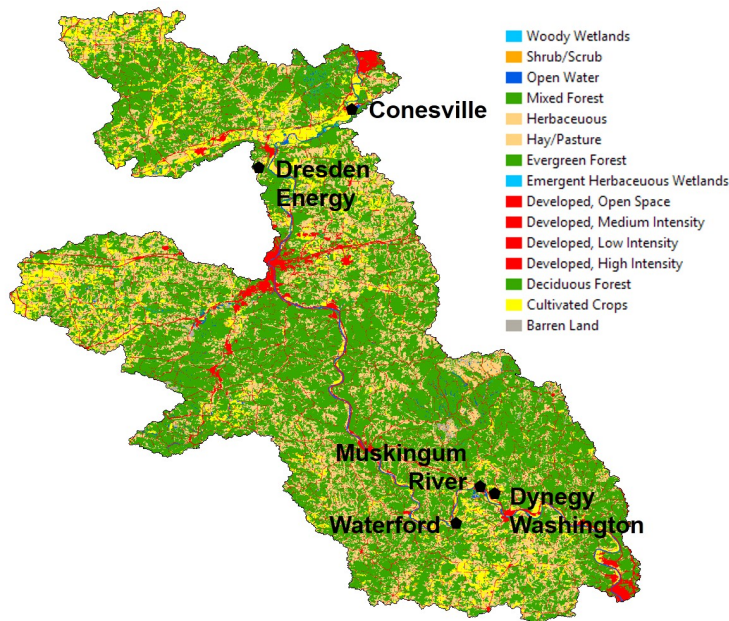


Figure 2: Two coal-fired steam turbine and three NG-fired combined cycle power plants in the Muskingum River Watershed.

In this study, three fuel types (coal, conventional NG, and shale gas), two power generation technologies (steam turbine and combined cycle turbine), and three cooling technologies (once-through, recirculating, and dry cooling) are considered as technological alternatives.

2.2 Other Activities

Although mining and thermoelectric activities account for most of the water use and pollutant emissions, other activities also use water and energy, and release emissions. Therefore, for the comprehensive analysis for the water-energy nexus in the MRW, all kinds of activities that include residential, commercial, industrial, transportation, and wastewater treatment, are included in the analysis.

2.3 Role of Ecosystems

Traditional analysis approaches, such as conventional life cycle assessment (LCA), account for environmental impacts on ecosystems but fail to consider if the capacity of ecosystems for those impacts is enough or not. Therefore, sustainability assessment methods should account for not only the demand for ecosystem goods and services but also the supply of ecosystem goods and services. The demand (D) corresponds to the environmental impacts, such as air and water emissions. The supply (S) corresponds to the provision of ecosystem goods and services, such as air quality regulation service and water resource provision. Techno-ecological synergy (TES) framework has been developed to include the role of ecosystems in the analysis [5, 6]. The TES sustainability index, $V_k = \frac{S_k - D_k}{D_k}$ ($V_k \geq -1$), is calculated for each type of ecosystem goods and services (k). The positive V_k value indicates that the

impacts do not overshoot the capacity of ecosystems.

Forest ecosystems and tree canopies provide climate change regulation and air quality regulation services. For greenhouse gas and air pollutant emissions from all activities including fossil power generation, V_k indexes are calculated to examine sustainability in the MRW.

To assess water provision in the watershed area, numerous factors about water cycle need to be considered as follows: precipitation, evapotranspiration from canopy and soil, infiltration into the soil, and surface/subsurface runoffs. Water Global Assessment and Prognosis (WaterGAP) hydrology model has been developed to calculate the amount of available water in the global scale while accounting for those factors [11]. In this study, Available Water Remaining (AWARE) model, which is based on the WaterGAP model, is used to calculate the amount of available water in the MRW [12].

Fossil resources are formed from organic matters in the earth through anaerobic decomposition over very long periods of time. In this work, the supply of natural gas is calculated to examine whether the use of fossil resources is sustainable or not. Two cases are considered depending on how the supply of NG is defined. One is the case where only newly-formed NG is the supply of NG. The other is the case where 2°C of global warming since the pre-industrial period is allowed for exploiting accumulated natural gas [13]. The exergy of NG is used to calculate the supply of NG for both cases [14].

2.4 Economic Feasibility

To investigate if aforementioned alternatives are economically profitable than other alternatives, the cost for operating power plants is calculated. Different technological alternatives have different efficiencies and installation costs. For example, once-through cooling technology is generally more efficient and cheaper than recirculating cooling technology, although once-through cooling technology withdraws much more water than recirculating cooling technology.

2.5 Data Collection and Allocation

Various activities and environmental interventions need to be accounted for in the analysis to address the nexus of different flows. Essentially, we need to rely on multiple databases and tools to collect those data. Table 1 shows major data sources for each activity and each intervention.

Since such a holistic analysis approach uses multiple data sources, it is important to keep the temporal and spatial consistency of data. The year 2014 is selected because most of the data for 2014 is available. The MRW region corresponds to one region where 8-digits of hydrologic unit code (HUC8) is assigned as 05040004. If data is not available for the HUC8 scale, the allocation method based on area or population is used to obtain data for the MRW region. For example, the AWARE model only has available water data for the HUC2 region, which represents much larger area than HUC8. This value for the Ohio region (HUC2: 05) is allocated to the MRW region (HUC8: 05040004) based on the ratio of HUC8 area to HUC2 area. For other activities, such as residential activity, that are more dependent on population rather than area, the allocation is performed based on the population.

Table 1: Data sources for each activity and each environmental intervention. If the spatial resolution of data is not the HUC8 scale, those data are allocated to the HUC8 scale based on area or population.

Activity	Environmental Intervention	Primary Data Source	Secondary Data Source	Data Spatial Resolution (P: Primary, S: Secondary)
Mining	GHG emissions	GREET [10]		US
	Air pollutants	EPA NEI (2014) [4]		County
	Water use	GREET	USGS (1995) [15]	US (P), Ohio (S)
	Natural gas use	EIA (2014) [16]		Ohio
	Electricity use	NREL [17]	GREET	US (P, S)
Thermoelectric	GHG emissions	EPA eGRID (2014) [18]		Facility
	Air pollutants	EPA NEI (2014)		Facility
	Water use	Form EIA-923 (2014) [19]		Facility
	Natural gas use	Form EIA-923 (2014)		Facility
	Electricity use	Form EIA-923 (2014)		Facility
Other activities (Residential, Commercial, Industrial, Agricultural, Transportation, Wastewater Treatment)	GHG emissions	EPA NEI (2014)	EPA eGRID (2014)	County (P), Facility (S)
	Air pollutants	EPA NEI (2014)		County
	Water use	EnviroAtlas [20]	USGS (2010 [1], 1995)	HUC8 (P), Ohio (S)
	Natural gas use	EIA (2014)		Ohio
	Electricity use	EIA (2015) [21]		Ohio
Ecosystem Supplies	CO ₂ sequestration	i-Tree Landscape [22]		HUC8
	Air pollutants removal	i-Tree Landscape		HUC8
	Natural gas formation /accumulation	[14]		Global
	Water provision	AWARE [12]		HUC2

3 Principal Findings and Results

3.1 Base Case Analysis

Figure 3 represents base case analysis results in terms of the demands and supplies of electricity and each of the ecosystem goods and services. The TES sustainability indexes are calculated for each ecosystem good and service and are shown in Fig. 4. For greenhouse gases and air pollutants, their demands, which correspond to the amounts of emissions, exceed their supplies. The TES indexes for climate change regulation service and air quality regulation service are all very close to negative one (-1). It indicates that those environmental interventions overshoot the capacity of ecosystems in the MRW, and therefore, it is unsustainable. Most of those interventions are attributed to the thermoelectric activity. This is not only because the thermoelectric activity causes much greater environmental impacts than other activities, but also because the MRW is the region where five fossil power plants are located in. As for the water use, the amount of water withdrawal is significantly large, but it is not considered as the demand for water provision since most of the withdrawn water returns to the waterbody. Instead, the amount of water consumption is considered as the demand for water provision. In that case, the water demand is larger than the water supply, which only includes the renewable portion of water provision.

With respects to the natural gas use, the TES index for natural gas provision is also very close to negative one (-1). This is because the supply of natural gas only includes the renewable portion of natural gas, which corresponds to the amount of natural gas formation. This result is expected since the rate of NG formation is significantly slower than the rate of natural gas consumption. According to the Intergovernmental Panel of Climate Change

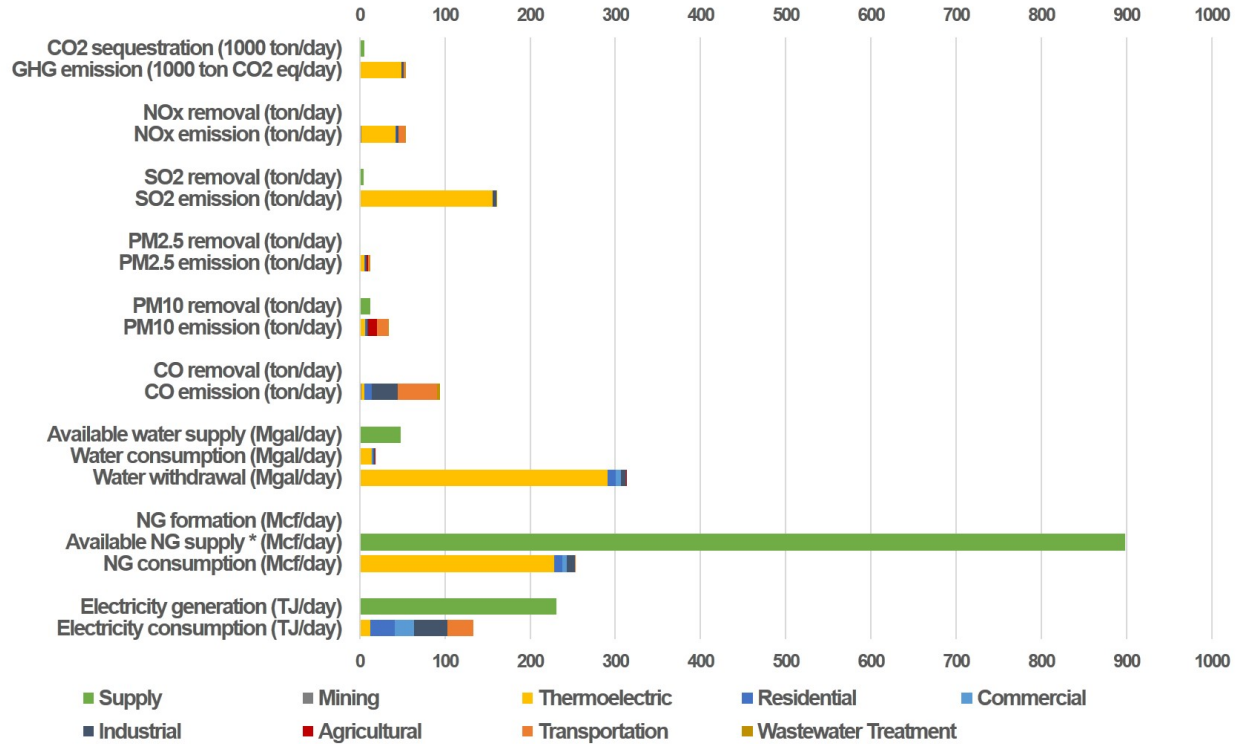


Figure 3: Base case analysis results in terms of the demands and supplies of electricity and each of the ecosystem goods and services. (* Available NG supply includes accumulated NG by allowing for 2 °C global warming since the pre-industrial period.)

(IPCC), the rise in global temperature must be limited to 2 °C above pre-industrial levels in order to avoid disastrous consequences of climate change. The IPCC has calculated the carbon budget that represents the amounts of global CO₂ emissions for keeping global warming under 2 °C. The budget is estimated to be one trillion tonnes of carbon. To stay within the carbon budget, roughly a quarter of accumulated fossil resources can be burned [13]. In that case, a quarter portion of accumulated NG is considered as an additional supply of NG, and thus, the TES index for natural gas provision shows a positive value, as shown in Figs. 3 and 4.

3.2 Scenario Analysis

To address the nexus of multiple flows in the analysis, multiple objectives that represent those flows need to be considered. In this analysis, a total of eleven objectives are considered as follows: a TES index for climate change regulation service ($V(\text{CO}_2)$), five TES indexes for air quality regulation services ($V(\text{NO}_x)$, $V(\text{SO}_2)$, $V(\text{PM}_{2.5})$, $V(\text{PM}_{10})$, and $V(\text{CO})$), a TES index for natural gas provision ($V(\text{NG})$), a TES index for water provision ($V(\text{Water})$), thermal water pollution from fossil power plants, net electricity generation, and cost for operating fossil power plants.

Various scenarios depending on which technological alternatives are employed are examined to identify how multiple flows interact in the watershed. The percentage change in

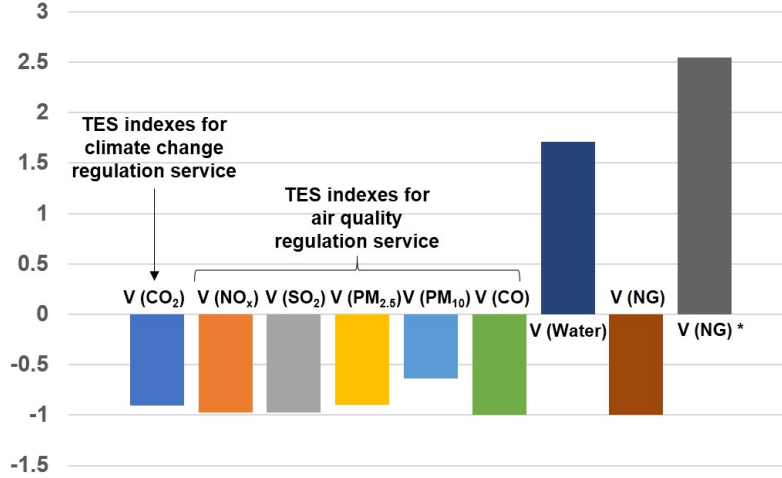


Figure 4: TES sustainability indexes calculated for each ecosystem good and service. (* This index considers accumulated NG as the supply of NG by allowing for 2°C global warming since the pre-industrial period.)

each objective value based on the base case is calculated for each scenario and plotted as a radar diagram. As a functional unit for the comparison between scenarios, five fossil power plants in the MRW are assumed to generate 98,094 GJ/day of electricity regardless of which alternatives are adopted. This corresponds to the amount of electricity generated from the five fossil plants in 2014.

Figure 5 shows eleven indicators for the percentage change in each objective based on the base case for the scenario where one type of fuel and generation technology is adopted for all five fossil power plants. For the convenience purpose, the negative sign is applied to the cost and thermal water pollution indicators, so that more positive values represent better results as other indicators do. That is, if the cost indicator and the thermal water pollution indicator are positive, it means the cheaper cost and less thermal water pollution are expected from the scenario than the base case.

For most of the indicators, the coal-fired steam turbine option is the worst among other fuel and generation technology options. This is simply because coal causes more air emissions when it burns than natural gas and the coal-fired plant has lower efficiency than the NG-fired plant. Also, the coal-fired steam turbine plant requires and consumes more water than the NGCC plant. Moreover, the coal mining and coal-fired steam turbine plant consume more electricity than the NG extraction and NGCC plant. Only the V(NG) indicator shows the coal-fired steam turbine option is slightly better than the other options because coal is selected to be used as a fuel instead of natural gas. In terms of the comparison between conventional natural gas and shale gas options, there are very minor differences. For instance, the V(Water) value for the conventional NG option is only 1.1% bigger than the shale gas option. This is because power generation technology is the same between those two options and the contribution from the mining activity to the overall environmental interventions is negligible compared to the contribution from the thermoelectric activity.

Different cooling technology options are compared for the NGCC plant as shown in Fig. 6.

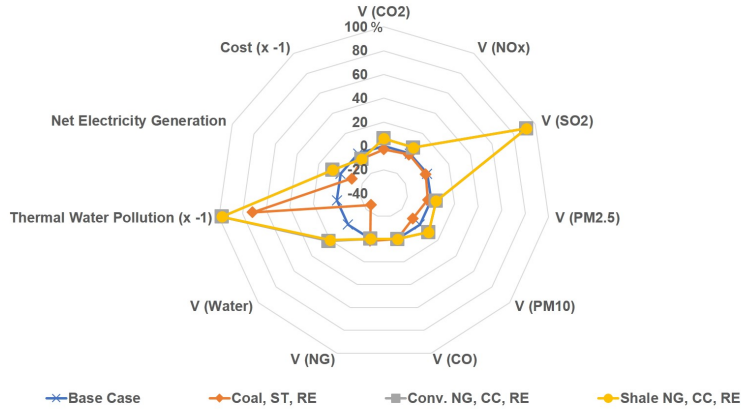


Figure 5: Percentage change in each objective based on the base case for the scenario where one type of fuel and generation technology is employed for five power plants. The negative sign is applied to the cost and thermal water pollution indicators.

Several trade-offs between objectives are identified. For water-related objectives, such as V (Water) and thermal water pollution indicators, the dry cooling option shows better results than the other options because it does not require water for cooling. However, since dry cooling is more expensive and less efficient than other cooling methods, its net electricity generation and cost indicator values are smaller than other cooling options. Also, since once-through cooling is more efficient than recirculating cooling by 1% and dry cooling by 2–3% [23], the once-through cooling requires slightly less amount of electricity and fuel, and thus, it results in fewer amounts of air emissions. Therefore, air emission-related indicators for the once-through cooling option is slightly more positive than the other options.

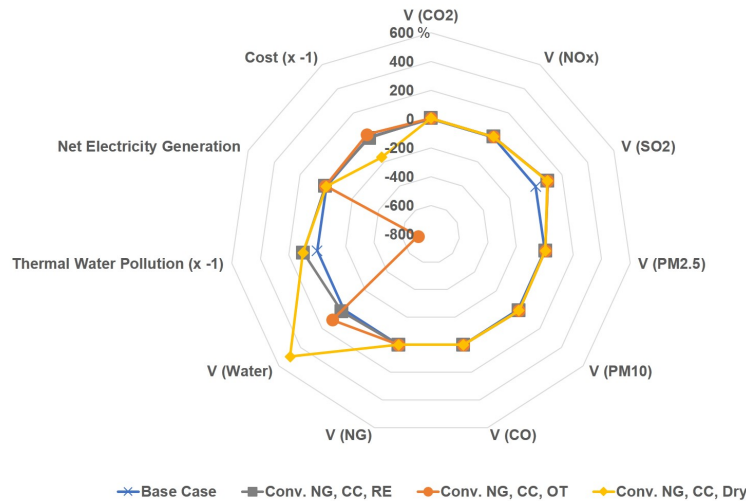


Figure 6: Percentage change in each objective based on the base case for the scenario where one type of cooling technology is employed for five power plants.

4 Finding Significance

In this work, various alternatives in terms of fossil power generation are investigated to identify interactions between multiple flows while addressing the nexus of water and energy in the watershed. Overall, the coal fuel option shows poor results compared to NG fuel options. In terms of cooling technology options, trade-offs between water quantity (V (Water)) and water quality (thermal water pollution) are identified for wet cooling technologies. Also, the dry cooling option shows better indexes in terms of water-related objectives than wet cooling options, however, exhibits worse indexes in terms of net electricity generation and cost. Although some trade-offs for water, cost, and net electricity generation objectives are identified depending on which alternatives are chosen, none of the scenarios show significantly better results in terms of greenhouse gas and air pollutant emissions since the TES indexes for these emissions are all negative. It indicates that there is a technological limitation to reduce those emissions. Therefore, we need to investigate agro-ecological options, such as land use change and farming practice change, to mitigate those emissions. For example, the land use change option can increase the supply of ecosystem services, such as air quality regulation and climate change regulation services, through the reforestation of barren lands. Also, according to the study from Ohio EPA, most of the phosphorous and nitrogen loads for the Muskingum River come from non-point sources, such as the use of fertilizers for agricultural activities, rather than point sources, such as power plants [24]. The study also notes that abating agricultural nutrient loadings is much cheaper than abatement at the regulated point sources [25]. Therefore, economic options based on nutrient trading schemes can be explored to avoid adverse impacts on water quality in the watershed. Moreover, since water supply and climate vary from one season to another, temporal variation needs to be considered for a more rigorous analysis.

Considering the energy-water nexus in the analysis will avoid shifting of the environmental impacts across multiple flows because interactions between flows are identified and all flows are included as objectives [2]. This work could be applied to any watershed and could be extended to address the food-energy-water nexus by including food productions from farming activities as another objective. Addressing the nexus could help businesses and policymakers in making decisions to improve the sustainability of the watershed.

References

- [1] M. A. Maupin et al. *Estimated use of water in the United States in 2010*. U.S. Geological Survey, Reston, Virginia, 2014.
- [2] B. R. Bakshi, T. G. Gutowski, and D. P. Sekulic. Claiming sustainability: Requirements and challenges. *ACS Sustain. Chem. Eng.*, 6:3632–3639, 2018.
- [3] USEPA. *Inventory of U.S. greenhouse gas emissions and sinks: 1990-2016*. U.S. Environmental Protection Agency, Washington, D.C., 2018.
- [4] USEPA. 2014 National Emissions Inventory (NEI). US Environmental Protection Agency. <https://www.epa.gov/air-emissions-inventories> Accessed on Feb 13, 2018.
- [5] B. R. Bakshi, G. Ziv, and M. D. Lepech. Techno-ecological synergy: A framework for sustainable engineering. *Environ. Sci. Technol.*, 49:1752–1760, 2015.
- [6] V. Gopalakrishnan, B. R. Bakshi, and G. Ziv. Assessing the capacity of local ecosystems to meet industrial demand for ecosystem services. *AIChE J.*, 62:3319–3333, 2016.
- [7] J. Inglis and T. Dutzik. *Wasting our waterways: Toxic industrial pollution and restoring the promise of the clean water act*. Environment America Research & Policy Center, Boston, MA, 2006.
- [8] Dan Gearino. AEP to close coal-fired power plant instead of converting, 2013. <http://www.dispatch.com/content/stories/business/2013/07/11/aep-to-close-coal-fired-power-plant-near-beverly.html> Accessed on May 15, 2018.
- [9] USEPA. Where Greenhouse Gases Come From. https://www.eia.gov/energyexplained/index.php?page=environment_where_ghg_come_from Accessed on Apr 15, 2018.
- [10] Argonne National Laboratory. The Greenhouse gases, Regulated Emissions, and Energy use in Transportation (GREET) Model, 2016 version.
- [11] Goethe University Frankfurt. Water – Global Analysis and Prognosis (WaterGAP) Model.
- [12] WULCA. Available WATER REmaining (AWARE) Model.
- [13] Water Resources Institute. The Carbon Budget. <http://www.wri.org/ipcc-infographics> Accessed on Apr 16, 2018.
- [14] I-Chun Hsiao. Global Climate and Energy Project at Stanford, 2009. <http://gcep.stanford.edu/research/exergycharts.html> Accessed on Apr 6, 2018.
- [15] Wayne B. Solley, Robert R. Pierce, and Howard A. Perlman. *Estimated use of water in the United States in 1995*. U.S. Geological Survey, Reston, Virginia, 1998.

- [16] USEIA. Natural Gas Summary. https://www.eia.gov/dnav/ng/NG_SUM_LSUM_DCU_SOH_A.htm Accessed on April 23, 2018.
- [17] National Renewable Energy Laboratory (NREL). U.S. Life Cycle Inventory Database, 2016.
- [18] USEPA. Emissions & Generation Resource Integrated Database (eGRID). <https://www.epa.gov/energy/emissions-generation-resource-integrated-database-egrid> Accessed on Feb 22, 2018.
- [19] USEIA. Form EIA-923 detailed data. <https://www.eia.gov/electricity/data/eia923/> Accessed on Apr 3, 2018.
- [20] USEPA. EnviroAtlas Interactive Map. <https://www.epa.gov/enviroatlas> Accessed on Jan 29, 2018.
- [21] USEIA. Total Energy Consumption, Price, and Expenditure Estimates, 2015. https://www.eia.gov/state/seds/data.php?incfile=/state/seds/sep_fuel/html/fuel_te.html&sid=US&sid=OH Accessed on April 23, 2018.
- [22] i-Tree Landscape. <https://landscape.itreetools.org/>.
- [23] Aviva Loew et al. Marginal costs of water savings from cooling system retrofits: A case study for texas power plants. *Environ. Res. Lett.*, 11:104004, 2016.
- [24] Ohio EPA. Nutrient Mass Balance Study for Ohio's Major Rivers, 2016.
- [25] Ohio EPA. Ohio Nutrient Reduction Strategy, 2013.

Remediation of Hydraulic Fracturing Fluid by Trace Element Extraction

Basic Information

Title:	Remediation of Hydraulic Fracturing Fluid by Trace Element Extraction
Project Number:	2017OH5690
Start Date:	3/1/2017
End Date:	2/28/2019
Funding Source:	Other
Congressional District:	OH-3
Research Category:	Engineering
Focus Categories:	Wastewater, Treatment, Methods
Descriptors:	
Principal Investigators:	Susan Welch, Julia Meyer Sheets, David Robert Cole

Publications

There are no publications.

Remediation of Hydraulic Fracturing Fluid by Trace Element Extraction

Susan A Welch, Julia M Sheets and David R Cole

School of Earth Sciences, The Ohio State University

Problem and Research Objectives

Hydraulic fracturing of lateral wells to extract unconventional hydrocarbon resources is generating enormous quantities of natural gas, with approximately 744 billion cubic feet produced from 2011 through the 1st quarter of 2015 in Ohio alone (Riley, 2015). As gas is produced, the water recovered from these wells is in the form of saline brines, typically with total dissolved solids (TDS) in the range 10s to 100s g/L. These brines also contain organic compounds, as well as elevated levels of trace elements such as barium, strontium, radium, transition metals and rare earth elements (Kondash et al., 2014; Nelson et al., 2015; Vengosh et al., 2014; Welch, Sheets and Cole unpub). The fluids are hazardous waste, they contribute to mineral scale that builds up in hydraulic fracturing equipment, and their compositions reflect pore waters derived from the rock formations with which they have interacted. From a hazardous waste standpoint, they are complicated by containing naturally occurring radioactive materials (NORM) derived from the rocks, that may then be concentrated, or technologically enhanced (TENORM). Understanding the nature of precipitates that form and settle out of the fluids in holding tanks is important for their safe handling and disposal. For example, radium has been identified in flowback fluids in water storage impoundments (Zhang et al., 2015). Microorganisms also are present that were either inserted along with input fluids or were indigenous to the subsurface environment and able to thrive in the fracking environment (Daly et al., 2016). Although hydraulic stimulation operations increasingly re-use these recovered brines, proper disposal of the fluids remains a problem because of their complex chemistry and potential toxicity. Deep injection of waste brines is prevalent in Ohio, and minimizing this activity is of interest to the general public.

Another view of these hydraulic fracturing flowback fluids (HFFF) is that the trace metals they contain also are a potential resource, given the opportunity to concentrate them so that they become economically viable. For example, it has been demonstrated that Fe, which is the most abundant transition metal element in Earth (and also abundant in these brines) can adsorb trace metals onto the surfaces of Fe oxy-hydroxides as they precipitate from natural waters (Webster et al., 1998; Smith, 1999; Bau, 1999) however, the sorption-coprecipitation behavior is complex, and depends on the properties of the solid phase formed (including surface area, mineralogy, and zero point of charge), solution properties (including acidity, salinity, and the concentrations of competing constituents), and the geochemical properties of the selected element. In general, experiments with hydrous ferric oxide phases, and studies of natural waters where Fe has oxidized, show that many trace elements, particularly transition and rare earth elements, are effectively sorbed onto FeOOH phases, however, there are fewer studies conducted on trace element sorption-coprecipitation in brines, where the elevated salinity can impact both element and mineral surface speciation, thus affecting sorptive properties. It would be advantageous to conduct laboratory experiments to determine conditions for the formation of secondary Fe- precipitates (or other phases) that could sequester and concentrate

valuable metals from hypersaline HFFF. If results of such experiments could eventually be scaled up and applied to HFFF storage facilities (holding tanks or storage ponds), then operators could potentially recover economically valuable metals from this waste product.

This research focused on three key goals:

- 1) To understand the evolution of the major and trace element composition of HFFF as it ages and secondary mineral phases precipitate, thereby potentially removing trace metals by sorption/co-precipitation reactions.
- 2) To investigate strategies to actively remove potentially toxic or economically important elements. These include inducing oxidation, addition of different chemical amendments to induce mineralization, or biologically mediated sorption-precipitation reactions.
- 3) To determine the feasibility of adding sulfate-rich acid mine drainage (AMD) waste to induce precipitation of sulfate minerals (barite, celestite) or jarosite group minerals, thereby removing both major and trace metals from solution.

Methods

Experiments were conducted on hydraulic fracturing flowback fluids collected from several unconventional hydrocarbon wells. Two sites were in the Utica/Point Pleasant shale in eastern Ohio, the UPP-W4 well was in the wet gas zone in Harrison county, and the UPP-S1-4 sample were collected from four wells on the same pad from a site in Monroe county Ohio. In addition, HFFF were sampled from two wells from a dry gas target in the Marcellus Shale from the Marcellus Shale Energy and Environment Laboratory (MSEEL) site in Morgantown, West Virginia. Major and trace constituents and biological properties of these fluids have been analyzed as part of several other studies (Welch, Sheets and Cole in prep, Daly et al., 2016). HFFF fluids were stored in large plastic carboys or in large Nalgene bottles and were allowed contact with the atmosphere so that the reduced species could oxidize. Analysis of these fluids and the precipitates that formed provided the basis for the Phase 1 experiments, determining how trace metals would partition between the fluids and the precipitates as the iron oxidizes.

Two additional sets of experiments (Phase 2 and Phase 3) were conducted on flowback fluids from the UPP-S3 and UPP-S4 wells collected in Sept, 2016. These fluids were stored at room temperature and exposed to the atmosphere for about a year before the experiments were started. The carboy of raw UPP-S3 (no chemical additions) flowback fluid was first vigorously shaken to re-suspend precipitate and make a homogeneous mixture for sampling. 200mL of the fluid was added into each of nine 250mL bottles. The addition of either H_3PO_4 or H_2SO_4 were to induce the formation of sulfate or APS (aluminum phosphate sulfate mineral phases $AB_3(XO_4)_2(OH)_6$ such as Alunite supergroup minerals (Bayliss et al., 2010), while the addition of sodium carbonate solution was to increase pH and induce the formation of carbonate minerals. The control and hydrochloric acid addition experiments were intended to serve as controls. A 1mL trace metal spike (1 ppm) was placed into each bottle. The additives for Phase 2 experiments are listed in Table 1.

Table 1. List of additives, concentrations, and volumes for Phase 2 experiments.

Bottle #	Additive	Volume/concentration
1	Control	No addition
2	Low H ₂ SO ₄	0.8 mL/2.5M
3	High H ₂ SO ₄	8.0 mL/2.5M
4	Low H ₃ PO ₄	1.3 mL/1.5M
5	High H ₃ PO ₄	13 mL/1.5M
6	Low HCl	2.0 mL/1.0M
7	High HCl	20 mL/1.0M
8	Low Na ₂ CO ₃	2.0 mL/1.0M
9	High Na ₂ CO ₃	20 mL/1.0M

Based on the results of these experiments, a third set of experiments (Phase 3) was conducted with mixtures of UPP-S4 flowback fluid, an artificial acid mine drainage fluid (1 N H₂SO₄, 0.01M FeCl₃, 0.01M FeSO₄) and a mixed trace metal solution (100 ppm each of Cu, Ag, Se, V, Zn, Ga, Y, Dy, Yb, and 1000 ppm La). These experiments were set up similarly to those in experiment two. Details of these additions are given in Table 2.

Table 2. Additives for Phase 3 experiments with artificial acid mine drainage fluid (AMD) and trace metal (TM) spike.

treatment	Additive
1 control	none
2 TM	10 ml TM spike
3 0.5 AMD	0.5 ml AMD
4 0.5 AMD TM	0.5 ml AMD and 10 ml TM
5 5.0 AMD	5.0 ml AMD
6 5.0 AMD TM	5.0 ml AMD and 10 ml TM
7 50 AMD	50 ml AMD
8 50 AMD TM	50 ml AMD and 10 ml TM
9 50 AMD	50 ml AMD

For the Phase 2 and 3 experiments, the first supernatant samples were collected within a few hours of the experimental set up, and then at one week and two weeks after the start of the experiments. Approximately 10 ml volume was removed from each bottle with a plastic syringe and then filtered with a 0.2 µm syringe filter into a clean 15 ml falcon tube. A small aliquot was removed for pH analysis. At the end of the two week long experiments a sample of the precipitates that formed were removed using a long pipet and placed on a 0.2 micron nucleopore filter in a polycarbonate filter flask. The solution was removed by vacuum filtration and the precipitates were rinsed with ~ 2 ml of milliQ water to remove the residual salts and the precipitates were allowed to air dry. An additional set of fluid and precipitate samples was collected from experiment three after approximately 8 months to investigate long-term changes in mineral composition and morphology.

Fluids and precipitates for the Phase 1 experiment were sampled similarly, except instead of collecting samples from a single bottle over time to determine changes in composition, samples were removed from larger volumes flowback fluids that had been collected previously and allowed to oxidize in the laboratory, and then compared to the original unoxidized sample.

Analytical methods

Because the total dissolved solids (TDS) of these brines is about 200g/L, solution samples had to be diluted before analysis using a Perkin-Elmer Optima 3000DV and 4300DV Inductively Coupled Plasma Optical Emission Spectrometer (ICP-OES) and a Perkin-Elmer Sciex ELAN 6000 Inductively Coupled Plasma Mass Spectrometer (ICP-MS). Two dilutions were made for each sample. The first was a 201-fold dilution in 2% HNO₃ with a 10ppb spike of indium for analysis of selected trace metals by ICP-OES and ICP-MS. This aliquot was diluted again (2211 fold) in 2% HNO₃ to measure major cations and silica by ICP-OES.

Precipitate samples were analyzed by scanning electron microscopy (SEM) using a FEI Quanta FEG 250 Field Emission Scanning Electron Microscope equipped with a Bruker EDX detector, and for X-ray diffraction (XRD) analysis with a PANalytical X'Pert Pro powder diffractometer. The SEM samples were placed on double sided carbon tape on aluminum specimen stubs and then coated with Au-Pd with a Denton Desk V precious metal coater before analysis. For XRD analysis, the filters with precipitate on them were placed on cut glass slides with double-sided tape and then placed on XRD sample mounts. Sample height was adjusted using modeling clay. Precipitate samples were typically scanned from 5 to 70 degrees 2-theta.

Principal Findings and Results

Phase 1 experiments

Analyses for Phase 1 experiments were conducted on fluids that were collected earlier and had already started to oxidize, in order to better determine the time scales required for geochemical changes occur. Aliquots were analyzed to characterize the supernatant fluid and secondary precipitates, the percent of trace elements associated with these phases, and the partitioning of trace elements into the solid phase(s).

The primary mineral phase formed from the oxidation of reduced iron from complex brines collected from the Utica/Point Pleasant is akaganeite (β -FeOOH). SEM analysis shows fine grained elongated nanometer sized precipitates in micron sized "tubular" and/or "hollow" aggregates that are reminiscent of mineralized microbial cells (Fig 1). However, EDX analysis of this phase reveals a more complex chemistry, (FeO(OH,Cl) with Si, however, it is not clear if Si substitutes into the mineral structure, is sorbed onto surfaces, or is present as a very fine grained silica precipitates intermixed within the akaganeite. XRD analysis of these precipitates are consistent with akaganeite. Other peaks for quartz, barite, halite (residual from evaporated brine) are frequently observed.

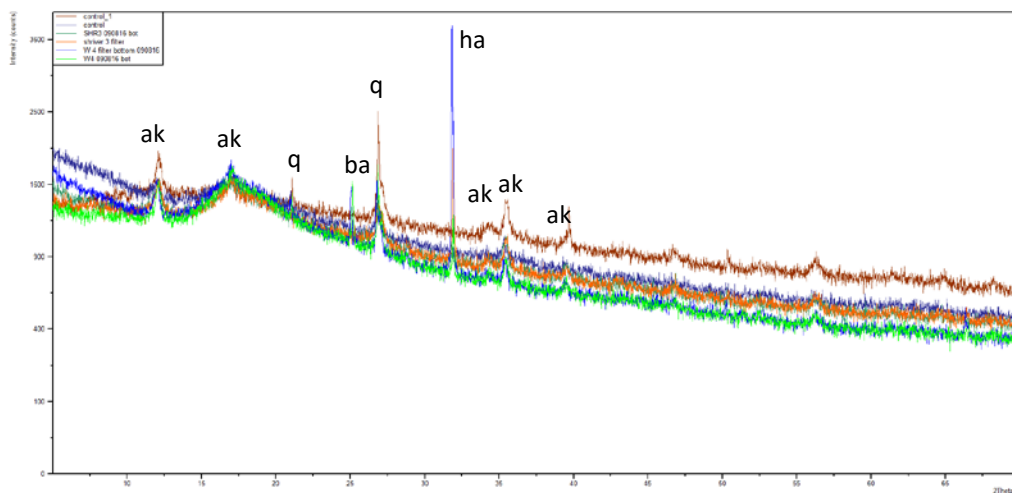
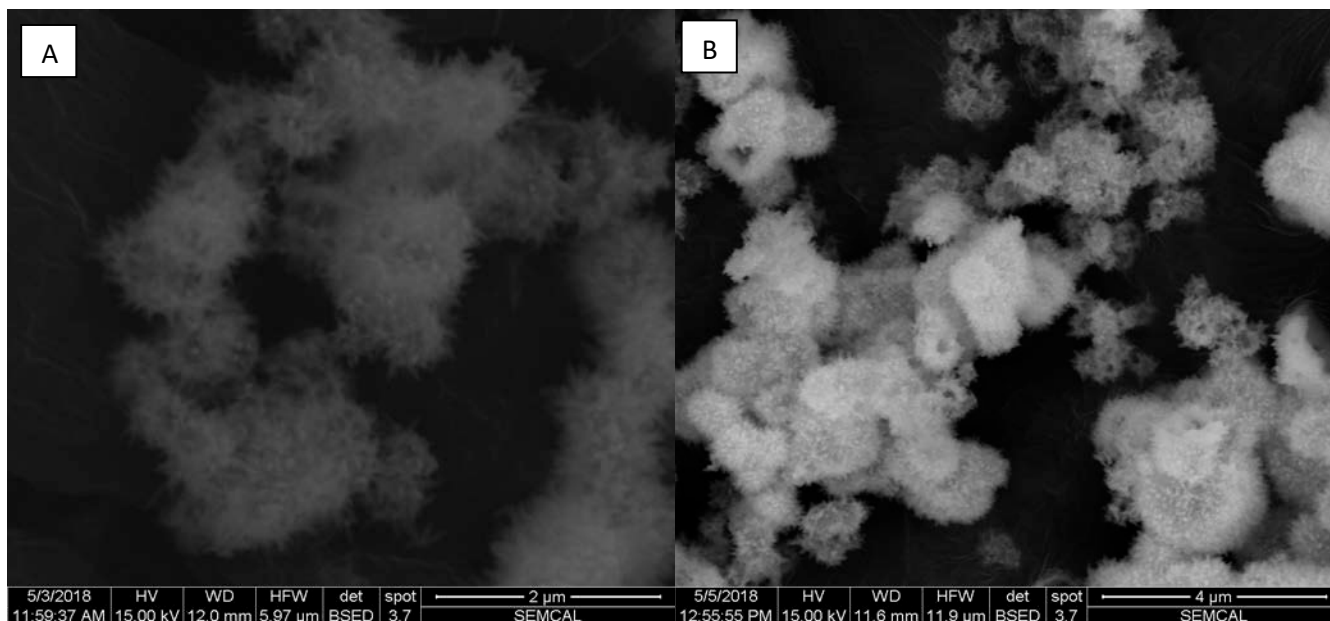


Figure 1- SEM images of fine grained akaganeite formed from the oxidation of HFFF from the A) UPP-W4 and B) UPP-S3 wells. EDX spectra reveals peaks for Fe, Cl and Si, suggesting these precipitates are akaganeite with SiO_2 either sorbed or coprecipitated. C) XRD spectra of precipitates from brines collected from Utica/Point Pleasant, the peaks in the spectra correspond to akaganeite (ak), quartz (q) and halite (ha).

Major and trace element uptake by these phases was determined by comparing the composition of an aliquot of the fluid sample that was filtered and acidified (FA) within hours of when the fluid was collected onsite at the well, to the residual supernatant after the fluid was allowed to age in the batch reactor (Raw). There was little difference in the major element concentrations (Na, Mg, K, Ca, Sr, Ba, Li

and even Mn) between the FA and Raw samples. However, approximately 50 % of the Fe in the UPP-W4, and 80-90% in the UPP-S1-4 samples precipitated as akaganeite, with a corresponding decrease in pH from near neutral (~ 6.4 to 6.6 at the well) to ~ 2.8 in the UPP W4 fluid, and ~ 3.1 in the UPP S1-4 samples. There was little evidence of uptake of alkali (Li, Rb, or Cs), alkaline earth metals (Sr, Ba) or transition metals (Ni, Cu, and Zn) into the solid phase in these acidic brines. Although several studies have shown that these elements can be sorbed onto akaganeite or other FeOOH phases, this behavior is strongly pH-dependent (eg Ponthieu et al., 2006 Webster et al., 1998; Smith, 1999; Bau, 1999; Verplanck et al., 2004) increasing with increasing pH. Therefore in these unbuffered experiments, acidity generated by iron oxidation and precipitation limits trace metal sorption onto these phases. The geochemical behavior of the rare earth and actinide elements measured was more complex. The light rare earth elements, for example La, remained in solution, while the middle and heavy rare earth elements were preferentially partitioned into the solid FeOOH phase. This behavior has been observed previously in both natural waters and in experiments (Bau, 1999; Verplanck et al., 2004) though the sorption-coprecipitation varies depending on solution speciation of the REE. Approximately 70 to 100% of the Th and U measured in the fresh flowback fluid was partitioned into the precipitates, while other toxic heavy elements, like Pb, do not appear to be partitioned into the solid phase under these conditions.

Table 3 Major and trace elements in fresh and oxidized (raw) HFFF for the Phase 1 experiments.

	Na mg/l	Mg mg/l	K mg/L	Ca mg/l	Si mg/l	Sr mg/l	Ba mg/l	Li mg/l	Fe mg/L	Mn mg/l	
W4	46486	2511	917	21045	17.3	3670	384	67.0	122.5	8.6	
shr 1	51726	2148	1240	18462	15.8	4525	1564	83.7	179.4	8.5	
shr 2	50433	2030	1267	17710	16.5	4127	1359	83.2	171.6	8.2	
shr 3	50941	2109	1223	17960	17.9	4455	1569	83.3	185.4	8.2	
Shr 4	53805	2199	1303	18725	17.9	4608	1664	85.8	172.6	8.4	
											pH
W4 raw	50555	2764	928	22829	11.9	3951	373	67.7	67.4	8.7	2.8
shr 1 raw	52998	2155	1315	18092	9.4	4599	1583	88.3	32.4	8.7	3.1
shr 2 raw	55872	2288	1287	19400	10.4	4566	1510	84.5	29.0	8.3	3.1
shr 3 raw	51450	2100	1285	17736	10.1	4435	1559	84.0	20.8	8.3	3.1
Shr 4 raw	55562	2268	1311	19031	11.5	4750	1730	89.5	26.5	8.6	3.1

	Rb µg/l	Cs µg/l	Ni µg/l	Cu µg/l	Zn µg/l	La µg/l	Ho µg/l	Th µg/l	U µg/l	Pb µg/l
W4	1203	191	727	68	92	11.3	4.63	9.25	3.56	29.4
shr 1	1909	395	631	154	239	20.5	1.25	4.77	1.17	21.8
shr 2	1949	385	532	148	229	16.6	0.82	1.86	0.35	20.5
shr 3	2027	410	609	160	269	17.6	0.58	1.06	0.22	17.0
Shr 4	2140	431	651	193	284	18.7	0.34	1.12	0.02	19.4
W4 raw	1170	155	819	70	82	6.1	1.02	1.14	0.94	26.2
shr 1 raw	2077	410	676	174	277	19.2	0.13	0.37	nd	23.7
shr 2 raw	2000	378	623	158	240	15.5	nd	0.34	nd	26.0
shr 3 raw	2005	392	692	197	280	18.7	nd	0.16	nd	24.2
Shr 4 raw	2137	421	698	207	340	19.4	nd	nd	nd	23.2

Phase 2 experiments

Phase 2 experiments were conducted with several different acid or base additives in order to induce precipitation of sulfate, phosphate, APS-Alunite supergroup, or carbonate phases that would sequester trace elements from these complex brines. Analysis of the solution compositions from these experiments shows that the concentrations of some elements did not change substantially over time after the various treatments, whereas others showed either a decrease or increase in concentration as a result of mineral precipitation/dissolution reactions. Analysis of the precipitates collected at the end of the bench scale experiments (by both XRD and SEM) show changes in mineralogy that are consistent with the measured changes in solution composition determined using ICP-OES and ICP-MS analyses.

Ba and Sr were removed by the addition of sulfuric acid, though their concentrations, and the resultant mineralogy, depended on the amount of sulfate added (Figure 2). In both the low and high SO₄ treatments, precipitation was instantaneous upon addition of the acid due to the formation of sulfate minerals. In the low SO₄ treatment, Ba decreased from ~ 1500 mg/L to ~ 600 mg/L within minutes, and then decreased slowly over the two week long experiment, while Sr varied only slightly. XRD and SEM analysis of the minerals formed indicate primarily barite (Figure 3). In the high SO₄ treatment, Ba concentrations decrease to undetectable before the first sample was collected, but in contrast, Sr decreased within the first hour after acid addition, and then increased over the two week experiment. XRD and SEM show minerals formed in the high SO₄ experiments were gypsum, and celestite [(Sr,Ba)SO₄]. However, despite the almost complete removal of Ba from solution, no discrete barite phases were observed (Fig 3). The changes in solution chemistry, as well as the SEM images of the solid phase in both sulfate treatments suggest that these minerals were undergoing dissolution-reprecipitation reactions throughout the experiments.

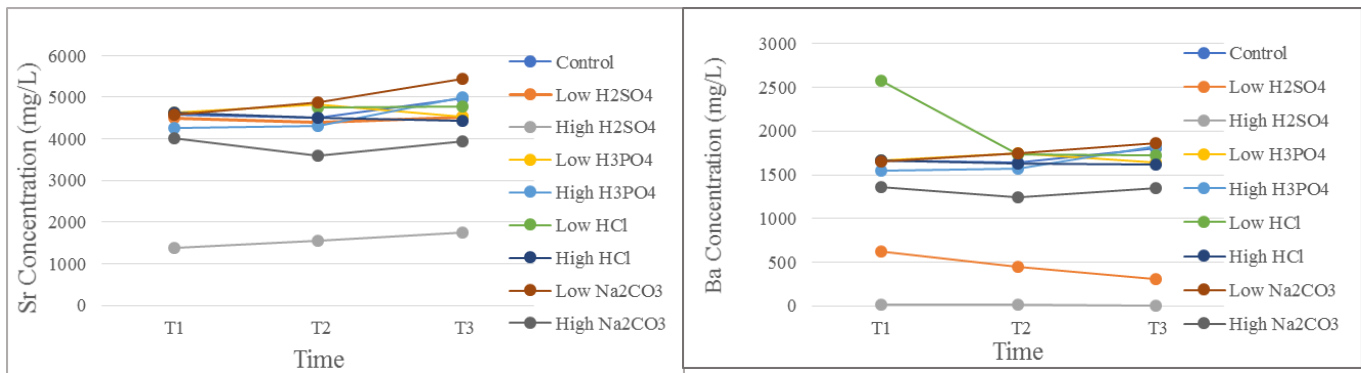


Figure 2 Sr and Ba in the phase two experiments with different acid and base amendments. Solutions were sampled after ~ 1-2 hours (T1), one week (T2) and two weeks (T3).

Addition of carbonate increased solution pH from an initial pH of ~ 2.4 up to ~ 6.5, and resulted in the precipitation of calcium carbonate (Fig 3C), however, with the exception of Ca, there was little change in the concentrations of other elements. Even Sr and Ba, which can substitute into calcite, exhibited only ~ 10% decrease in concentration in the high carbonate treatment.

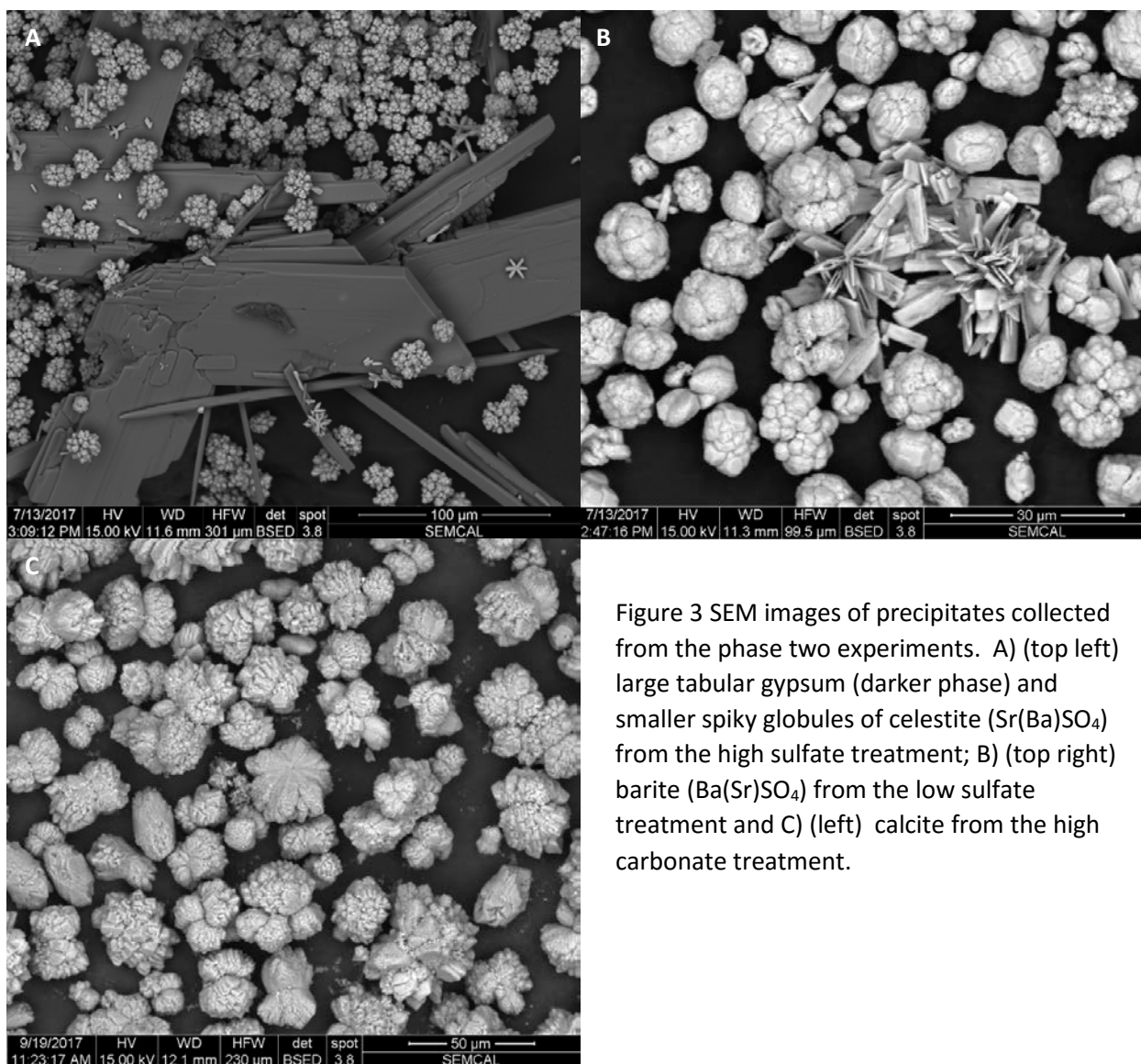


Figure 3 SEM images of precipitates collected from the phase two experiments. A) (top left) large tabular gypsum (darker phase) and smaller spiky globules of celestite ($\text{Sr}(\text{Ba})\text{SO}_4$) from the high sulfate treatment; B) (top right) barite ($\text{Ba}(\text{Sr})\text{SO}_4$) from the low sulfate treatment and C) (left) calcite from the high carbonate treatment.

The geochemical behavior of trace elements in these experiments was complex. The addition of sulfuric acid, or sodium carbonate and subsequent precipitation of barite, celestite, gypsum and calcite had no measureable effect on the concentrations of alkali metals (Li, Rb, or Cs) and surprisingly, had very little effect on most of the transition metals measured (Ni, Cu, and Zn), with only small decreases (< 10 %) observed in the high carbonate treatment. Most of the REE elements showed little to no change in concentrations in solution in any of the acid addition treatments compared to the control, but were effectively scavenged by the carbonate addition treatments (Figure 4). In contrast, La was removed in both the carbonate and sulfate addition experiments, suggesting that larger ions like La can substitute into the sulfate phases.

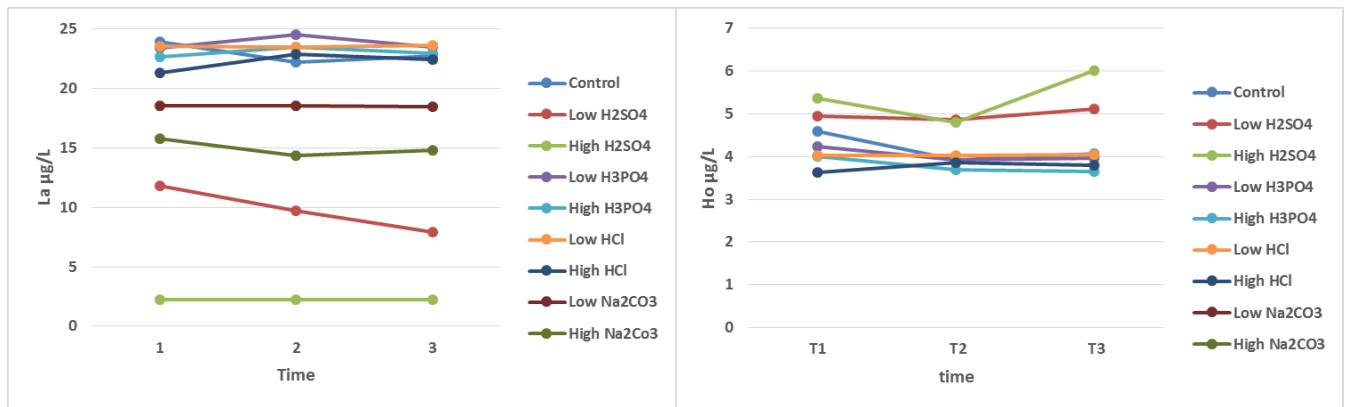


Figure 4 La and Ho concentrations in the phase two experiments. La was scavenged from solution in both the sulfate and carbonate amendment treatments while heavier REE like Ho were primarily scavenged in the carbonate addition treatments where its concentration was below detection.

Phase 3 experiments

Based on the results of the phase 2 experiments, we conducted third set of experiments using HFFF, a synthetic acid mine drainage fluid, and a trace metal solution to investigate the formation of sulfate and APS mineral phases from mixtures of these solutions, the stability of these phases over time (several months), and their potential to incorporate trace elements from solution. The sulfate minerals observed in SEM images, the chemistry from spot analysis from EDX, and the mineralogy determined by XRD were consistent with the changes in solution chemistry. The sulfate phases formed immediately upon addition of the artificial AMD to HFFF, but varied among the three different sulfate addition experiments, and also appeared to change in morphology and relative abundance over time. The sulfate phases observed in the 0.5 AMD treatment were small (~ 5 µm) nearly pure endmember barite with characteristic barite rose morphology, as well as euhedral rectangular crystals (Figure 5). The formation of these phases is consistent with the changes in solution chemistry- Sr in the 0.5 AMD treatment is not significantly different than the control experiment, while Ba is approximately 10 % lower. The chemistry and morphology precipitates in the 5 ml AMD are very different, precipitates are barite-celestite balls and euhedral bricks, but these phases appear to be extensively etched and have sharp features that are indicative of dissolution-precipitation reactions. Analysis of precipitates formed early on in these experiments showed some discrete SrSO₄ phases were present as elongated needles or as fibrous aggregates resembling sheaths, however these were not abundant and were not observed in samples collected after several months. Solution chemical analysis from the first week of the experiment showed that both Sr and Ba varied, indicating dissolution-precipitation occurs. In the 50 ml AMD treatment, large tabular crystals of gypsum as well as smaller elongated crystals of celestite were observed in SEM images and by XRD. Although barium was completely removed from solution in this treatment, and geochemical modelling using PHREEQC indicated solutions were supersaturated with respect to barite, there were no discrete barite phases observed in the precipitates. Ba was detected as a trace element in both the gypsum and celestite by EDX spot analysis. Trace elements, Cu and La, were sorbed/co-precipitated into the solid phase, however their concentrations varied over time, particularly in the 50 AMD treatment, suggesting continued exchange between the solution and precipitates.

Figure 5 SEM images from A, B), 0.5 ml AMD; C, D), 5 ml AMD; and E,F), 50 ml AMD.

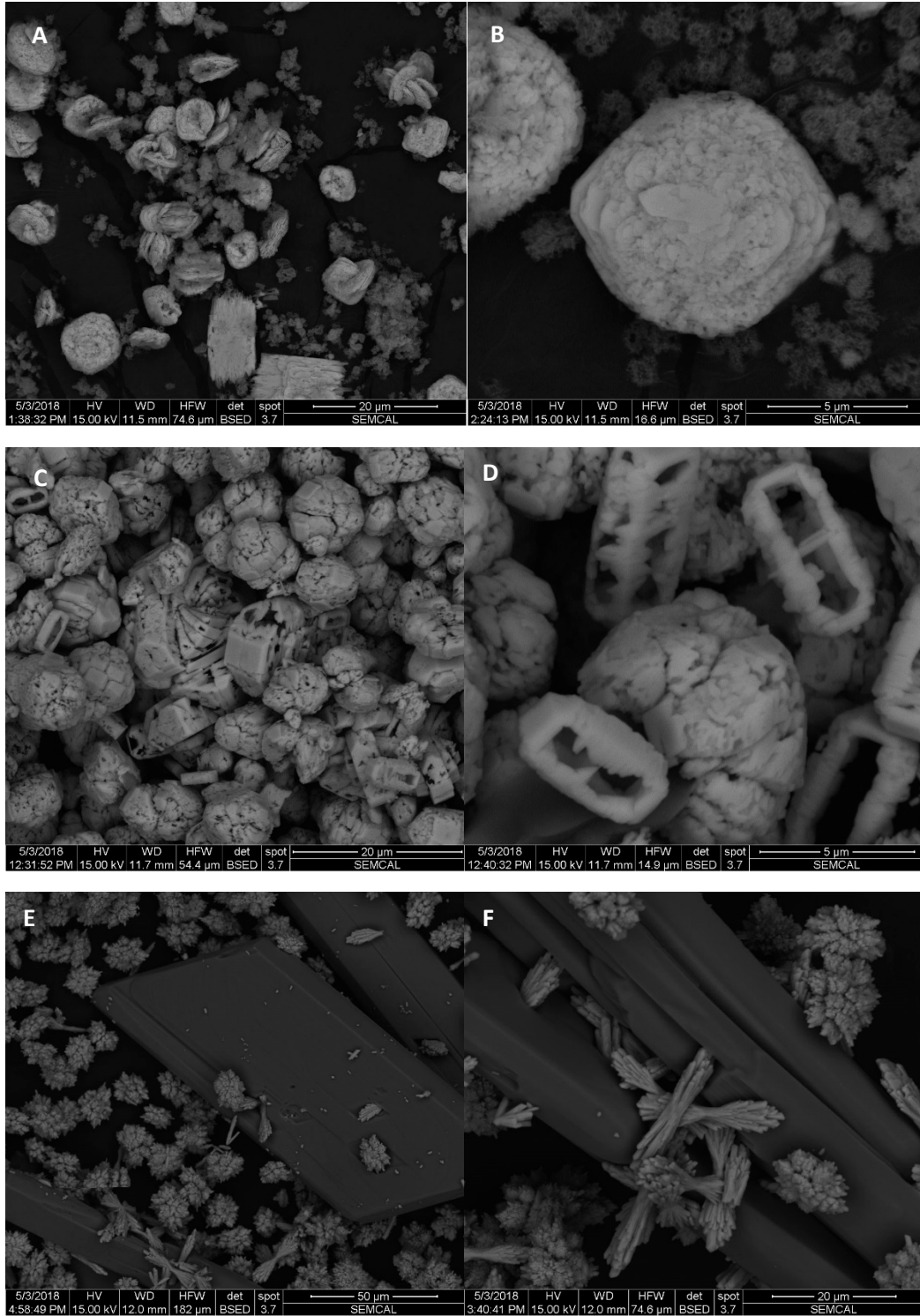
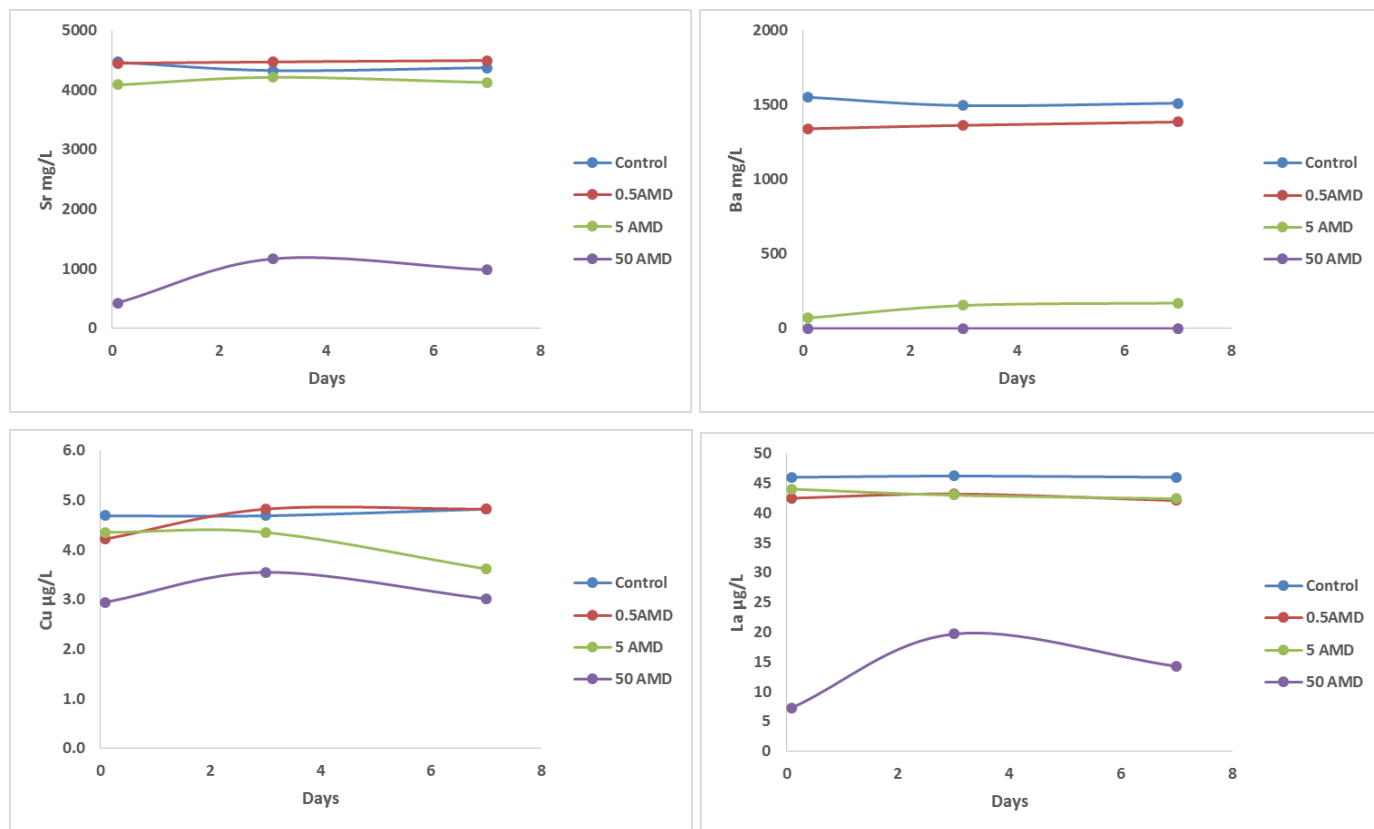


Figure 6 – Sr, Ba, Cu and La in the Phase 3 experiments.



Summary and Conclusions

Considering the Utica-Point Pleasant (UPP W4; UPP S3 and S4) hydraulic fracturing flowback fluids measured in this study, akaganeite is the major Fe oxy-hydroxide phase identified in all control samples as well as samples prepared with chemical additives. Both XRD data, which provide crystallographic (mineral atomic structural) data, and EDS microanalytical elemental data support this result. This phase contains significant Cl and Si. Akaganeite of this composition has been synthesized in the laboratory for its unique physical properties as a nano-scale material (Tadic et al., 2015). Because it is not as common as a ferric iron phase in most geological materials it has received less attention as compared to the more abundant natural Fe³⁺ (hyd)oxide minerals, such as goethite (Cornell, 1992). Akaganeite does occur in nature in brines (Font et al., 2017; Chilkoor et al., 2018). Cornell (1992) synthesized akaganeite in the presence of silica to form a structure that she suggests incorporates about 4 percent Si into the crystal structure, with some silica also sorbing to the surface of hollow rods of the akaganeite crystals. The potential for akaganeite to sorb trace elements from hydraulic fracturing fluids is likely to be dramatically different as compared to more common natural Fe oxyhydroxide phases.

The mineralogical composition of precipitates varies with the type and concentrations of chemical additions mixed with the flowback fluids. As expected, sulfates precipitate with the introduction of

sulfuric acid, and carbonates precipitate with introduction of sodium bicarbonate. But in the case of sulfuric acid addition, the concentration of the acid determines the phases that precipitate. This result has important implications for the sequestration of cations with large atomic radii into the sulfate, including some that are of environmental concern, such as radium (Rosenberg et al., 2014; Zhang et al., 2015).

References

Bau M, 1999, Scavenging of dissolved yttrium and rare earths by precipitating iron oxyhydroxide: Experimental evidence for Ce oxidation, Y-Ho fractionation, and lanthanide tetrad effect. *Geochim. Cosmochim. Acta*, **63**, 67–77.

Bayliss P., Kolitsch U, Nickel EH, and Pring A, 2010, Alunite supergroup: recommended nomenclature. *Mineralogical Magazine*, 74, 919-927.

Chilkoor G., Shrestha N, Soeder D, Gadhamshetty V, 2018, Corrosion and environmental impacts during the flowback water disposal associated with the Bakken shale, *Corrosion Science*, 133, 48-60.

Cornell RM, 1992, Preparation and properties of Si substituted akaganeite (Beta-FeOOH). *ZEITSCHRIFT FÜR PFLANZENNAHRUNG UND BODENKUNDE*, 155, 449-453.

Dia A, Graua G, Olivie-Lauquet G, Riou C, Molénat J, Curm P, 2000, The distribution of rare earth elements in groundwaters: assessing the role of source-rock composition, redox changes and colloidal particles. *Geochim. Cosmochim. Acta*, 64, 4131-4151

Daly RA, Borton MA, Wilkins MJ, Hoyt DW, Kountz DJ, Wolfe RA, Welch SA, Marcus DN, Trexler RV, MacRae JD, Krzycki JA, Cole DR, Mouser PJ, and Wrighton KC. 2016 Microbial metabolism in new 2.5 km deep ecosystem created by hydraulic fracturing in shales. *Nature Microbiology* 16146 | DOI: 10.1038/NMICROBIOL.2016.146

Font E, Carlut J, Remazeilles C, Mather TA, Mirao J and Casale S. End-Cretaceous akaganeite as a mineral marker of Deccan volcanism in the sedimentary record (2017) *Nature Scientific Reports* 7 no. 11453

Kondash AJ, Warner NR, Lahav O, Vengosh A, 2014, Radium and Barium Removal through Blending Hydraulic Fracturing Fluids with Acid Mine Drainage. *ENVIRONMENTAL SCIENCE & TECHNOLOGY* 48, 1334-1342.

Nelson AW, Eitheim ES, Knight AW, May D, Mehrhoff MA, Shannon R, Litman R, Burnett WC, Zorbes TZ, Schultz MK, 2015, Understanding the Radioactive In-growth and Decay of Naturally Occurring Radioactive Materials in the Environment: An Analysis of Produced Fluids from the Marcellus Shale, *Environmental Health Perspectives*, 123, 689-696

Pontieu M., Julliot F., Hiemstra T, van Riemsdijk WH, and Benedetti MF, 2006, Metal ion binding to iron oxides. *Geochimica et Cosmochimica Acta*, 70, 2679-2698.

Riley RA, 2015, Regional drilling activity and production, in Patchen, DG and Carter, KM, eds., *A geologic play book for Utica Shale Appalachian basin exploration, Final report of the Utica Shale Appalachian basin exploration consortium*, p. 11-19, Available from: <http://www.wvgs.wvnet.edu/utica>

Rosenberg YO, Sadeh Y, Metz V, Pina CM, and Ganor J, 2014, Nucleation and growth kinetics of $Ra_xBa_{1-x}SO_4$ solid solution in NaCl aqueous solutions. *Geochimica et Cosmochimica Acta*, 125, 290-307.

Smith KS, 1999, Metal sorption on mineral surfaces: An overview with examples relating to mineral deposits. Chapter 7 Reviews in Economic Geology, Volumes 6A Published by the Society of Economic Geologists, pp 161-182.

Tadic M., Milosevic I, Kralj S., Mbodji M., Motte L, 2015, Silica-Coated and Bare Akaganeite Nanorods: Structural and Magnetic Properties. *Journal of Physical Chemistry C* 119, 13868-13875.

Vengosh, A.; Jackson, R. B.; Warner, N.; Darrah, T. H.; Kondash, A. A critical review of the risks to water resources from unconventional shale gas development and hydraulic fracturing in the United States. *Environ. Sci. Technol.* 2014, 48 (15), 8834–8348.

Verplank PL, Nordstrom DK, Taylor HE, and Kimball BA, 2004, Rare earth element partitioning between hydrous ferric oxides and acid mine water during iron oxidation. *Applied Geochemistry*, 19, 1339-1354.

Webster JG, Swedlund PJ, and Webster KS, 1998, Trace Metal Adsorption onto an Acid Mine Drainage Iron(III) Oxy Hydroxy Sulfate, *Environ. Sci. Technol.*, 1998, 32 (10), pp 1361–1368

Welch, Sheets and Cole in prep Geochemistry of Flowback fluids from the Utica-Point Pleasant.

Zhang, T, Hammack, RW, Vidic, RD, 2015, Fate of Radium in Marcellus Shale Flowback Water Impoundments and Assessment of Associated Health Risks *ES&T* (2015), 49, 9347-9354.

Design of a self-cleaning membrane-assisted bioreactor for enhanced removal of nutrients from wastewater

Basic Information

Title:	Design of a self-cleaning membrane-assisted bioreactor for enhanced removal of nutrients from wastewater
Project Number:	2017OH5700
Start Date:	3/1/2017
End Date:	2/28/2019
Funding Source:	Other
Congressional District:	OH-001
Research Category:	Engineering
Focus Categories:	Wastewater, Nutrients, Treatment
Descriptors:	
Principal Investigators:	Soryong Chae

Publications

1. Noe T. Alvarez, Ryan Noga, So-Ryong Chae, George A. Sorial, Hodon Ryu and Vesselin Shanov, Heatable carbon nanotube composite membranes for sustainable recovery from biofouling, *Biofouling*, 33(10), 847-854, 2017. (<https://doi.org/10.1080/08927014.2017.1376322>)
2. So-Ryong Chae and Yoshimasa Watanabe, Performance and fouling characteristics of poly-vinylidene fluoride (PVDF) ultrafiltration membranes with pre-coagulation/sedimentation, sand filtration, and chlorination. The 5th Busan Global Water Forum, Busan, South Korea, September 6-7, 2017.
3. So-Ryong Chae, Environmental implications and applications of carbon nanomaterials, American Industrial Hygiene Association (AIHA) - Ohio Valley Section meeting, March 21, 2018.

Project title: Design of a self-cleaning membrane-assisted bioreactor for enhanced removal of nutrients from wastewater

Project number: 2017OH518B

PI: Soryong Chae, Ph.D., Assistant Professor, Department of Chemical and Environmental Engineering, University of Cincinnati

1. Problem and Research Objectives

Eutrophication is a key driver causing a number of pressing aquatic environmental problems including reductions in light penetration and increases in harmful algal blooms (HABs) [1]. The major factors affecting eutrophication are mineral nutrients such as nitrogen and phosphorus in municipal and industrial wastewater [2]. In Ohio's lakes and rivers, the key symptom of eutrophication is cyanobacterial blooms [3]. The increasing occurrence of HABs in fresh water due to eutrophication of surface water has become an emerging concern threatening human and environmental health because cyanobacteria, more commonly known as blue-green algae, can produce and release potent toxic compounds, which are known as "cyanotoxins" such as microcystins, cylindrospermopsin, saxitoxin, and anatoxin-a [4-7].

The United States has the world's highest water consumption rate per capita (approximately 215 cubic meters per year) [8]. The ever-increasing demand for water leads to need for new sources of longer distance and/or greater depth, however, which would lead to increased environmental costs and economic exploitation. Development of an expanded water portfolio is even more challenging given the high cost of maintenance and upgrade of existing aging and overloaded centralized wastewater conveyance and treatment infrastructures currently serving large metropolitan areas in the U. S. [9]. It is estimated that water infrastructure maintenance and upgrade for the wastewater treatment sector alone would cost more than \$200 billion over the next 20 years in the U. S. [10]. Given the rising burden on centralized water conveyance and treatment systems, wastewater reuse has emerged as a viable approach toward water sustainability.

In nutrient-sensitive estuaries, municipal and industrial water resource recovery facilities are required to implement more advanced treatment methods in order to meet increasingly stringent effluent guidelines for nutrients. According to literature, biological nutrient removal processes that incorporate coupled nitrification/denitrification have the potential to remove total nitrogen (TN) down to about 5 - 12 mg/L, in selected cases, down to 3 mg/L. The TN concentration in effluent is known as less than 10 mg/L at most inland municipal WRRFs. In case of phosphorus, very stringent effluent total phosphorus (TP) limits (0.03 - 0.10 mg P/L) are required in the U.S. but it is challengeable to reach the goal by only biological nutrient removal processes [11, 12].

Achieving these limits demands **very low soluble P and essentially a biomass-free effluent**. In particular, biological nutrient removal systems with a settling tank discharge approximately 10 mg/L of total suspended solids in the effluent. The phosphorus content of the solids contributes approximately 0.3 mg/L to the effluent [13]. Biological nutrient removal systems incorporating membrane technology, which are able to produce solids-free effluent are becoming an attractive technology [14-19].

Membrane bioreactor (MBR) technology can provide complete retention of biomass allowing higher sludge retention time with effective bacterial cultures that can degrade certain types of recalcitrant constituents. However, **membrane fouling** is identified as a major hurdle to the wide

applications of MBRs [20]. Membrane fouling in MBRs takes place mainly due to two reasons: (i) cake layer formation by biomass and (ii) precipitation of inorganics on the membrane surface. In particular, the cake formation that includes sludge particles and biopolymers such as proteins, polysaccharides, and humic substances has been identified as a dominant feature contributing to the deterioration of membrane performance [21-23]. To recover the reduced water permeability through membranes due to fouling, routine membrane cleaning using chemicals is required. However, conventional polymeric membranes that have been widely used for MBRs are sensitive to oxidising disinfectants and the frequent use of chemicals shortens the membrane life-time [24]. Therefore, it is desirable to develop new membranes and approaches for mitigating of membrane fouling.

Due to the continuously increasing occurrence of HABs in Ohio's lakes and rivers and the inefficient or impractical technologies for the elimination of nutrients, there is a critical need to develop an effective solution for a satisfactory removal of nutrients from wastewater sources in order to achieve clean and safe drinking water supplies and protect human health. The main objective of this project is to fabricate a self-cleaning membrane for the efficient removal of nutrients from municipal wastewater. A bench-scale MBR (treatment capacity = 10 L/day) was developed and optimized for simultaneous removal of nitrogen and phosphorus to prevent HABs combined with the self-cleaning carbon nanotube (CNT) membrane.

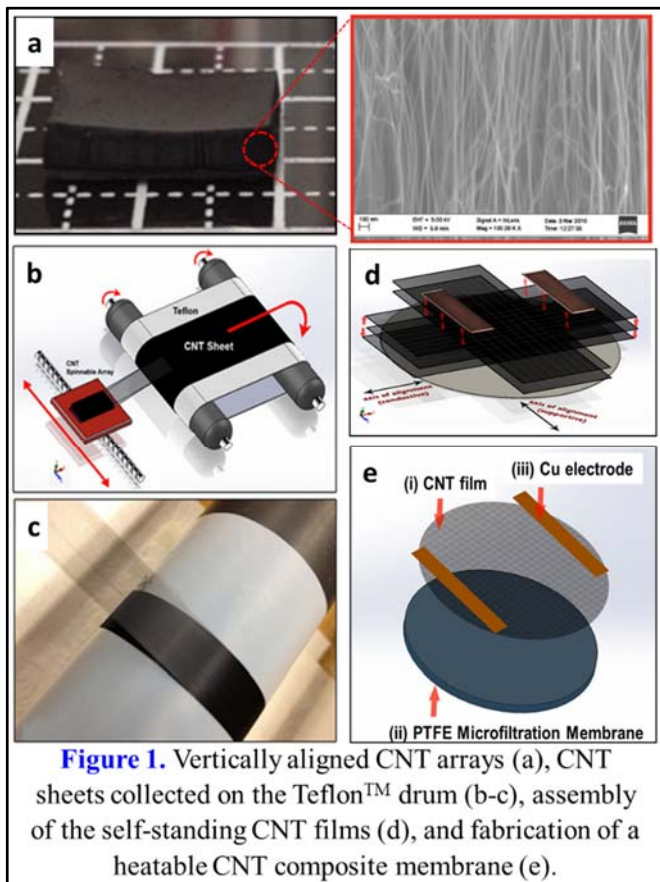
2. Methodology

2.1 Fabrication and surface modification of self-cleaning membranes

We have successfully synthesized prototype **self-standing and electrically heatable CNT composite membranes** (100 cm²). Firstly, **vertically aligned CNT arrays** (**Figure 1a**) ~0.45 mm long with 7~10 nm pore diameter were synthesized through a chemical vapor deposition (CVD) as described in the PI's previous work [51]. CNTs with a production rate of ~ 600 kg/h can be obtained using an industrial-scale catalytic CVD reactor and the average cost of CNTs with these proposed processes lies in the range of **\$25 - \$38/kg** [52].

The synthesis process uses a thin film catalyst of iron and cobalt, sputtered over a 5-nm aluminum oxide buffer layer on a 4-inch silicon wafer. The catalyst-coated silicon wafers are cut into 2-inch pieces of variable width, and loaded into a modified commercial CVD reactor (ET3000, CVD Equipment Corporation) at 740 Torr and 750°C.

Fabrication of **porous CNT sheets** (water contact angle > 140°) (**Figure 1b**)



starts by drawing one edge of the vertically aligned CNT arrays. Approximately each linear millimeter of vertically aligned CNT arrays can be drawn into a linear meter of CNT sheet using a machine at speeds up to 16 m/s by using collecting drums connected to a high-speed motor and collecting the CNT sheets onto the Teflon™ drum (**Figure 1c**).

The CNT sheets were stacked layer-by-layer to form **self-standing CNT films (Figure 1d)** on a 0.20 μm flat-sheet **hydrophilic PTFE membranes** (Sterlitech). The entire hybrid membrane was wetted with ethanol (99.5%, Acros Organics) in order to increase the adsorption of CNTs to the polymeric membrane and improve densification, which occurs after solvent evaporation. Loading of CNTs, surface area, and porosity were controlled by varying number of CNT sheets and orientation on the membrane surface. Finally, a **CNT composite membrane (Figure 1e)** was synthesized by combining 1) the self-standing CNT films on the PTFE membrane and 2) Cu electrodes on the surface of the CNT films.

We modified the surface of the CNT composite membrane using atmospheric pressure plasma facility (**Figure 2**), which allows dry functionalization of CNTs creating hydroxyl (-OH) and amine (-NH) functional groups. Hydroxyl functional groups were created on CNTs by using atmospheric pressure Helium/Oxygen plasma. Also, amine reactive species were created using NH₃ combined with helium flow and generating plasma at atmospheric pressure.

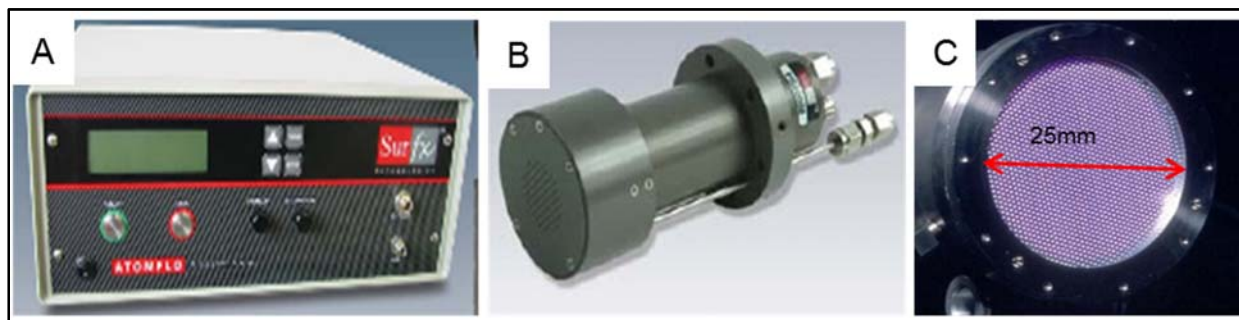


Figure 2. Plasma functionalization of CNTs: The Surfx Atomflo 400D plasma controller (A) with a cylindrical plasma deposition headset (B), and plasma discharge unit (C).

2.2 Electric heating of the CNT composite membrane for mitigation of biofouling

This type of material is easily scalable and electrically conducting to produce heat when connected to electrodes and voltage is applied. For electrical heating of the CNT composite membranes, a bench top direct current (DC) power supply (E3612A, Hewlett Packard) was connected to each sample and electric potentials of 10 V, 15 V, 20 V and 25 V were run for 5 minutes. The surface temperatures were monitored with a FLIR T-640 IR camera. FLIR Tools+ software was used to record, plot, and prepare images and reports from the resulting thermal data.

2.4 A bench-scale MBR system

A bench-scale anoxic and oxic MBR system (treatment capacity = 10 L/day at HRT = 12 hr) (**Figure 3**) was operated at room temperature over 4 months with synthetic wastewater (**Table 1**). The reactor was operated without electrical heating of the CNT composite membranes for about two months (Period I) and then the CNT membrane was electrically heated to remove membrane foulants for about one month (Period II). During these periods, mixed liquor suspended solids (MLSS) concentration in the reactors was maintained at 6.2 ± 0.4 g/L at 30-day SRT. Water permeability through polymeric membrane and the CNT composite membranes was maintained at 10 L/m²/hr (LMH).

Table 1. Characteristic of synthetic wastewater.

Item	Chemical formula	Concentration (mg/L)
Glucose	C ₆ H ₁₂ O ₆	150 (as COD)
Ammonium sulfate	(NH ₄) ₂ SO ₄	30 (as N)
Potassium phosphate	KH ₂ PO ₄	6 (as P)
Sodium bicarbonate	NaHCO ₃	200 (as CaCO ₃)
Calcium chloride	CaCl ₂ ·2H ₂ O	0.50
Cobalt chloride	CoCl ₂ ·6H ₂ O	0.35
Cupric sulfate	Cu SO ₄ ·5H ₂ O	0.15
Ferric chloride anhydrous	FeCl ₃	0.80
Magnesium sulfate	Mg SO ₄ ·7H ₂ O	0.34
Manganese chloride	MnCl ₂ ·4H ₂ O	0.50
Sodium molybdate dihydrate	Na ₂ MoO ₄ ·2H ₂ O	0.20
Yeast extract	-	10
Zinc sulfate	ZnSO ₄ ·5H ₂ O	0.55

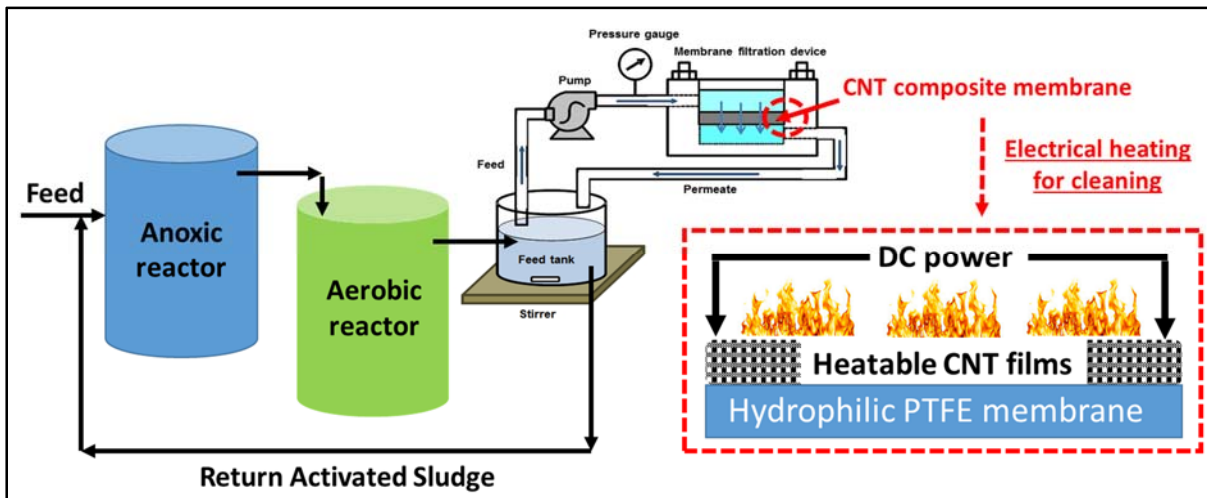


Figure 3. Schematic diagram of a bench-scale MBR system with the electrically heatable CNT composite membrane.

2.5 Analysis of membrane fouling

To determine the effects of the electric heating of the CNT composite membrane in membrane fouling, the resistance-in-series model was used to analyze membrane fouling resistances, which describes the permeate flux - transmembrane pressure (TMP) relationship over the entire domain of pressure as described in the previous study [28]. Based on the model, the permeate flux on the applied TMP can be described by Darcy's law as Eq. (1):

$$J_v = \frac{1}{A} \frac{dV}{dt} = \frac{\Delta P}{\mu R_t} \quad (1)$$

where J_v is the permeate flux ($\text{m}^3/\text{m}^2/\text{s}$), V is the total volume of permeate (m^3), A is the membrane area (m^2), ΔP is the TMP (Pa), μ is the dynamic viscosity of permeate ($\text{Pa}\cdot\text{s}$), and R_t is the total membrane resistance (m^{-1}).

2.6 Characterization of the CNT composite membranes

Characterization of the CNT composite membranes were conducted as follows: **Hydrophobicity** or hydrophilicity of the membranes was examined by contact angle measurements using the sessile drop Young–Laplace method (Drop Shape Analyzer, DSA25E, Krüss). **Surface charge** (or streaming potential) of the membranes was determined by measuring streaming potential and streaming current on the material surface (SurPASS, Anton Paar). **Surface area and pore properties** of the composite membranes was investigated using a micropore physisorption analyzer (ASAP 2060, Micromeritics).

2.7 Characterization of wastewater and membrane permeate

Concentrations of various ions such as NO₂-N, NO₃-N, and ortho-P were analyzed using ion chromatography (IC) (Dionex DX-120, U.S.A) after filtering with a 0.45 μm membrane filter (ADVANTEC MFS Inc., Dublin, CA, U.S.A). Temperature and pH were measured using temperature and pH electrodes connected with a pH meter (Orion Model 420A, Orion Research Inc., U.S.A). Concentrations of COD, MLSS, total suspended solid (TSS), TN, and TP of wastewater were measured according to *Standard Methods* [29]. All experiments of this study were performed at least three times. Analysis of variance (ANOVA) was applied for the statistical analysis and differences from controls was considered significant when $p \leq 0.05$.

3. Principal Findings and Results

3.1 Changes in membrane temperature by electric heating

Figure 4 shows the effects of electric potential and power on temperature changes on the surface of the CNT composite membranes. The max temperature is the warmest point recorded by the IR camera and the average temperature is the average values of five different spots on the membrane surface. As electric voltage increased from 10 (0.75 W) to 20 V (3 W), average temperature increased from 53°C to 110°C. However, temperature slightly decreased at 25 V (3.5 W) due to damage of the membrane sustained at the corners where the CNT layers first meets the Cu electrode.

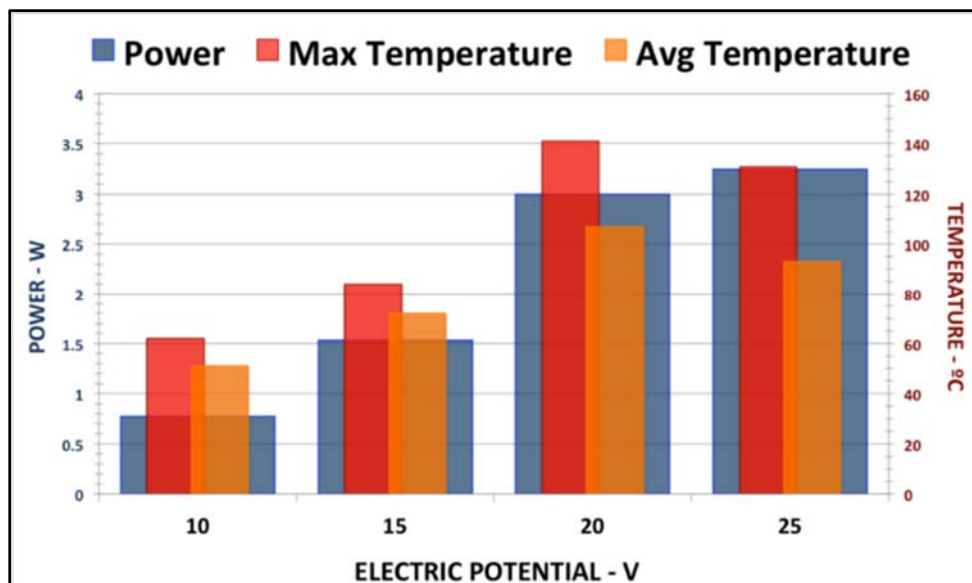


Figure 4. Effects of electric potential on membrane temperature.

In this study, the surface temperature of the CNT membrane increased from 25 to 140°C (Spot 3 in **Figure 5(C-1)**) by electric heating with DC power (20 V). When this membrane was employed, *Escherichia coli* K12 filtered and collected on its surface were successfully annihilated within ten seconds.

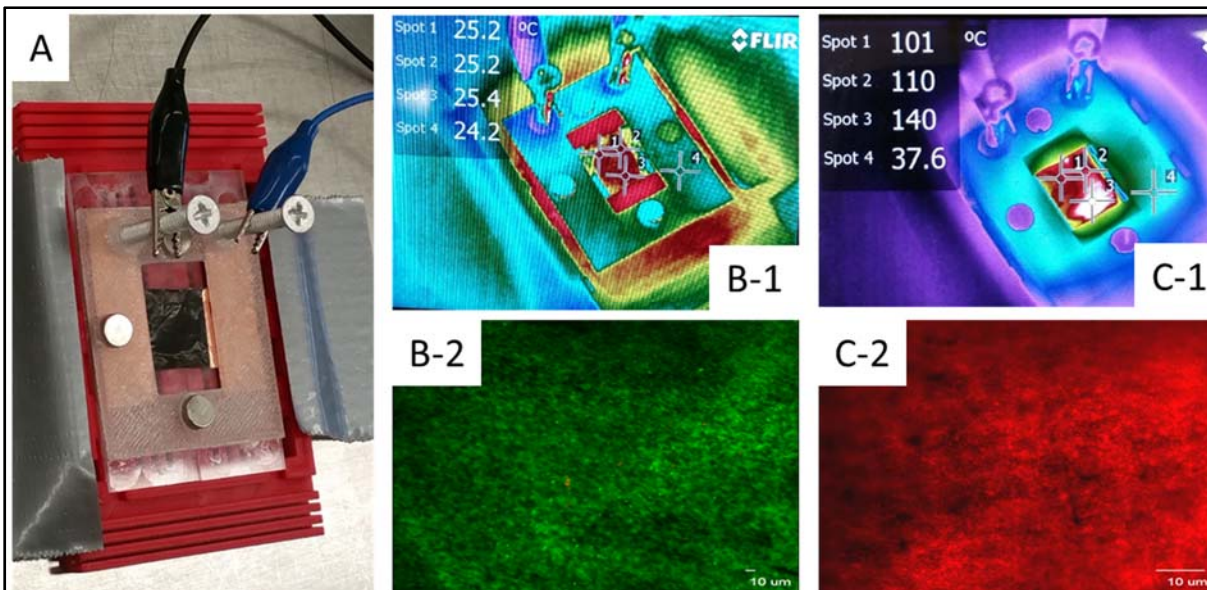


Figure 5. Electric heating device (A) with a DC power supply, IR temperature profile of the CNT arrays (B-1) and *Escherichia coli* (ATCC 25922) stained using the Live/Dead BacLight Bacterial viability kits (B-2) before DC power supply, IR temperature profile of the CNT arrays (C-1) and *Escherichia coli* (ATCC 25922) stained using the Live/Dead BacLight Bacterial viability kits (C-2) after 10-second at 20 V.

3.2 Removal efficiency of organic matter and nutrients by the bench-scale MBR system

As shown in **Table 2**, the bench-scale MBR system showed good performance in removing organic matter and nutrients from synthetic wastewater. Typical removal efficiencies of COD, TN, and TP by the MBR were 95~96%, 83~84%, and 63~65%, respectively. Also, the both polymeric membrane and the CNT composite membrane effectively separate biomass from the final effluent (over 99.9% removal of TSS).

Table 2. Average removal efficiencies of COD, nutrients, and TSS by the bench-scale MBR system.

Removal efficiency	Period I (0 ~ 60 days)	Period II (61 ~ 97 days)
COD	95 ± 3%	96 ± 4%
TN	83 ± 2 %	84 ± 3%
TP	65 ± 5%	63 ± 2%
TSS	Over 99.9 %	Over 99.9 %

3.3 Membrane fouling and recovery from membrane fouling in the MBR system

The bench-scale MBR system was operated at constant flux (*i.e.*, 10 LMH) with the 0.20 μm PTFE membrane for 60 days. **Figure 6** shows variations of TMP during the operation. When the

TMP increased over 50 kPa, there is decreased in water flux so the membrane was replaced with new one. As shown in this figure, the TMP increased over 50 kPa within 6-7 days due to membrane fouling. This was consistent for each experiment during the operation.

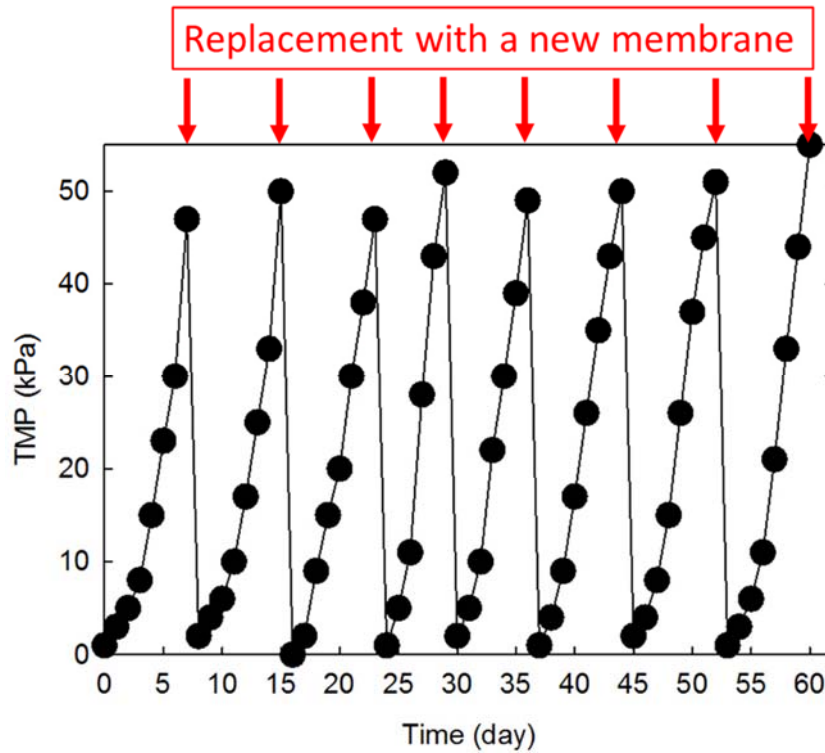


Figure 6. Changes in membrane fouling (*i.e.*, TMP) during the experimental period I.

After 60 days, the PTFE membrane was replaced with the CNT composite membrane (water contact angle $< 20^\circ$) and the MBR system was operated for about one month under the same operating conditions. During this period, the CNT composite membrane was heated over 100°C for 30 seconds using DC power (E3612A, Hewlett Packard) to remove membrane fouling when the TMP increased over 50 kPa. As shown in **Figure 7**, the CNT composite membrane was able to treat wastewater for 9-10 days without cleaning and the membrane was effectively recovered from fouling using electric heating. During this period, any physical damage of the CNT composite membrane was not found by the electric heating.

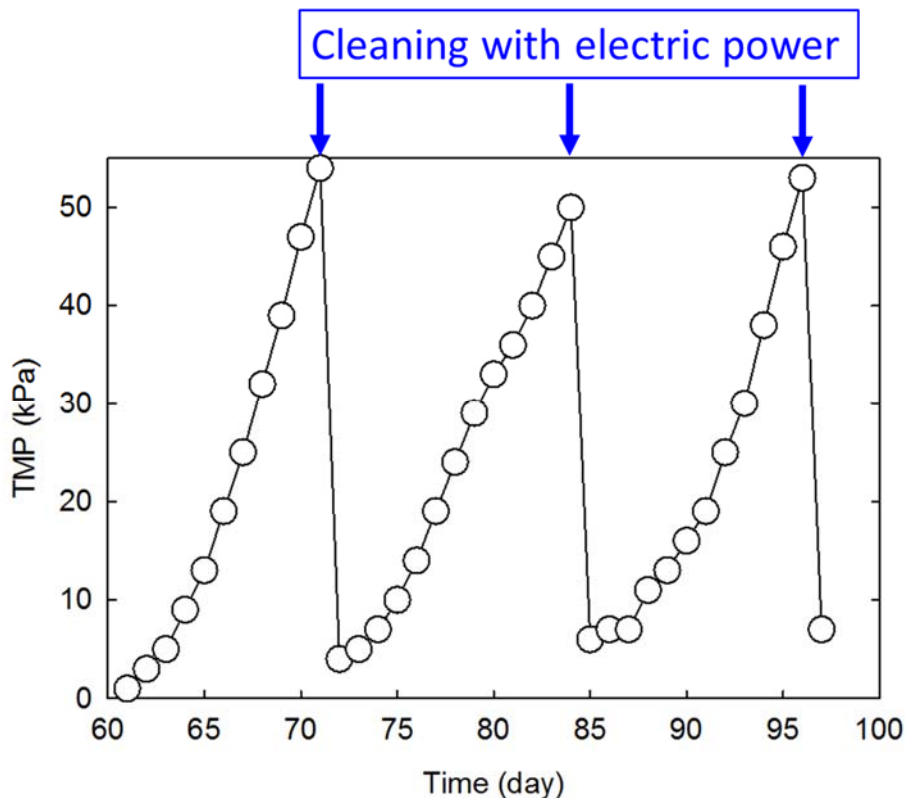


Figure 7. Changes in membrane fouling (*i.e.*, TMP) during the experimental period II.

4. Finding Significance

HABs have a significant impact on drinking water quality, fish and animal habitat as well as ecosystem services. The need to reduce anthropogenic nutrient inputs to aquatic ecosystems in order to protect drinking-water supplies and to reduce eutrophication, including the proliferation of HABs and “dead zones” in coastal marine ecosystems has been widely recognized. MBR is one of the most cost-effective treatment technologies for removal of nutrients from wastewater. However, membrane fouling is identified as a major hurdle to the wide applications of MBRs for wastewater treatment with high MLSS concentration.

From this study, it was found that the CNT composite membrane has an anti-fouling function and electric heating is a sustainable method to clean the CNT membrane after fouling. The results allow for development of novel engineering solutions for the mitigation of membrane fouling and/or recovery from membrane fouling that eventually increase performance of MBR systems and also reduce HABs’ risks to public health and the environment.

References

1. Mesfioui, R.; Love, N. G.; Bronk, D. A.; Mulholland, M. R.; Hatcher, P. G., Reactivity and chemical characterization of effluent organic nitrogen from wastewater treatment plants determined by Fourier transform ion cyclotron resonance mass spectrometry. *Water Res.*, *46*(3), 622-634, 2012.
2. Correll, D. L., The Role of Phosphorus in the Eutrophication of Receiving Waters: A Review. *Journal of Environmental Quality*, *27*(2), 261-266, 1998.
3. Schindler, D. W., Eutrophication and Recovery in Experimental Lakes: Implications for Lake Management. *Science*, *184*(4139), 897-899, 1974.
4. Chorus, I.; Falconer, I. R.; Salas, H. J.; Bartram, J., Health risks caused by freshwater cyanobacteria in recreational waters. *J. Toxicol. Env. Health-Pt b-Crit. Rev.*, *3*(4), 323-347, 2000.
5. Vasconcelos, V. M.; Sivonen, K.; Evans, W. R.; Carmichael, W. W.; Namikoshi, M., Hepatotoxic microcystin diversity in cyanobacterial blooms collected in Portuguese freshwaters. *Water Res.*, *30*(10), 2377-2384, 1996.
6. Pitois, S.; Jackson, M. H.; Wood, B. J. B., Sources of the eutrophication problems associated with toxic algae: An overview. *J. Environ. Health*, *64*(5), 25-32, 2001.
7. Kotak, B. G.; Lam, A. K. Y.; Prepas, E. E.; Kenefick, S. L.; Hruday, S. E., VARIABILITY OF THE HEPATOTOXIN MICROCYSTIN-LR IN HYPEREUTROPHIC DRINKING-WATER LAKES. *J. Phycol.*, *31*(2), 248-263, 1995.
8. Maupin, M. A.; Kenny, J. F.; Hutson, S. S.; Lovelace, J. K.; Barber, N. L.; Linsey, K. S., Estimated use of water in the United States in 2010. *U.S. Geological Survey Circular 1405*, <http://pubs.usgs.gov/circ/1405/>, 2014.
9. Agency, U. S. E. P., Drinking Water Infrastructure Needs Survey and Assessment: Fourth Report to Congress; U.S. Environmental Protection Agency, Office of Water, Office of Ground Water and Drinking Water, Drinking Water Protection Division: Washington, D.C., 2009.
10. Agency, U. S. E. P., Clean Watersheds Needs Survey 2004 Report to Congress, Washington, D.C., 2008.
11. Villaverde, S., Recent developments on biological nutrient removal processes for wastewater treatment. *Re/Views in Environmental Science & Bio/Technology*, *3*(2), 171-183, 2004.
12. Ekama, G. A., Recent developments in biological nutrient removal. *Water SA*, *41*(4), 515-524, 2015.
13. Liu, W.-j.; Hu, Z.-r.; Walker, R. L.; Dold, P. L., Enhanced nutrient removal MBR system with chemical addition for low effluent TP. *Water Sci. Technol.*, *64*(6), 1298-1306, 2011.
14. Moeslang, H.; Brockmann, M. In *Membrane bioreactors keytechnology for water reuse*, The 11th International Workshop on Information Security Applications, Jeju Island, Korea, 2010; Jeju Island, Korea, 2010.
15. Melin, T.; Jefferson, B.; Bixio, D.; Thoeye, C.; De Wilde, W.; De Koning, J.; van der Graaf, J.; Wintgens, T., Membrane bioreactor technology for wastewater treatment and reuse. *Desalination*, *187*(1), 271-282, 2006.
16. Judd, S., *The MBR Book: Principles and Applications of Membrane Bioreactors for Water and Wastewater Treatment* 2nd ed.; Elsevier Ltd.: UK, 2011.
17. Adam, C.; Gnirss, R.; Lesjean, B.; Buisson, H.; Kraume, M., Enhanced biological phosphorus removal in membrane bioreactors. *Water Sci. Technol.*, *46*(4-5), 281-286, 2002.

18. Lesjean, B.; Gnirss, R.; Adam, C.; Kraume, M.; Luck, F., Enhanced biological phosphorus removal process implemented in membrane bioreactors to improve phosphorous recovery and recycling. *Water Sci. Technol.*, 48(1), 87-94, 2003.
19. Monti, A.; Hall, E. R.; van Loosdrecht, M. M. C., Kinetics of phosphorus release and uptake in a membrane-assisted biological phosphorus removal process. *Journal of Environmental Engineering-Asce*, 133(9), 899-908, 2007.
20. Visvanathan, C.; Abeynayaka, A., Developments and future potentials of anaerobic membrane bioreactors (AnMBRs). *Membr. Water Treat.*, 3(1), 1-23, 2012.
21. Shon, H. K.; Phuntsho, S.; Vigneswaran, S.; Kandasamy, J.; Aryal, R.; Jegatheesan, V., *Physical, chemical, and biological characterization of membrane fouling*. American Society of Civil Engineers (ASCE): Reston,, 2012; p 457-503.
22. Wu, B.; Yi, S.; Fane, A. G., Microbial behaviors involved in cake fouling in membrane bioreactors under different solids retention times. *Bioresour. Technol.*, 102(3), 2511-2516, 2011.
23. Le-Clech, P.; Chen, V.; Fane, T. A. G., Fouling in membrane bioreactors used in wastewater treatment. *Journal of Membrane Science*, 284(1-2), 17-53, 2006.
24. Puspitasari, V.; Granville, A.; Le-Clech, P.; Chen, V., Cleaning and ageing effect of sodium hypochlorite on polyvinylidene fluoride (PVDF) membrane. *Sep. Purif. Technol.*, 72(3), 301-308, 2010.
25. ElMekawy, A.; Diels, L.; De Wever, H.; Pant, D., Valorization of Cereal Based Biorefinery Byproducts: Reality and Expectations. *Environmental Science & Technology*, 47(16), 9014-9027, 2013.
26. Suslick, K. S., Sonochemistry. *Science*, 247(4949), 1439-1445, 1990.
27. Beckett, M. A.; Hua, I., Elucidation of the 1,4-Dioxane Decomposition Pathway at Discrete Ultrasonic Frequencies. *Environmental Science & Technology*, 34(18), 3944-3953, 2000.
28. Chae, S. R.; Ahn, Y. T.; Kang, S. T.; Shin, H. S., Mitigated membrane fouling in a vertical submerged membrane bioreactor (VSMBR). *J. Membr. Sci.*, 280(1-2), 572-581, 2006.
29. APHA/AWWA/WEF, Standard Methods for the Examination of Water and Wastewater, 18th ed. Washington, DC. 1992.
30. Henze, M., Capabilities of Biological Nitrogen Removal Processes from Wastewater. *Water Science and Technology*, 23(4-6), 669-679, 1991.
31. Chae, S.-R.; Jeong, H.-S.; Lim, J.-L.; Kang, S.-T.; Shin, H.-S.; Paik, B.-C.; Youn, J.-H., Behaviors of Intercellular Materials and Nutrients in Biological Nutrient Removal Process Supplied with Domestic Wastewater and Food Waste. *Water Environment Research*, 76(3), 272-279, 2004.
32. Grabińska-Loniewska, A., Biocenosis diversity and denitrification efficiency. *Water Research*, 25(12), 1575-1582, 1991.



Figure. A graduate student (Brindha Murugesan, M.S. candidate) is optimizing a bench-scale membrane bioreactor system with the carbon nanotube composite membrane for efficient removal of nitrogen and phosphorus from municipal wastewater.

Concentration-discharge behavior of dissolved and particulate metals in a mining impacted stream

Basic Information

Title:	Concentration-discharge behavior of dissolved and particulate metals in a mining impacted stream
Project Number:	2017OH571O
Start Date:	3/1/2017
End Date:	2/28/2018
Funding Source:	Other
Congressional District:	OH-013
Research Category:	Water Quality
Focus Categories:	Hydrogeochemistry, Geochemical Processes, Water Quality
Descriptors:	None
Principal Investigators:	Elizabeth Maureen Herndon

Publications

1. Shaw, M.E. (2018) Concentration-discharge behavior of contaminants in a stream impacted by acid mine drainage. MS Thesis, Kent State University.
2. Klein, M., Herndon, E. (2018) Developing a protocol for extracting mineral-associated organic matter in soils developed from coal mine waste. Kent State Undergraduate Research Symposium, Kent State University, Kent, OH. Undergraduate presenter.
3. Shaw, M.E., Klein, M., and Herndon, E. (2017) Concentration-discharge behavior of contaminants in a stream impacted by acid mine drainage. American Geophysical Union Fall Meeting, New Orleans, LA, USA. Graduate presenter.
4. Shaw, M. and Herndon, E. (2017) Investigation of trace metal transport in an AMD-impacted stream and treatment system in northeastern Ohio. GSA Joint Northeastern/North Central Section Meeting, Pittsburgh, PA, USA. Graduate presenter.

Ohio WRC Final Report

Project Title: Concentration-discharge behavior of dissolved and particulate metals in a mining impacted stream

Principal Investigator: Dr. Elizabeth Herndon, Department of Geology, Kent State University

1. Problems and Research Objectives

Background

Water resources in the United States are degraded by contamination from legacy mining operations. More than 5,000 miles of streams throughout eastern Ohio and the Appalachian coal region have been impaired by unnatural concentrations of acid, metals, and other dissolved substances that originate as acid mine drainage (AMD) from legacy mines (Herlihy et al., 1990). Although billions of dollars have been spent to remediate AMD-impacted streams, the associated abandoned mine lands represent a persistent source of pollutants to water bodies (Blowes and Jambor, 1990; Nordstrom, 2011). Specifically, piles of mine spoil and tailings that were deposited within watersheds following coal extraction contain pyrite and other sulfide minerals that weather and release sulfuric acid and toxic metals to stream water and groundwater (Cravotta et al., 1994; Cravotta, 2008; Cravotta et al., 2010; Cravotta et al., 2014). Runoff and leachate from waste rock in mined watersheds is a major contributor to non-point source pollution (Herlihy et al., 1990).

Deciphering contributions to headwater streams and solute transport into higher order stream networks is complicated by both the spatial complexity of hydrologic flow paths and the geochemical reactions that occur along those flow paths (Kirchner, 2003; Bishop et al., 2004; Zimmer et al., 2013; Kim et al., 2014; Trostle et al., 2016). Streams in AMD-impacted watersheds can receive inputs from rainwater, groundwater, AMD-treatment cells, and undiscovered mine outflows that vary in contribution as a function of stream discharge. The mixing of these different water sources generates pH gradients that influence metal mobility. For example, an influx of acidic, metal-rich water into a circumneutral stream (or a limestone treatment system) promotes rapid, pH-dependent precipitation of iron oxyhydroxysulfate and oxyhydroxide minerals (Ferris et al., 1989; Bigham et al., 1990; Bigham et al., 1996). These poorly crystalline minerals can either be transported downstream by flowing water or accumulate in thick deposits on the stream bed. Initial iron precipitates (e.g., ferrihydrite, schwertmannite) readily bind toxic elements, e.g., As, Se, Cu, Zn, but undergo mineral transformation over time into jarosite, goethite, and hematite phases that can re-release metals into solution (Webster et al., 1998; Schroth and Parnell, 2005; Acero et al., 2006; Burton et al., 2009; Cruz-Hernández et al., 2016). Thus, the iron minerals that form in AMD-impacted streams may serve as temporary sinks but long-term sources of toxic metals to downstream water bodies.

Surveys of water quality typically only measure the dissolved component of stream water (operationally defined as < 450 nm) and do not consider colloidal or particulate fluxes. Colloids (1 – 100 nm) are generally measured within the “dissolved” fraction but have different geochemical and physical properties than true dissolved ions, which affect transport and toxicity. Particles enter the stream through runoff or are re-suspended from stream bed sediments. In AMD systems, colloidal and particulate iron oxides may represent a poorly understood but potentially substantial flux of iron and associated metals into downstream water bodies (Kimball et al., 1994). Moreover, little is known about how partitioning of these metal contaminants between size fractions varies as a function of stream discharge. The concentration-discharge (CQ) behaviors of different elements can reveal how sources of these elements (e.g., soil water, groundwater, mine outflow) become hydrologically connected to the stream under different flow regimes. When the

Ohio WRC Final Report

discharge (Q) of a stream increases, concentrations of solute and particulate elements (C) can either increase (enrichment behavior), decrease (dilution behavior), or remain relatively constant (chemostatic behavior) (Kirchner, 2003; Godsey et al., 2009; Clow and Mast, 2010; Zhang et al., 2016). Chemostasis for solutes has been proposed to result from rapid equilibration of infiltrating water with exchangeable cations or readily weatherable minerals (Bishop et al., 2004; Godsey et al., 2009; Maher, 2011), whereas non-chemostatic behaviors (dilution and enrichment) result from hydrologic connection of a concentrated water source to the stream under either high or low flow regimes (Johnson et al., 1969; McGlynn and McDonnell, 2003; Hood et al., 2006; Herndon et al., 2015). These behaviors can be influenced by seasonal hydrogeochemical reactions that occur along the flowpaths (Kim et al., 2014; Trostle et al., 2016).

Project Objectives

This project examined metal dynamics in the Huff Run watershed, an AMD-impacted watershed in northeast Ohio. The landscape at Huff Run is dominated by un-reclaimed refuse piles that either remain barren or have naturally developed successional vegetation over time. Restoration efforts costing \$4.6 million have reduced acid loading and improved aquatic biodiversity in the Huff Run stream and its tributaries; however, metal loads and concentrations in the stream remain elevated because of inputs from undiscovered mines, contaminated groundwater, and piles of coal refuse (Bowman and Johnson, 2013). Our research focused on the HR25 subcatchment where restoration efforts were compromised by undocumented inputs of AMD. Our objectives were as follows:

- Identify potential sources of contamination to the HR25 tributary by conducting spatial surveys of water chemistry in the catchment
- Evaluate concentration-discharge behaviors of solutes, colloids, and particles by establishing methods for continuous, simultaneous collection of solutes and particles

2. Methodology

Site Description

The Huff Run watershed (13.9 mi²) is located near Mineral City, OH in the unglaciated portion of the Appalachian Plateau. The watershed is primarily underlain by shale, siltstone, and sandstone bedrock of the Pennsylvanian Allegheny group that contains thinly bedded limestone and 1-5 ft thick coal seams (Lamborn, 1956). The regional climate is humid continental with mean annual temperature ~10°C and mean annual precipitation ~100 cm (NOAA, 2015). While the eastern, headwaters portion of the watershed was developed for agriculture and remains unmined, the western, downstream portion has experienced numerous anthropogenic

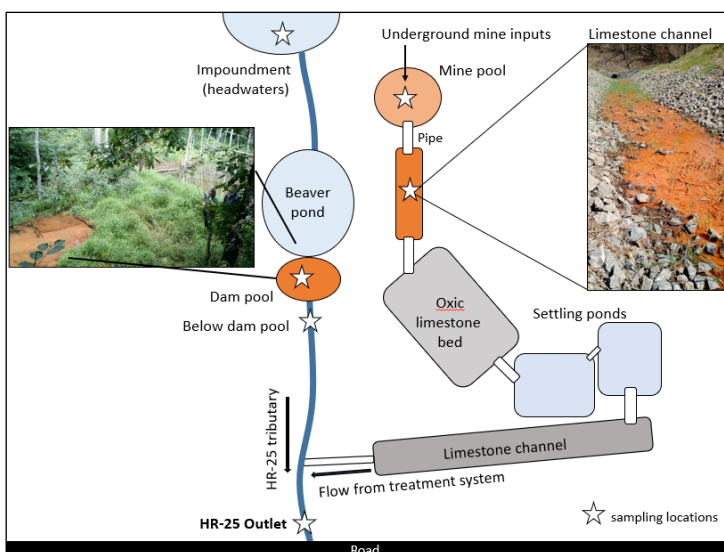


Figure 1. Schematic of the HR25 tributary and treatment system. The stream at the outlet receives inputs from both the tributary and treatment system. Sampling locations indicated with stars.

perturbations that include deep mining (1810 – 1946), surface mining (1950 – present), and oil and gas production (AMDAT, 2000). Fourteen reclamation projects completed over the past 14 years have substantially reduced acid loads in the stream and led to increases in biological diversity; however, the Huff Run stream and its tributaries remain impaired by acidic, metal-rich inputs from deep mine discharge, water-filled impoundments, and runoff from unclaimed coal refuse piles (Kinney, 2013). Ongoing reclamation efforts seek to restore water quality and biological diversity to levels necessary to obtain a warmwater habitat designation from Ohio EPA.

This project focused on a small tributary, site 25 within Huff Run (HR-25), that was the largest acid contributor and fourth largest metal contributor to the Huff Run stream under medium flow conditions prior to reclamation (Kinney, 2013). Despite efforts to treat mine discharge, stream water at the catchment outlet is impaired by low pH (< 4) and high dissolved metals (average $40 \pm 21 \text{ mg L}^{-1}$ Fe and $43 \pm 11 \text{ mg L}^{-1}$ Mn from 2001-2013) (watersheddata.com). HR-25 shows an abrupt change in color below a beaver dam that was investigated in this study as a site of undocumented contaminant inputs. Further downstream, HR-25 receives inputs from limestone channel that drains a treatment system.

Sample collection

To evaluate concentration-discharge behavior of metals in the stream, stream water was collected at (1) low frequency sampling intervals over long periods, i.e., semi-daily collection from early spring through late autumn; and (2) high frequency over short periods, i.e., hourly collection during multiple storm events (~24 hour period). This sampling timeline allowed us to investigate both event-based and seasonal CQ behavior. To record stream discharge, we installed an area velocity meter (Teledyne 2150 Flow Module) to obtain continuous measurements at 15 min intervals. An automatic water sampler (Teledyne ISCO 6712 portable sampler) was installed in the stream at the watershed outlet. ISCO samplers typically collect unfiltered water that is stored until retrieval, which is often unsuitable for metal analysis due to precipitation and dissolution of mineral phases during storage (Kim et al., 2012). We implemented a sampling protocol modified from Kim et al. (2012) to filter and preserve water samples immediately upon collection. Briefly, a gravity filtration system was used to immediately filter and acidify water injected into the sampling bottle in order to maintain sample integrity during storage (Figure 2).

Spatial surveys of stream chemistry were conducted approximately biweekly during the sampling period to evaluate potential inputs of solutes and particles to stream water. Surface water was collected from along the length of the tributary and AMD treatment system (Figure 1). Shallow subsurface water was collected from piezometers installed in the stream bed near the contaminant source.

Sample analysis and characterization

Water samples were analyzed for temperature, specific conductance, and pH and filtered in the field ($0.45 \mu\text{m}$ Supor



Figure 2. *In situ* gravity filtration system used to filter stream water during collection by the ISCO autosampler. Water delivered to the syringe was filtered through a $0.45 \mu\text{m}$ polyethersulfone filter into a bottle that was either pre-acidified with ultrapure nitric acid for cation analysis or left unacidified for anion analysis.

Ohio WRC Final Report

syringe filters). Concentrations of major (e.g., Ca, Mg, Na, K, Fe, Mn, Al, P, etc.) were determined by inductively coupled plasma optical emission spectrometry (PerkinElmer ICP-OES; Department of Biological Sciences, KSU) in filtered water samples acidified with ultrapure nitric acid (HNO₃). Anion concentrations (F⁻, Cl⁻, Br⁻, NO₃⁻, NO₂⁻, SO₄²⁻, and PO₄³⁻) were determined by ion chromatography (Dionex ICS-2100; Dept. of Geology, KSU) in filtered non-acidified samples (Fishman et al., 1989). DOC was measured in filtered samples acidified with HCl and stored in combusted amber glass bottles prior to analysis on a Shimadzu TOC-L (Dept. of Geology, KSU).

To assess the proportion of metals present as colloids, a subset of water samples was filtered through pre-cleaned < 10 kDa molecular weight cutoff Amicon Ultra-15 centrifugal filter units. Dissolved species, i.e., free ions, pass through the filter whereas mineral colloids such as iron oxides did not. Differences in metal concentrations between the < 0.45 μm and < 10 kDa filtrates were used to define the colloidal phase (Aiken et al., 2011). Filters used for particle analysis (Supor) were weighed prior to installation in the ISCO system. Following filtration, filters were oven dried at low temperature (60°C) and reweighed to determine particle mass captured for a known volume of water.

3. Principal Findings and Results

Identifying sources of AMD to the stream

Our results indicate that the treatment system effectively neutralized contaminated water draining the mine pool, but that additional contamination entered the tributary near a beaver dam, leading to high metal concentrations and low pH in the stream. Specifically, the pH of the surface water in the treatment system increased from 4.6 ± 0.7 in the mine pool to 7.8 ± 0.8 in the second settling pond. Concentrations of AMD-associated metals Fe and Mn were high in the mine pool but decreased to below detection limit in the settling ponds. In the stream during the autumn dry period, pH decreased while Fe and Mn concentrations increased from the headwaters to the outlet. The pH of the surface water was circumneutral (7.05 ± 0.08) from the headwaters to the beaver pond but decreased to 2.9 ± 0.3 at the outlet. Iron and Mn concentrations in the surface water increased from below detection limit ($< 0.02 \text{ mmol L}^{-1}$) in the headwater pond to $1.03 \pm 0.06 \text{ mmol L}^{-1}$ and $0.56 \pm 0.02 \text{ mmol L}^{-1}$ respectively at the outlet.

It is possible that the beaver dam directly contributed to contaminant inputs by altering flow paths and promoting mixing between surface and subsurface water, but this explanation has not been thoroughly explored. It is also possible that subsurface flow paths between the mine pool and stream persist and continue to deliver contaminated water. Additional research would be necessary to untangle these factors and determine precisely how contamination enters the stream.

Concentration-discharge behavior of solutes

Concentrations of contaminant metals in the stream generally decreased with increasing stream discharge due to inputs from the treatment system that only occurred at high flow. A decrease in pH from March (~6) through November (~3) was concurrent with a decrease in stream discharge and declining inputs from the treatment system (Figure 3). Correspondingly, AMD-derived

Ohio WRC Final Report

contaminants (Fe, Mn, Al) increased in concentration from March through November. These trends reflect mixing of contaminated baseflow and intermittent inputs from the treatment system, indicating that the treatment system was only effective at neutralizing stream acidity and removing metals when flow was present.

The response of stream chemistry to increased discharge during storm events differed between spring and fall due to differing inputs from the treatment system. Though storm events monitored on July 7, 2017 and October 8-9, 2017 had similar discharge, the pH was higher and more variable in July (3.3 to 5.3) than October (2.9 to 3.4). In July, the stream signal was influenced by circumneutral, metal-poor water flowing from the treatment system. In October, no water flowed from the limestone channel into the stream, thus the stream at the outlet consisted primarily of contaminated water derived from upstream.

Concentration-discharge behaviors were examined by generating log-log plots of concentrations versus discharge for all samples collected between March to November (Figure 4). AMD-derived metals Fe, Mn, and Al all showed dilution behavior, while sulfate and base cations Ca, Mg, Na, and K were chemostatic. We attributed dilution behavior to inputs from the limestone channel that occurred at high flow and diluted high concentrations of metals in baseflow. Chemostatic behavior was attributed to mixing of chemically similar waters given that contaminated baseflow and the treatment system contained similar concentrations of these solutes.

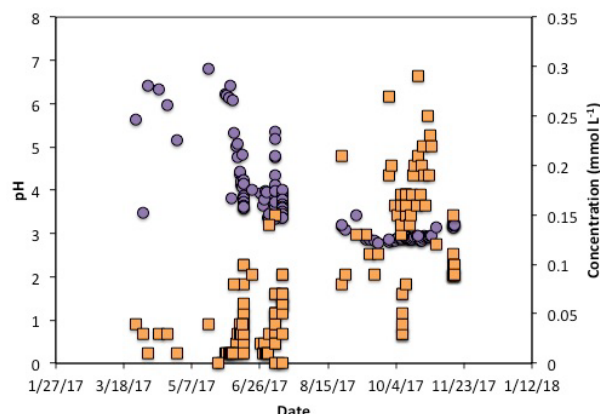
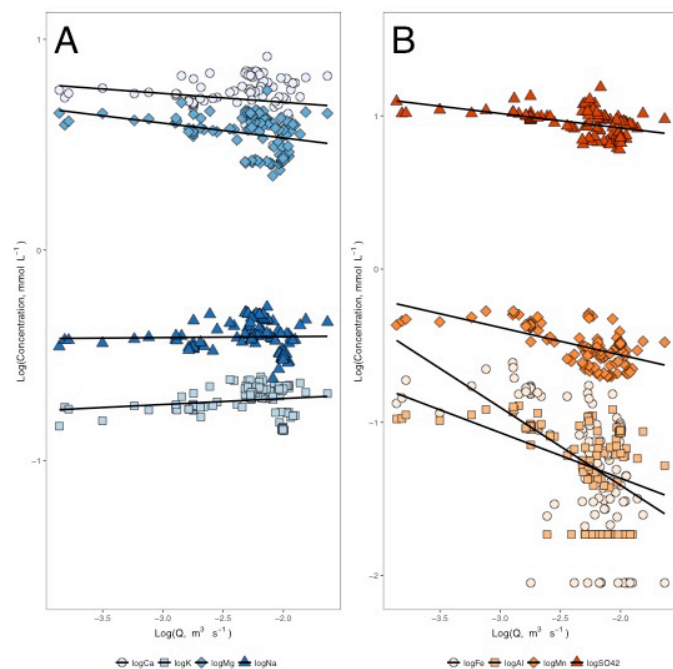


Figure 3. Dissolved Fe (mmol L⁻¹) and pH in the stream at the outlet plotted versus sampling date. Stream pH (purple circles) decreased from spring to autumn while concentrations of dissolved Fe (orange squares) increased.

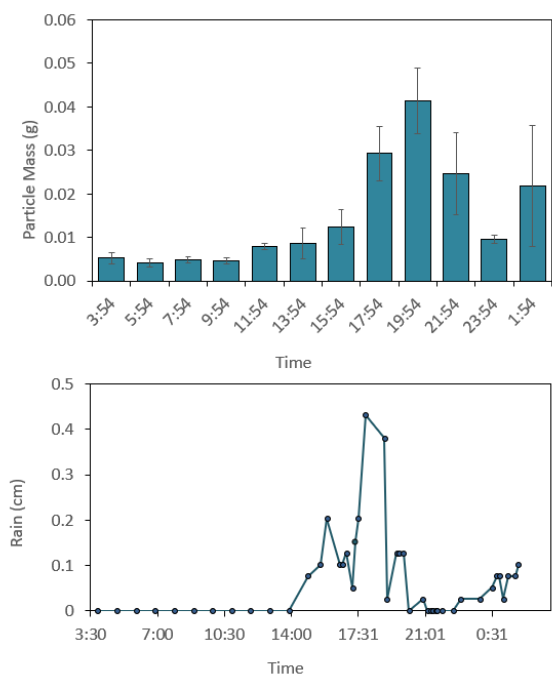
Ca, Mg, Na, and K were chemostatic. We attributed dilution behavior to inputs from the limestone channel that occurred at high flow and diluted high concentrations of metals in baseflow. Chemostatic behavior was attributed to mixing of chemically similar waters given that contaminated baseflow and the treatment system contained similar concentrations of these solutes.

Figure 4. Log-log plots of solute concentration (mmol L⁻¹) versus stream discharge (m³ s⁻¹) in the HR25 stream at the catchment outlet. Base cations exhibit chemostasis. AMD-derived solutes (right panel) show either chemostatic (sulfate) or dilution (Fe, Mn, Al) behaviors.

Concentration-discharge behavior of colloids and particles

The mass of particles (g) retained by gravity filtration in the ISCO sampler increased with increasing stream discharge during a storm event (Figure 5). These particles consisted primarily of iron oxides and iron-oxide coated sediment, from which we infer that particle transport is dominated by scouring of iron oxides from the stream bed during high flow conditions. Colloid composition was determined in stream water collected near the outlet of the catchment. Iron that passed through a 0.45 μm filter was presently largely as colloids (~70%) while Mn was almost entirely dissolved. High proportions of Ca and Mg were also present in colloids (~50%), possibly indicating that these cations participate in colloid aggregation, although these trends require further exploration.

Figure 5. (top panel) Particle mass contained within 60 ml of stream water collected once every two hours by the ISCO autosampler and injected into the gravity filtration system. (bottom panel) Rainfall recorded during the storm event.



4. Finding Significance

In this study, we investigated the concentration-discharge behavior of base cations and AMD-derived solutes in a stream in Northeastern Ohio. We determined that constructed treatment systems can act as ephemeral tributaries to the stream and control CQ behavior at the stream outlet. Through long-term and storm-event sampling, we demonstrated that base cations and sulfate behaved chemostatically in the stream exiting the catchment while AMD-derived metals (Fe, Mn, Al) showed dilution behavior. Chemostatic behavior was explained by the mixing of chemically similar waters. Sulfate and base cations concentrations remained high in both treated and untreated water, leading to chemostatic behavior at the stream outlet. The dilution behavior could be explained by reactive transport processes that removed dissolved Fe from the stream coupled with dilution of contaminated baseflow by ephemeral inputs from the limestone treatment system. Overall, the treatment system effectively neutralized acidity and reduced contaminant loads in the tributary, but only under high flow conditions. During baseflow conditions when flow from the treatment system into the tributary was negligible, stream pH was low (< 4) and metal concentrations were high.

This study emphasizes the importance of understanding hydrologic flowpaths and geochemical processes in complex AMD-impacted sites. Many factors contribute to the efficacy of treatment systems, including flow paths from the source of contamination, multiple sources of stream and groundwater contamination, and the fate of treated water. Flow from AMD-impacted streams, even in watersheds with treatment systems in place, may ultimately contaminate sources of drinking water such as rivers or wells. If contamination is not caught and mitigated by the treatment system then it will further contaminate surface and groundwater and create more health issues for communities near AMD-impacted watersheds.

Ohio WRC Final Report

References

- Acero P., Ayora C. and Torrento C. (2006) The behavior of trace elements during schwertmannite precipitation and subsequent transformation into goethite and jarosite. *70*, 4130–4139.
- Abandoned Mine Abatement and Treatment Plan (2000) Huff Run Watershed.
- Aiken G. R., Hsu-kim H. and Ryan J. N. (2011) Influence of Dissolved Organic Matter on the Environmental Fate of Metals, Nanoparticles, and Colloids. *Environ. Sci. Technol.* **45**, 3196–3201.
- Bigham J. M., Schwertmann U., Carlson L. and Murad E. (1990) A poorly crystallized oxyhydroxysulfate of iron formed by bacterial oxidation of Fe (II) in acid mine waters. *Geochim. Cosmochim. Acta* **54**, 2743–2758.
- Bigham J. M., Schwertmann U., Traina S. J., Winland R. L. and Wolf M. (1996) Schwertmannite and the chemical modeling of iron in acid sulfate waters. *Geochim. Cosmochim. Acta* **60**, 2111–2121.
- Bishop K., Seibert J., Köhler S. and Laudon H. (2004) Resolving the Double Paradox of rapidly mobilized old water highly variable responses in runoff chemistry. *Hydrol. Process.* **18**, 185–189.
- Blowes D. W. and Jambor J. L. (1990) The Pore-Water Geochemistry And The Mineralogy Of The Vadose Zone Of Sulfide Tailings, Waite-Amulet, Quebec, Canada. *Appl. Geochemistry* **5**, 327–346.
- Bowman J. and Johnson K. (2013) *2012 Stream Health Report: An evaluation of water quality, biology, and acid mine drainage reclamation in five watersheds: Raccoon Creek, Monday Creek, Sunday Creek, Huff Run, and Leading Creek.*
- Burton E. D., Bush R. T., Johnston S. G., Watling K. M., Hocking R. K., Sullivan L. A. and Parker G. K. (2009) Sorption of arsenic (V) and arsenic (III) to schwertmannite. *Environ. Sci. Technol.* **43**, 9202–9207.
- Clow D. W. and Mast M. A. (2010) Mechanisms for chemostatic behavior in catchments: Implications for CO₂ consumption by mineral weathering. *Chem. Geol.* **269**, 40–51.
- Cravotta C. A. (2008) Dissolved metals and associated constituents in abandoned coal-mine discharges, Pennsylvania, USA. Part 2: geochemical controls on constituent concentrations. *Appl. Geochemistry* **23**, 203–226.
- Cravotta C. A., Goode D. J., Bartles M. D., Risser D. W. and Galeone D. G. (2014) Surface water and groundwater interactions in an extensively mined watershed, upper Schuylkill River, Pennsylvania, USA. *Hydrol. Process.* **28**, 3574–3601.
- Cravotta III C. A., Brightbill R. A. and Langland M. J. (2010) Abandoned mine drainage in the Swatara Creek Basin, Southern Anthracite Coalfield, Pennsylvania, USA: 1. Stream water quality trends coinciding with the return of fish. *Mine Water Environ.* **29**, 176–199.
- Cruz-Hernández P., Pérez-López R., Parviainen A., Lindsay M. B. J. and Nieto J. M. (2016) Trace element-mineral associations in modern and ancient iron terraces in acid drainage environment. *Catena* **147**, 386–393.
- Ferris F. G., Tazaki K. and Fyfe W. S. (1989) Iron oxides in acid mine drainage and their association with bacteria. *Chem. Geol.* **74**, 321–330.
- Fishman M. J., Friedman L. C. and others (1989) *Methods for determination of inorganic substances in water and fluvial sediments.*, US Department of the Interior, Geological Survey.
- Godsey S. E., Kirchner J. W. and Clow D. W. (2009) Concentration--discharge relationships reflect chemostatic characteristics of US catchments. *Hydrol. Process.* **23**, 1844–1864.
- Herlihy A. T., Kaufmann P. R., Mitch M. E. and Brown D. D. (1990) Regional estimates of acid mine drainage impact on streams in the mid-Atlantic and southeastern United States. *Water, Air, Soil Pollut.* **50**, 91–107.
- Herndon E. M., Dere A. L., Sullivan P. L., Norris D., Reynolds B. and Brantley S. L. (2015) Landscape heterogeneity drives contrasting concentration-discharge relationships in shale headwater catchments. *Hydrol. Earth Syst. Sci.* **19**, 3333–3347.
- Hood E., Gooseff M. N. and Johnson S. L. (2006) Changes in the character of stream water dissolved organic carbon during flushing in three small watersheds, Oregon. *J. Geophys. Res. Biogeosciences* **111**, 1–8.

Ohio WRC Final Report

- Johnson N. M., Likens G. E., Bormann F. H., Fisher D. W. and Pierce R. S. (1969) A working model for the variation in stream water chemistry at the Hubbard Brook Experimental Forest, New Hampshire. *Water Resour. Res.* **5**, 1353–1363.
- Kim H., Bishop J. K. B., Dietrich W. E. and Fung I. Y. (2014) Process dominance shift in solute chemistry as revealed by long-term high-frequency water chemistry observations of groundwater flowing through weathered argillite underlying a steep forested hillslope. *Geochim. Cosmochim. Acta* **140**, 1–19.
- Kim H., Bishop J. K. B., Wood T. J. and Fung I. Y. (2012) Autonomous water sampling for long-term monitoring of trace metals in remote environments. *Environ. Sci. Technol.* **46**, 11220–11226.
- Kimball B. A., Broshears R. E., Bencala K. E. and McKnight D. M. (1994) Coupling of Hydrologic Transport and Chemical Reactions in a Stream Affected by Acid Mine Drainage. *Environ. Sci. Technol.* **28**, 2065–2073.
- Kinney C. (2013) *Huff Run Acid Mine Drainage Abatement and Treatment Plan Addendum.*, New Philadelphia OH.
- Kirchner J. W. (2003) A double paradox in catchment hydrology and geochemistry. *Hydrol. Process.* **17**, 871–874.
- Lamborn R. E. (1956) *Geology of Tuscarawas County (vol.55).*,
- Maher K. (2011) The role of fluid residence time and topographic scales in determining chemical fluxes from landscapes. *Earth Planet. Sci. Lett.* **312**, 48–58.
- McGlynn B. L. and McDonnell J. J. (2003) Quantifying the relative contributions of riparian and hillslope zones to catchment runoff. *Water Resour. Res.* **39**, 1310.
- National Atmospheric and Ocean Administration (2015) National Climatic Data Center.
- Nordstrom D. K. (2011) Hydrogeochemical processes governing the origin, transport and fate of major and trace elements from mine wastes and mineralized rock to surface waters. *Appl. Geochemistry* **26**, 1777–1791.
- Schroth A. W. and Parnell R. A. (2005) Trace metal retention through the schwertmannite to goethite transformation as observed in a field setting, Alta Mine, MT. *Appl. Geochemistry* **20**, 907–917.
- Trostle K. D., Runyon J. R., Pohlmann M. A., Redfield S. E., Pelletier J., McIntosh J. and Chorover J. (2016) Colloids and organic matter complexation control trace metal concentration-discharge relationships in Marshall Gulch stream waters. *Water Resour. Res.*
- Webster J. G., Swedlund P. J. and Webster K. S. (1998) Trace Metal Adsorption onto an Acid Mine Drainage Iron (III) Oxy Hydroxy Sulfate. *Environ. Sci. Technol.* **32**, 1361–1368.
- Zhang Q., Harmon C. J. and Ball W. (2016) An improved method for interpretation of riverine concentration-discharge relationships indicates long-term shifts in reservoir sediment trapping. *Geophys. Res. Lett.*
- Zimmer M. A., Bailey S. W., McGuire K. J. and Bullen T. D. (2013) Fine scale variations of surface water chemistry in an ephemeral to perennial drainage network. *Hydrol. Process.* **27**, 3438–3451.

Photos

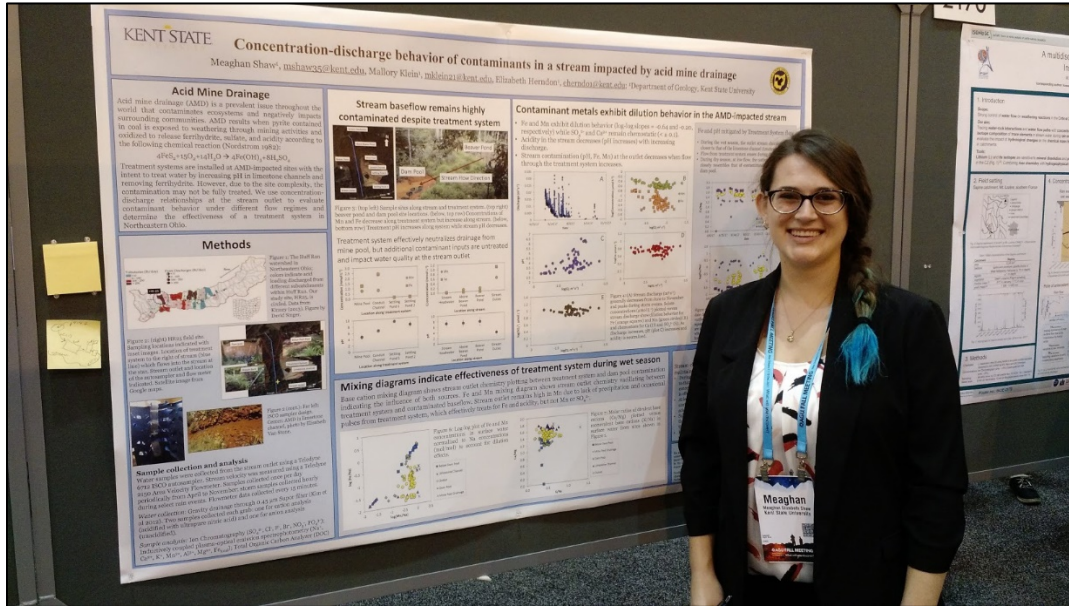


Figure 1. Kent State Geology MS student Meaghan Shaw presents her OWRC-funded research at the American Geophysical Union Fall Meeting in New Orleans, LA in December 2017.



Figure 2. Kent State Geology MS student Lindsey Yazbek collects surface water during winter from a stream receiving acid mine drainage.

Information Transfer Program Introduction

The Ohio WRC conducted a number of activities designed to transfer water related information to a wide range audience throughout Ohio, including state, federal, county, and municipal agencies, as well as to the academic community of researchers and students. In addition, many of our efforts target non-professional audiences including children, and private citizens. The Ohio WRC conducted information transfer by (1) promoting center activities, researchers, and research projects via newsletters, the Ohio WRC website, email correspondence, brochures, booths at conferences, personal meetings with water professionals and agency representatives; (2) organizing, sponsoring, and participating in workshops, seminars, guest lectures and conferences; (3) serving and volunteering in various water organizations and their advisory boards; and (4) leading one information transfer project. Specific activities included:

1) Promoting Ohio WRC research, results of projects, and investigators a) Preparation of Ohio WRC website content (wrc.osu.edu), website updates of events and news, and general maintenance of website. We had over 150 website hits per month b) Preparing one page summaries of completed research projects, including the importance of the research topic for the State, relevant outcomes and results, and investigator background. These summaries were distributed to our Advisory Board members and other stakeholders. c) Publishing research project summaries and investigators research highlights in the Ohio Water Table, a quarterly newsletter published by the Water Management Association of Ohio (WMAO). During the reporting period, the highlighted researchers and projects were: Dr. Hornbeek's project #2015OH445B, Dr. Costello's project #2016OH490B, Dr. Bohrerova's information transfer project #2015OH482O and Dr. Davies' project highlight #2017OH534B. This newsletter is distributed to about 600 professionals and organizations in Ohio in the water resources field from private sector (33%), universities (8%), nonprofit/citizens (17%) and federal, state and local government agencies (42%) d) Preparing and publishing an Ohio WRC brochure highlighting the annual activities and projects of the Ohio WRC. Brochure is distributed at various events and conferences. e) Responding to questions from public regarding water resources issues in the State of Ohio. f) Maintaining and updating statewide database of investigators in Ohio universities with research interests related to water. Currently, the database contains around 250 researchers from 15 different Ohio Universities. g) Meeting with Ohio Congress and Senate members' office staff to discuss Ohio WRC activities, research results, and their impact for the State.

2) Organizing and sponsoring information transfer events a) Co-organized quarterly Ohio WRC-WMAO luncheon seminars, which includes assisting with luncheon administration and securing speakers. This past year the four luncheons were attended by approximately 108 water professionals from government, academia, NGOs and industry. The speakers and topics in this reporting period were: Audrey Sawyer (OSU): "Hidden Chemical Exchange Due to Lake-Groundwater Interactions"; Fernanda Craig (Muskingum Watershed Conservancy District): "Water Quality Monitoring within Muskingum Watershed Conservancy District"; David Costello (KSU): "Macro- and Micro-nutrient Control of Algal Growth in Great Lakes Aquatic Ecosystems"; Greg Nageotte (ODA) and Kurt Keljo (Franklin SWCD): "Overview and Updates - Ohio Watershed Coordinator Program" b) Sponsored 46th Annual Water Management Association of Ohio (WMAO) conference titled: "Partnerships at the Confluence of Challenge and Opportunity". In 2017 around 266 professionals attended the conference. We also helped with selecting the student candidate for WMAO award, moderated a session and set up a booth at the conference to discuss Center activities. c) Organizing and leading a 25 minute, hands-on workshop for about 90 5th grade students on principles of buoyancy in the 2017 Central Ohio Children's Water Festival d) Co-organized workshop and seminar of James Olson, expert on drinking water treatment privatization. Workshop title: "Water and Public Trust Law and Rights", seminar title: "Privatization of Drinking Water Utilities — Can the Public's Interest Still be Protected?" e) Collaborate with North Central Regional Network on project to identify youth water education gaps in the region

Information Transfer Program Introduction

3) Serving in multiple water organizations a) Serving on Water Management Association of Ohio (WMAO) board as a Director of Research and Data Management. In this role, we focus on promoting water resources research in the State, and attend bimonthly meetings. b) Member of WMAO student awards committee – evaluating student proposals and deciding the best candidate for the award. c) National Institute of Water Resources Regional Representatives of the Great Lakes Region. d) Participating in quarterly meetings of the Ohio Water Resources Council meetings, forum for collaboration and coordination among state agencies. e) Serving on board to plan mission and goals of new established Lake Erie Area research Network (LEARN) – collaboration with Ohio Sea Grant f) Serving on Friend of Lower Olentangy Watershed (FLOW) NGO Science committee, helping organize events, write outreach and education proposals. g) Member of Water Resources Working Group under the Mid-Ohio Regional Planning Commission. h) Member of Water Technology Board of Ohio American Water Works Association

4) Information Transfer Projects Dr. Bohrerova's project (conducted by Ohio WRC but funded by other funds) titled "Adopt Your Waterway" focuses on citizen volunteer lead monitoring of streams in urbanized areas around Columbus, OH for water chemistry and macroinvertebrates. The goal is to educate public about stream health and support water stewards in the area.

Adopt Your Waterway

Basic Information

Title:	Adopt Your Waterway
Project Number:	2015OH4820
Start Date:	6/1/2016
End Date:	8/31/2017
Funding Source:	Other
Congressional District:	3rd
Research Category:	Not Applicable
Focus Categories:	Education, Water Quality, Surface Water
Descriptors:	Membrane separations; water treatment; biomimetic
Principal Investigators:	Zuzana Bohrerova

Publications

There are no publications.

FINAL PROJECT REPORT

Adopt Your Waterway Training June 1, 2015 through December 31, 2017

1. **Project Summary and Achievements:** The main objective of our project was to increase citizen's awareness about three aspects of water quality – physical, chemical and biological. The Ohio Sierra Club training on water pollution and water chemistry together with macroinvertebrate sampling were used to help us achieve this goal. We exceeded our goals and managed to train 69 volunteers not only using broad water quality lecture, but they have an opportunity to go through hands on measurement training and most of them sample at least once in the field. We are currently developing materials (“stream report card”) that will be disseminated to watershed citizens and given to our water stewards so they can share it with people they are approach by while sampling. We also expanded the program from original four tributaries and eight sampling sites to eleven tributaries and twenty-one sampling sites due to large number of citizen's interested in the program. Throughout the program we strengthened partnership between FLOW, Ohio Water Resources Center and Sierra Club and created new partnerships with Ohio Sea Grant, Franklin Soil and Water Conservancy District and Del-Co. Generally, the program was very successful with using limited resources and we are committed to continue the program beyond the project end.
2. **Collaborators:** This project brought together three FLOW Science Committee members that had not collaborated on a project before: Friends of the Lower Olentangy Watershed (FLOW), Sierra Club's Ohio Chapter and the Ohio Water Resources Center. Our collaboration has been successful and yielded significant amounts of coordination, knowledge and resources leveraged. Several FLOW student contractors (Marci Bird, Joe Bevan and Danielle Johnson) and Zuzana Bohrerova from Ohio Water Resources Center did jointly most of the program coordination. Sierra Club conducted the Water Alert Reporting Network (WARN) and Water Sentinel Chemistry training and provided materials as a match. They are benefiting from recruitment of many new stream monitoring volunteers and are pleased with FLOW finding suitable sampling locations. Ohio Water Resources Center is helping coordinate volunteers' involvement and interest in water resources by organizing sampling and data dissemination while getting staff support and volunteer recruitment and organization from FLOW. In addition to these collaborators on the project, many other people were involve in various positions and levels, such as Erin Monaco from Ohio Sea Grant, Kurt Keljo from the Franklin Soil and Water Conservation district, Jeff Kauffman from Del-Co.
3. **Project Objectives and Associated Activities**
 - a. Objective: Increase awareness and participation of individuals in water quality related issues
 - i. Activity: *Broad Public Education on Watershed Issues and Water Quality Monitoring Techniques*. The main activity under this objective

was to educate public about water quality issues (conducted by Ohio Sierra Club). This training Water Alert Reporting Network (WARN) is designed to help Ohioans record and report suspected incidents of pollution or misconduct that could potentially harm our natural environment. During the training citizens are presented with potential water quality issues and incidents and are given card that includes emergency numbers if potential water quality issues are observed. The example of this card is in appendix A.

Although large number of people were trained we did not see an increase in WARN reported incidents on the Sierra Club website. During the two and half years of program, four incidents directly connected to our stream volunteers while sampling were reported to FLOW.

- ii. Activity: *Hands-on Volunteer Training to Monitor Stream Water Quality*. We expected that portion of the broadly educated volunteers will be interested in further training and water quality monitoring of Olentangy tributaries. The number of trainings conducted and participants trained are summarized in the table below.

After one year of the program, the amount of volunteers interested in actual monitoring was so high, that we expanded the program from four Olentangy tributaries (two sampling locations at each) to about thirteen tributaries, most of them with two sampling locations. From our WARN participants, 88% percent continued further water sentinel training and macroinvertebrate training. This number was so overwhelming that in 2017 we combined the WARN and sentinel training into one training session and added (based on response from volunteers) special classroom macroinvertebrate training (previously we just had hands-on macro training). Furthermore, we did not advertise the program broadly to public in 2017 and only recruited limited amount of volunteers to fill in sampling spots on the 13 tributaries from 2016.

About five groups of the volunteers were comfortable sampling in 2017 by themselves without any additional support (except of replenishing supplies and sampling reminders) from FLOW and their collaborators.

Metrics:

Activity	Goal	Actual #			
		2015	2016	2017	Sum
# of WARN training conducted	2	2	3	3	8
WARN training (# participants)	100	16	50	31	97
WARN incidents (# incidents reported to FLOW)	NA		3	1	4

# Hands-on training conducted (sentinel and macroinvertebrates)	4	2	4	2	8
Hands-on training # participants	30	16	39	14	69
New in-depth macroinvertebrate training (# participants)	NA	NA	NA	19	19

b. Objective: Support and coordination of citizens to foster water stewards

i. Activity: *Train the trainer*. To improve volunteers retention and foster water stewards for the Olentangy tributaries, we assigned trainer (experienced water quality professional) per about 8 volunteers (2 – 3 sampling sites). Some of the trainers were trained in the beginning of the program (FLOW staff), but most of them were recruited from the professionals in the area (OSU graduate students, Kurt Keljo, Erin Monaco etc.). The trainers were helping to train the group of volunteers on sites, so that they become confident in their monitoring and start sampling individually, potentially becoming trainers themselves. Although none of the FLOW recruited volunteers became trainer yet, in 2017 few of the groups accepted additional volunteer and trained the volunteer on their site. This tiered trainer – volunteer program was started to help with volunteers’ retention. Some of our volunteers are sampling with FLOW all three year, many sampled two years in a row. Despite of this system, a lot of volunteers stopped sampling, often due to changed life circumstances – new jobs, moving away, disease, new family etc.

We schedule yearly collaborators and trainers meeting before the start of the season (January/February), where we discuss the modification to the program and plan for next year. So far we had a large turn over in the trainers, almost every year we had to find new set of trainers.

ii. Activity: *Follow up meeting with the FLOW Water Stewards*. This activity was again designed to improve retention and create FLOW Water Steward community. After the first year meeting where the results were presented and the program discussed with our volunteers, and following on survey to our volunteers, we also created a closed facebook group for our stewards, where we post information. This facebook group now contains photos of the collected macroinvertebrates to create online library.

Metrics:

Activity	Goal	Actual #		
		2015	2016	2017
# Trainers : Volunteers ratio	1:10	1:8	1:7	1:8
# of Trainers	NA	2	6	5
% retention	NA	---	56	62
Meeting attendance	NA	6	20	---

c. Objective: Summarize and disseminate water quality data on the lower Olentangy watershed

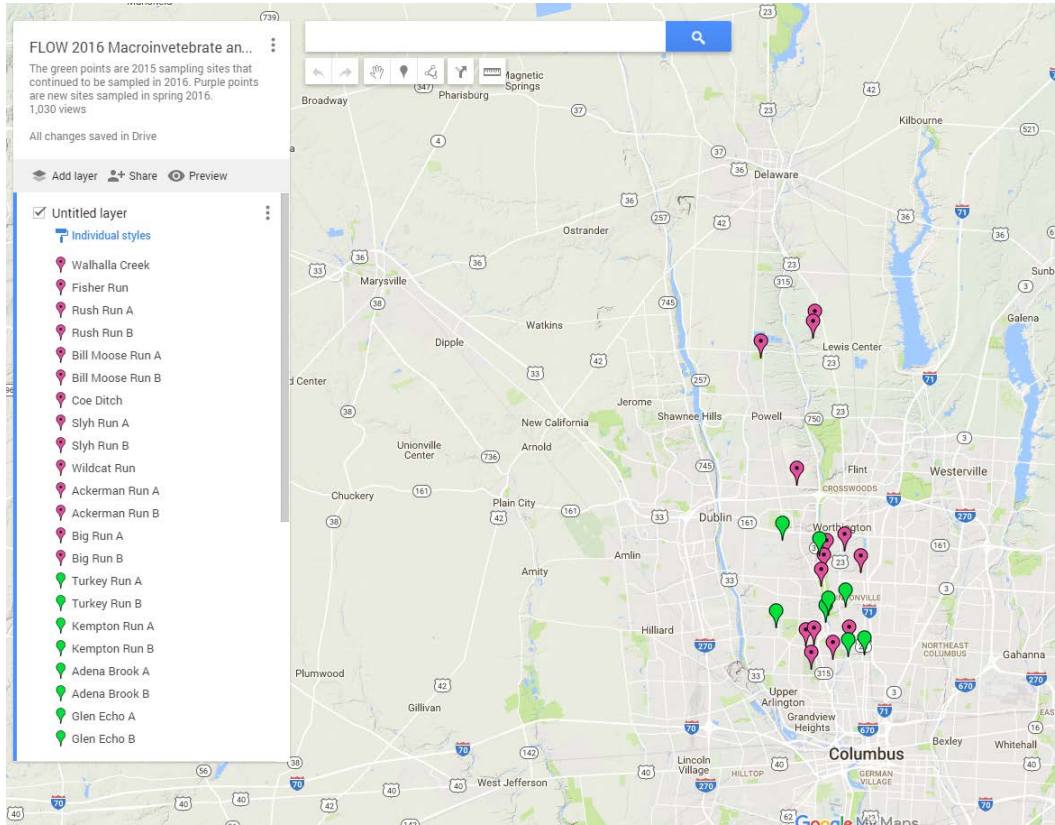
- i. Activity: *Maintenance and sharing of quality data* – the sentinel data are shared with Ohio Chapter of Sierra Club on their website. The macroinvertebrates and sentinel data are also sent to FLOW and shared with the volunteers in summarized version on the facebook page and during annual meetings. It seems that the volunteer macroinvertebrate data slightly underestimate the actual numbers, but this difference does not seem significant. In 2017, due to unavailability of nutrient testing strips from Sierra Club, different testing strips were ordered independently. These strips were showing slightly different results for nitrates, hardness and alkalinity. Additionally, the data are summarized and shared on FLOW Wiki website: <http://wiki.olentangywatershed.org/> and shared with ODNR Scenic River program coordinators.
- ii. Activity: *Presentation of the program water quality data*. Currently FLOW volunteer is working on creating “Stream Report Cards” – easily summarized macroinvertebrates results for the various tributaries with suggestions about helping to maintain water quality of your stream. These cards (example shown in Appendix) will be ready in spring for dissemination to landowners in the watershed. They will also be provided to our volunteers, since they often get questions from citizen while sampling.

4. Volunteers – Currently our volunteers are a diverse group of people including retirees, young professionals, OSU students, and Upper Arlington high school students along with their science teacher. We also have two organizations/groups involved in our program – OSU student organization TerAqua and the Cap City Biohackers.

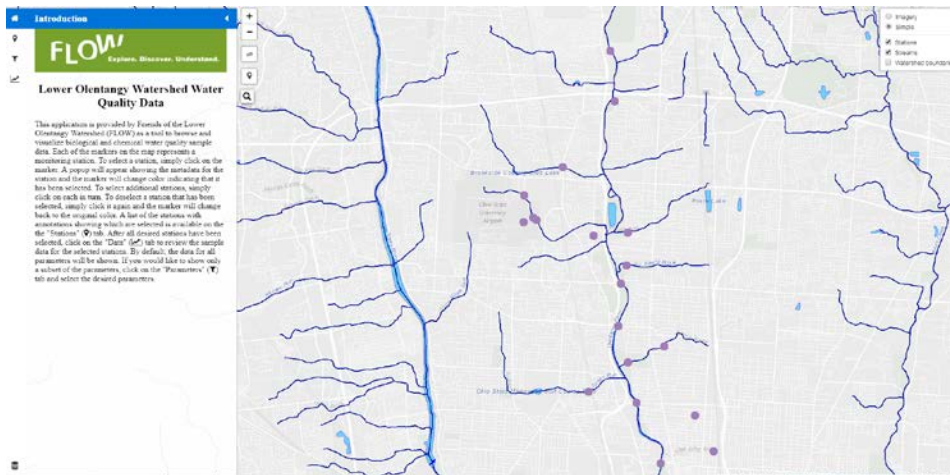
5. Continuation and Replication – We are excited about this program and are planning to continue it next year and possibly beyond. We will be meeting with program coordinators and trainers in February and discussing continuation plan – some things to discuss will be frequency of sampling, the areas we are sampling (do we want to expand, drop some sites etc.) and the parameters to measure. Many of our volunteers already expressed interest in continuing next year. This program did not require big fiscal resources but still needs a lot of involvement and time from collaborators and trainers. Though it seems that the program could be easily replicated to other areas, there is need for quite extensive administrative support to run this program.

SamplingLocationMap:

https://www.google.com/maps/d/u/0/edit?mid=1OCXPHgUi5R4aHf_9iITGAz5MBS0&ll=40.15001641395445%2C-83.00653957355956&z=11



FLOW has an application under development that will eventually allow residents to see our current grant data along with other data. <https://adamporr.github.io/FLOWWaterQuality/>



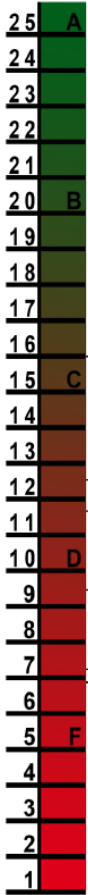
Data summary macroinvertebrates – Stream Quality Rating (SQM) is based on macroinvertebrates diversity, note that higher rating means higher diversity and better stream, usually we denote values <11 as Poor streams, 11-16 Fair, 17-22 Good and >22 as Excellent streams. Most of the sampled tributaries locations were in the fair to poor range.

Tributary	Average SQM
Ackerman Run A	9.4
Ackerman Run B	3.4
Adena Brook A	14.8
Adena Brook B	17.3
Big Run A	13.8
Big Run B	14.3
Bill Moose Run A	11.7
Bill Moose Run B	9.4
Glen Echo A	7.0
Glen Echo B	9.8
Kempton Run A	15.8
Kempton Run B	11.8
RUSH RUN A	7.2
Rush Run B	10.8
Slyh Run A	2.8
Slyh Run B	8.0
Turkey Run A	5.5
Turkey Run B	14.2
Walhalla	13.8
Wildcat Run B	11.7
Wildcat Run C	15.3

Data summary – sentinel measures temperature, total dissolved solids (TDS), conductivity and salinity using meter and hardness, alkalinity, nitrates, chlorines and phosphates using measurements strips (semi-quantitative). Average values from two or three sampling years (n=5-8) are presented in the table.

Row Labels	Temp (C)	TDS (mg/L)	Total Chlorine (ppm)	Average of Total Hardness (ppm)	pH	Conductivity (uS)	Total Alkalinity (ppm)	Nitrate (ppm)	Phosphate ppm	Salinity ppm
Ackerman Run A	23.4	544.8	0.4	130.0	7.9	717.0	210.0	10.0	5.0	454.8
Ackerman Run B	20.4	755.3	0.5	237.5	8.3	1491.8	255.0	0.4	12.0	706.8
Adena Brook A	17.0	542.6	0.2	274.4	8.0	756.9	220.0	2.3	1.9	370.0
Adena Brook B	17.8	460.0	0.6	121.4	7.7	718.1	200.0	1.1	6.4	310.9
Big Run A	20.2	561.8	0.3	259.0	8.2	646.8	230.0	2.0	0.0	379.7
Big Run B	19.4	581.3	0.1	265.0	8.4	741.0	223.3	2.0	1.7	424.2
Bill Moose Run A	17.7	543.3	0.1	405.0	8.4	942.3	220.0	12.5	14.2	466.0
Bill Moose Run B	19.8	580.0	0.4	250.0	8.0	806.0	200.0	8.1	2.0	400.5
Glen Echo A	20.3	713.7	0.6	223.6	8.2	1018.4	214.3	0.5	15.0	481.3
Glen Echo B	18.6	657.8	0.9	267.5	7.7	863.0	186.7	1.3	9.2	536.5
Kempton Run A	17.5	598.4	0.3	308.3	8.1	812.2	230.0	2.0	5.8	400.3
Kempton Run B	19.4	545.8	0.2	166.4	7.9	779.5	245.0	3.8	8.1	392.9
RUSH RUN A	20.6	848.4	0.5	390.0	8.4	1111.0	240.0	0.3	3.0	610.2
Rush Run B	18.5	665.1	0.2	339.0	8.0	1012.6	198.0	0.0	17.0	533.8
Slyh Run A	20.7	831.6	0.4	390.0	8.2	1387.0	216.0	2.8	9.4	747.1
Slyh Run B	18.9	976.5	0.3	275.0	8.4	1370.5	270.0	20.7	15.0	702.8
Turkey Run A	20.0	566.1	0.3	182.2	7.9	747.3	195.0	0.9	7.9	393.0
Turkey Run B	25.5	832.4	0.5	159.0	8.1	952.9	224.0	4.3	11.0	611.0
Walhalla	18.4	642.7	0.3	174.0	8.0	854.7	184.0	8.3	24.2	452.8
Wildcat Run B	21.6	678.0	0.3	250.0	8.4	967.0	220.0	1.5	0.0	476.7
Wildcat Run C	21.3	469.6	0.3	308.3	8.2	927.0	220.0	0.5	6.7	451.3

Stream Report Card DRAFT



Rush Run

Your Stream Report Card!!!

Volunteer Stream Quality Monitors from the Friends of the Lower Olentangy Watershed (FLOW) have sampled 14 Olentangy tributaries in 28 locations over the past 2 years. The Cumulative Index Value (CIV) is a score assigned based on the number of different organisms found in these streams. This method of sampling is used in a volunteer capacity by other agencies such as ODNR. Increased diversity leads to a high CIV, but a score of 9.5 in Rush Run reflects that many species are absent due to poor water quality and an unhealthy system.



The Causes for your score....

- Fertilizers and Pesticides
- Road Salt
- Pet Waste
- Trash
- Oil and Fuels

How You Can Help Improve Your Stream Quality...

- Consider that **all local drains lead to your stream**- they are not filtered so anything you can do to prevent pollution will help
- Reduce **fertilizers and pesticides** used in lawn care
- **Do not mow up to the edge** of your stream- leaving a barrier will help filter rain runoff
- Clean up **pet waste and litter**
- **Wash vehicles in your lawn**
- Plant **native species**- Consider a prairie or pollinator garden.

Adena Brook-16.0

Kempton Run-12.5

Bill Moose-11.6

Rush Run-9.5

Glen Echo-7.3

Sivh Run-6.9

FLOW

For more information and ways you can get involved in your watershed please visit

FLOWohio.org

Email: info@olentangywatershed.org

Phone: (614)-267-3386.

Picture FLOW Water Steward Facebook group page

<https://www.facebook.com/groups/224663261215502/>

Check out the videos that we have to help our volunteers with their D net technique

<https://www.facebook.com/groups/224663261215502/videos/>

FLOW Watershed Wiki Page – Sample for Big Run

<http://wiki.olentangywatershed.org/watersheds/big-run>

Watersheds >
Big Run

The Lewis Center tributary enters the Olentangy River at RM 18.15. It drains less than 10 square miles in Delaware County. The Ohio EPA monitored this tributary in 1999 at RM 0.10. The results are listed in the table below. This is a perennial stream (flows all year long). The effect of nearly every affessor within the basin was likely made more acute by significantly diminished stream flow within the entire catchment (EPA pg. 59). As classified by the Palmer Drought Severity Index, severe to extreme drought conditions were indicated for the period between July and October 1999 (Ohio DNR 1999). Big Run Preserve is a 75 acre area along Big Run that is within the Delaware County Preservation Parks system. FLOW partnered with Preservation Parks naturalists to conduct a bird survey in July of 2009 for the Ohio Bird Atlas. More information on the park can be found at <http://www.preservationparks.com/parks/bcr.asp>

FLOW Water Stewards are monitoring Big Run three times a year (spring, summer and fall) at two locations in Shale Hollows park. The Big Run stream winds along a twisting corridor lined by 20- to 40-foot tall shale cliffs. You can see many remnants of concretions (round rock formations) in the cliffs and along the stream bed. Our citizen scientists monitor water chemistry parameters such as total dissolved solids, conductivity, salinity, hardness, alkalinity, nitrate, phosphates and others. The overall water quality is fair, with average total dissolved solids 563 mg/l (just above the desired <500 for healthy streams), conductivity 706 uS, healthy salinity levels of 408 ppm, total hardness 245 ppm and total alkalinity 218 ppm. The nitrates are around 2 ppm which indicates nutrient enrichment, and phosphates are 0 ppm. FLOW water stewards also monitor macroinvertebrate diversity in water and though their results indicate fair water quality (SQM index average of 12), volunteers saw mayfly and stonefly nymphs, water pennies larvae, caddisfly and alderfly larvae, and riffle beetles (indicators of good water quality), in addition to scuds, damselfly nymphs, sowbugs and other organisms. Our water stewards' data can be found below in excel spreadsheet named Big Run data.



Location	Date	Temp (C)	TDS (mg/L or ppm)	Conductivity (uS)	Salinity (ppm)	Total Hardness (ppm)	Total Chlorine (ppm)	Free Chlorine (ppm)	Total Alkalinity (ppm)	pH	Nitrate (ppm)
Big Run A	6/12/2016	23	629	874	440	250	0.5	0.5	240	8.4	2
Big Run B	6/12/2016	22	640	933	454	250	0	0	240	8.4	2
Big Run A	7/31/2016	23.7	468	668	319	120	0	0	240	8.4	2
Big Run B	7/31/2016	22.7	396	566	393	120	0	0	180	8.4	2
Big Run A	9/25/2016	18.8	525	747	364	250	0	0	240	8.4	2
Big Run B	9/25/2016	18.5	543	798	386	120	0	0	240	8.4	2
Big Run A	6/4/2017	19	627	89.5	437	425	0.5	0	120	7.8	NA
Big Run B	6/4/2017	21	677	969	472	425	0.5	0	240	8.4	NA

Nitrite (ppm)	Phosphate (ppm)	Stream Assessment Quality Rating:	SQM word		
0	0	12	fair	low	spring
0	0	17	good	low	spring
0	0	9	POOR	normal	summer
0	0	5	POOR	normal	summer
0	0	10	POOR	normal	fall
0	0	5	POOR	normal	fall
NA	0	21	Good	normal	spring
NA	5	16	Fair	normal	spring

KIT Possession:					
Name(s): Megan and JB					
Date: (MM/DD/YYYY)					6/12/2016
Time:					9:30
Site:				Big Run A	
Site Description: log jam					
Sampling occurred for a minimum of 30 minutes					X
Sampling occurred over multiple habitats					X
Sampling did NOT occur with in 48 hours of a precipitation event					X

Macroinvertebrate Tally

Group 1 Taxa	Letter Code	Group 2 Taxa	Letter Code	Group 3 Taxa	Letter Code
Water Penny Larvae	a	Damselfly Nymphs		Blackfly Larvae	
Mayfly Nymph	a	Dragonfly Nymphs		Aquatic Worms	
Stonefly Nymph		Crane Fly Larvae		Midge Larvae	
Dobsonfly Larvae	a	Beetle Larvae		Pouch Snails	a
Caddisfly Larvae	a	Crayfish	a	Leeches	
Riffle Beetle Adult		Scuds			



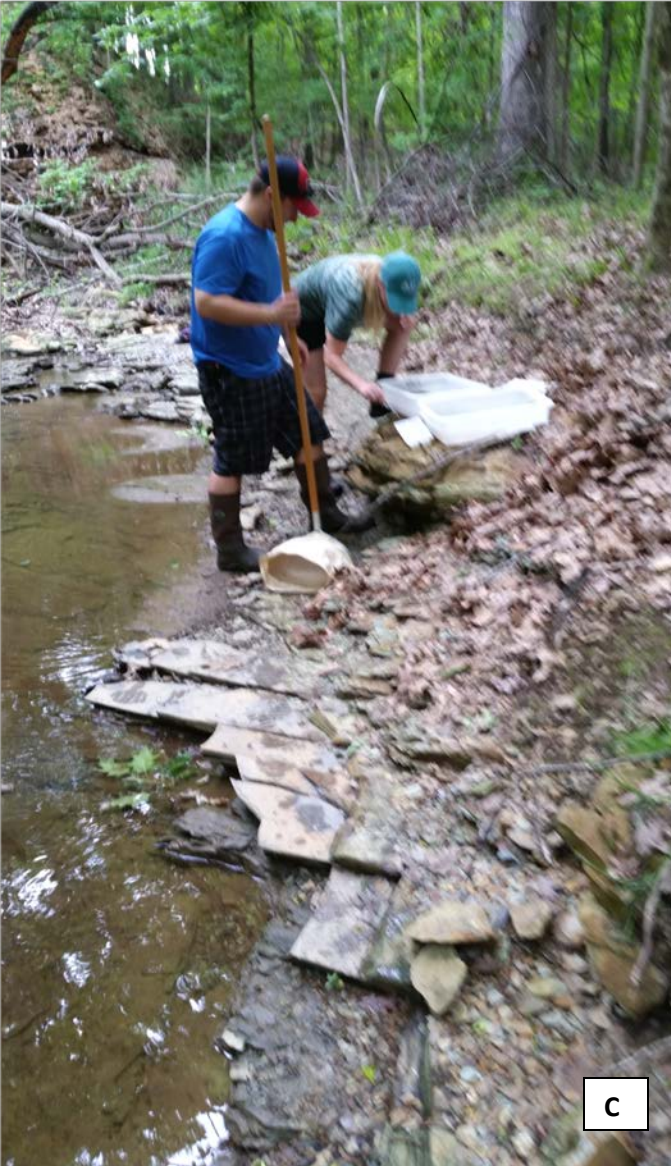
From Left to Right: Rush Run B Macros Crane fly Larvae, Damselfly Larvae, and Salamander- Eurycea Cirrigera (which isn't recorded but was an interesting find for volunteers!)



A



B



C

Sampling Teams at 4 Sites:
A: Kempton Run B
B: Glen Echo A
C: Big Run
D: Bill Moose Run



D

USGS Summer Intern Program

None.

Student Support					
Category	Section 104 Base Grant	Section 104 NCGP Award	NIWR-USGS Internship	Supplemental Awards	Total
Undergraduate	8	0	0	6	14
Masters	3	0	0	3	6
Ph.D.	5	0	0	1	6
Post-Doc.	1	0	0	0	1
Total	17	0	0	10	27

Notable Awards and Achievements

2016OH506O Omaghomi, T and Buchberger, S. (2017) “Residential Water Demand Calculator” 2nd place poster competition at OVALS Conference Cincinnati, Ohio

2016OH507B MICMoR Graduate Student Fellowship, Karlsruhe Institute of Technology, 2016-2018. To Chante Vines (Trainee)

2017OH533B Deon Knights received the School of Earth Sciences’ Distinguished Graduate Student Award for a post-candidacy doctoral student. Cited among his accomplishments was his Journal of Hydrology publication.

2017OH534B PhD Student Camilo Rey Sanchez received the prestigious OSU Presidential Fellowship for the final year of his studies in recognition of his outstanding progress to date.

2017OH532B Megan Berberich – J. Robie Vestal Award for Outstanding MS Student, University of Cincinnati Biological Sciences Department (2017)

2017OH532B Ishi Buffam - Faculty Development Council Grant, University of Cincinnati: Presenting Research and Establishing Collaborations on Carbon Connectivity of Watersheds, Lakes and Streams at the American Water Resources Association Conference (2017)

Publications from Prior Years

1. 2014OH312B ("Scenario Analysis for the Impact of Hydraulic Fracturing on Stream Low Flows and Water Supplies: A Case Study of Muskingum Watershed in Eastern Ohio") - Articles in Refereed Scientific Journals - A Shrestha, S Sharma, CE McLean, BA Kelly, SC Martin (2017). Scenario analysis for assessing the impact of hydraulic fracturing on stream low flows using the SWAT model. Hydrological Sciences Journal, 62(5): 849-861, DOI:10.1080/02626667.2016.1235276
2. 2014OH327B ("Linked geomorphic and ecological responses to river restoration: Influence of dam removal on river channel structure and fish assemblages") - Articles in Refereed Scientific Journals - S. Ma, eika P. Sullivan, D.W.P. Manning (2017). Seasonally distinct taxonomic and functional shifts in macroinvertebrate communities following dam removal. PeerJ, open access, DOI 10.7717/peerj.3189
3. 2014OH447B ("Spatial Demand Estimation: Moving Towards Real-Time Distribution System Network Modeling") - Articles in Refereed Scientific Journals - T Quin, DL Boccelli (2017). Grouping Water-Demand Nodes by Similarity among Flow Paths in Water-Distribution Systems. Journal of Water Resources Planning and Management, 143(8): 04017033-1, DOI: 10.1061/(ASCE)WR.1943-5452.0000788
4. 2016OH508B ("Co-Optimizing Enhanced Water Recovery and CO2 Sequestration in Ohio") - Articles in Refereed Scientific Journals - Y Wang, J Bielicki (2018). Acclimation and the response of hourly electricity loads to meteorological variables. Energy, 142: 473-485, DOI: <https://doi.org/10.1016/j.energy.2017.10.037>